CONF-9205234--

BNL 47972

Proceedings of the

Workshop on Hadron Structure from Photo-reactions at Intermediate Energies

Brookhaven National Laboratory
May 28-29, 1992

Editors: A.M. Nathan and A.M. Sandorfi

BROOKHAVEN NATIONAL LABORATORY
ASSOCIATED UNIVERSITIES INC.
Under Contract No. DE-AC02-76CH00016 with the
UNITED STATES DEPARTMENT OF ENERGY

BNL--47972

DE93 001904

Proceedings of the

Workshop on Hadron Structure from Photo-reactions at Intermediate Energies

Brookhaven National Laboratory
May 28-29, 1992

Editors: A.M. Nathan and A.M. Sandorfi

This Workshop concentrated on two aspects of hadron structure: the polarizabilities of nucleons and mesons, and nucleon deformation as reflected in an E2 component in the excitation of the delta isobar.

Sponsorship was provided by Brookhaven National Laboratory, Associated Universities Inc., the University of Illinois, Hamamatsu Corp., Phillips Scientific Inc., and LeCroy Corp., and is gratefully acknowledged.

Printed in the United States of America
Available from
National Technical Information Service
U.S. Department of Commerce
5285 Port Royal Road
Springfield, VA 22161

NTIS price codes:
Printed Copy: A07; Microfiche Copy: A01

Proceedings of the Workshop on Hadron Structure from Photo-reactions at Intermediate Energies

Contents

The Proton Compton Effect: Recent Measurements of the Electric and Magnetic Polarizabilities of the Proton

F. J. Federspiel
Los Alamos Meson Physics Facility
Los Alamos National Laboratory
Los Alamos, New Mexico 87545

ABSTRACT

A review of the experimental situation regarding the electric and magnetic polarizabilities of the proton is presented. The polarizabilities extracted from an analysis of two recent experiments are: $\bar{\alpha} = (10.8 \pm 1.0 \pm 1.0) \times 10^{-4}\ fm^3$ and $\bar{\beta} = (3.4 \mp 1.0 \mp 1.0) \times 10^{-4}\ fm^3$.

1. Introduction

The electric and magnetic polarizabilities, labelled α and β respectively, measure the ease with which an electric or magnetic dipole moment can be induced in a composite system through the application of static external electric or magnetic fields.[1] These structure constants are therefore fundamentally as important as the charge or magnetic radius of the system, although in the case of the nucleon they are considerably less well known. With the high present–day interest in QCD–based theoretical descriptions of the nucleon, it is clear that the additional information represented by an accurate determination of its polarizabilities would be of substantial importance.

Simple constituent quark models[2] relate α to the size and energy scales of the proton, and experimental measurements for these quantities typically lead to values in the range $\alpha \sim 10 \times 10^{-4}\ fm^3$. The simplest bag model calculations lead to similar values.[3] However, these results are possibly misleading, since these models suffer from the inherent difficulty that their size and energy scales are incompatible. Furthermore, only contributions due to excited states of the nucleon are included; potentially important contributions due to states of the pion–nucleon system are omitted. These deficiencies are partially remedied in a chiral bag model, where the valence quark core is surrounded by a pion cloud. Using this model, Weiner and Weise[4] reproduce both the size scale, which is largely determined by the pion cloud, and the energy scale, which is determined by the quark core. They find $\alpha \approx (7-9) \times 10^{-4}\ fm^3$; interestingly, only a small part of the result is due to excited states of the quark core, while the dominant contribution comes from the pion cloud.

The magnetic polarizability β is believed to be smaller than α due to a strong cancellation between the positive contribution of the low-lying $\Delta(1232)$ resonance and the negative contribution of virtual quark–antiquark pairs.[1,2] The degree to which the cancellation occurs is highly model-dependent, and at this point in time even the sign of β is uncertain. Typically the calculations span the range $(-3 \leq \beta \leq 3) \times 10^{-4}\ fm^3$. An accurate determination of β would be of great value in constraining the model calculations.

Measurements of the proton polarizabilities have exclusively come from Compton scattering experiments. These measurements rely on a theorem to establish a unique relation between a low-energy expansion of the Compton scattering cross section and the static polarizabilities. For photon energies small compared to the pion mass, this low-energy expansion (LEX) reads[1]:

$$\frac{d\sigma}{d\Omega}(E,\theta) = \frac{d\sigma^{pt}}{d\Omega}(E,\theta) - r_0 \left[\frac{E'}{E}\right]^2 \left[\frac{EE'}{(\hbar c)^2}\right] \left\{ \frac{\bar{\alpha}+\bar{\beta}}{2}(1+\cos\theta)^2 + \frac{\bar{\alpha}-\bar{\beta}}{2}(1-\cos\theta)^2 \right\}, \tag{1}$$

where E and E' are the energies of the incident and scattered photon, respectively; r_0 is the classical radius of the proton; and $d\sigma^{pt}/d\Omega$ is the exact cross section for a structureless proton with an anomalous magnetic moment.[5] E and E' are related by the usual Compton formula. The quantities $\bar{\alpha}$ and $\bar{\beta}$ are the static polarizabilities, corrected for recoil and retardation,[1] and are the only unknown parameters in Eq. (1). They are the quantities one seeks to extract from the measured scattering cross sections. Eq. (1) shows that the forward cross section is sensitive mostly to $\bar{\alpha}+\bar{\beta}$, whereas the backward cross section is sensitive mostly to $\bar{\alpha}-\bar{\beta}$.

The sum $\bar{\alpha}+\bar{\beta}$ is also constrained by a model-independent dispersion sum rule[6]:

$$\bar{\alpha}+\bar{\beta} = \frac{\hbar c}{2\pi^2}\int_{m_\pi c^2}^{\infty} \frac{\sigma_\gamma(E)dE}{E^2} = (14.2 \pm 0.03)\ \text{x}\ 10^{-4}\ \text{fm}^3, \tag{2}$$

where $\sigma_\gamma(E)$ is the total photoabsorption cross section on the proton. The integral is evaluated using both the available experimental data and a reasonable theoretical assumption for continuing the integral to infinite energy.[7] Thus, a combination of the above dispersion sum rule and a measurement of the scattering cross section at a backward angle can determine both $\bar{\alpha}$ and $\bar{\beta}$. Alternately, measurements at forward and backward angles can determine both $\bar{\alpha}$ and $\bar{\beta}$ as well as test experimental systematics through comparisons with the sum rule.

The choice of photon energy requires some discussion. On the one hand one wants the photon energy to be large, since the effect of the polarizability on the cross section is quadratic in energy. On the other hand, if the photon energy becomes too large, the LEX breaks down, thereby introducing theoretical uncertainty into the extraction of the polarizabilities from the measured cross sections. Various attempts have been made to estimate corrections to the LEX. The most successful of these

is due to L'vov,[8] whose calculations are based on dispersion relations in which a variety of experimental data and theoretical *ansatzen* are used to evaluate numerically the dispersion integrals. The parameter $\bar{\alpha} - \bar{\beta}$ appears as an unknown subtraction constant, which can be adjusted to fit an experimental cross section. The range of validity of the LEX is an important consideration in the analysis of the experimental data.

2. Review of Compton Scattering Experiments

2.1. Experiments Prior to 1980

A common feature of these experiments has been the use of continuous-energy bremsstrahlung photon beams and photon detectors having poor energy resolution. These factors have made it difficult to determine the incident photon flux accurately. Consequently, all but one of these experiments quote systematic uncertainties that are too large to provide meaningful constraints on the polarizabilities.[9] The exception is the Moscow experiment of Baranov, *et al.*,[10] in which the systematic errors were reduced by measuring the yield of photons scattered from the proton to those scattered from the atomic electrons, for which the scattering cross section is well known. Data were taken in the 80–110 MeV range at scattering angles of 90° and 150° . Using the L'vov cross section to extract the polarizabilities from this data yields $\bar{\alpha} = 11.2 \pm 1.3$ and $\bar{\beta} = -5.7 \pm 1.8$, both in units of $10^{-4} fm^3$. Despite the small error bars and the claim of small systematic uncertainty, this result is very problematic since it is inconsistent with the dispersion sum rule (Eq. 2). It is this problem that provided the principal motivation for the new experiments, which are now discussed.

2.2. The Illinois Tagged Photon Experiment

The Illinois experiment[11] had two distinct technical advantages over the previous experiments, allowing systematic errors to be held to a very low level. This experiment made use of a monochromatic tagged photon beam and large $NaI(Tl)$ photon detectors with high intrinsic resolution ($\Delta E/E \sim 3\%$). As shown below, the result is a considerable improvement on experimental knowledge of the proton polarizabilities.

Electrons from the 100% duty factor accelerator MUSL–2 were incident on a 34 mg/cm^2 Al radiator foil. The post–bremsstrahlung electrons were momentum–analyzed in a magnetic spectrometer and detected in a staircase array of 32 plastic scintillator counters, thereby tagging the associated photons and determining their energy. The photons were collimated and directed onto a 889 mg/cm^2 target of liquid hydrogen contained in a thin–walled Mylar vessel. Scattering data were taken with the vessel both full and empty, in order to be able to subtract the events due to scattering in the Mylar. Photons scattered from the target were detected in one of the two large NaI detectors, which were positioned at scattering angles of 60° and

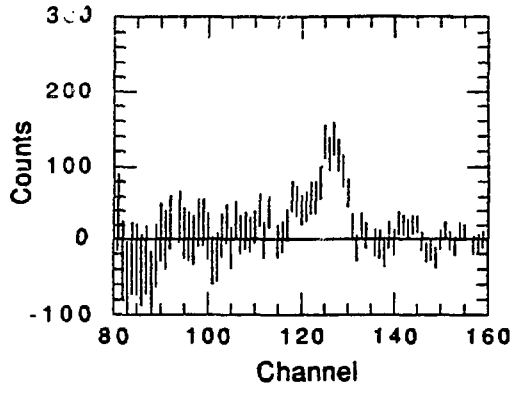

Figure 1: Pulse height spectrum from the scattering of 70 MeV tagged photons from hydrogen at 135° . Contributions from the empty target and from chance coincidences have been subtracted.

135°, respectively. A valid event consisted of a time–correlated coincidence between an electron in a tagging counter and the associated photon in one of the NaI detectors. The incident photon flux was determined directly by counting the tagging electrons; calibration measurements were done in which each of the NaI detectors was separately put directly into the photon beam in order to determine the number of tagged photons per tagging electron. Data were taken between 32 and 72 MeV incident photon energy, in four steps, each covering a total tagged photon range of 8 MeV. In the off–line analysis, the data were combined into two 4 MeV-wide bins. A typical pulse–height spectrum in one of the NaI detectors is shown in Fig. 1; chance coincidences, as well as the contribution of the empty Mylar vessel, have been subtracted out.

The scattering cross section is related to the measured quantities by the following expression:

$$\frac{d\sigma}{d\Omega} = \frac{1}{\kappa\Omega}\left[\frac{Y_\gamma^s/N_e^s}{Y_\gamma^c/N_e^c}\right]. \tag{3}$$

The numerator and denominator of the bracketed expression are the number of detected tagged photons per tagging electron in the scattering and calibration measurements, respectively; these were determined by summing over the appropriate regions of the pulse–height spectra. The systematic errors are as follows: incident photon flux, ±1%; number of target nuclei per unit area (κ), ±1%; photon detector solid angle (Ω), ±1.4%. Combining all the systematic errors in quadrature, the systematic

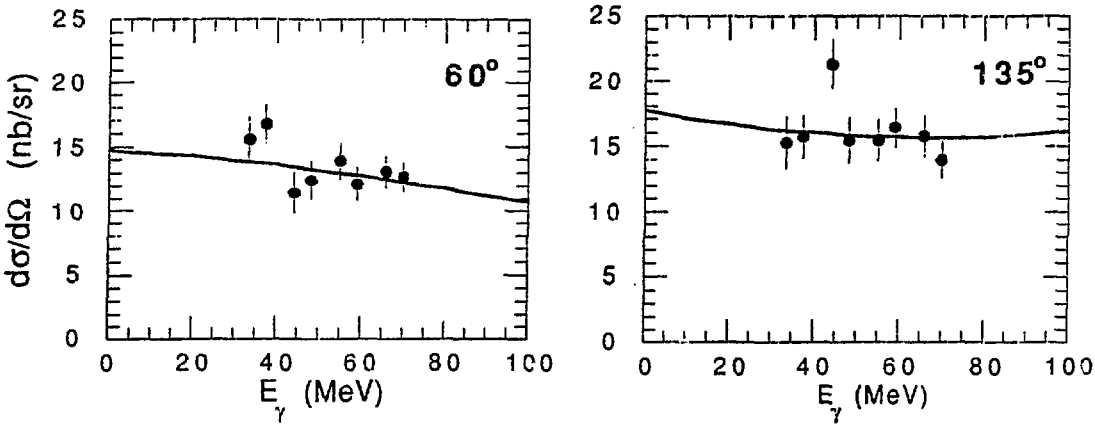

Figure 2: Compton–scattering cross sections on hydrogen obtained in the Illinois experiment. The error bars include statistical errors only. The curves are the cross sections of L'vov fitted to our data.

uncertainty in the absolute scale of the cross sections is estimated to be ±2.0%. The resulting cross sections are shown in Fig. 2 along with their statistical errors.

The polarizabilities were extracted from these cross sections in two steps. First, the two parameters $(\bar{\alpha}+\bar{\beta})$ and $(\bar{\alpha}-\bar{\beta})$ were adjusted to fit L'vov's theory to the data. This results in $(\bar{\alpha}+\bar{\beta}) = 11.9 \pm 3.9 \pm 1.7$ and $(\bar{\alpha}-\bar{\beta}) = 8.0 \pm 4.4 \pm 2.2$. Comparison of this result to the sum rule constraint from Eq. 2 shows that the Illinois data is not in disagreement with the sum rule. The second step was to *assign* the sum rule value to $(\bar{\alpha}+\bar{\beta})$ and allow only $(\bar{\alpha}-\bar{\beta})$ to vary in the fitting procedure. This results in

$$(\bar{\alpha}-\bar{\beta}) = 7.6 \pm 4.3 \pm 2.5. \qquad (4)$$

In the results above, the first error shown is statistical; the second represents the effect of changing the absolute normalization of the data by the systematic error in that data.

As a demonstration of the model independence of these results, Figure 3 shows the 135° Illinois data with both L'vov's calculation and the LEX evaluated at $(\bar{\alpha}+\bar{\beta}) = 14.2$, $(\bar{\alpha}-\bar{\beta}) = 7.6$. Further details of the experimental setup, data reduction, various corrections, and systematic errors can be found in the thesis of Federspiel.[11]

2.3. The Mainz 180° Experiment

The Mainz experiment[12] used a continuous-energy bremsstrahlung beam to measure the 180° Compton scattering cross section by detecting the forward recoiling protons in a magnetic spectrometer. Using the theoretical calculation of L'vov,

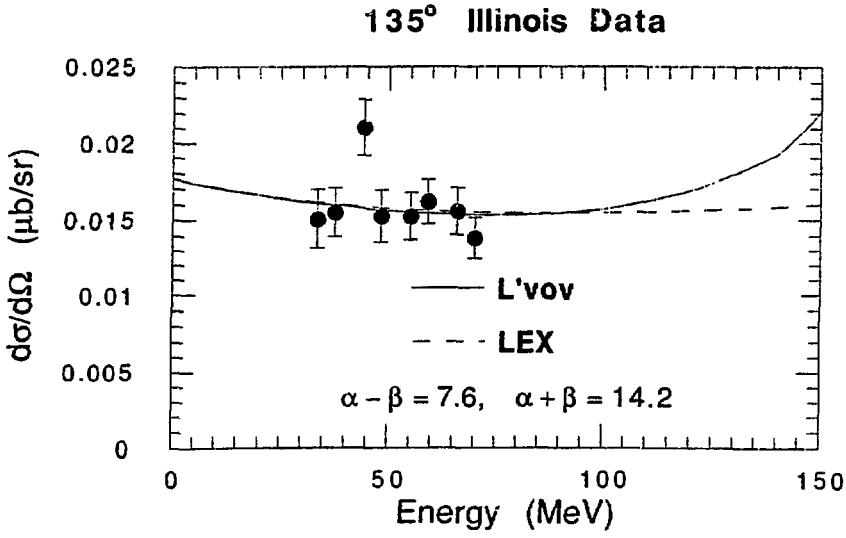

Figure 3: The 135° Illinois cross sections. The overlap of the two theoretical curves in the region of the data indicates that the high-energy breakdown of the LEX has negligible effect on the polarizabilities extracted from the Illinois data.

polarizabilities can be extracted from the Mainz calculations that are in excellent agreement with the Illinois values. By measuring at relatively high energy, the Mainz cross sections place tighter statistical constraints on the polarizabilities at the expense of introducing a degree of model-dependence to the result.

Photons were produced by the 350 MeV electron beam passing through an 837 mg/cm^2 Al radiator, and directed toward one of two liquid hydrogen targets (thickness 40 mg/cm^2 or 72 mg/cm^2). Cross section measurements were made at two nominal settings of the magnetic spectrometer, one corresponding to protons scattered elastically from 98 MeV incident photons, the other to 132 MeV photons. Downstream of the target, the photon flux was monitored during each run by a P2 ionization chamber. A rate was calculated for each run by dividing the observed yield in the spectrometer by the charge collected in the ionization chamber. This ionization chamber was calibrated by measuring the well-known Compton electron yield in the same magnetic spectrometer used to detect the protons.

The subtraction of empty target contributions required two types of empty target measurements: one to account for the protons produced in the target upstream of the liquid hydrogen, and one to account for the protons produced downstream of the liquid. During a full target run, the protons produced *upstream* of the liquid chamber passed through the liquid and lost energy on their way to the spectrometer. When the target was empty, these same background protons arrived at the spectrometer at a higher energy. Also, during full target runs, some fraction of these protons

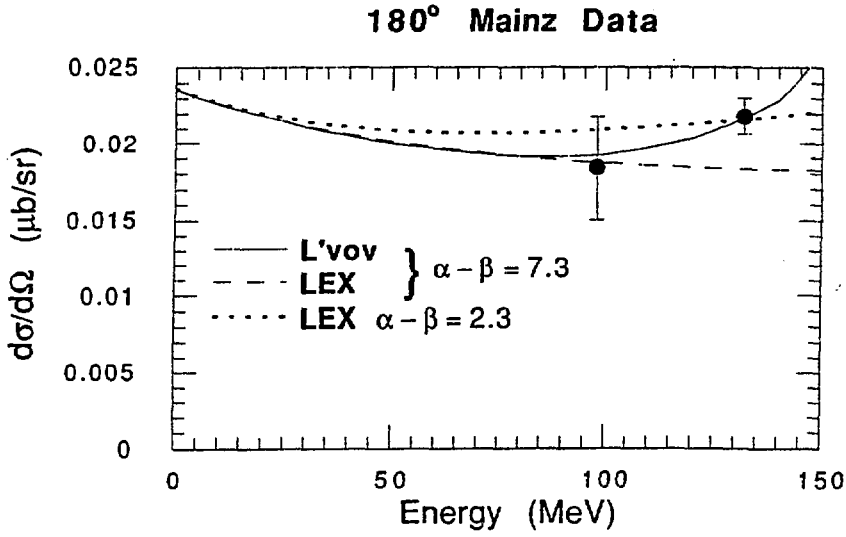

Figure 4: The Mainz cross sections. The solid curve and the short–dashed curve are fits to the data. The long–dashed curve shows the high–energy divergence of the LEX from the L'vov calculation, imparting some degree of theoretical uncertainty to the polarizabilities derived from the Mainz cross sections.

were also scattered out of the spectrometer's acceptance by the layer of liquid. To account for the energy difference, one set of empty target measurements was made with the spectrometer at a higher momentum setting than in the full target runs. Monte Carlo techniques were used to account for the difference between full target background acceptance and empty target background acceptance. The background from the *downstream* part of the target was dealt with simply by measuring the rate from the empty target at the nominal spectrometer setting.

The Mainz cross sections are shown in Figure 4 along with three theoretical calculations. The solid curve results from fitting the L'vov theory to the data. This fit results in

$$(\bar{\alpha} - \bar{\beta}) = 7.3 \pm 2.3 \pm 2.1, \tag{5}$$

where the second error corresponds to the systematic uncertainty in the cross sections. The long–dashed line in Fig. 4 is the LEX evaluated at that same value of $(\bar{\alpha} - \bar{\beta})$, showing that the high–energy measurement is well above the energy at which the LEX is valid. The short–dashed curve is the result of fitting the LEX to the Mainz data.

3. Summary of Experimental Results

There are four potential constraints on the polarizabilities:

- The sum rule result for $(\bar{\alpha} + \bar{\beta})$,

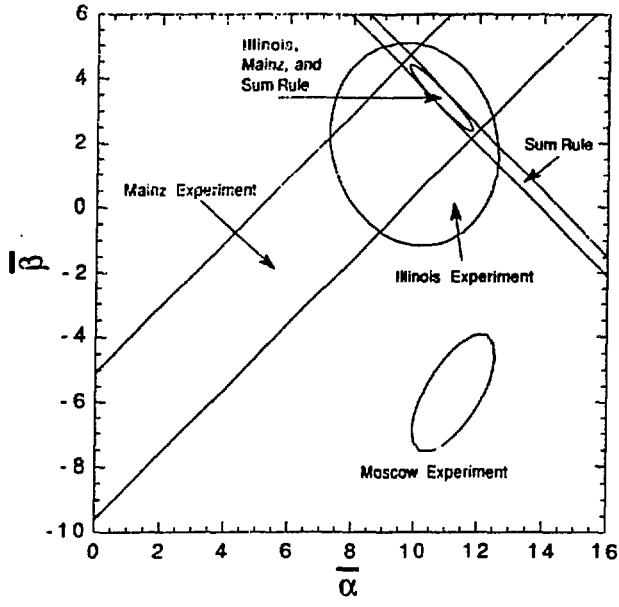

Figure 5: Shown are 1–σ boundaries in the $\bar{\alpha}$ –$\bar{\beta}$ plane of the various constraints on the polarizabilities

- The Moscow data,
- The Illinois data, and
- the Mainz data.

As stated earlier, the Moscow measurements at 90° and 150° are not both compatible with the sum rule result. Because of this, the approach taken in this analysis will be to disregard the Moscow data in the global fitting process. The polarizabilities extracted from the Illinois measurements have rather large error bars, but they do agree with the sum rule and they are measured at energy low enough so that model–dependency is not an issue. Using the cross sections of L'vov, values extracted for $\bar{\alpha}$ and $\bar{\beta}$ from the Mainz data are in excellent agreement with the Illinois results. Note that if the Mainz measurement at 98 MeV had a smaller error bar, the Mainz data could distinguish between the two fits (the solid curve and the short–dashed curve) in Fig. 4. This points out the importance of an accurate mapping of the Compton cross section as a function of energy. As things stand now, the low–energy Illinois measurements together with the higher energy Mainz measurement lend support to the theory of L'vov.

Figure 5 shows the good agreement between the Illinois measurement and the sum rule, and between the Illinois measurement and the Mainz result derived from

the L'vov calculation. The narrow ellipse is the $1-\sigma$ boundary resulting from these three constraints on the polarizabilities, assuming that the error in L'vov's calculation contributes negligibly to the error in the Mainz polarizabilities. Numerically, this ellipse can be represented as

$$\bar{\alpha} = 10.8 \pm 1.0 \pm 1.0, \tag{6}$$

and

$$\bar{\beta} = 3.4 \mp 1.0 \mp 1.0, \tag{7}$$

where the errors on $\bar{\alpha}$ and $\bar{\beta}$ are anticorrelated because of the tiny error bar on the sum rule. The systematic error shown is solely due to the systematic error in the Mainz 132 MeV measurement.

References

1. V. A. Petrun'kin, Fiz. Elem. Chastits At. Yadra **12** (1981) 692 [Sov. J. Part. Nucl. **12** (1981) 278].
2. D. Drechsel and A. Russo, Phys. Lett. **137B** (1984) 294.
3. A. Schäfer, B. Müller, D. Vasak, and W. Greiner, Phys. Lett. **143B** (1984) 323.
4. R. Weiner and W. Weise, Phys. Lett. **159B** (1985) 85.
5. J. L. Powell, Phys. Rev. **75** (1949) 32.
6. M. Gell-Mann, M. L. Goldberger, and W. E. Thirring, Phys. Rev. **95** (1954) 1612.
7. M. Damashek and F. J. Gilman, Phys. Rev. D **1** (1970) 1319.
8. A. I. L'vov, Yad. Fiz. **34** (1981) 1075 [Sov. J. Nucl. Phys. **34** (1981) 597], and private communication.
9. C. L. Oxley, Phys. Rev. **110** (1958) 733; L. G. Hyman, *et al.,* Phys. Rev. Lett. **3** (1959) 93; V. I.Gol'danski, *et al.,* Zh. Eksp. Teor. Fiz. **38** (1960) 1695 [Sov. Phys. JETP **11** (1960) 1223].
10. P. S. Baranov, *et al.,* Yad. Fiz. **21** (1975) 689 [Sov. J. Nucl. Phys. **21** (1975) 355].
11. F. J. Federspiel, *et al.,* Phys. Rev. Lett. **67** (1991) 1511. See also F. J. Federspiel, Ph.D. dissertation, University of Illinois, 1991 (unpublished).
12. A. Zieger, *et al.,* Phys. Lett. **278B** (1992) 34.

Experiments on the Electric Polarizability of the Neutron

JÖRG SCHMIEDMAYER

Institut für Experimentalphysik Universität Innsbruck, A-6020 Innsbruck, Austria

Department of Physics, Massachusetts Institute of Technology, Cambridge, Massachusetts, USA

Abstract:

The experimental situation regarding the electric polarizability of the neutron is reviewed. The experiments provides for the first time a nonzero value for the electric polarizability of the neutron $\alpha_n^o = (12.0\pm1.5\pm2.0)\times10^{-4}$ fm^3.

Electron-nuclear scattering experiments at GeV energies showed that the nucleons: neutrons and protons, are not point like objects. Therefore, their internal structure may be deformed by external forces. The deformations induced by strong electro - magnetic fields are characterized to lowest order by the electric (α) and magnetic (β) polarizabilities [1,2,3]. They are defined such that a particle placed in an external electric (magnetic) field **E** (**B**) acquires an induced electric (magnetic) dipole moment $\mathbf{d}=\alpha\mathbf{E}$ ($\mathbf{d}=\beta\mathbf{B}$). With the recent advance in QCD based models of the nucleon, knowledge of the polarizabilities may give new tests to be met by the models.

Electric and magnetic polarizabilities of elementary particles have been calculated recently using various models. The simple valence quark models [4] and bag models [5] provide a qualitative description of the electric polarizabilities and predict $\alpha\sim10\times10^{-4}$ fm^3. In the chiral bag model, the quark core contributes only 20% to the total polarizability, most of which comes from the distortion of the surrounding pion cloud [6]. This calculation gives $\alpha\sim(7\text{-}9)\times10^{-4}$ fm^3 and $\beta<2\times10^{-4}$ fm^3 for the nucleon. Recent calculations in chiral perturbation theory even suggest that the polarizability is entirely due to the pion cloud [7]. A chiral soliton model leads to $\alpha=13.4\times10^{-4}$ and $\beta=-1.1\times10^{-4}$ fm^3 [8]. In recent work, attempts were made to calculate the electric polarizabilities of hadrons in a quenched lattice QCD model [9]. In the light quark limit, a value of $\alpha\sim10\times10^{-4}$ fm^3 was obtained.

In most of the models the electric polarizability of the nucleon is calculated and is significantly larger than the magnetic polarizability. For the latter, even the sign of β is uncertain. Except for the chiral perturbation theory calculation, no significant differences between the neutron and proton are expected.

The electric polarizability of the neutron predicted by these models is approximately 18 orders of magnitude smaller than the polarizability of the hydrogen atom. This can be qualitatively understood because of the smaller volume and the stronger interaction, 100 times that of the Coulomb interaction, binding the neutron together.

Due to the small size of the electric polarizability of the neutron α_n, a measurement using macroscopic laboratory fields which can be controlled by the experimentalist, seems far beyond the possibilities of present technology. Even with the unrealistically high laboratory electric field of $E=10^8$ V/m and an expected value of $\alpha=10\times10^{-4}$ fm^3 one only finds an induced electric dipole moment of $d=3.5\times10^{-30}$ [ecm], which is about 4 orders of magnitude smaller than the present limit on the *static* electric dipole moment [10]. All measurable effects by the *induced* electric dipole moment would therefore be masked by a possible *static* dipole moment. Even neutron interferometry [11] and spin rotation experiments [12] cannot measure the potential energy change of $V=-1.7\times10^{-24}$ eV by a neutron in the above electric field. The largest controllable electric fields (up to 5 V/Å) are of microscopic size and are found around sharp tips, like those used in the scanning tunneling and the field emission microscope [13]. Even then the induced moment is still 2 orders of magnitude smaller than the limit on the static electric dipole moment.

There are two distinctly different ways to measure the electric polarizability of the neutron. One consists of measuring the energy change of the neutron ground state ($-\frac{1}{2}\alpha E^2$) in the presence of a strong electric field (corresponding to the DC stark shift). The other being Compton scattering experiments on the neutron. The first method was pursued over the last 30 some years using neutron scattering (tab.1). These experiments collimated recently in the first determination of the electric polarizability by the Vienna - Oak Ridge experiment [14]. The second method has only recently become possible with the advent of accelerator based high luminosity gamma ray sources and may provide an independent confirmation. A summary of experiments is given in table 1.

Review of neutron scattering experiments:

The strongest electric fields in nature up to 10^{21} V/m are found in an atom, near the surface of heavy nuclei like lead. The interaction potential due to the electric polarizability of the neutron near the nuclear surface is given by $V=-\frac{1}{2}\alpha_n Z^2e^2\frac{1}{r^4}$. The corresponding scattering amplitude for a point like nucleus with charge Ze was first calculated in the late 50's by Alexandrov [15] and independently by Thaler [16], and also Breit and Rustgi [17]. In a more detailed calculation [18,19], the complete nonmagnetic neutron-atom scattering cross section was calculated, including neutron - nucleus potential and resonant scattering, Schwinger scattering (spin-orbit scattering), the neutron-electron interaction, the electric polarizability and all interference terms. The neutron - nucleus potential and resonant scattering were considered in the framework of R-matrix theory. Schwinger scattering (spin-orbit scattering), the neutron-electron interaction and the electric polarizability

interactions were calculated in the Born approximation assuming a homogeneously charged sphere of radius R_N with total charge Z e for the nucleus and a realistic charge distribution for the atom. The scattering due to the electric polarizability of the neutron is dominated by the nuclear Coulomb field. The contributions of the atomic charge distribution is smaller by the ratio $R_N / R_e \approx 10^{-5}$ and can be neglected (R_e being the charge radius of the atom). For the complete scattering amplitude due to the electric polarizability, f_{Pol} calculated in first Born approximation (which is nearly proportional to $Z^{5/3}$) we find for $qR_N << 1$:

$$f_{Pol}(q) = \alpha_n Z^2 \frac{e^2 m}{\hbar^2} \frac{1}{R_N} \left[\frac{6}{5} - \frac{\pi}{4} qR_N + \frac{1}{7}(qR_N)^2 - \frac{1}{540}(qR_N)^4 + \ldots \right], \qquad (1)$$

where the second term (proportional to qR_N) is characteristic of the long range $1/r^4$ interaction potential of an induced electric dipole moment in the Coulomb field of a spherical charge. This term, linear in the momentum transfer $\hbar q$, gives the best possibility to separate $f_{Pol}(q)$ from the nuclear scattering amplitude which is about 2 orders of magnitude larger. Nevertheless, the electric polarizability of the neutron constitutes about 0.5% of the total neutron atom scattering cross section for a heavy nucleus.

It is interesting to note an interaction proportional to E^2 also arises in a QED treatment of the interaction of a point particle with a magnetic moment and an electric field [20]. Anandan showed in the nonrelativistic limit of the Dirac equation a term $\frac{\mu^2}{2mc^2} E^2$ arises which will give a contribution to our measured polarizability of $\Delta\alpha = -\frac{e^2}{4m^3} \kappa^2$. This is exactly the difference between the polarizabilities $\bar{\alpha}$ as described in quantum field theory and $\alpha^o$the static electric polarizability. For the neutron, $\Delta\alpha = -0.62 \times 10^{-4}$ fm^3 is small compared to the statistical uncertainty.

There are 2 possibilities to separate f_{Pol} from the f_{Nuc} :

* One, used in the early experiments (see table 1), measures the *differential cross section* of the neutron-nucleus scattering. Here, one examines the change of the contributions of p-wave scattering P(k) with incoming neutron momentum, $\hbar k$. P(k) can be expanded:

$$P(k) = P(0) + ak + bk^2 + O(k^4), \qquad (2a)$$

where $k = 2.1968 \times 10^{-4} \sqrt{E} \frac{A}{A+1}$ (k in [fm^{-1}] and E in [eV]) is the wave-vector of the incoming neutron. The parameter a depends only on the electric polarizability of the neutron. b and higher order parameters in the expansion (2) come mainly from the neutron-nucleus interaction.

* The other method is to measure the *total neutron-nucleus potential scattering cross section* σ_s as a function of neutron energy [19]. Below 50 keV ($k < 0.05$ fm^{-1}), σ_s can be expanded:

$$\sigma_s(k) = \sigma_s(0) + ak + bk^2 + O(k^4), \qquad (2b)$$

Here, the parameter a again depends only on the electric polarizability of the neutron while b and higher order parameters in the expansion (2) come mainly from the effective range of the neutron-nucleus interaction.

The characteristic term proportional to the momentum $\hbar k$ of the incoming neutron in Eq.2a, 2b can be separated from neutron-nucleus scattering via its characteristic energy dependance in the region 50 eV < E < 50 keV (k < 0.05 fm^{-1}). At very low energies the corrections from atomic scattering (neutron electron scattering and Schwinger scattering) become too large. At energies above 50 keV, even without resonant scattering higher order terms in Eq.2 become large and may mask a small term proportional to k.. An accuracy of 1 part in 1000 for each measured cross section is required for 100 different energies in the energy range 50 eV to 40 keV to achieve a statistical uncertainty of 2×10^{-4}fm^3 in α_n. Both methods have about the same sensitivity. But it turns out that the atomic and nuclear physics corrections are much smaller in the total cross section experiments [19].

The first experiments using total cross section measurements were carried out by various groups in Dubna, Munchen and Vienna-Harwell using natural Pb and Bi as heavy nuclear scattering targets. They were limited both in statistical accuracy and by unknown neutron-nuclear resonance scattering contributions.

In the Vienna-Oak Ridge experiment we choose to use ^{208}Pb because there are only p-wave (which give corrections $O(k^2)$ in Eq.2) and d-wave (which give corrections $O(k^4)$ in Eq.2) resonances below 500 keV [21]. Furthermore it has a negligible thermal absorption cross section $\sigma_a=(0.49\pm0.02)\times10^{-3}$ b [22]. The resulting energy dependent resonance corrections are smaller by more than an order of magnitude compared to the previous experiments. ^{208}Pb has the best properties of any heavy isotope to separate the potential scattering and the term proportional to k in Eq.2 from the resonant scattering contribution.

The total neutron-^{208}Pb cross section was measured by neutron transmission at a 80m and 200m flight path at the ORELA pulsed neutron source at Oak Ridge National Laboratory in the energy range 10 eV to 5 MeV. We remeasured all the relevant neutron resonances up to a few MeV. Analysis of the energy dependence of the data in the range from 50 eV to 40 keV gives the electric polarizability to $\alpha_n^0 = (12.0 \pm 1.5 \pm 2.0)\times10^{-4}$ fm^3 [14].

Neutron Compton scattering experiments.

Similar to the proton, the electric polarizabilities of the neutron can also be determined in Compton scattering. These experiments are much more difficult for the following two reasons:

* First, the neutron has no charge; therefore, the Thompson scattering amplitude vanishes. In addition,he polarizabilities $\bar{\alpha}_n$ and $\bar{\beta}_n$ enter the differential Compton cross section via the square of the Raleigh amplitude. This makes the cross sections below 100 MeV photon energy much smaller than for the proton.

* Second there is no dense, free neutron target. Even in the core of high flux reactors the neutron density corresponds to a gas pressure of about 5×10^{-2} torr. Compton scattering experiments on the neutron can therefore only be done only for neutrons bound in a nucleus. To extract the Compton scattering cross sections of the free neutron the experiments have to be carried out in the kinematically quasi free regime where the proton in the deuteron is only a spectator. Care has to be taken to include all competing processes and final state interactions.

Recently the first neutron Compton scattering experiments on the neutron in the deuteron where carried out by a Göttingen-Mainz collaboration at MAMI-A. The experiment measured the neutron Compton scattering cross section at 90° and 135°, with a tagged photon beam with energies ranging form 40 MeV to 80 MeV. To distinguish quasi free neutron-Compton scattering from the other competing processes in the photo-deuteron breakup both the outgoing photon energy and the outgoing neutron energy and angle was measured.

From measured differential cross sections for quasi free Compton scattering by the neutron in the deuteron at 90° and 135° Rose and al. [23] obtain an upper limit of $\bar{\alpha}_n=14.\times10^{-4}$ fm^3, but no lower limit. Assuming $\bar{\alpha}_n$ to be positive, they give $\bar{\alpha}_n=(10.7^{+3.3}_{-10.7})\times10^{-4}$ fm^3 .

With the advent of the new MAMI-B accelerator and an improved setup allowing the use of higher energy γ-rays, it will be possible to test the Vienna-Oak Ridge result. An interesting test of the above method, using quasi free scattering, will be to measure proton Compton scattering for protons in the deuteron. This will allow a better understanding of the corrections involved in these types of experiments.

Discussion:

The sum of the Compton electric $\bar{\alpha}_n$ and magnetic $\bar{\beta}_n$ polarizabilities $(\bar{\alpha}_n+\bar{\beta}_n)$ can be estimated model-independently with the help of the Kramers-Kroning dispersion sum rule for the total photoabsorption cross section $\sigma_T(\omega)$ of the neutron [1].

$$(\bar{\alpha}_n+\bar{\beta}_n) = \frac{1}{2\pi^2}\int_{\omega_0}^{\infty} d\omega \frac{\sigma_T(\omega)}{\omega^2} = (15.8\pm0.5)\times10^{-4}\ \text{fm}^3$$

With $\bar{\alpha} = \alpha^0 - \Delta\alpha$, we predict the magnetic polarizability of the neutron to be $\bar{\beta}_n = (3.2 \pm 1.6 \pm 2.0) \times 10^{-4}$ fm^3. This indicates that β is positive and much smaller than α.

In conclusion we want to point out that after 30 years of effort the Vienna-Oak Ridge experiment provides for the first time a value for the electric polarizability of the neutron and an estimate for its magnetic polarizability. With the recent advance in QCD based models of the nucleon, these polarizabilities may give new tests to be met by the theories.

I would like to thank H. Leeb for many fruitful discussions and all my collaborators in Vienna and Oak Ridge for their invaluable contributions to the experiment. This work was supported by by the *Austrian Fonds zur Förderung der Wissenschaftlichen Forschung* proj. No. 6849 and the Division of Nuclear Physics, U.S. Dep. of Energy, under contract No. DE AC05-840R21400. J.S. was supported in part by an *Erwin Schrödinger* Fellowship.

Table 1: Experimental values for the electric polarizability of the neutron.

method	α [10^{-4} fm^{-3}]	references	
differential cross section	800 ± 350	Alexandrov (1958)	[15]
	< 200	Thaler (1959)	[16]
	< 200	Breit,Rustgi (1959)	[17]
	7 ± 54	Alexandrov (1966)	[24]
	2600 ± 1000	Anikin (1972)	[25]
total cross section	15 ± 33	Alexandrov (1986)	[26]
	30 ± 40	Koester (1986)	[27]
	12 ± 10	Schmiedmayer (1987)	[28]
	8 ± 10	Koester (1988)	[29]
	$12 \pm 1.5 \pm 2$	Schmiedmayer (1991)	[14]
Compton scattering	$1.17^{+0.33}_{-10.7}$	Rose et al (1990)	[23]

References:

[1] V.A. Petrun'kin , Sov. J. Part. Nucl. **12**, 278 (1981) [Fiz. Elem. Chastits At. Yadra, **12**, 692 (1981)]; J.L. Friar, in "*Workshop on Electron-Nucleus Scattering*", A.Fabrocini, S.Fantoni, S.Rosati, and M.Viviani, eds.(World Scientific,Singapore,1989), p.3 ; A.I. L'vov and V.A. Petrun'kin, P.N.Lebedev Physical Institute Moscow, Preprint 258, (1988); A.I. L'vov, P.N.Lebedev Physical Institute Moscow, Preprint 344, (1987).. and references therein.

[2] A. L'vov in: *Baryons'92* and this procedings (1992).

[3] An overview on experiments on the electric polarizability is given in: J.Schmiedmayer, H.Rauch, P.Riehs, I.L.L. Workshop on *Fundamental Physics with slow Neutrons*, Nuc.Inst.Meth. **A284**, 137 (1989).

[4] T.E.O.Ericson, in Interaction Studies in Nuclei, Editors H.Jochim, B.Ziegler, North-Holland, 1975; G.Dattoli, G.Matone, D.Prosperi, Lett.al Nuovo Cimento **19**, 601 (1977).

[5] P.Hecking and G.F.Bertsch, Phys.Lett. **B99**, 237 (1981); H.Krivine, J.Navarro, Phys.Lett. **B171**, 331 (1986); V.Bernard, B.Hiller, W.Weise, Phys.Lett. **B205**, 16 (1988); A.Schäfer, B.Müller, D.Vasak, W.Greiner, Phys.Lett. **B143**, 323 (1984).

[6] R.Weiner, W.Weise, Phys.Lett. **B159**, 85 (1985).

[7] V. Bernard, N. Kaiser, U.-G. Meissner, Phys.Rev.Lett. **67**, 1515 (1991).

[8] N.N.Scoccola and W. Weise, Phys.Lett **B232**, 287 (1989).

[9] H.R.Fiebig, W.Wilcox, R.M.Woloshyn, Nuc.Phys. **B324**, 47 (1989).

[10] Pendlebury J.M., et.al., Phys.Lett. 136B, 237 (1984); see also these proceedings.

[11] Badurek G., Rauch H., Tuppinger D., Phys.Rev A34, 2600 (1986).

[12] Mezei F., Physica 137B, 295 (1986).

[13] Fink H.W., Physica Scripta 38, 260 (1988).

[14] J. Schmiedmayer, P.Riehs, J.Harvey and N.Hill, Phys.Rev.Lett. **66** 1015 (1991).

[15] Alexandrov I.A., Sov.Phys.JETP **6** 228 (1958);

[16] R.M. Thaler, Phys.Rev. **114**, 827 (1959);

[17] G. Breit and M.L. Rustgi, Phys.Rev. **114**, 830 (1959).

[18] H. Leeb, G. Eder, H. Rauch, J. de. Phys **45C**, 47 (1984).

[19] J. Schmiedmayer, Ph.D thesis, Technische Universität Wien (1987).

[20] J.Anandan, PhysLett **A138**, 347 (1989); J. Anandan, *Proc. 3rd Int. Symp. Foundations of Quantum Mechanics, Tokyo, 1989, p98 (1989).*

[21] Horen D.J. et al., Phys.Rev.C 34 429 (1986).

[22] S.F. Mughabghab, M. Divadeenam and N.E. Holden, *Neutron Cross Sections* Vol.1, Part B, Academic Press (1985).

[23] K.W. Rose et al. , Nucl.Phys. **A514**, 621 (1990).

[24] Y.A. Alexandrov,G.S. Samosvat, Z. Sereeter and T.G. Sor, JETP Lett. 4, 134 (1966).

[25] G.V.Anikin and Kotukhov I.I., Sov.J.Nucl.Phys. **14**, 152 (1972)

[26] Y.A.Alexandrov, et al., Yad.Fiz. **44**, 1384 (1986) [Sov.J.Nucl.Phys. **44**, 900 (1986)]

[27] L. Koester, W. Waschkowski and A. Klüver, Physica **B137**, 282 (1986).

[28] J.Schmiedmayer, H.Rauch, P.Riehs, Phys.Rev.Lett **61**, 1065 (1988).

[29] L. Koester, W. Waschkowsky, and J. Meier, Z. Phys. **A 239**, 229 (1988).

[30] An overview of the experimental details is given in: J.Schmiedmayer, M.Pernicka, M.C.Moxon, Nuc.Inst.Meth, **A276**, 250 (1989); J.Schmiedmayer, Kerntechnik, **53**, 218 (1989).

CHIRAL SYMMETRY AND NUCLEON POLARIZABILITIES *

Ulf-G. Meißner|†

Universität Bern
Institut für Theoretische Physik
Sidlerstr. 5
CH-3012 Bern, Switzerland

ABSTRACT

I consider the nucleon polarizabilities in the framework of chiral perturbation theory to one loop order. The chiral expansion of the Compton scattering amplitude in forward direction is worked out. The non-trivial information about the nucleon structure is embodied in the electric ($\bar{\alpha}$) and magnetic ($\bar{\beta}$) polarizabilities of the proton and the neutron. The one-loop calculation sheds light on the two most prominent empirical features that a) the sum $\bar{\alpha}+\bar{\beta}$ is approximatively the same for the proton and the neutron and that b) the proton and the neutron behave essentially as electric dipoles. I also discuss the inclusion of resonances, the calculation within the framework of heavy baryon chiral perturbation theory and the hyperon polarizabilities.

1. INTRODUCTION

With the advent of CW machines, the electromagnetic structure and interactions of hadrons at low energies can be investigated with a superbe accuracy. Such an improvement on the experimental side is an enormously fruitful trigger for improved theoretical investigations. Although hadrons are built from quarks and gluons, at low energy they show a different face. In fact, the spontaneous breakdown of the chiral symmetry of QCD leads to massless pseudoscalar particles, the Goldstone bosons (pions). These govern the dynamics at low energies. The theoretical precision tool to take this into account together with the pertinent Ward-Takahashi identities of QCD is called chiral perturbation theory (CHPT) – a systematic and simultaneous expansion of the QCD Greens functions in external momenta and quark masses. In the following I will discuss the calculation of a presently very much debated photon-nucleon process, the electromagnetic polarizabilities, in the framework of CHPT.

---

* talk presented at the workshop on "Hadron Structure from Photo-Reactions at Intermediate Energies", Brookhaven, May 1992, to be published in the proceedings (eds. A. Nathan and A. Sandorfi).

|† Heisenberg Fellow

2. CHPT WITH BARYONS

At low energies, the QCD Greens functions can be systematically determined. For that, one replaces the fundamental QCD lagrangian $\mathcal{L}_{QCD}$ by an effective lagrangian $\mathcal{L}_{eff}$ expressed in terms of the asymptotically observed nucleon (Ψ) and pion (π) fields.|1,2,3,4 This effective lagrangian is constructed in harmony with the underlying discrete and continuous symmetries of the fundamental theory and it abides to the pertinent Ward-Takahashi identities. Furthermore, the effective theory admits a systematic expansion in external momenta and quark masses. This framework is called chiral perturbation theory (CHPT). In what follows, we will work in the one-loop approximation. The two main reasons to consider loops are unitarity and the possible infrared singular structure of certain Greens functions. In the presence of baryon fields (here, the nucleons), complications arise from the fact that the nucleon mass in the chiral limit is non-vanishing, $\mathring{m} \simeq 800$ MeV.|5 This is in sharp contrast to the meson sector, where the pseudoscalars related to the spontaneous chiral symmetry breaking become massless in the chiral limit of vanishing quark masses. This means that in the baryon sector there is no exact one-to-one mapping of the loop expansion onto the expansion in external momenta and quark masses. Stated differently, there is no strict proof (as can be done in the meson sector) that the leading infrared singularities in the Greens functions are completely given by the one-loop graphs.* Nevertheless, such a behaviour is plausible and no explicit counter example has been worked out so far. A detailed account of the low-energy structure in the baryon sector for the case of πN scattering can be found in Ref.[3]. Many of these problems can be overcome in the extreme non-relativistic limit discussed in section IV.

The effective lagrangian relevant to one-loop order reads (we work in SU(2) and the isospin limit $m_u = m_d = \hat{m}$):

$$\begin{aligned} \mathcal{L}_{eff} &= \mathcal{L}_1 + \mathcal{L}_2 \\ \mathcal{L}_1 &= \mathcal{L}_{\pi N}|(1) + \mathcal{L}_{\pi\pi}|(2) \end{aligned} \tag{2.1}$$

where the superscript (i) denotes terms of order $E|i$ in the low-energy expansion.** In the one-loop approximation, the structure of the effective theory is rather simple:

---

* Here, one-loop graphs means meson loops, *i.e.* closed fermion lines are not considered.

** $E|i$ stands for any term of the type $q|n\hat{m}|(i-n)/2$, with q a generic baryon 3-momentum or a generic meson 4-momentum.

One has to evaluate tree and one-loop diagrams involving the vertices from $\mathcal{L}_1$ and tree graphs involving $\mathcal{L}_2$ vertices. Explicitely, $\mathcal{L}_1$ can be written as:|3,4

$$\begin{aligned}\mathcal{L}_{\pi N}|(1) &= \bar{\Psi}(i\gamma|\mu D_\mu - \mathring{m})\Psi + \frac{\mathring{g}_A}{2}\bar{\Psi}\gamma_\mu\gamma_5 u|\mu\Psi \\ \mathcal{L}_{\pi\pi}|(2) &= \frac{F|2}{4}\,\mathrm{Tr}\,(\nabla_\mu U|\dagger\,\nabla|\mu U + M|2(U + U|\dagger))\end{aligned} \tag{2.2}$$

where U embodies the pion fields

$$\begin{aligned}U &= u|2 = \sigma + i\phi/F, \qquad \sigma|2 + \phi|2/F|2 = 1 \\ \phi &= \begin{pmatrix} \pi|0 & \sqrt{2}\,\pi|+ \\ \sqrt{2}\,\pi|- & -\pi|0 \end{pmatrix}\end{aligned} \tag{2.3}$$

The covariant derivatives $\nabla_\mu U$ and $D_\mu\Psi$ are given by

$$\begin{aligned}\nabla_\mu U &= \partial_\mu U - ieA_\mu[Q, U| \\ D_\mu\Psi &= \partial_\mu\Psi + \Gamma_\mu\Psi \\ \Gamma_\mu &= \frac{1}{2}\{u|\dagger\,(\partial_\mu - ieA_\mu Q)u + u(\partial_\mu - ieA_\mu Q)u|\dagger\}\end{aligned} \tag{2.4}$$

where $Q = \mathrm{diag}(1, 0)$ is the (nucleon) charge matrix. Furthermore,

$$u_\mu = iu|\dagger\,\nabla_\mu U u|\dagger \tag{2.5}$$

and A_μ denotes the photon field (I restrict myself here to those terms which are explicitely needed.). $F, \mathring{g}_A$ and $\mathring{m}$ denote the pion decay constant, the axial vector coupling constant and the nucleon mass in the chiral limit $\hat{m} = 0$, respectively,

$$(F, \mathring{g}_A, \mathring{m}) = (F_\pi, g_A, m)_{\hat{m}=0} \tag{2.6}$$

and $M|2$ stands for the leading term in the expansion of the pion mass squared in the current quark mass

$$M_\pi|2 = M|2\,\{1 + \mathcal{O}(\hat{m})\}\ . \tag{2.7}$$

To leading order, the Goldberger-Treiman relation is exact, $\mathring{g}_{\pi N} = \mathring{g}_A\,\mathring{m}/F$, with $\mathring{g}_{\pi N}$ the pion-nucleon coupling constant in the chiral limit. It is instructive to expand $\mathcal{L}_1$ in powers of the pion and the photon fields. One finds

$$\begin{aligned}\mathcal{L}|(1)_{\pi N} =& \bar{\Psi}\{i\partial\!\!\!/ - \mathring{m} + \frac{e}{2}(1 + \tau_3)A\!\!\!/ + \frac{i}{8F|2}[\phi, \partial\!\!\!/\phi] \\ &- \frac{\mathring{g}_A}{2F}\partial\!\!\!/\phi\,\gamma_5 + \frac{i\,e\,\mathring{g}_A}{4F}[\tau_3, \phi]\,A\!\!\!/\,\gamma_5\}\Psi + \ldots\end{aligned} \tag{2.8}$$

which embodies the conventional pseudovector pion-nucleon coupling as well as the celebrated $NN\gamma\pi$ and $NN\pi\pi$ contact terms (Kroll-Ruderman and Weinberg terms).

At next-to-leading order in CHPT, one has two kinds of contributions. First, there are the pion loop graphs with all vertices from $\mathcal{L}_1$. These account for unitarity corrections as well as vertex and mass renormalization and secondly, there are polynomial counter terms up to and including order $\mathcal{O}(q|3)$. In the meson sector, the two lowest order constants F and M are not changed by the loops, which is different for the baryon sector – the values of $\mathring{m}$ and $\mathring{g}_A$ are in fact influenced by one-loop contributions. Therefore one has to add appropriate counter terms in $\mathcal{L}_2$. The full expression for $\mathcal{L}_2$ reads:

$$\mathcal{L}_2 = \Delta\mathcal{L}_{\pi N}|(0) + \Delta\mathcal{L}_{\pi N}|(1) + \mathcal{L}_{\pi N}|(2) + \mathcal{L}_{\pi N}|(3) + \mathcal{L}_{\pi\pi}|(4) \tag{2.9}$$

Here, $\Delta\mathcal{L}|(0,1)_{\pi N}$ are the terms necessary for the renormalization of the nucleon mass and the axial vector coupling constant in the chiral limit. I do not give the explicit form of the polynomial terms $\mathcal{L}|(2,3)_{\pi N}$ and $\mathcal{L}|(4)_{\pi\pi}$. A complete list of these terms can be found in Ref.[4].

3. ELECTROMAGNETIC POLARIZABILITIES

The electric charge radii of the neutron and the proton as well as their magnetic moments are known to a high accuracy. Low–energy Compton scattering reveals further important information about the internal structure of the nucleon, parametrized by the so–called electric and magnetic polarizabilities. These are the first non–trivial structure constants in two–photon observables. Let us place a neutron/proton into an external electric (magnetic) field $\vec{E}$ ($\vec{B}$). The particle will acquire an induced electric (magnetic) dipole moment,

$$\vec{d}_E = \alpha\vec{E} \;\; ; \;\; \vec{d}_M = \beta\vec{B} \tag{3.1}$$

The electric (α) and magnetic (β) polarizabilities therefore characterize the ease with which a dipole moment can be induced in a composite system. This information is as fundamental as the one related to the one–photon processes (charge radii, magnetic moments).

Before discussing the CHPT calculation of the polarizabilities, let me give a brief overview about the experimental situation:

- The sum of the electric and the magnetic polarizabilities of the proton and the neutron can be determined rather precisely by use of a forward dispersion relation sum rule,

$$\bar{\alpha}+\bar{\beta}=\frac{1}{2\pi|2}\int_{E_{\gamma,\mathrm{thr}}}|\infty d\omega\frac{\sigma_\gamma(\omega)}{\omega|2} \tag{3.2}$$

with $\sigma_\gamma(\omega)$ the total photoabsorption cross section of the proton or neutron, and $\omega = E_\gamma$ the photon energy in the lab frame. The threshold value $E_{\gamma,\mathrm{thr}}$ is given in (3.1). The most commonly quoted values are $\bar{\alpha}_p+\bar{\beta}_p = (14.3\pm0.3)\cdot10|{-4}\,\mathrm{fm}|3$ and $\bar{\alpha}_n+\bar{\beta}_n = (15.8\pm0.5)\cdot10|{-4}\,\mathrm{fm}|3$.

- The separation into the individual contributions ($\bar{\alpha}_{p,n}$, $\bar{\beta}_{p,n}$) is afflicted with much larger uncertainties. However, there exists clear evidence that the proton and the neutron behave as electric dipoles, $\bar{\alpha}_{p,n} >> \bar{\beta}_{p,n}$. Typical values quoted in the literature span the ranges $\alpha_n \approx \bar{\alpha}_p \approx 8\ldots12\cdot10|{-4}\,\mathrm{fm}|3$ and $\bar{\beta}_n \approx \bar{\beta}_p \approx -1\ldots4\cdot10|{-4}\,\mathrm{fm}|3$. There is also some evidence that the intrinsic electric polarizability is larger for the neutron than for the proton.*

To perform a systematic one–loop calculation, we need an operational definition of the polarizabilities. Consider the low–energy expansion of the spin–independent Compton scattering amplitude. In the rest frame it takes the form

$$T(\gamma N\to\gamma N)=T_0+\bar{\alpha}\,\omega'\omega\,\vec{\epsilon}\,'\cdot\vec{\epsilon}+\bar{\beta}\,(\vec{\epsilon}\,'\times\vec{k}\,')\cdot(\vec{\epsilon}\times\vec{k})+\mathcal{O}(\omega|4) \tag{3.3}$$

with $(\omega,\vec{k},\vec{\epsilon})$ and $(\omega',\vec{k}',\vec{\epsilon}')$ the frequencies, momenta and polarization vectors of the incoming and outgoing photon, respectively. The constant term T_0 is nothing but the Thomsom scattering amplitude which carries only information about the charge and mass of the particle the photon scatters off. The internal structure is, therefore, embodied in the two structure constants $\bar{\alpha}$ and $\bar{\beta}$ which parametrize the corrections to T_0 at order $\omega|2$. In quantum field theory, the calculation of these structure constants (the polarizabilities) proceeds as follows. Obviously, we need the Fourier transformed matrix–element of two electromagnetic currents in a nucleon state,

$$T_{\mu\nu}(p,k)=\int d|4x\,e|ik\cdot x<N(p)T\,J|em_\mu(x)J|em_\nu(0)N(p)> \tag{3.4}$$

---

* The bar on α and β refers to the fact that we are dealing with the so-called Compton polarizabilities. In what follows, I will only consider these. They differ from the static polarizabilities (3.1) by recoil effects and alike. In the literature, one can find a variety of prescriptions how to relate these two definitions (mostly in terms of non-relativistic physics). Although it would be worthwhile to clarify this connection in more detail, lack of space forbids to do so.

with p and k the nucleon and photon four–momentum, respectively. From this, we can form the spin–averaged Compton tensor in forward direction,|6, 7

$$\theta_{\mu\nu} = \frac{1}{4}\,\mathrm{Tr}\,\{(\not{p} + m)\; T_{\mu\nu}(p,k)\} = e|2\,\{g_{\mu\nu}\,A(s) + k_\mu k_\nu\,B(s) + (p_\mu k_\nu + p_\nu k_\mu)\,C(s) + p_\mu p_\nu\,D(s)\} \tag{3.5}$$

with $e|2/4\pi = 1/137$ the fine structure constant. The kinematics is rather simple here. The Mandelstam variables are $s = (p+k)|2,\ t = 0$ and $u = (p-k)|2 = 2m|2 - s$ (in forward direction,

Chiral model predictions for electromagnetic polarizabilities of the nucleon: A "Consumer Report" †

Wojciech Broniowski *

Department of Physics and Astronomy, University of Maryland, College Park, Maryland 20742-4111

This contribution has two parts:

1) We critically discuss predictions for the electromagnetic polarizabilities of the nucleon obtained in two different approaches: a) hedgehog models (HM), such as Skyrmions, chiral quark models, hybrid bags, NJL *etc.*, and b) chiral perturbation theory (χPT).

2) We show new results[1] obtained in HM: N_c-counting of polarizabilities, splitting of the neutron and proton polarizabilities (we argue that $\alpha_n > \alpha_p$ in models with pionic clouds), relevance of dispersive terms in the magnetic polarizability β, important role of the Δ resonance in pionic loops, and the effects of non-minimal substitution terms in the effective lagrangian.

The basic claims in the literature are that HM naturally predict the smallness of β by providing a cancellation mechanism between the pionic sea-gull term and the paramagnetic $N-\Delta$ term[2]. It is also claimed that χPT (at the one-loop level) leads to beautiful agreement with the data[3]. We show, that these statements are inconsistent with the basic organizational principles behind the two approaches. HM and χPT are based on two different limits of QCD: the large-N_c limit, and the chiral ($m_\pi \to 0$) limit. Rigorously, little is known about the formal properties of these expansions (Are they convergent? If yes, what is the region of convergence? *etc.*). A physisist's approach is to calculate the leading term and, if possible (usually not!), the next term in the expansion. The next term should be smaller than the leading term, and the leading term should roughly reproduce the data for the approach to be viable. With these principles, we show that the claims of Refs. [2,3] do not hold, since either the N_c-counting rules, or the chiral counting rules are violated to obtain the agreement with experiment. In other words, chiral models have problems in describing the polarizabilities.

We study the role of the Δ in pionic loops in the two approaches. HM overestimate these contributions since they ignore the $N-\Delta$ mass splitting, while χPT drops them altogether (at the leading chiral singularity level). We propose how to estimate these effects for the physical value of the $N-\Delta$ mass splitting, using a framework of a modified chiral expansion. It is found that the Δ contribution to pionic loops in this scheme is as large as the nucleon contribution! In this context we also show an interesting connection between HM and χPT predictions for various physical observables.

† Research done with T. D. Cohen

* On leave of absence from Institute of Nuclear Physics, 31-342 Cracow, POLAND.

[1] W. Broniowski, M. K. Banerjee, and T. D. Cohen, DOE/ER/40322-144, U. of MD PP # 92-130, 1991, to appear in *Phys. Lett.* **B**; W. Broniowski and T. D. Cohen, DOE/ER/40322-155, U. of MD PP # 92-193, 1992; T. D. Cohen and W. Broniowski, DOE/ER/40322-154, U. of MD PP # 92-191, 1992.

[2] E. M. Nyman,Phys. Lett. **142B**, 388 (1984); M. Chemtob, Nucl. Phys. **A473**, 613 (1987); N. N. Scoccola and W. Weise, Nucl. Phys. **A517**, 495 (1990).

[3] V. Bernard, N. Kaiser and U.-G. Meissner, Phys. Rev. Lett. **67** (1991) 1515.

The Polarizabilities of Bound Nucleons

D. P. Wells
Nuclear Physics Laboratory and Department of Physics. GL-10
University of Washington, Seattle, WA 98195

Abstract

Photon scattering cross sections of ^{4}He, ^{12}C, ^{16}O and ^{208}Pb at energies between the giant resonances and pion photo-production threshold have been measured at Mainz, Illinois and Lund and have been interpreted in terms of bound-nucleon polarizabilities. Those results that are published all find the polarizibilities of bound nucleons to be essentially the same as free nucleons. However, we find that the extraction of these polarizabilities depends critically on the reliability of total photoabsorption data. Thus the significant discrepancies between photon scattering data and photoabsorption data imply large uncertainties in the polarizibilities of bound nucleons.

Introduction

The electromagnetic polarizabilities of nucleons measure the proportionality between an applied static electric (magnetic) field and the induced electric (magnetic) dipole moment. They are the fundamental second-order electromagnetic structure constants comparable to the first-order structure constants of the charge and magnetic moment of the nucleon. Nevertheless, while the charge and magnetic moment are known to at least eight significant figures, the polarizabilities of free nucleons are known to only approximately 10% [5, 6, 7]. The investigation of nucleon polarizabilities has attracted considerable theoretical and experimental interest due to their fundamental importance in understanding the internal structure of nucleons, and more specifically, as a test of quark models of the nucleon. For nucleons bound in a nucleus, the question arises as to whether binding-effects can significantly alter the internal structure of nucleons. For example, the electric polarizibility of a system is proportional to its size, and hence if bound nucleons are "swollen" the electric polarizibility of a bound nucleon should be larger than a free nucleon.

The polarizability of the proton has been measured using nuclear Compton scattering at energies below pion-production threshold. Similarly, it is expected[8, 9] that the polarizability of bound nucleons can be measured using Compton scattering at energies intermediate between nuclear giant resonances and nucleon resonances. At these energies the coherent scattering from individual nucleons significantly contributes to the total scattering amplitude. In particular, it has been shown that the polarizabilities of bound nucleons have a large effect on the nuclear Compton scattering amplitude [8, 3, 4, 2].

Experimental work on this question has been done on ^{208}Pb [1] and ^{12}C [3] at Mainz, ^{4}He [2] at Illinois, and ^{12}C and ^{16}O[4] at Lund. The results from Mainz and Lund find that the polarizability of bound nucleons differs very little, if at all, from the free nucleon value. In contrast, the Illinois results imply that while the bound electric polarizability

is consistent with the free value, the magnetic polarizability is substantially larger than for the free nucleon. The latter result is surprising and raises the question as to whether the polarizability of bound nucleons has a large A-dependence or whether there is some significant error in the Illinois experiment or its interpretation.

In order to answer these questions it is useful to study existing data on ^{12}C, which has received more relevant experimental attention than any other nucleus. In particular the total photoabsorption of ^{12}C has been measured from 10 to 140 MeV [15], and Compton scattering on ^{12}C has been measured at many labs[11, 10, 3, 4] covering 20 to 140 MeV and many angles. We argue that the significant discrepancies between photon scattering cross sections and photoabsorption cross sections introduce large uncertainties into the analysis of the scattering data, and hence the polarizability of a bound nucleon is largely an open question.

Formalism

The formalism for the interpretation of photon scattering has been described many times [13, 10, 12, 9] and will only be briefly summarized here. The photon scattering cross section is the square of a scattering amplitude:

$$d\sigma/d\Omega(E,\theta) \;=\; \mid R(E,\theta) \mid^2 . \tag{1}$$

Unitarity relates the imaginary part of the forward scattering amplitude to the total photoabsorption σ_γ

$$Im[R(E,\theta=0)] \;=\; \frac{E}{4\pi\hbar c}\sigma_\gamma. \tag{2}$$

Causality relates the real part of the forward scattering amplitude to the imaginary part, and hence the total photoabsorption, through a dispersion relation

$$Re[R(E,\theta=0)] \;=\; \frac{E^2}{2\pi^2\hbar c}\int_0^\infty \frac{\sigma_\gamma(E')dE'}{(E'^2-E^2)} + D. \tag{3}$$

where D is the classical Thomson amplitude. It is typically assumed that these relations hold for each multipole. The scattering amplitude for angles larger than zero is found by summing the contributions from each multipole, each of which has its own angular distribution.

At energies intermediate between nuclear giant resonances and nucleon resonances the scattering amplitude has significant contributions from both *nuclear* excitations and *nucleon* excitations. At these energies ($\approx$ 100 MeV), which are small compared to excitation energies of the nucleon ($\approx$ 300-1000 MeV), the principle contributions to the scattering amplitude from nucleon degrees of freedom comes from their electromagnetic polarizabilities. Drechsel and Russo [8] were the first to show how one could extract these polarizabilities. Essentially, one only includes photoabsorption due to nuclear excitations, which is the total photoabsorption up to pion photoproduction threshold, in eq.3. The remaining part of the dispersion integral, due to nucleon degrees of freedom, is phenomenologically added to D to form an effective Thomson amplitude $\bar{D}$. To

lowest order, the correction to the Thomson amplitude due nucleon polarizabilities is proportional to

$$A(\bar{\alpha}g_{E1} + \bar{\beta}g_{M1})E_\gamma^2 F(q) \tag{4}$$

where A is the number of nucleons in the nucleus, $F(q)$ is the charge form factor as measured in electron scattering and the g's are angular distribution functions. Thus the effect on scattering due to these polarizabilities increases quadratically with photon energy. In addition, it is useful to note that forward scattering is primarily sensitive to the sum $\bar{\alpha}+\bar{\beta}$, while back-angle scattering is primarily sensitive to the difference $\bar{\alpha}-\bar{\beta}$.

Experimental Summary

Photon scattering cross sections for a number of nuclei have been measured with both tagged and untagged photons. The advantage of tagged photons is excellent control of systematic errors. This is primarily achieved by measuring the photon flux with the same detector that is used to measure scattered photons; thus largely eliminating the detector efficiency from the determination of cross sections. The other major advantage is the monochromaticity of the photon beam, resulting in a elastic scattering yield easily resolved from inelastic backgrounds. The major disadvantage is statistics, which is the primary strength of bremsstrahlung scattering experiments. Both techniques have been used in photon scattering studies to probe the polarizabilities of bound nucleons. In addition, one typically uses total photoabsorption data, if it exists, to constrain the nuclear photoabsorption.

The first published results on the polarizabilities of bound nucleons came from Mainz[1], where the nucleus studied was ^{208}Pb. They measured elastic photon scattering cross sections with both tagged and untagged photons at several angles and energies from 10 to 100 MeV. They found $\bar{\alpha}+\bar{\beta} = 16.9\pm1.0\cdot10^{-4}fm^3$. However, the extraction of $\bar{\alpha}-\bar{\beta}$ was limited by the large effects of nuclear form factors in the angular distribution.

More recently the same group published results from scattering experiments on ^{12}C, where again they used both bremsstrahlung and tagged photon scattering techniques [3]. They measured cross sections at several angles and energies from 15 to 140 MeV. They found $\bar{\alpha}+\bar{\beta} = 11.9 \pm 0.7 \cdot 10^{-4}fm^3$. Curiously, though they measured cross sections at several angles and nuclear form factors only play a modest role in the angular distribution for a nucleus as light as ^{12}C, they did not report a value for the difference $\bar{\alpha}-\bar{\beta}$.

Most recently, Ludwig et al. [4] have measured photon scattering cross sections at energies of 61 and 77 MeV and an angle of 90 degrees, which is sensitive to $\bar{\alpha}$ only, on ^{12}C and ^{16}O using the photon tagging facility at Lund. They used the constraint $\bar{\alpha}+\bar{\beta} = 14\cdot10^{-4}fm^3$ from total photoabsorption studies above pion threshold [16] to extract $\bar{\alpha} = 11.5 \pm 0.8 \pm 2.1 \cdot 10^{-4}fm^3$ and $\bar{\beta} = 2.5 \mp 0.8 \mp 2.1 \cdot 10^{-4}fm^3$. They have also measured angular distributions, but these have not yet been published.

A consistent picture emerges from these experiments, namely that the polarizabilities of bound nucleons differ very little, if at all, from the polarizabilities of a free nucleon.

There are also unpublished scattering data on ^{4}He from Illinois [2]. They measured scattering cross sections from 23 to 73 MeV and angles of 45 and 135 degrees. They found $\bar{\alpha} = 16.4 \pm 6.6 \pm 1.0 \cdot 10^{-4}fm^3$ and $\bar{\beta} = 10.0 \pm 1.3 \pm 1.0 \cdot 10^{-4}fm^3$. Thus, while

the extracted electric polarizability was consistent with the free value. the magnetic polarizability was dramatically different. This raises the question as to whether this experiment has some significant error, or whether there is a strong A-dependence to the polarizabilities of bound nucleons?

To answer these questions it is useful to examine the differences between ^{4}He and the other published cases. First, ^{4}He is the smallest nucleus, which means that nuclear form factors play less of a role in the analysis of these data than any other nucleus. However, even in the case of ^{12}C and ^{16}O, uncertainties due to form factors are sufficiently small to rule out this as a problem. Second, and significantly, unlike the other nuclei studied, there is no data for the total photoabsorption of ^{4}He. Thus, in the case of ^{4}He, the scattering data has both to constrain the nuclear photoabsorption and $\bar{\alpha}$ and $\bar{\beta}$; whereas in the other cases one can constrain the nuclear photoabsorption with photoabsorption data. This apparently strong sensitivity of extracted polarizabilities to nuclear photoabsorption suggests one should examine, where possible, how consistent scattering and absorption data are.

A Test Case: ^{12}C

It is useful to consider ^{12}C as a test case for the following reasons: the scattering data on ^{12}C are more complete in terms of coverage of angles and energy than any other nucleus, the total photoabsorption has been measured over the relevant energy range, and it is a sufficiently light nucleus such that nuclear form factors only play a small role. In what follows, we consider only the *tagged* photon scattering data because, as we will see, absolute normalization is critical to accurately extract the polarizabilities of bound nucleons.

The existing scattering data comes from many labs: NBS, Illinois, Mainz, and most recently Lund. In analyzing these data one can take several approaches. One can analyse the scattering data, with the absorption constrained by the measured absorption in which case (essentially) the only free parameters are the nucleon polarizabilities. One can alternatively allow the scattering data to constrain both the nuclear absorption and the nucleon polarizabilities, and ignore the measured absorption; or one can give equal weight to the scattering and absorption data and use them both to constrain the nuclear absorption, while using the scattering data to constrain the nucleon polarizabilities. We have tried all of these approaches.

In the first approach, we have fit the measured photoabsorption of ^{12}C [15] with a multi-lorentzian fit. Then, the scattering data of NBS, Illinois, Mainz and Lund are combined and used to constrain $\bar{\alpha}$ and $\bar{\beta}$. We find $\bar{\alpha} = 15 \pm 1$ and $\bar{\beta} = 13 \pm 1$. While $\bar{\alpha}$ is roughly consistent with the free value, $\bar{\beta}$ is radically different. We then simultaneously fit the nuclear photoabsorption to the scattering and absorption data and used the scattering data to constrain $\bar{\alpha}$ and $\bar{\beta}$. We find $\bar{\alpha} = 10 \pm 1$ and $\bar{\beta} = 8 \pm 1$. Finally, we ignored the measured photoabsorption and used only the scattering data to constrain both the nuclear photoabsorption and the nucleon polarizabilities. We find $\bar{\alpha} = 1 \pm 1$ and $\bar{\beta} = 8 \pm 1$. These results are summarized in table 1, along the integrated nuclear photoabsorption up to 140 MeV in units of TRK sum rules and the reduced χ^2 of the fits.

The extreme sensitivity of these results to assumptions about the nuclear photoabsorption is astonishing. In all cases the fitted photoabsorption is reasonably consistent with the known systematics of nuclear photoabsorption, both in terms of energy dependence and sum rules. In particular, at 100 MeV the difference between the absorption fitted to scattering data and the absorption fitted to absorption data is only 20%. Figure 1 shows the measured photoabsorption of Ahrens *et al.* [15], along with the multilorentzian fit to that data (solid curve), and the absorption found by fitting the scattering data only (dashes). The most prominent discrepancy is in the region $30 < E_\gamma < 45$MeV. This discrepancy between scattering data and absorption data was first noted by Wright *et al.* [10], and has large consequences on the scattering (see fig. 2). It is important to note that in this energy region the effects of nucleon polarizabilities and nuclear form factors are very small, and thus this discrepancy represents a fundamental disagreement between the scattering and absorption data. Above this energy region the effects of form factors and polarizabilities grow in importance, and hence one cannot unambiguously conclude that a fundamental disagreement exists between scattering and absorption. These differences at higher energies are shown in figs. 1 and 2.

Conclusions

Photon scattering has been shown to be sensitive to internal structure properties of the nucleon, specifically the electric and magnetic polarizabilities of the nucleon. However, at present the quantitive interpretation of such data in terms of nucleon polarizabilities is largely phenomenological. New theoretical efforts to produce a model-independent formalism for the interpretation of photon scattering data at energies intermediate between nuclear giant resonances and nucleon resonances are badly needed. Nevertheless, the existing phenomenological formalism is sufficient to show that the existing photon scattering data is insufficient, by itself, to constrain both nuclear absorption and nucleon polarizabilities.

Moreover, in the case of ^{12}C, which is the most carefully examined nucleus to date, it can be said that the scattering and absorption data are not consistent with each other. This inconsistency is sufficiently large to make extraction of bound nucleon polarizabilities impossible. Moreover, we conclude that it is essential to have high accuracy photoabsorption data available in order use scattering data to constrain bound nucleon polarizabilities. We suggest that future and ongoing work at Lund and Saskatoon in this field must include measurements of the total nuclear photoabsorption with an emphasis on the absolute normalization. Thus, we argue that new experimental efforts are needed in order to resolve these differences before one can confidently extract bound nucleon polarizabilities.

Acknowledgements

I would like to thank our colleague Prof. M. Schumacher for useful correspondence and for supplying us with the scattering cross sections from Mainz and Lund and Prof. A. M. Nathan for many fruitful discussions on this topic. I also would like to thank the

organizers of this conference, Dr. A. Sandorfi and Prof A. M. Nathan for inviting me to speak at this conference.

References

[1] K. P. Schelhaas, J. M. Henneberg, M. Sanzone-Arenhovel, N. Wieloch-Laufenberg, U. Zurmuhl, B. Ziegler, M. Schumacher and F. Wolf, Nucl. Phys. **A489**, 189 (1988).

[2] D. P. Wells, Ph.D. thesis, University of Illinois, 1990 (unpublished).

[3] K. P. Schelhaas, J. M. Henneberg, N. Weiloch-Laufenberg, U. Zurmuhl, B. Ziegler, M. Schumacher, and F. Wolf, Nucl. Phys. **A506**, 307 (1990).

[4] M. Ludwig, B. E. Anderson, A. Baumann, K. I. Blomqvist, K. Fuhrberg, E. Hayward, G. Muller, D. Nilsson, A. Sandell, B. Schroder, and M. Schumacher, Phys. Lett. B **274**, 275 (1992).

[5] F. J. Federspiel *et al.*, Phys. Rev. Lett. **67**, 1511 (1991).

[6] J. Schmeidmayer *et al.*, Phys. Rev. Lett. **66**, 1015 (1991).

[7] A. Zieger *et al.*, Phys. Lett. B **278**, 34 (1992).

[8] D. Drechsel and A. Russo, Phys. Lett. B **137**, 294 (1984).

[9] M. Schumacher, P. Rullhusen, and A. Baumann, Nuovo Cimento **100A**, 339 (1988).

[10] D. H. Wright, P. T. Debevec, L. J. Morford, and A. M. Nathan, Phys. Rev. C **32** 1174 (1985).

[11] W. R. Dodge, E. Hayward, R. G. Leicht, M. McCord, and R. Starr, Phys. Rev. C **28**, 8 (1983).

[12] B. Ziegler, *New Vistas in Electro-Nuclear Physics*, eds. E. L. Tomusiak, H. S. Caplan, and E. T. Dressler, pp. 293-329, (Plenum Press,New York, 1986).

[13] J. J. Sakurai, *Advanced Quantum Mechanics*, Chap. 2 (1984).

[14] Y. M. Arkatov, P. I. Vatset, V. I. Voloshchuk, V. A. Zolenko, I. M. Prokhorets and V. I. Chmil, Sov. J. Nucl. Phys. **19**, 598 (1980).

[15] J. Ahrens *et al.*, Nucl. Phys. **A251**, 479 (1975).

[16] J. Ahrens, Nucl. Phys. **A446**, 229c (1985).

Table 1: Results for bound nucleon polarizabilities with various constraints on the nuclear photoabsorption.

Technique Used	$\bar{\alpha}$ $(10^{-4} fm^3)$	$\bar{\beta}$ $(10^{-4} fm^3)$	Σ_{140} (MeV- mb)	χ^2_τ
Scattering data only used to constrain σ_{abs}, $\bar{\alpha}$, $\bar{\beta}$	1 ± 1	8 ± 1	1.5	1.4
σ_{abs}, $\bar{\alpha}$, $\bar{\beta}$ are fit to both scattering and absorption data	10 ± 1	8 ± 1	1.8	2.5
σ_{abs} constrained by absorption data $\bar{\alpha}$, $\bar{\beta}$ constrained by scattering data	15 ± 1	13 ± 1	1.7	7.5

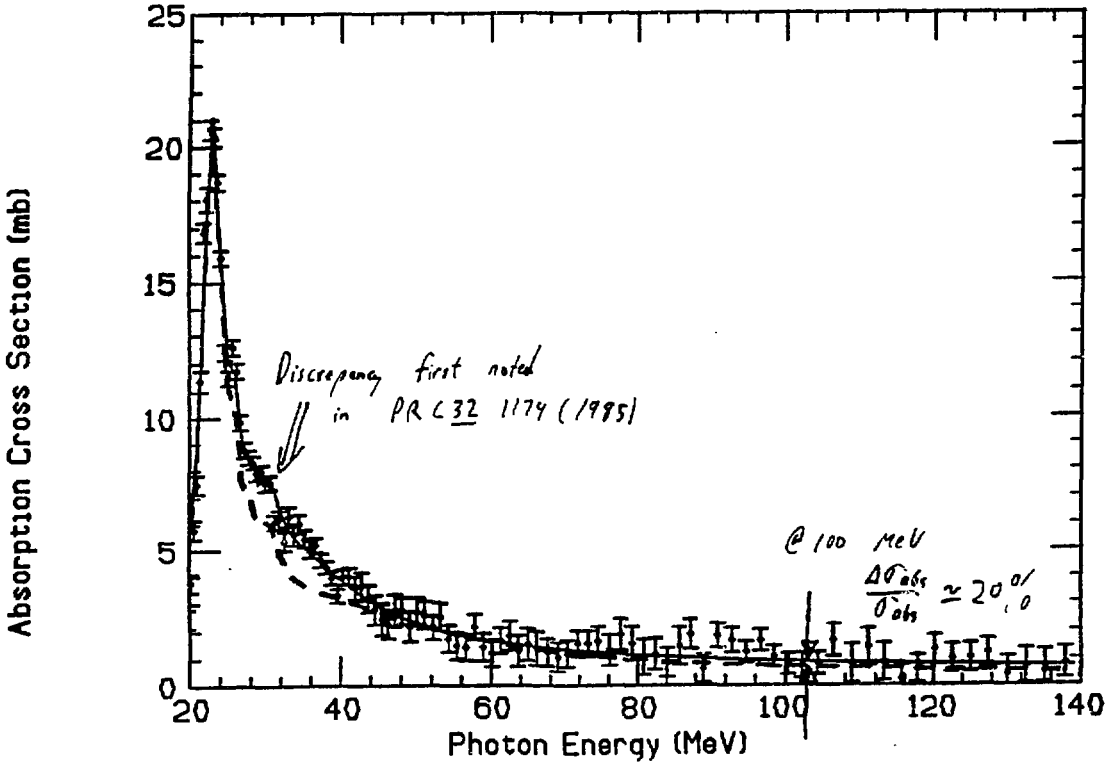

Figure 1: The measured total photoabsorption of ^{12}C, along with a multi-lorentzian fit to this data (solid line), and the photoabsorption inferred by considering only the scattering data (dashed line).

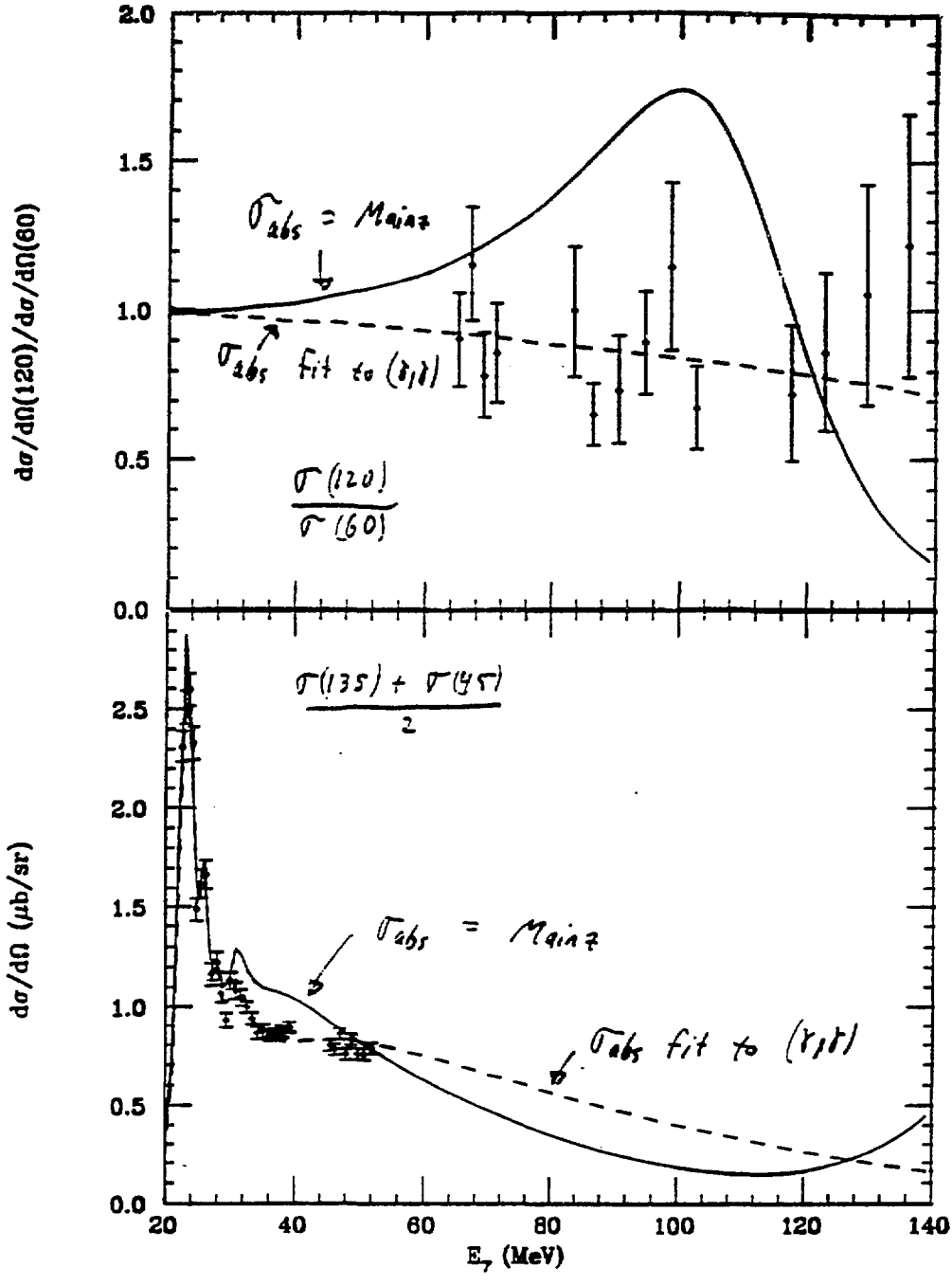

Figure 2: (a)(upper) The ratio of backward (120 degrees) to forward (60 degrees) scattering cross sections (from Mainz data). The dashed curve is a fit to the scattering data only, while the solid curve is a fit with σ_{abs} constrained by the measured absorption. (b) The mean of 135 and 45 degree cross sections (from Illinois) showing the large discrepancy for $30 < E_\gamma < 45$ MeV.

Nucleon Polarizability in Free Space and in Nuclear Matter

G. G. Bunatian
Joint Institute for Nuclear Research, Dubna, Russia.

In the framework of the cloudy bag model, CBM [1], we calculate the nucleon electric dipole moment $d=\langle\hat{d}\rangle=\alpha E$ induced by external static electric field **E**, and then get the electric polarizability α-the response on the field. When the field is turned on, the total CBM lagrangian L includes the quarks L and pions L interactions with the electric field. In the lowest (second) order in the quark-pion interaction L, the quantity α is represented by the diagrams

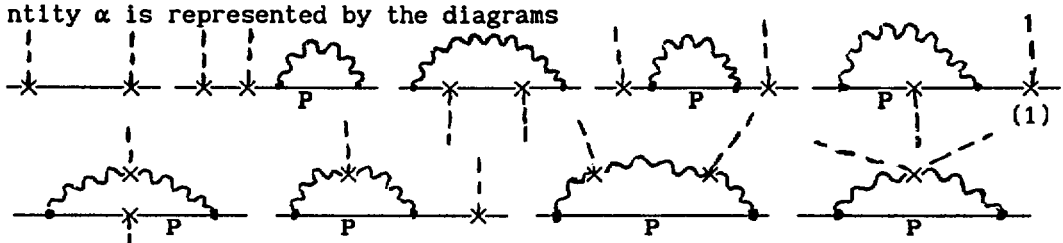

Here the solid lines stand for propagators G_B of the various baryons both in ground and in exited states, the wavy lines correspond to pion propagators D and the crosses with dashed line denote the interaction of the electric dipole field with quarks and pions. Our calculations give for the free nucleon polarizability value $\alpha=0.87\ 10^{-3}\text{fm}^3$ (the value of nucleon size being R=0.9fm) which is in good enough agreement with experimental data. The main share of the α value, ≈90% its magnitude, is contributed by the last diagram which itself is arisen as the reduction of the last bat one.

The nucleon polarizability in the nuclear medium differs from one in free space because of two main reasons. First, a nucleon in processes (1) may not arrive at the intermediate states with momentum P less than the Fermi momentum P_F. As a result, if the nuclear medium influenced on nucleon via Pauli principal only, the α value should be bring down to magnitude $\tilde{\alpha}= 0.35\ 10^{-3}\ \text{fm}^3$. On the other hand, the pion propagator D and interaction $L_{\pi N}$ change in medium because of the pion modification which is accounted for by availability of the pion polarization operator $\Pi(\rho)$ in the CBM pion lagrangian L_π [2]. According to the previous investigations, the influence of the medium leads to pion mode softening which causes the significant increase of the contributions of the diagrams, involving D [2], especially of the most important last one in (1), to quantity $\tilde{\alpha}$. Eventually, when both Pauli-blocking and pion mode softening are taken into account, the nucleon polarizability reduces in medium to value $\tilde{\alpha}=(1.5\text{-}2.8)10^{-3}\ \text{fm}^3$, which is appreciably greater then the α value of a free nucleon. The experimental data [3] allow to infer that α value in medium is at any rate greater then in free space, $\tilde{\alpha}_{exp}=(1.4\text{-}2.5)10^{-3}\text{fm}^3$ As we have seen, when the pion mode softening had not been taken into account, the $\tilde{\alpha}$ value would have become very small. So we have got unambiguous evidence of the considerable pion mode modification in nuclear matter as compare to free space.

References

1. A.V. Thomas, Adv. Nucl. Phys. **13** (1984) 1
2. G.G. Bunatian, Sov. J. Nucl. Phys. **49** (1989) 664; **49** (1989) 847; **43** (1986) 188; **51** (1990) 790. Nucl. Phys. **A509** (1990) 736
3. E. Hayward, Phys. Rev. **C40** (1989) 467. M. Ericson and M. Rosa-Clot, Z. Phys. **A324** (1986) 373. Baumann et al., Phys Rev. **C38** (1988) 1940

MECHANISMS OF PHOTON SCATTERING ON NUCLEONS AT INTERMEDIATE ENERGIES

A.I. L'vov
P.N. Lebedev Physical Institute, Leninsky Prospect 53
Moscow 117924, Russia

1. What can we study in photon scattering?

The principal question for studies of photon scattering by nucleons and nuclei is the following: Can photon scattering say somewhat new about structure of these objects in comparison with photo- and electroproduction investigations? There is a general reason to believe that it is indeed the case. The Hamiltonian of electromagnetic interaction,

$$H_{e.m.} = j_\mu A_\mu - \tfrac{1}{2} S_{\mu\nu} A_\mu A_\nu + \dots \,, \tag{1}$$

has, in general, a piece quadratic in the electromagnetic field (the so-called two-photon seagull [1]) which is seen only in two-photon processes, such as Compton scattering. Although longitudinal part of this seagull is constrained by the gauge invariance,

$$\frac{\partial}{\partial x_\mu}\Big[i\,\mathrm{T}(j_\mu(x) j_\nu(y)) + S_{\mu\nu}(x,y)\Big] \equiv i\,[j_0(x), j_\nu(y)]\,\delta(x_0 - y_0) + \frac{\partial}{\partial x_\mu} S_{\mu\nu}(x,y) = 0\,, \tag{2}$$

its transverse part is decoupled from the e.m. current and cannot be found in photoabsorption processes.

The seagull $S_{\mu\nu}$ depends on explicit degrees of freedom included into the Hamiltonian. E.g. non-relativistic Schrödinger equation has an effective seagull due to the kinetic energy $(\vec{p} - e\vec{A})^2/2M$. Its parent relativistic Dirac equation has no seagull at all but has the same low-energy consequences due to additional degrees of freedom (antiparticles). In low-energy nuclear physics, with explicit mesonic degrees of freedom disregarded, some effective seagull appear which replace effects of meson exchanges [2] and meson clouds (i.e. internal polarizability of the nucleons) [3-4]. By explicit including the mesons into the Hamiltonian we can remove part of the seagulls. Then the rest of them will be a signal for degrees of freedom invisible in photoabsorption at energies of the considered scale. Some seagulls are related with t-channel exchanges in Compton scattering. The π^0-exchange is seen in γp-scattering but has no counterpart in photoproduction off the proton.

Thus, a complementary study of one- and two-photon reactions provides a way to look in a region of higher energies where direct studies via photoproduction processes may be hard.

The photon scattering amplitude contains a standard dispersion piece and its cross partner, the seagull being producing a term surviving at high energies and seen as a subtraction function in dispersion relations:

$$T_{\mu\nu} = \sum_n \frac{\langle f|j_\mu|n\rangle\langle n|j_\nu|i\rangle}{E_n - E_i - \omega} + \text{cross-term} + \langle f|S_{\mu\nu}|i\rangle\,. \tag{3}$$

Generally, the sum over n in (3) has additional substructure due to possibility to produce particles from vacuum, so that the intermediate state $|n\rangle$ can include initial or final nucleon $|i\rangle$ or $|f\rangle$ (or both) together with other particles. Four contributions shown in Fig. 1 have energy denominators with different energy behavior. As a consequence, the contribution of vector

states in Fig. 1 dominates at high energies, thus supporting the model of vector meson dominance. At low ω the contribution of nucleon excitations is the most important one; the other pieces are then smaller relativistic corrections which, however, are important for understanding the nature of the correction $\Delta\alpha$ to the nucleon electric polarizability $\bar{\alpha}$.

Apart from studying the seagulls, photon scattering experiments can be aimed also onto investigation of photoabsorption, as it is done in photonuclear physics where photon scattering is widely used to study giant resonances [5-7]. Both these aims are supported by dispersion approach which is a very convenient equivalence of the formula (3).

2. Dispersion look at γN-scattering

Dispersion approach is based on the analyticity of the photon scattering amplitudes and represents the amplitudes in terms of their imaginary parts which are principally known from photoabsorption.

In the simplest case of spin-0 target there are two independent Compton amplitudes: photon-helicity-flip one and helicity-non-flip one. Technically it is more convenient to work with so-called invariant amplitudes, A_1 and A_2, free from trivial angular factors:

$$T_{1-1}(s,u,t) = Mt\,A_1(s,u,t) = -2M\omega^{*2}(1-\cos\theta^*)\,A_1 \quad ,$$
$$T_{11}(s,u,t) = \frac{su-M^4}{M}\,A_2(s,u,t) = -2M\omega^2(1+\cos\theta^*)\,A_2 \quad . \tag{4}$$

Unsubtracted fixed-t dispersion relations for these amplitudes look like

$$\mathrm{Re}\,A_i(s,u,t) = \frac{1}{\pi}\int_{M^2}^{\infty}\left[\frac{1}{s-s'}+\frac{1}{u-s'}\right]\mathrm{Im}\,A_i(s',u',t)\,ds' \quad . \tag{5}$$

However, for the helicity-flip amplitude A_1 it is necessary to introduce a subtraction or to use a dispersion loop of finite size to overcome bad convergence of the dispersion integral for A_1 at high energies. In this case we can write down, instead of (5),

$$\mathrm{Re}\,A_1 = \frac{1}{\pi}\int_{M^2}^{s_M}(\ldots) + A_1^{as} \tag{6}$$

where the asymptotic contribution [8,9] takes into account both photoproduction at higher energies and the seagull generating a non-vanishing contribution to the Compton amplitude (Fig.2). This asymptotic term (or subtraction function) can be further analyzed by virtue of a dispersion relation over t [10-13] which provides a link between Compton scattering on the nucleon and that on the pion but does not allow, of course, to find the scattering amplitude in terms of photoabsorption only.

Imaginary parts of the helicity amplitudes appeared in (5)-(6) are found through multipoles of photoabsorption:

$$\mathrm{Im}\,T_{1\pm1}(s,\theta^*) = \sum_J (s-M^2)\,d^J_{1\pm1}(\theta^*)\left[\sigma_{EJ}(s) \pm \sigma_{MJ}(s)\right] \quad . \tag{7}$$

Therefore, ingredients of actual dispersion calculations of Compton scattering are: 1) multipoles of photoabsorption, and 2) asymptotic pieces for badly convergent dispersion relation.

Real case of the spin-1/2 proton is more complicated since there are six various types of multipoles (namely, the transitions $EL \to EL$, $ML \to ML$, and $EL \leftrightarrow M(L\pm1)$ with $J = L\pm\frac{1}{2}$) and, respectively, six invariant amplitudes A_i two of which need in subtractions. However, the main features of the dispersion calculations are the same as in the case of spin-0 target.

What do we know about photoabsorption at medium energies and its multipole structure? The most clear situation is for the channel $\gamma N \to \pi N$ where reliable partial-wave analyses are available up to 1-2 GeV [14-15]. We have much worse knowledge of the channels with ≥ 2 pions which are opened above the Δ-resonance and dominate at $\omega > 600\,\mathrm{MeV}$ (Fig. 3). Their joint cross section can be restored from measurements of total photoabsorption cross sections [16] but further multipole decomposition can be made only in a very model-dependent way.

Approximately 30-40% of the $\gamma N \to (\geq 2\pi) + N$ cross section is related with production of resonances decaying into channels with ≥ 2 pions. This part of the cross section is easily decomposed into partial waves by using amplitudes of resonance photoexcitation found from $\gamma N \to \pi N$ data [14,15]. The remaining non-resonance cross section is, in part, related with production of $\pi\Delta$ which we can split further into low partial waves (actually we imply only s-wave) and higher ones and calculate the latter through one-pion-exchange model. There is also the channel $\rho^0 N$ which can be assumed to be produced by a diffractive mechanism conserving s-channel helicities of the particles and therefore having known multipole structure. The other channels and the remaining s-wave in $\gamma N \to \pi\Delta$ can be rather arbitrary ascribed to electric dipole absorption.

This is the model we use to calculate the dispersion integrals.

The asymptotic contributions which are required for two of six Compton amplitudes are mainly related with t-channel exchanges by scalar (σ) and pseudoscalar (π^0) mesons [8,9]. In the case of the scalar exchange its magnitude is badly known but can be adjusted from knowledge of or assumption on nucleon polarizabilities $\bar{\alpha} - \bar{\beta}$; its t-dependence at $-t \leq 0.5 - 1\,\mathrm{GeV}^2$ is assumed to be the same as t-dependence of Compton amplitude as measured in few-GeV region: $\propto \exp(\frac{B}{2}t)$, $B \simeq 5 - 6\,\mathrm{GeV}^{-2}$.

Both these asymptotic contributions appear in photon helicity-flip amplitudes. Due to their relation to seagulls it is of great interest to study them in details. For this aim data on the asymmetry of photon scattering with linearly-polarized photons are very useful because the asymmetry is just proportional to helicity-flip amplitudes:

$$\Sigma = \frac{\sigma_\perp - \sigma_\parallel}{\sigma_\perp + \sigma_\parallel} = \frac{2\,\mathrm{Re}\,(T_{11}T_{1-1}^*)}{|T_{11}|^2 + |T_{1-1}|^2}\,. \tag{8}$$

Unfortunately, we have almost no data for Σ. Their obtaining could be a nice job for polarized photon facilities such as LEGS.

The described inputs into dispersion calculations result in rather satisfactory description of various data on γp-scattering. At very low energies the cross sections are mainly sensitive to proton polarizabilities, so that the latters can be fixed there (see [17] and the talk by F. Federspiel at this workshop). After this step the theory described has no free parameters and can be directly compared with different data. Then a pretty good agreement of the theory with Mainz measurements at 100–130 MeV [18] and recent measurements from Saskatoon at 140–290 MeV, as discussed in talks by F. Federspiel and E. Hallin, provides a strong support to our present understanding of mechanisms of photoabsorption and Compton scattering at energies up to Δ-resonance. With advent of the Saskatoon data no visible disagreements are seen between the dispersion theory predictions and data. The old disagreement at the Δ-resonance energy at 90° seems to be not confirmed by new data from Mainz [19]. Hence, we can rely on the theory in attempts to improve information on photoproduction. Important application could be to γp-scattering at the Δ-resonance energy. The angular distribution of the scattered photons is sensitive to the quadrupole amplitude of the Δ-resonance excitation (Fig. 4), so that Compton scattering can provide useful constraints to this physically very interesting value.

At energies above the Δ-resonance the described theory is less determined, mainly because

of uncertainties in double-pion photoproduction cross sections. Nevertheless, its results [20] look to be not very bad both for differential cross sections and polarization observables (Fig. 5) and this provides a hope to use Compton data for improving our knowledge of the photoabsorption and seagulls at these energies too.

Again measurements with linearly-polarized photons are very informative for this job because of their sensitivity to helicity-flip contributions.

It is worth to stress that non-resonance photoabsorption plays dominating role in photon scattering above the Δ-resonance, so that simple resonance models [21-22] ignoring this feature cannot provide a reliable base for extracting information on photoabsorption. Between 0.5 and 0.9 GeV only $D_{13}(1520)$ resonance is clearly seen over the non-resonance background. A study of other resonances in γN-scattering, which are masked by the background, seems to be rather hard.

3. Dispersion look at the nucleon polarizabilities

Dispersion analysis of Compton scattering gives very useful hints for understanding of fundamental structure parameters of the nucleon, its electric and magnetic polarizabilities [23]. Recently they have been measured both for proton [17-18] and, for the first time, for the neutron [24]. In low-energy Compton scattering the polarizabilities are seen as coefficients determining deviation of the scattering amplitude from its point-like magnitude which involves the mass M, charge Q and anomalous magnetic moment κ of the nucleon:

$$\frac{1}{8\pi M} T = \text{point-like} + \omega\omega' \bar{\alpha} (\vec{e}\vec{e}') + (\vec{k} \times \vec{e})(\vec{k}' \times \vec{e}') \bar{\beta} + O(\omega^3) . \qquad (9)$$

The polarizability $\bar{\alpha}$ entering Eq. (9) can be expressed in terms of electric dipole transitions as [25-27]

$$\bar{\alpha} = \alpha^0 + \Delta\alpha, \quad \alpha^0 = 2 \sum_n{}' \frac{|\langle n|D_z|0\rangle|^2}{E_n - E_0}, \quad \Delta\alpha = \frac{e^2}{3M} Q^2 \langle r_E^2 \rangle + \frac{e^2}{4M^3}(\kappa^2 + Q^2) \qquad (10)$$

where the term $\Delta\alpha$ has, at least in non-relativistic theory, the meaning of retardation correction determined by the electric radius of the particle. In relativistic theory this correction becomes be inherent part of the polarizability and always appears together with α_0, even in energy shift for the particle placed into electric field [27]. Because of complicated cluster structure of the sum α_0, as shown in Fig. 1, the value α_0 turns out to be non-zero even for point-like electron due to contribution of antiparticles or, in other words, negative energy states. Nevertheless, $\bar{\alpha}$ is zero in this case, in accordance with intuitive feeling that the point-like electron has no intrinsic polarizability.

Somewhat similar is occurred with the retardation correction $\propto \langle r_E^2 \rangle$. Due to vector contributions the value α_0 is not zero for the particle which has no excited states and interacts with photons through intermediate vector mesons. But $\bar{\alpha} = 0$ in this case also.

These examples, together with the following dispersion formulae, show that namely $\bar{\alpha}$, not α_0, is determined by nucleon excitations.

Dispersion approach which gives the Compton scattering amplitude enables us to find polarizabilities through the same relations (5)-(6). Dispersion relation for helicity-non-flip amplitude results in the well-known sum rule [28]:

$$\bar{\alpha} + \bar{\beta} = \frac{1}{2\pi^2} \int_0^\infty \sigma_{tot}(\omega) \frac{d\omega}{\omega^2} . \qquad (11)$$

Another relation is derived from dispersion relation for helicity-flip amplitude [8]:

$$\bar{\alpha}-\bar{\beta}= \int_0^{\omega_M}\frac{1}{4\pi^2\omega^2}\left(1+\frac{2\omega}{M}\right)\{1\cdot 2\cdot[\sigma_{B1}(\omega)-\sigma_{M1}(\omega)]+ 2\cdot 3\cdot[\sigma_{B2}(\omega)-\sigma_{M2}(\omega)]+\ldots\}\,d\omega+(\bar{\alpha}-\bar{\beta})^{as} \quad . \tag{12}$$

Using the same inputs for photoproduction cross sections we can find integrands determining the nucleon polarizabilities (Fig. 6). The main feature of these integrands are the following. There is a large paramagnetic contribution from Δ-resonance but we see almost no diamagnetism. The contribution to $\bar{\alpha}$ is equally shared between the near-threshold regions of single- and double-pion photoproduction, both contributions being essentially non-resonant and related with OPE-mechanism in $\gamma N\to\pi N$ and $\gamma N\to\pi\Delta$ reactions.

Then the immediate conclusion is drawn that the main part of electric polarizability of the nucleon is due to pion cloud, as was earlier inferred from analysis of cloudy bag model [29].

Numerically (in units of $10^{-4}\,\mathrm{fm}^3$)

$$\bar{\alpha}_p=6+\tfrac{1}{2}(\bar{\alpha}-\bar{\beta})_p^{as}\,,\qquad \bar{\beta}_p=8-\tfrac{1}{2}(\bar{\alpha}-\bar{\beta})_p^{as}\,,$$
$$\bar{\alpha}_n=8+\tfrac{1}{2}(\bar{\alpha}-\bar{\beta})_n^{as}\,,\qquad \bar{\beta}_n=8-\tfrac{1}{2}(\bar{\alpha}-\bar{\beta})_n^{as}\,, \tag{13}$$

and experimental data on the nucleon polarizabilities [17,18,24] imply the following value of the asymptotic contributions:

$$(\bar{\alpha}-\bar{\beta})_p^{as}\simeq(\bar{\alpha}-\bar{\beta})_n^{as}=5\text{ to }13\,. \tag{14}$$

That means that about 30-50% of the electric polarizability of the nucleon and the main part of the nucleon diamagnetism is related with degrees of freedom invisible below 1 GeV.

A possible mechanism explaining Eq. (14) is the excitation of pions in the meson cloud of the nucleon. This possibility is supported by dispersion analysis [12] of the diagram in Fig. 7 which results in a linear relation between polarizabilities of the nucleon and the pion:

$$\Delta(\bar{\alpha}-\bar{\beta})_N\simeq 0.7\,(\bar{\alpha}_{\pi^+}-\bar{\beta}_{\pi^+}) \tag{15}$$

Due to small mass of the pion the energy required to excite the pion is indeed very high, $\sim(m_\rho^2-m_\pi^2)/2m_\pi\approx 2\,\mathrm{GeV}$.

Further tests can be made by comparing ω- and t-dependence of the asymptotic contributions as seen in experiment and according to Fig. 7. Accurate data on Compton scattering, especially at backward angles and with polarized photons, would be very useful to study this question.

4. Conclusions

Theoretical investigations of dynamics of photon scattering on nucleons at intermediate energies are needed in improving our knowledge of mechanisms of double-pion photoproduction and those of helicity-flip in the scattering at high energies. Both direct data on $\gamma N\to\pi\pi N$ and linearly-polarized photon scattering could be very helpful.

Polarizabilities of the nucleon are still needed to be explained. Appropriate theoretical models apparently must take into account lessons found in dispersion analysis. They must include not only excitations of constituent quarks (i.e. resonances) but also excitation of the pion cloud and, probably, internal polarizability of the constituent pions and even constituent quarks.

References

1. L.S. Brown, Phys. Rev. **150** (1966) 1338.
2. P. Christillin and M. Rosa-Clot, Nuovo Cim. **28A** (1975) 29.
3. D. Drechsel and A. Russo, Phys. Lett. **137B** (1984) 294.
4. A.I. L'vov and M. Schumacher, Nucl. Phys. **A**, in press.
5. R. Leicht et al., Nucl. Phys. **A362** (1981) 111.
6. A.M. Nathan et al., Phys. Rev. **C34** (1986) 480.
7. K.P. Schelhaas et al., Nucl. Phys. **A506** (1990) 307.
8. A.I. L'vov, V.A. Petrun'kin and S.A. Startsev, Yad. Fiz. **29** (1979) 1265.
9. A.I. L'vov, Yad. Fiz. **34** (1981) 1075.
10. J. Bernabeu and R. Tarrach, Phys. Lett, **69B** (1977) 484.
11. I. Guiasu, C. Pomponiu and E.E. Radescu, Ann. Phys. 114 (1978) 296.
12. V.M. Budnev and V.A. Karnakov, Yad. Fiz. **30** (1979) 440.
13. D.M. Akhmedov and L.V. Fil'kov, Yad. Fiz. **33** (1981) 1083.
14. W.J. Metcalf and R.L. Walker, Nucl. Phys. **B76** (1974) 253.
15. R.A. Arndt et al., Phys. Rev. **C42** (1990) 1853 and R. Arndt, private communication.
16. T.A. Armstrong et al., Phys. Rev. **D5** (1972) 1640; Nucl. Phys. **B41** (1972) 445.
17. F.J. Federspiel et al., Phys. Rev. Lett. **67** (1991) 1511.
18. A. Zieger et al., Phys. Lett. **278B** (1992) 32.
19. M. Sanzone, private communication.
20. A.I. L'vov and V.A. Petrun'kin, in progress.
21. T. Ishii et al., Nucl. Phys. **B165** (1980) 189.
22. Y. Wada et al., Nucl. Phys. **B247** (1984) 313.
23. V.A. Petrun'kin, Fiz. Elem. Chast. At. Yadra **12** (1981) 692.
24. J. Schmiedmayer et al., Phys. Rev. Lett. **66** (1991) 1015.
25. V.A. Petrun'kin, Nucl. Phys. **55** (1964) 197.
26. V.M. Shekhter, Yad. Fiz. **7** (1968) 1272.
27. A.I. L'vov, Preprint FIAN # 344 (1987).
28. A.M. Baldin, Nucl. Phys. **18** (1960) 310.
29. R. Weiner and W. Weise, Phys. Lett. **159B** (1985) 85.

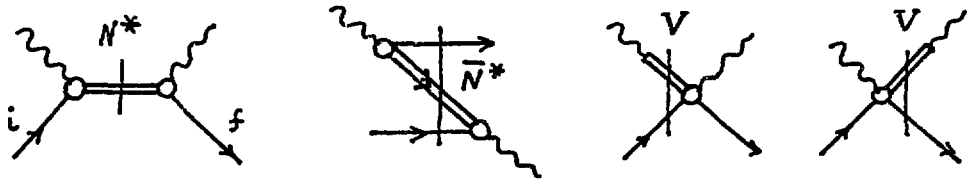

$(E_{N^*} - E_i - \omega)^{-1}$ $(E_{\bar{N}} + E_f - \omega)^{-1}$ $(E_V - \omega)^{-1}$ $(E_V - \omega')^{-1}$

Figure 1: Cluster structure of the photon scattering amplitude and corresponding energy denominators.

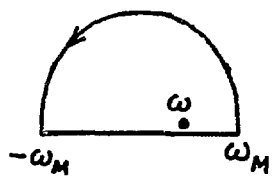

$$A^{as}(\omega,t) = \frac{1}{2\pi}\mathrm{Im}\int_{\omega_M}^{-\omega_M}\left(\frac{1}{\omega'-\omega}+\frac{1}{\omega'+\omega}\right)A(\omega',t)\,d\omega'$$

Figure 2: Dispersion loop of finite size and the corresponding asymptotic contribution (integral over the semicircle).

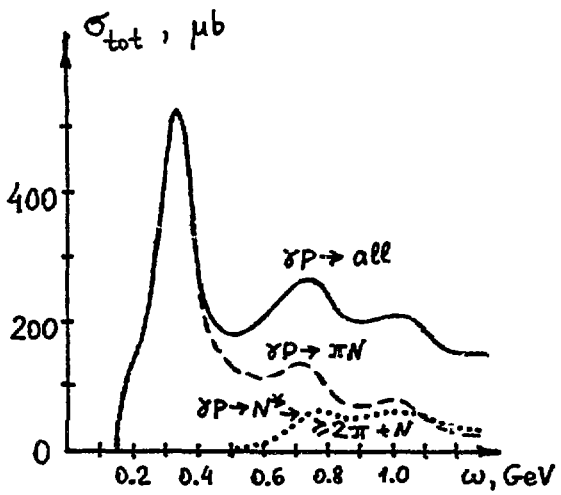

Figure 3: Cross sections of photoproduction by the proton.

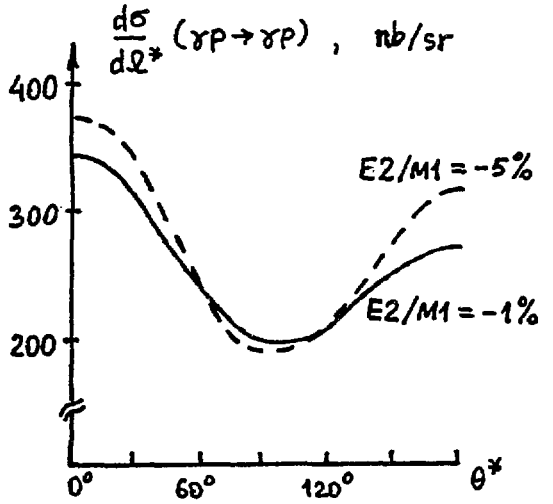

Figure 4: Angular distribution at ω=320 MeV and various $E2/M1$-admixture in the photoexcitation of Δ.

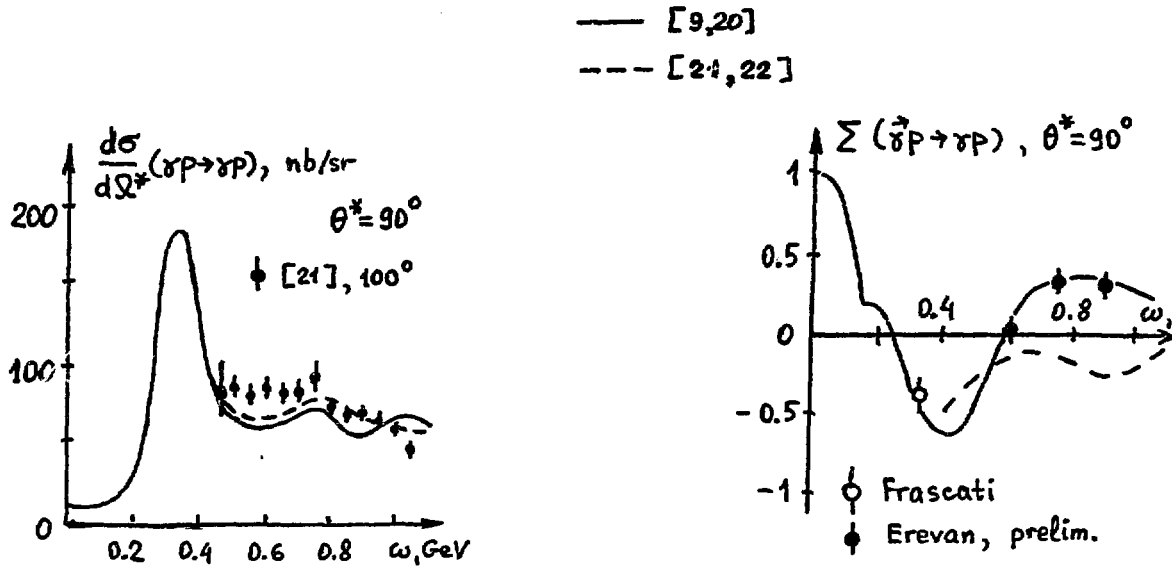

Figure 5: Predictions of the dispersion theory [9,20] and the resonance model [21].

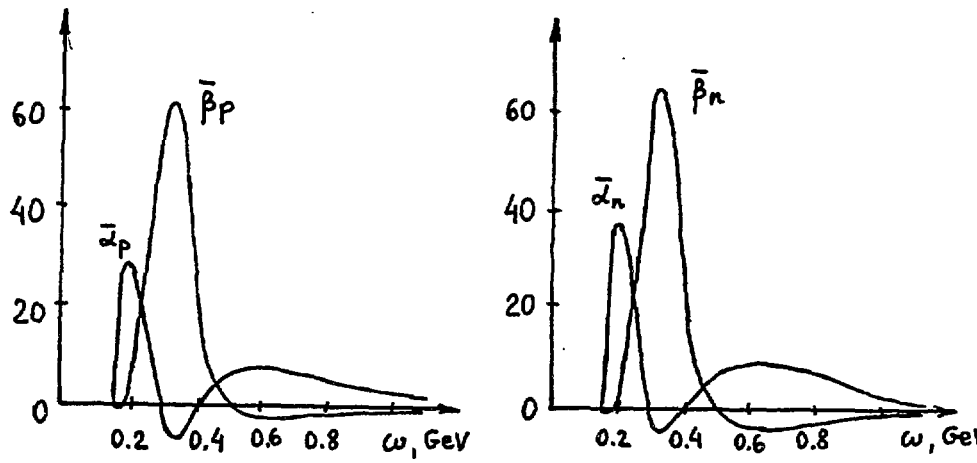

Figure 6: Integrands in dispersion integrals for $\bar{\alpha}_N$ and $\bar{\beta}_N$, units are $10^{-4}\,\mathrm{fm}^3\,\mathrm{GeV}^{-1}$.

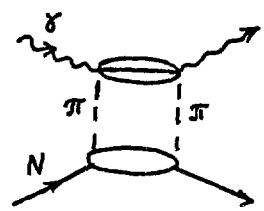

Figure 7: Possible mechanism responsible for arising the asymptotic contributions, Eq. (14).

Pion Polarizabilities in Chiral Perturbation Theory

D. Babusci, S. Bellucci, G. Giordano, G. Matone
INFN - Laboratori Nazionali di Frascati, Italy

The electric (α) and magnetic (β) polarizabilities of any composite system are fundamental quantities that are inherently sensitive to their internal structure and, together with the charge, mass and the magnetic moment, fully determine the expression of the Compton amplitude at low energy. Their experimental determination constitute an important testing ground for any hadron model. In recent years, a great deal of interest has been expressed in the literature for the polarizabilities of the pion [1] which belongs to the pseudoscalar meson octet and thus is believed to be one of the Goldstone bosons associated with the spontaneously broken chiral symmetry.

Following a standard formalism, the general form of the photon scattering amplitude by a pseudoscalar meson can be written in the following form (see Fig.1):

$$\begin{aligned} \mathcal{A}(\gamma\pi \to \gamma\pi) &= \epsilon_1^\mu \epsilon_2^\nu M_{\mu\nu} , \\ M_{\mu\nu} &= A(s,t) T_{\mu\nu}^{(1)} + B(s,t) T_{\mu\nu}^{(2)} , \end{aligned} \tag{1}$$

where ϵ_1, ϵ_2 are the initial and final photon polarizations and the two gauge-invariant Lorentz tensors are given by :

$$\begin{aligned} T_{\mu\nu}^{(1)} &= -(\frac{t}{2} g_{\mu\nu} + k_{2\mu} k_{1\nu}) , \\ T_{\mu\nu}^{(2)} &= \frac{1}{t}[\frac{1}{2}(s - m_\pi^2)(u - m_\pi^2) g_{\mu\nu} + t p_{1\mu} p_{1\nu} + \\ &\quad (s - m_\pi^2) k_{2\mu} p_{1\nu} - (u - m_\pi^2) p_{1\mu} k_{1\nu}] . \end{aligned} \tag{2}$$

The two structure functions A(s,t) and B(s,t) may be decomposed in two terms:

$$A(s,t) = A_p(s,t) + A_s(s,t) , \quad B(s,t) = B_p(s,t) + B_s(s,t) . \tag{3}$$

The first terms (A_p,B_p) describe the scattering from a point-like charge (Born) and the second terms (A_s,B_s) arise from the inner structure of the pion. The Born terms are given by [2]:

$$\begin{aligned} A_p(s,t) &= 0 , \\ B_p(s,t) &= 16\pi\alpha_f \frac{t}{(s - m_\pi^2)(u - m_\pi^2)} \mid q \mid , \end{aligned} \tag{4}$$

where α_f is the fine structure constant and $|q| = 1(0)$ for the charged(neutral) pion. The two structure functions $A_s(s,t)$ and $B_s(s,t)$ contain the dinamycs of the process and resemble very closely the role that the hadron form factors have in electron scattering. The non- relativistic limit for the Compton scattering amplitude at low energy can be written as follows:

$$\mathcal{A}^{NR}(\gamma\pi \to \gamma\pi) = [-\frac{\alpha_f}{m_\pi} + \alpha_\pi \omega\omega'](\hat{\epsilon}\cdot\hat{\epsilon'}) + \beta_\pi \omega\omega'(\hat{\epsilon}\wedge\hat{k})\cdot(\hat{\epsilon'}\wedge\hat{k'}) \,, \qquad (5)$$

where $\omega(\omega')$, $\hat{k}(\hat{k'})$ and $\hat{\epsilon}(\hat{\epsilon'})$ are the energy, momentum and polarization versors of the incoming and outgoing photons respectively. It can be easily verified that the low energy limit of Eq.(1) reproduces exactly Eq.(5) if the two structure constants α_π and β_π of Eq.(5) are identified as:

$$\begin{aligned}
\alpha_\pi &= -\frac{1}{8\pi m_\pi} \quad \lim_{s\to m_\pi^2, t\to 0} \quad [A_s(s,t) + \frac{(s-3m_\pi^2)}{t} B_s(s,t)] \,, \\
\beta_\pi &= \frac{1}{8\pi m_\pi} \quad lim_{s\to m_\pi^2, t\to 0} \quad [A_s(s,t) + \frac{(s-m_\pi^2)}{t} B_s(s,t)] \,, \qquad (6) \\
(\alpha+\beta)_\pi &= \frac{m_\pi}{4\pi} \quad lim_{s\to m_\pi^2, t\to 0} \quad \frac{1}{t} B_s(s,t) \,.
\end{aligned}$$

Thus, the static electric and magnetic polarizabilities that characterize the pion-photon coupling in the non-relativistic limit, are defined by the low energy limit of the two structure functions $A_s(s,t)$ and $B_s(s,t)$ of Eqs.(3).

Chiral perturbation theory (χPT) [3] appears today as one of the most successful ideas in describing the electromagnetic interactions of pions. Its approach is to describe the interactions of the Goldstone bosons at low energy in terms of a so called chiral Lagrangian which stems directly from QCD with the only assumptions of chiral symmetry $SU(3)_L \times SU(3)_R$, Lorentz invariance and low momentum transfer. In particular, with a perturbative expansions of this effective Lagrangian limited to terms of increasing order in the external momenta and quark masses, the method is capable of establishing a network of relationships between different processes in terms of a common set of renormalized parameters L_i^r (tree level coefficients). At $O(p^4)$-level, the perturbative expansion is truncated at terms quartic in the photon momentum and 12-coupling constants are needed. The $O(p^4)$ expressions for the structure functions of Eqs.(3) have been calculated by different authors [4],[5] and can be written as

$$\begin{aligned}
A_s^{(\pm)}(s,t) &= -16\pi\alpha_f\{\frac{2}{F_\pi^2}(L_9^r + L_{10}^r) - \frac{1}{32\pi^2 F_\pi^2}[\frac{3}{2} + \frac{1}{t_\pi} ln^2 Q_\pi(t) + \frac{1}{2t_K} ln^2 Q_K(t)]\} \,, \qquad (7) \\
B_s^{(\pm)}(s,t) &= 0 \,,
\end{aligned}$$

for the charged pion, and

$$\begin{aligned}
A_s^{(0)}(s,t) &= \frac{\alpha_f}{4\pi F_\pi^2}[4(1-\frac{1}{t_\pi})(1+\frac{1}{t_\pi} ln^2 Q_\pi(t)) + (1+\frac{1}{t_K} ln^2 Q_K(t))] \,, \qquad (8) \\
B_s^{(0)}(s,t) &= 0 \,,
\end{aligned}$$

for the neutral pion. In Eqs.(7,8) both the contribution from pion and kaon loops have been considered, and

$$t_i = \frac{t}{m_\pi^2}\,, \qquad Q_i = \frac{\sqrt{t_i - 4} + \sqrt{t_i}}{\sqrt{t_i - 4} - \sqrt{t_i}}\,, \qquad (i = \pi, K)\,. \tag{9}$$

$F_\pi = 93.1$ MeV is the pion decay constant. Moreover Eqs.(7) show that, at $O(p^4)$, only the combination (L_9+L_{10}) intervenes in the expression of the Compton amplitude. This is the same combination that intervenes in the pion radiative decay where the ratio of the vector and axial vector coupling constants is related to (L_9+L_{10}) by the very well known expression[1]

$$L_9^r + L_{10}^r = \frac{1}{32\pi^2}\frac{h_A}{h_V}\,. \tag{10}$$

From the experimental value[6] of $h_A/h_V = 0.46 \pm 0.09$ one obtains $L_9+L_{10} = (1.43 \pm 0.27)\ 10^{-3}$. On the contrary, Eqs.(8) are parameter free predictions for the neutral pion. Thus, following Eq.(6), the $O(p^4)$ expressions for the pion polarizabilities are [1]:

$$\begin{aligned} \alpha_{\pi^\pm} &= \frac{4\alpha_f}{m_\pi F_\pi^2}(L_9^r + L_{10}^r) = 2.65 \pm 0.50\,, \\ \alpha_{\pi^0} &= -\frac{\alpha_f}{96\pi^2 m_{\pi^0} F_\pi^2} = -0.49\,. \end{aligned} \tag{11}$$

In the exact chiral limit where the pion mass vanishes, one has [1]:

$$(\alpha + \beta)_\pi = 0\,, \tag{12}$$

and from Eqs.(6,7,8) the same result holds in χPT up to the $O(p^4)$-level. This is not surprising because a strong cancellation effect in $(\alpha+\beta)$ can indeed be expected from classical considerations based on the Lorentz invariance of the interaction hamiltonian. Potential problems to this conclusion can arise from the finite sizes of the forward angle dispersion sum rules

$$(\alpha + \beta)_{\pi^\pm} = 0.39 \pm 0.04\,, \quad (\alpha + \beta)_{\pi^0} = 1.04 \pm 0.07\,, \tag{13}$$

which stem directly from the optical theorem and have been evaluated in a model dependent way in Ref.[7]. According to χPT, these sum rules express only the contributions that come from the $O(p^6)$ (and higher) corrections to the lowest order result of Eq.(12). However, these higher order corrections have never been fully calculated and thus a cross-check between the full chiral predictions and Eqs.(13) has never been done.

In a recent paper [5] we have discussed in some detail the experimental knowledge that is presently available on the pion polarizabilities. We have shown that these quantities can be extracted directly from two reactions, related to each other by crossing symmetry: Compton scattering ($\gamma\pi \to \gamma\pi$) and photon-photon interaction ($\gamma\gamma \to \pi\pi$). We demonstrated that both these cross sections can be expressed in a

[1] in the present paper the polarizabilities are expressed in Gaussian units of 10^{-43} cm^3

very similar way:

$$
\begin{aligned}
(\frac{d\sigma}{d\Omega})_{\gamma\pi^{\pm}\to\gamma\pi^{\pm}} &= \frac{\alpha_f^2}{2s}[\mid B_1 + \frac{m_\pi}{2\alpha_f}\bar{\alpha}_\pi(t)t \mid^2 + \mid B_2 + \frac{m_\pi}{2\alpha_f}\bar{\alpha}_\pi(t)t \mid^2] \,, \\
(\frac{d\sigma}{d\Omega})_{\gamma\gamma\to\pi^+\pi^-} &= \frac{\alpha_f^2}{2s}\frac{\beta_v}{2}[\mid \tilde{B}_1 + \frac{m_\pi}{2\alpha_f}\bar{\alpha}_\pi(s)s \mid^2 + \mid \tilde{B}_2 + \frac{m_\pi}{2\alpha_f}\bar{\alpha}_\pi(s)s \mid^2] \,,
\end{aligned}
\tag{14}
$$

where β_v is the velocity of the final pions in the CM-system and

$$
B_1 = \tilde{B}_1 = 1 \,, \qquad B_2 = -1 + \frac{t}{G(s,u)} \,, \quad \tilde{B}_2 = -1 + \frac{s}{G(t,u)} \,,
\tag{15}
$$

$$
G(x,u) = \frac{(x-m_\pi^2)(u-m_\pi^2)}{2m_\pi^2} \,.
$$

Similarly for the neutral pion we obtained:

$$
\begin{aligned}
(\frac{d\sigma}{d\Omega})_{\gamma\pi^0\to\gamma\pi^0} &= \frac{m_\pi^2}{4s} \mid \bar{\alpha}_{\pi^0}(t) \mid^2 t^2 \,, \\
(\frac{d\sigma}{d\Omega})_{\gamma\gamma\to\pi^0\pi^0} &= \frac{1}{2}\frac{m_\pi^2}{4}\frac{\beta_v}{2} \mid \bar{\alpha}_{\pi^0}(s) \mid^2 s \,.
\end{aligned}
\tag{16}
$$

In all these equations we introduced an "effective polarizability function":

$$
\bar{\alpha}_\pi = \frac{1}{8\pi m_\pi} A_s(s,t) \,,
\tag{17}
$$

whose absolute value is shown in Fig.2(a,b). Table I summarizes the results which have been obtained considering all the data available for the charged pion both in the Compton and photon-photon channels.

The wide range of values they are spread over is a clear indication of the large systematic uncertainties that affect all these experimental determinations. The most significative values come from the MARK-II and Serpukov's experiments. The former is consistent with the chiral prediction (see Fig.3) but the latter differ by more than two standard deviations from the value of Eq.(11). As for the π^0, the only source of information comes from the Crystal Ball data [14] on the $\gamma\gamma \to \pi^0\pi^0$ reaction. Following our discussion of Ref.[5], this data set determines an experimental value for the π^0 polarizability of $0.69 \pm 0.07(\text{stat.}) \pm 0.04(\text{syst.})$ which is 40% larger than the chiral prediction of Eq.(11). It is interesting to notice that this result is perfectly consistent with the value of (0.4 ± 1.0) that has been obtained in [15] by analyzing the same Crystal Ball data set with a completely different approach.

However, in spite of Eqs.(13), practically all the data have been analyzed with the constraint of Eq.(12). This can be easily criticized because, in principle, can lead to erroneous results. The extent of the higher order corrections to $(\alpha + \beta)$ is not expected to be neglegible: according to [1] $(\alpha+\beta)/\alpha$ is estimated of the order of 25% for the charged pion. The effect appears to be even larger for the π^0 if we compare the values of Eqs.(11) and (13). On the other hand the quality of all the examined data

does not allow for an independent and reasonable determination of $(\alpha+\beta)$. It is true that the second analysis of the Serpukov experiment [13] shows that, by releasing the constraint of Eq.(12), $(\alpha+\beta)$ results largely consistent with zero. But the consequence is that the statistical errors in the determination of α and β worsen so much that the issue loses most of its significance. In conclusion, the present determinations suffer from the limitation imposed by Eq.(12) and the question of the experimental test of Eqs.(13) is left up to the next generation experiments.

On the theoretical side, a complete $O(p^6)$ calculation is still lacking. However, the t-channel vector meson contributions to the photon-photon interaction that have been calculated [16] in connection with the Crystal Ball data are contributions to $O(p^6)$. We know that they can not be ignored in the energy region above threshold even though they are not sufficient to give a satisfactory description of the Crystal Ball data (see Fig.4). We also know that they are neglegible in the threshold region. Nevertheless, they can constitute a sizeable contribution in the crossed channel reaction (Compton scattering) at $t = 0$ where the $O(p^4)$ contribution to the cross section vanishes both for the charged and neutral pion. As a matter of fact, this effect has to be expected because a substantial contribution to the sum rules of Eqs.(13) comes from the vector meson photoproduction and this necessarely has to affect the forward Compton amplitude.

This effect can be fully calculated following Ref.[16] and using crossingsymmetry. The result indicates that the two structure functions of Eqs.(3) acquire indeed extra contributions. By neglecting the ϕ-meson, these come from the ρ and ω-exchanges in the case of the π^0

$$\begin{aligned} A_s^{(0)}(s,t) &= A_s^{(0)}(O(p^4)) - \frac{1}{2}\sum_V G_V\left(\frac{s+m_\pi^2}{s-M_V^2} + \frac{u+m_\pi^2}{u-M_V^2}\right), \\ B_s^{(0)}(s,t) &= B_s^{(0)}(O(p^4)) - \frac{1}{2}\sum_V G_V t\left(\frac{1}{s-M_V^2} + \frac{1}{u-M_V^2}\right), \end{aligned} \tag{18}$$

$(V \equiv \omega, \rho)$

and from the ρ-exchange only for the charged pion

$$\begin{aligned} A_s^{(\pm)}(s,t) &= A_s^{(\pm)}(O(p^4)) - \frac{1}{2}G_\rho\left(\frac{s+m_\pi^2}{s-M_\rho^2} + \frac{u+m_\pi^2}{u-M_\rho^2}\right), \\ B_s^{(\pm)}(s,t) &= B_s^{(\pm)}(O(p^4)) - \frac{1}{2}G_\rho t\left(\frac{1}{s-M_\rho^2} + \frac{1}{u-M_\rho^2}\right), \end{aligned} \tag{19}$$

where M_V is the mass of the vector resonance and

$$G_V = 96\pi M_V^3 \frac{\Gamma(V\to\pi\gamma)}{(M_V^2-m_\pi^2)^3}. \tag{20}$$

Using Eqs.(19) and following Eq.(6) one can see that the α-values remain unaffected and the β-values become:

$$\begin{aligned} \beta_{\pi^\pm} &= -\alpha_{\pi^\pm} + \frac{m_\pi}{4\pi}\frac{G_\rho}{M_\rho^2-m_\pi^2} = -2.59, \\ \beta_{\pi^0} &= -\alpha_{\pi^0} + \frac{m_\pi}{4\pi}\sum_V \frac{G_V}{M_V^2-m_\pi^2} = 1.26. \end{aligned} \tag{21}$$

Consequently, the new estimated values for the sum rules are:

$$\begin{aligned}(\alpha+\beta)_{\pi^\pm} &= \frac{m_\pi}{4\pi}\frac{G_\rho}{M_\rho^2-m_\pi^2} = 0.062\ , \\ (\alpha+\beta)_{\pi^0} &= \frac{m_\pi}{4\pi}\sum_V \frac{G_V}{M_V^2-m_\pi^2} = 0.77\ .\end{aligned} \tag{22}$$

These numerical results have been obtained assuming the following experimental values for the $\rho\pi^0\gamma$ and $\rho\pi\gamma$ coupling constants [6]

$$G_\omega = 0.495\ GeV^{-2},\quad G_\rho = 0.044\ GeV^{-2}, \tag{23}$$

Although these results account only for partial $O(p^6)$ corrections, they deserve some comments. The vector meson contributions do not help much in reproducing the value of the sum rule of Eq.(13) for charged pions. On the contrary they account for more than 70% of the sum rule for the neutral pions. This is quite remarkable if one considers that they contribute very little in the threshold region for the $\gamma\gamma \to \pi^0\pi^0$ channel.

In a recent paper, M.A.Ivanov and T.Mizutani [17] presented a full calculation of the pion polarizabilities in the framework of the Dubna Quark Confinement Model (DCQM) with the explicit inclusion of scalar,vector and axial-vector mesons exchanges. They find that the axial-vector contributions are always almost neglegible and can be safely omitted. The major effects come from the scalar exchanges which contribute with opposite signs to α and β and thus cancel out in the sum. Therefore the only contributions to the sum rules come from the vector exchanges that are found to be small and affecting only the β-values. Qualitatively, these results are perfectly consistent with our claim that the vector-meson exchanges could be the dominant $O(p^6)$ contributions to the sum rules. But there are numerical differences and several problems. From the set of values they found:

$$\begin{aligned}(\alpha+\beta)_{\pi^\pm} &= 0.22\ , \quad \alpha_{\pi^\pm} = 3.63\ , \\ (\alpha+\beta)_{\pi^0} &= 0.44\ , \quad \alpha_{\pi^0} = 0.74\ ,\end{aligned} \tag{24}$$

the value for $\alpha_{\pi^\pm}$ results higher than the chiral prediction and α_{π^0} has the right magnitude but opposite sign. Moreover both the sum rules appear underestimated by approximatively a factor two with respect to Eqs.(13). Our numerical evaluations for $(\alpha+\beta)$ differ from the values of Eq.(24) : they do a better job for the π^0 but not for the $\pi^\pm$.

In conclusion the vector-meson contributions are certainly important corrections to the $O(p^4)$ results but do not seem to fully account for the values of the sum rules (13) as quoted in Ref.[7].

References

[1] B.R.Holstein, Comments Nucl. Part. Phys. 19, 239 (1990); J.F.Donoghue, B.R.Holstein and Y.C.Lin, Phys. Rev. D37, 2423 (1988)

[2] J.D.Bjorken and S.Drell, Relativistic Quantum Mechanics, Mc Graw-Hill (1964)

[3] J.Gasser and H.Leutwyler, Nucl. Phys. B250, 465 (1985)

[4] J.Bijnens and F.Cornet, Nucl. Phys. B296, 557 (1988)

[5] D.Babusci et al., Phys. Lett. B277, 158 (1992)

[6] Particle Data Group(G.P.Yost et al.), Review of Particle Properties, Phys. Lett. B239, 1 (1990)

[7] V.A.Petrun'kin, Sov. J. Part. Nucl. 12, 278 (1981)

[8] PLUTO Coll.(C.Berger et al.), Z. Phys. C26, 199 (1984)

[9] D.Morgan and M.R.Pennington, Phys. Lett. 192B, 207 (1987)

[10] MARK-II Coll.(J.Boyer et al.), Phys. Rev. D42, 1350 (1990)

[11] T.A.Aybergenov et al., Czech. J. Phys. 36, 948 (1986)

[12] Yu.M.Antipov et al., Phys. Lett. 121B, 445 (1983)

[13] Yu.M.Antipov et al., Z. Phys. C-Particles and Fields 26, 495 (1985)

[14] Crystal Ball Coll.(H.Marsiskie et al.), Phys. Rev. D14, 3324 (1990)

[15] A.E.Kaloshin and V.V.Serebryakov, Phys. Lett. B278, 198 (1992)

[16] P.Ko, Phys. Rev. D41, 1531 (1990); J.Bijnens, S.Dawson and G.Valencia, Phys. Rev. D44, 3555 (1991); S.Bellucci and D.Babusci, LNF-91/033(R) (1991)

[17] M.A.Ivanov and T.Mizutani, Phys. Rev. D45, 1580 (1992)

FIGURE CAPTION

FIG. 1 - Compton scattering kinematics.
FIG. 2 - Effective polarizability function for charged (a) and neutral pion (b) from χPT with $(L_9^r+L_{10}^r) = 1.4\ 10^{-3}$. $x \leq 0$ corresponds to Compton (t-variable) ; $x \geq 4m_\pi^2$ corresponds to $\gamma\gamma \rightarrow \pi\pi$ (s-variable).
FIG. 3 - MARK-II total cross-section data for $M_{\pi\pi} \leq 0.5$ GeV. The theoretical curves are : Born (dashed line) ; χPT with $(L_9^r+L_{10}^r) = 1.4\ 10^{-3}$ (full line). The region above $M_{\pi\pi} = 0.5$ GeV considered to be outside the domain of validity of χPT.
FIG. 4 - The cross-section for $\gamma\gamma \rightarrow \pi^0\pi^0$ including : i) both the 1-loop diagrams and the $O(p^6)$ contribution due to the vector-meson resonace exchange in the t-channel (full line) ; ii) the 1-loop contribution only (dashed line). The data are taken from the Crystal Ball experiment.

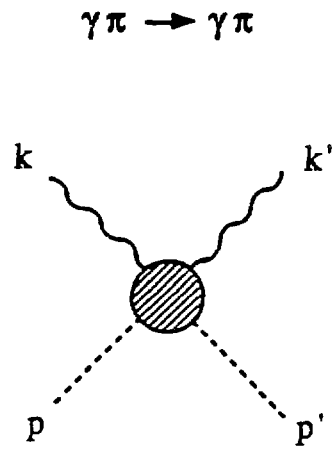

$$s = (k+p)^2$$

$$t = (k-k')^2$$

$$u = (k+p')^2$$

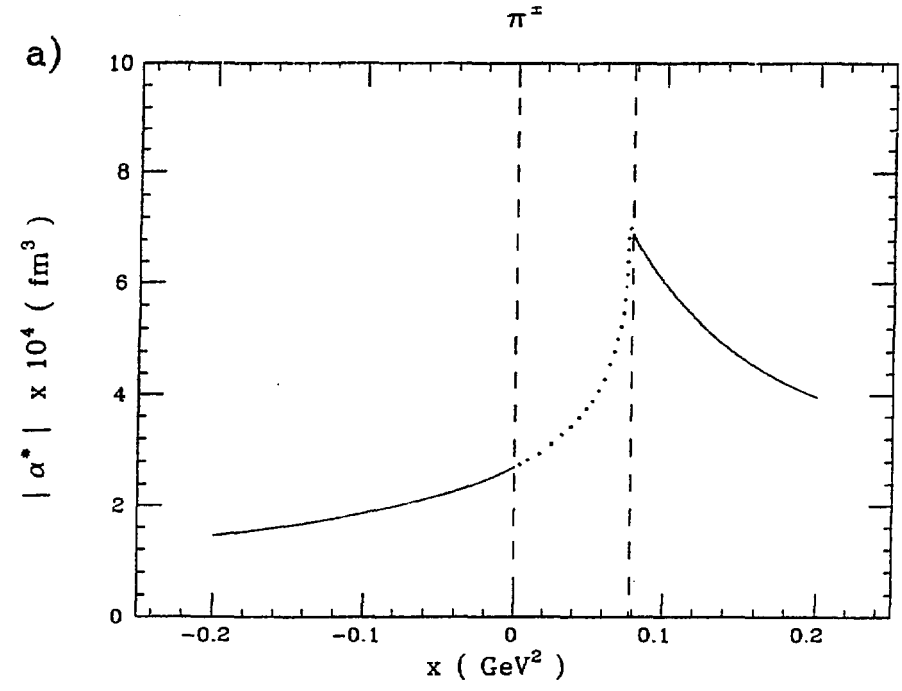
a)
$\pi^{\pm}$
$|\alpha^*|$ x 10^4 (fm^3)
x (GeV^2)
10
8
6
4
2
0
-0.2
-0.1
0
0.1
0.2

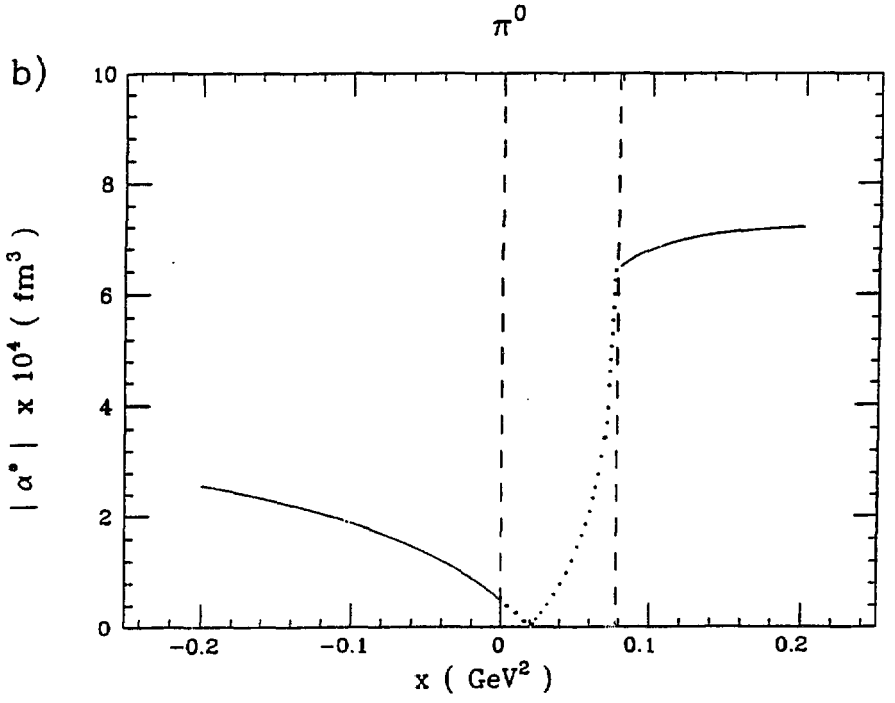
b)
π^0
$|\alpha^*|$ x 10^4 (fm^3)
x (GeV^2)
10
8
6
4
2
0
-0.2
-0.1
0
0.1
0.2

$\gamma\gamma \rightarrow \pi^+\pi^-$

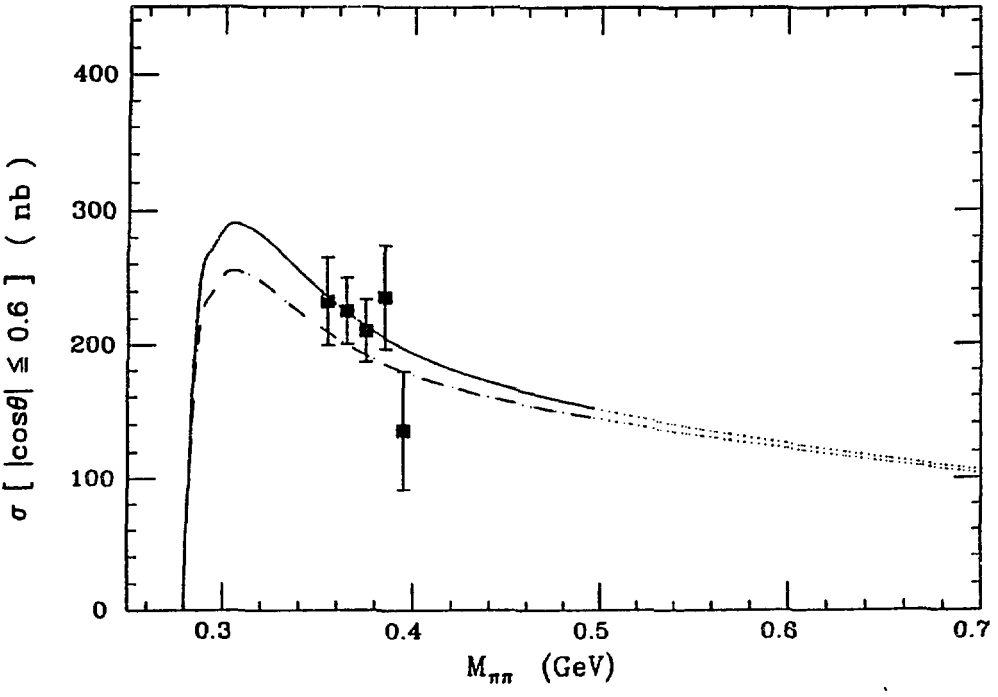

$\gamma\gamma \rightarrow \pi^0\pi^0$

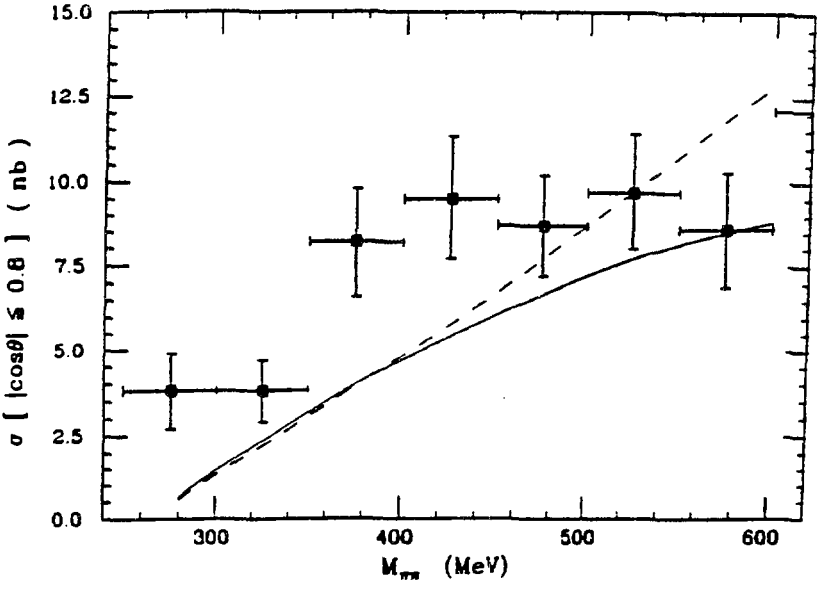

Pion Polarizabilities and the Shielding of the $\sigma(700)$-Meson Exchange in $\gamma\gamma \to \pi\pi$ Processes

A. Bramon,
Grup de Fisica, Universitat Autónoma de Barcelona, 08193 Bellaterra (Barcelona) Spain
A. N. Ivanov and N. I. Troitskaya,
State Technical University, 195251 Sankt Petersburg, Russia (USSR).
M. Nagy,
Institute of Physics, Slovak Academy of Sciences, CS-84248 Bratislava, Czechoslovakia
M. D. Scadron
Department of Physics, University of Arizona, Tucson, AZ, USA

First we develop a soft-pion theorem (SPT) whereby a $\gamma\gamma \to \pi\pi$ quark box graph in s-wave is cancelled by a scalar meson σ pole graph $\gamma\gamma \to \sigma \to \pi\pi$ when either pion four momentum becomes soft [1]. The linear σ model (LσM) field theory underlying this SPT in turn generates an internal electric polarizability respectively from quark and meson loops $\alpha_{\pi^+} = \alpha(8\pi^2 m_\pi f_\pi^2)^{-1}\left(1 - \frac{1}{3}\right) \sim 4 \times 10^{-4}\text{fm}^3$. This SPT result has already been obtained from the $\gamma\pi \to \gamma\pi$ low energy theorem (LET) with the LσM predicting [2] $\alpha_{\pi^+} = \alpha/(12\pi^2 m_\pi f_\pi^2)$ along with the $\pi^+ \to e^+\nu\gamma$ structure-dependent form factor ratio [3] $\gamma = h_A/h_V = 1 - \frac{1}{3}$, respectively from quark and meson loops. These SPT and LET predictions are internally consistent because they require $\alpha_{\pi^+} = \alpha(8\pi^2 m_\pi f_\pi^2)^{-1}\gamma$, which is the model-independent relation of Terent'ev [4].

[1] A. N. Ivanov, M. Nagy and M. D. Scadron, Phys. Lett. B273 (1991) 137.
[2] A. I. L'vov, Sov. J. Nucl. Phys. 34 (1981) 289.
[3] P. Pascal and R. Tarrach, Nucl. Phys. B146 (1978) 520; A. Bramon and M. D. Scadron, submitted for publication.
[4] M. V. Terent'ev, Sov. J. Nucl. Phys. 16 (1973) 87; J. F. Donoghue and B. R. Holstein, Phys. Rev. D40 (1989) 2378.

Pion and kaon polarizabilities in the quark confinement mode

M. A. Ivanov[1,2] & **T. Mizutani**[2]

[1] *Joint Institute for Nuclear Research, SU-141980 Dubna, Russia.*
[2] *Physics Department, Virginia Polytechnic Institute, Blacksburg, Va. 24061.*

The quark confinement model (QCM) which is based on quark confinement and th composite nature of hadrons, is applied to the study of electromagnetic polarizabiliti of the π and K mesons [1]. The Compton scattering amplitude for pseudoscalar meso in the QCM obtains contributions from the following processes (or diagrams): (1) th photon scattering by a point charge, (2) diagrams which involve only one quark loo (3) the scalar, vector, and axial meson exchanges. The presence of quark loops in QC diagrams introduces nontrivial momentum dependences which do not exist in the effecti Lagrangian scheme with only meson degrees of freedom.

Our principal findings may be summarized as follows. (Numerical results are give in the Gaussian system. The unit is $10^{-43}\mathrm{cm}^3$)

(1) The pion polarizabilities:

$$\alpha_{\pi^+} = 3.63 \qquad \alpha_{\pi^+} + \beta_{\pi^+} = 0.22,$$

$$\alpha_{\pi^0} = 0.74 \qquad \alpha_{\pi^0} + \beta_{\pi^0} = 0.44.$$

(2) The kaon polarizabilities:

$$\alpha_{K^+} = 2.28 \qquad \alpha_{K^+} + \beta_{K^+} = 0.97,$$

$$\alpha_{K^0} = 0.33 \qquad \alpha_{K^0} + \beta_{K^0} = 0.04.$$

For charge mesons, quark loop contributions have a strong mass dependence, which ma not be inferred easily from other existing models. As a consequence, the charged kao polarizability becomes considerably larger than what chiral models predict. This gives u hope that it may be measured experimentally without much difficulty.

In the chiral limit, when $m_\pi = m_K \to 0$ and the scalar mesons become degenerat $m_\epsilon = m_{f_0} = m_{a_0} \equiv m_S$, we obtain

$$\alpha_{\pi^+} = -\beta_{\pi^+} = 2.8 \qquad \alpha_{\pi^0} = 0,$$

$$\alpha_{K^+} = -\beta_{K^+} = 0.8 \qquad \alpha_{K^0} = 0,$$

which is just the prediction of the chiral perturbative theory [2].

[1] M. A. Ivanov and T. Mizutani, Phys. Rev. **D45**, 1580 (1992).
[2] J. F. Donoghue and B. R. Holstein, Phys. Rev. **D40**, 2378 (1989).

RADIATIVE PION PHOTOPRODUCTION AND PION POLARIZABILITIES

L.V.Fil'kov
Lebedev Physical Institute, Moscow 117924, Russia

1. The information on pion polarizabilities [1] can be obtained by investigation of the reaction $\gamma\pi \longrightarrow \gamma\pi$ [2–5] or $\gamma\gamma \longrightarrow \pi\pi$ [6–8]. Determination of the pion polarizabilities from the process $\gamma\gamma \longrightarrow \pi\pi$ is model–dependent. It is a result of necessity of a $\pi\pi$–interaction consideration. An expression for polarizability contributions into $\gamma\pi$–scattering cross section is obtained by expanding the scattering amplitude at low energy. This expression is more model independent. However information on $\gamma\pi$–scattering can be obtained only from indirect experiments.

One such experiment is the study of the scattering of high–energy pions in a Coulomb field of nuclei [9–11]: π+A $\longrightarrow$ γ+π+A. The experiments performed at IHEP at energy E_{π^-}= 40 GeV [2] permitted determination of polarizability of π meson: α_{π^-}= $(6.8\pm1.4\pm1.6)\cdot10^{-43}$cm^3. At FNAL, radiative scattering of π^- and π^+ mesons on nuclei of Cu and Pb [3] at energy E_π = 150 GeV did not show polarizability of pions.

Since in these experiments the information on $\gamma\pi$–scattering was obtained under a certain assumption, we should also study other possibilities of obtaining information on Compton scattering on pions.

The $\gamma\pi$–scattering cross section can be found by extrapolation of experimental data on the radiative pion photoproduction on proton

$$\gamma + p \longrightarrow \gamma + \pi + N \qquad (1)$$

to pion pole [12,13] (Fig.1).

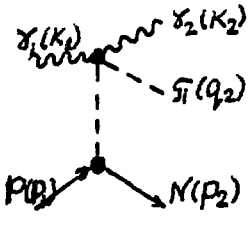

Fig.1. Pion pole diagram

This method was first suggested in [14] and broadly used for determination of the cross section and phases of elastic $\pi\pi$–scattering from reaction $\pi N \longrightarrow \pi\pi N$.

2. Let us obtain expressions for the $\gamma\pi$–scattering cross section through the polarizability of the pions [15]. D.Babusci et al. [7] have obtained such expressions using chiral perturbation theory and assuming $\alpha_\pi = -\beta_\pi$ (where α_π and β_π are the electric and magnetic pion polarizabilities). We will not imply $\alpha_\pi \neq \beta_\pi$ and will start with the one–subtracted dispersion relations for the $\gamma\pi$–scattering amplitudes [16]

$$T_i(s_1,t_1) = B_i + t_1 \Phi_i(t_1) + \frac{s_1-\mu^2}{\pi}\int_{4\mu^2}^{\infty} dx\ \mathrm{Im}\,T_i(x,t_1)\left[\frac{1}{(x-s_1)(x-\mu^2)} - \frac{1}{(x-u_1)(x-\mu^2+t_1)}\right], \qquad (2)$$

where B_i is the Born term, s_1 is the square of the total energy, t_1 is the square of the momentum transfer, μ is the pion mass, $s_1+u_1+t_1 = 2\mu^2$ and $t\Phi_i(t)$ is the t–dependent part of the subtraction function. In the expansions of $\Phi_i(t)$ with respect to t/m_ε^2 and t/m_ρ^2 (m_ε is the mass of the ε meson and m_ρ is the mass of the ρ meson) we limit ourselves to the first term

$$t_1\Phi_i(t) = t_1\Phi_i(0). \qquad (3)$$

In the expansion of the integral expression in (2) we omit the terms

$$\left(\frac{S_1-\mu^2}{x-\mu^2}\right)^n \approx \left(\frac{S_1}{m_\rho^2}\right)^n, \quad n \geq 3.$$

Then, using the relations [16] $\Phi_1(0) = -4\pi\mu\alpha_\pi$, $\Phi_2(0) = 4\pi\mu\beta_\pi$ and $T_1(s_1,t_1=0) = -T_2(s_1,t_1=0)$ we obtain for the amplitudes of $\gamma\pi^+$ scattering

$$T_1 = -2e^2\left[1-2\frac{(S_1-\mu^2)^2+S_1t_1}{(S_1-\mu^2)(\mu^2-U_1)}\right]-4\pi\mu\left[\alpha_{\pi^\pm}t_1 + \right.$$
$$\left. + \frac{(S_1-\mu^2)(\mu^2-U_1)}{2\mu^2}(\alpha_{\pi^\pm}+\beta_{\pi^\pm})\right], \qquad (4)$$

$$T_2 = -2e^2+4\pi\mu\left[\beta_{\pi^\pm}t_1 + \frac{(S_1-\mu^2)(\mu^2-U_1)}{2\mu^2}(\alpha_{\pi^\pm}+\beta_{\pi^\pm})\right],$$

where $e^2/4\pi$ is the fine structure constant and the amplitudes T_i is related to the differential $\gamma\pi$ scattering cross section as follows:

$$\frac{1}{r_0^2}\frac{d\sigma_{\gamma\pi}}{d\Omega} = \frac{\mu^2}{8e^4S_1}\left[|T_1|^2+|T_2|^2\right]. \qquad (5)$$

As result for $\gamma\pi^\pm \to \gamma\pi^\pm$ we find:

$$\frac{1}{r_0^2}\frac{d\sigma_{\gamma\pi}}{d\Omega} = \frac{1}{r_0^2}\left(\frac{d\sigma_{\gamma\pi}}{d\Omega}\right)_B + \frac{4\pi}{e^2}\frac{\mu^3(S_1-\mu^2)^2}{4S_1}\left\{\frac{1-z}{S_1}\left[\frac{(S_1-\mu^2)+(S_1+\mu^2)z}{(S_1+\mu^2)+(S_1-\mu^2)z}\alpha_{\pi^\pm}+\right.\right.$$
$$\left.\left. + \beta_{\pi^\pm}\right] - \frac{1+z}{\mu^2}(\alpha_{\pi^\pm}+\beta_{\pi^\pm})\right\}, \qquad (6)$$

$$\frac{1}{r_0^2}\sigma_{\gamma\pi} = \frac{1}{r_0^2}\sigma_B - \frac{4\pi}{e^2}\frac{2\pi\mu^3}{S_1}\left\{\left[\frac{(S_1-\mu^2)^3-6S_1\mu^4+2\mu^6}{2\mu^2S_1}+\right.\right.$$
$$\left.\left. + \frac{2\mu^2S_1}{S_1-\mu^2}\ln\frac{S_1}{\mu^2}\right]\alpha_{\pi^\pm} + \frac{(S_1-\mu^2)^3}{2\mu^2S_1}\beta_{\pi^\pm}\right\}, \qquad (7)$$

where $(d\sigma/d\Omega)_B$ and σ_B are cross sections corresponding to the Born term only; $z \equiv \cos\theta^Q_{\gamma\pi}$ in c.m.s. If the initial photon is polarized then we have

$$\frac{1}{r_0^2}\frac{d\sigma_{\parallel}}{d\Omega} = \frac{\mu^2}{S_1}\left[1-\frac{2S_1(1+z)}{(S_1+\mu^2)+(S_1-\mu^2)z}\right]^2 - \frac{4\pi}{e^2}\frac{(S_1-\mu^2)^2\mu^3}{4S_1^2}\left[1-\right.$$

$$- \frac{2 s_1 (1+z)}{(s_1+\mu^2)+(s_1-\mu^2)z}\Big]\Big[(1-z)(\alpha_{\pi^\pm}-\beta_{\pi^\pm}) - \frac{s_1}{\mu^2}(1+z)(\alpha_{\pi^\pm}+\beta_{\pi^\pm})\Big], \qquad (8)$$

$$\frac{1}{r_0^2}\frac{d\sigma_1}{d\Omega} = \frac{\mu^2}{s_1} - \frac{4\pi}{e^2}\frac{(s_1-\mu^2)^2\mu^3}{4 s_1}\Big[(1-z)(\alpha_{\pi^\pm}-\beta_{\pi^\pm}) +$$

$$+ \frac{s_1}{\mu^2}(1+z)(\alpha_{\pi^\pm}+\beta_{\pi^\pm})\Big]. \qquad (9)$$

The analysis [15] shows that the expressions (6) and (7) are correct with a high degree of accuracy in the region $s_1 \lesssim 10\ \mu^2$. The results of calculations of the relative contribution of pion polarizability to $d\sigma_{\gamma\pi}/d\Omega$ at $\theta^Q_{\gamma\gamma} = 180^0$ and to $\sigma_{\gamma\pi}$ as a function of s_1 are shown in Fig.2.

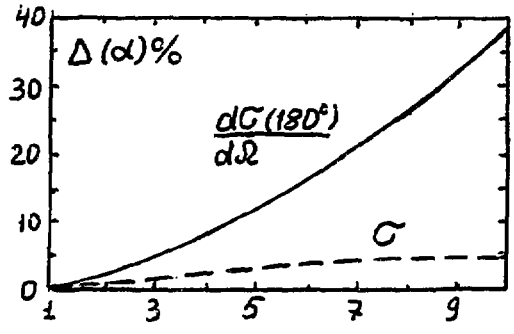

Fig.2. Relative contribution of pion polarizability to $d\sigma_{\gamma\pi}/d\Omega$ at $\theta^Q_{\gamma\gamma}=180^0$ and to $\sigma_{\gamma\pi}$ as a function of s_1.

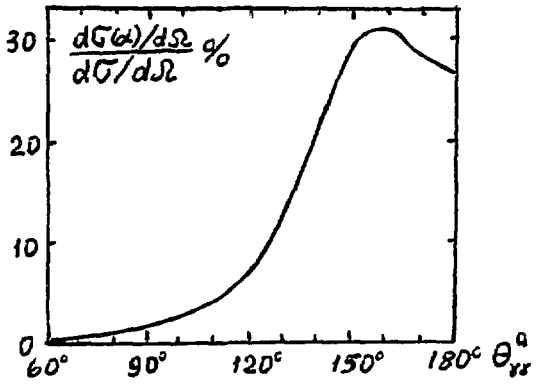

Fig.3. Relative contribution of pion polarizability to $d\sigma_{\gamma\pi}/d\Omega$ at $s_1=8\mu^2$ as a function of $\theta^Q_{\gamma\gamma}$.

Fig.3 shows the relative contribution of polarizability to the angular distribution of $d\sigma/d\Omega$ at $s_1 = 8\ \mu^2$. In these calculations we assumed $\alpha_{\pi^\pm} = -\beta_{\pi^\pm} = 7\cdot10^{-43}\text{cm}^3$. The contribution of the polarizability to $d\sigma/d\Omega$ is the largest for backward scattering; at $s\approx10\mu^2$ it reaches ~37%. The contributions of polarizability to the $\sigma_{\gamma\pi}$ for $s_1\lesssim10\mu^2$ is less than 5%.

For $\gamma+\pi^0 \longrightarrow \gamma+\pi^0$ scattering the Born term is equal to zero and the polarizabilities appear in the cross section as quadratic terms

$$\frac{1}{r_0^2}\frac{d\sigma_{\gamma\pi^0}(\alpha^2_{\pi^0})}{d\Omega} = \left(\frac{4\pi}{e^2}\right)^2\frac{\mu^4\omega^4}{4 s_1}\Big[(1-z)^2(\alpha_{\pi^0}-\beta_{\pi^0})^2 + \frac{s_1^2}{\mu^4}(1+z)^2(\alpha_{\pi^0}+\beta_{\pi^0})^2\Big], \qquad (10)$$

$$\frac{1}{r_0^2}\sigma_{\gamma\pi^0}(\alpha^2_{\pi^0}) = \left(\frac{4\pi}{e^2}\right)^2\frac{4\pi\mu^4\omega^4}{3 s_1}\Big[(\alpha_{\pi^0}-\beta_{\pi^0})^2 + \frac{s_1^2}{\mu^4}(\alpha_{\pi^0}+\beta_{\pi^0})^2\Big]. \qquad (11)$$

where $\omega = (s_1-\mu^2)/2\sqrt{s_1}$. For estimates we will take $\alpha_{\pi^0} = -2{,}8\cdot10^{-43}\text{cm}^3$ and $\beta_{\pi^0} = 3{,}8\cdot10^{-43}\text{cm}^3$ what is result of the dispersion sum rules calculation [17]. For $\theta^{Q}_{\gamma_1\gamma_2}=0$ expression (10) is enough accurate up to $s_1=10\mu^2$. However, at large scattering angles the discarded terms become important. Therefore, in order to expand the region of applicability of expressions (10) and (11), let us introduce an additional free parameter by including the following term in the expansion of $\Phi_1(t_1)+\Phi_2(t_1)$

$$\delta = \frac{1}{2}\frac{d}{dt_1}[\Phi_1(t_1)+\Phi_2(t_1)]_{t_1=0} \tag{12}$$

This parameter is related to quadrupole polarizabilities of the π^0 meson

$$\delta = \frac{\pi\mu}{6}(\beta_2-\alpha_2)_{\pi^0} \tag{13}$$

From dispersion sum rules we have: $(\alpha_2-\beta_2)_{\pi^0} = 2{,}8\cdot10^{-3}\text{fm}^5$. As a result we obtain

$$\frac{1}{r_0^2}\frac{d\sigma_{\gamma\pi^0}}{d\Omega} = \frac{1}{r_0^2}\frac{d\sigma_{\pi^0}(\alpha^2_{\pi^0})}{d\Omega} + \left(\frac{4\pi}{e^2}\right)^2\frac{\mu^3 t_1^3}{16\pi s_1}(\beta_{\pi^0}-\alpha_{\pi^0})\delta + \left(\frac{4\pi}{e^2}\right)^2\frac{\mu^2 t_1^4}{64\pi^2 s_1}\delta^2, \tag{14}$$

$$\frac{1}{r_0^2}\sigma_{\gamma\pi^0} = \frac{1}{r_0^2}\sigma_{\gamma\pi^0}(\alpha^2_{\pi^0}) - \left(\frac{4\pi}{e^2}\right)^2\frac{4\mu^3\omega^6}{s_1}(\beta_{\pi^0}-\alpha_{\pi^0})\delta + \left(\frac{4\pi}{e^2}\right)^2\frac{16\mu^2\omega^8}{5\pi s_1}\delta^2. \tag{15}$$

These expressions are correct for all angles in the region $s_1 \lesssim 9\mu^2$ with an accuracy better than 80%.

3. For the reaction $\gamma p \longrightarrow \gamma\pi N$ there are five independent invariant variables:

$$s=(p_1+k_1)^2 = m^2+2m\nu_1, \quad t=(p_2-p_1)^2=-2m(E_2-m),$$
$$t_1=-2\nu_1\nu_2(1-\cos\theta_{\gamma_1\gamma_2}), \quad s_2=(p_2+q_2)^2 = s+t_1-2m\nu_2, \tag{16}$$
$$s_1=(k_2+q_2)^2 = \mu^2+2\nu_2(q_0-q\cos\theta_{\gamma_2\pi}) = -2(\nu_1+m)(E_2-m)+2\nu_1 p\cos\theta_{\gamma_1 N},$$

where, in the system in which the target is at rest, ν_1 and ν_2 are the energies of the initial and final photons; E_2 and p are the energy and momentum of the final nucleon; q_0 and q are the energy and momentum of the pion. In addition to set (16) there are other five invariant variables. They depend linearly on the set (16)

$$s_3 = (k_2+p_2)^2 = s-s_1-s_2+m^2+\mu^2,\ t_4 = (p_1-k_2)^2 = s_2-s-t_1+m^2,$$
$$t_2 = (p_1-q_2)^2 = t_1-t-s_2+2m^2+\mu^2,\ t_5 = (k_1-p_2)^2 = s_1-s-t+2m^2,$$
$$t_3 = (k_1-q_2)^2 = t-t_1-s_1+\mu^2 \tag{17}$$

The cross section of the elastic $\gamma\pi$–scattering can be obtained by extrapolation of experimental data on reaction $\gamma+p \longrightarrow \gamma+\pi+N$ with respect to t to the pion pole $t=\mu^2$ (Fig.1) [13,18]

$$\frac{d\sigma_{\gamma\pi}}{d\Omega} = -K(s_1,s)\lim_{t\to\mu^2} F(t,s,s_1,t_1,s_2), \tag{18}$$

$$F(t, s, s_1, t_1, s_2) = (t-\mu^2)^2 \frac{d\sigma_{\gamma p \to \gamma\pi N}}{dt_1\, ds_1\, d\Omega} \qquad (19)$$

where

$$K = \left(\frac{4\pi}{g^2}\right) \frac{2\pi (s-m^2)^2}{\mu^2 (s_1-\mu^2)}, \quad \frac{g^2}{4\pi} = 14.6 . \qquad (20)$$

It is worth noting that doing the extrapolation we must fix 4 independent kinematic variables, for instance s, s_1, t_1 and s_2. Instead of fixing s_2 one can fix the Treiman–Yang angle φ between the planes formed by the momentums $\vec{k}_1$, $\vec{p}_1$ and $\vec{k}_1$, $\vec{q}_2$. However in this case singularities near the path of the extrapolation may appear. Analysis of expressions (16) and (17) for the invariant variables with fixed φ has shown [13] that at $t=0$ there are poles $1/(s_3-m^2)$ and $1/(t_4-m^2)$ for back scattering in the system $\gamma\pi \longrightarrow \gamma\pi$. Furthermore, the poles $1/(s_2-m^2)$ and $1/(t_2-m^2)$ arise at the end point of extrapolation $t=\mu^2$ for forward scattering ($t_1=0$), plus the pole $1/(t_3-\mu^2)$ at point $s_1=\mu^2$, $t_1=0$, $t=\mu^2$.

Thus, to avoid ambiguities in the extrapolation of experimental data with fixed φ, it is recommended that data will be selected in the region of scattering angles $30^0 \leq \theta^{Q}_{\gamma\gamma} \leq 150^0$ for $s_1 \gtrsim 2\mu^2$. Another method of avoiding singularities in s_2, t_2, s_3, t_4 is to fix variable s_2 and, consequently, use 4π–geometry.

To perform the extrapolation, let us represent the function $F(t)$ from (19) as

$$F(t) = e^{A(t-\mu^2)} \left[A_0 + A_1 (t-\mu^2) + A_2 (t-\mu^2)^2 + \dots\right] \qquad (21)$$

where the absorption effects are represented by exponent. The parameters $A, A_0, A_1 \dots$ are determined from the fit of the experimental data.

A rate of convergence of the expansion (21) can be improved by using a conformal mapping of the analytic region of the scattering amplitude [19–21]. Another method allowing reliable approximation is the Pade approximants method [22]. Pade approximants are constructed from the coefficients of the Taylor series and allow approximate summation of a diverging series. A Pade approximant has a larger region of convergence than the polynomial representation of an analytic function. It converges quite rapidly and allows stable analytic continuation. The [1/1] Pade approximant for the function $F(t)$ in (21) can be represented as

$$F(t) = e^{A(t-\mu^2)} \left[A_0 + \frac{A_1^2 (t-\mu^2)}{A_1 - A_2 (t-\mu^2)}\right] \qquad (22)$$

In order to a result of extrapolation will be reliable it is necessary to obtain experimental data as close as possible to the point $t=0$. The maximum possible experimental values of t are listed in the Table 1.

Results of calculation of the function $F_{\pi^+}(t)$ for the process $\gamma p \longrightarrow \gamma\pi^+ n$ at $s_1=3\mu^2$, $\nu_1=310$ MeV, $\theta^{Q}_{\gamma\gamma}=180^0$, $s_2=60\mu^2$ are presented in Fig.4. In the calculation we took into consideration the Born diagram (Fig.1) and $\Delta(1232)$ resonance in s–channel. The obtained behaviour of the function $F_{\pi^+}(t)$ puts on possibility to perform the extrapolation. It is worth noting that the calculated value of the function $F_{\pi^+}(t=0)$ is not equal to zero ($F_{\pi^+}(t=0) = 0{,}97 \cdot 10^{-33} \mathrm{cm}^2/\mathrm{str}$).

On the other hand, analysis of the process $\gamma p \longrightarrow \gamma\pi^0 p$ shows that the contribution of the Born diagram (Fig.1) into $F_{\pi^0}(t)$ is very small in this region of energies. As result the

ν_1(GeV)	t_{max}/μ^2			
	$s_1=2,5\mu^2$	$s_1=3\mu^2$	$s_1=6\mu^2$	$s_1=8\mu^2$
0.31	–0.51	–0.88	–	–
0.5	–0.14	–0.22	–1.20	–3.4
0.7	–0.07	–0.10	–0.46	–0.92
1.0	–0.03	–0.05	–0.200	–0.375
1.5			–0.084	–0.153
2.0			–0.046	–0.083

Table 1. The values of t_{max}

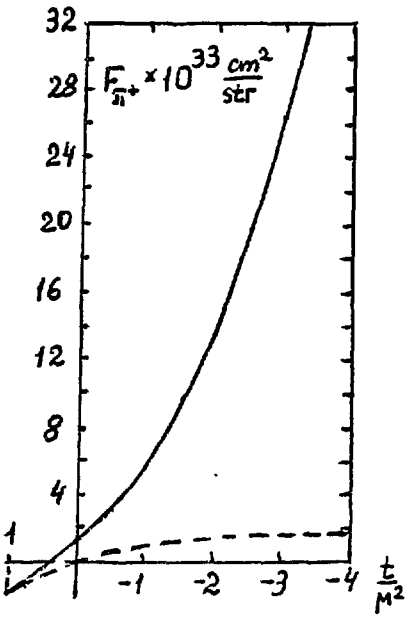

Fig.4. Function F_{π^+} for the process $\gamma p \to \gamma\pi^+ n$. Dash line shows contribution of the Born diagram (Fig.1).

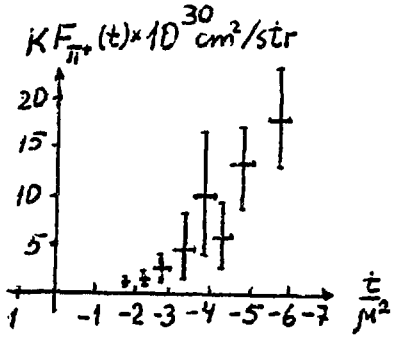

Fig.5. Experimental data for the function $F_{\pi^+}(t) \cdot K$

extrapolation of the function F_{π^0} is impossible in this case. Possibility of the extrapolation is more real at larger values of s_1 ($s_1 \approx 8$–$10\mu^2$) and ν_1 ($\nu_1 \approx 2$ GeV) where the contribution of polarizabilities is considerable and contribution of nucleon resonances become not so essential.

4. The process $\gamma p \to \gamma\pi^+ n$ was measured at Lebedev Physical Institute in a bremsstrahlung beam of 1.2 GeV electron synchrotron PACHRA. The measurement consisted of two run.

The first run was taken at low energies $\sqrt{s_1}$ where polarizability contribution is small comparing to the Born term. In order to perform the extrapolation of the experimental data the function $F_{n^+}(t)$ was represented as

$$F(t)=A_0+A_1(t-\mu^2)+A_2(t-\mu^2)^2.$$

As result the following value for cross section of $\gamma\pi^+$–scattering has been obtained [23,5]

$$\frac{d\sigma_{\gamma\pi^+}}{d\Omega} = \left(0.2^{+1,1}_{-0,2}\right) \times 10^{-30} \frac{cm^2}{str} \quad (23)$$

at $s_1=(1,5\pm0.5)\mu^2$, $\Theta^{Q}_{\gamma\gamma} \approx 150^0 \pm 30^0$, $\nu = 510^{+120}_{-130}$ MeV, $\varphi=0$. This value of the cross section agrees with the Born one.

The second run data were taken at higher values of s_1, and were used to evaluate the pion polarizability [4,5]. Experimental data for $F_{\pi^+}(t)$ are presented in Fig.5. Unfortunately, due to the lack of experimental data at $-t<1.5\mu^2$, we are forced to assume that function $F_{\pi^+}(t)$ passes through 0 when t=0. A similar suggestion was made in [24] to extract the partial $\pi\pi$–scattering cross sections from data on the reaction $\pi p \to \pi\pi N$. This suggestion is strictly correct for diagram at Fig.1. Our calculations [13] have shown that actually $F_{\pi^+}(t=0) \neq 0$.

After extrapolation the following values for cross section of the process $\gamma\pi^+ \to \gamma\pi^+$ has been obtained

$$\frac{d\sigma_{\gamma\pi^+}}{d\Omega} = (5.4 \pm 1.0) \times 10^{-32} \frac{cm^2}{str} \qquad (24)$$

at $s_1 = (6.5\pm0.5)\mu^2$, $\theta^Q_{\gamma\gamma} = 130^0\pm30^0$, $\nu = 650^{+150}_{-300}$ MeV, $\varphi=0$. This allowed the following value to be determined for polarizability of a π^+–meson

$$\alpha_{\pi^+} = -\beta_{\pi^+} = (20\pm12)\cdot10^{-43}\text{cm}^2 \qquad (25)$$

More correct result could be obtained using the beam of monochromatic photons and 4π–geometry.

The author thanks Dr. T.A.Aybergenov for helpful discussion.

References

1. V.A.Petrun'kin. Sov. J. Part. Nucl. 12 (1981) 278.
2. Yu.M.Antipov, V.A.Batarin, et al. Phys. Lett. B121 (1983) 445.
3. R.V.Kowalewski, D.Berg, et al. Phys. Rev. D29 (1984) 1000; M.Zelinski, D.Berg, et al. Phys. Rev. D29 (1984) 2633.
4. T.A.Aybergenov, P.S.Baranov, et al. Sov. Phys.–Lebedev Inst. Reports, N°6 (1984) 32.
5. T.A.Aybergenov, P.S.Baranov, et al. Czech. J. Phys. B36 (1986) 948.
6. A.A.Belkov and V.N.Pervushin. Yad. Fiz. 40 (1984) 966.
7. D.Babusci, S.Bellucci, et al. Phys. Lett. (to be published).
8. A.E.Kaloshin and V.V.Serebryakov. Yad. Fiz. 54 (1991) 1732.
9. I.Ya.Pomeranchuk and I.M.Shmushkevich. Nucl. Phys. 23 (1961) 452.
10. N.I.Starkov, L.V.Fil'kov and V.A.Tsarev. Krat. soobshch. po fizike FIAN N°3 (1980) 24; Yad. Fiz. 36 (1982) 1212.
11. A.S.Galperin, G.V.Mitsel'makher, et al. Yad. Fiz. 32 (1980) 1053.
12. L.V.Fil'kov. Proceedings of the Lebedev Phys. Inst. 41 (1969) 1.
13. T.A.Aybergenov, P.S.Baranov, et al. Proceedings of the Lebedev Phys. Inst. 186 (1988) 169.
14. C.Goebel. Phys. Rev. Lett. 1 (1958) 337; G.F.Chew and F.E.Low. Phys. Rev. 113 (1959) 1640.
15. L.V.Fil'kov. Sov. J. Nucl. Phys. 41 (1985) 636.
16. D.M.Akhmedov and L.V.Fil'kov. Sov. J. Nucl. Phys. 33 (1981) 573.
17. L.V.Fil'kov, I.Guiasu, E.E.Radescu. Phys. Rev. D26 (1982) 3146.
18. D.M.Akhmedov and L.V.Fil'kov. Preprint of Lebedev Phys. Inst. N°214 (1978).
19. S.Dubnicka, O.V.Dubrais and F.Nichitiu. Nucl. Phys. A217 (1973) 535.
20. S.Chulli, K.Pomponiu and I.Sabba–Shtefanesku. Phys. of Element. Part. and Atomic Nuclei, 6 N°1 (1975) 72.
21. J.P.Baton, G.Laurens and J.Reigner. Phys. Lett. B33 (1970) 525.
22. J.L.Basdevant. Fortschr. Phys. 20 (1972) 283.
23. T.A.Aybergenov, P.S.Baranov, et al. Sov. Phys.–Lebedev Inst. Reports, N°5 (1982) 28.
24. Ye.A.Alekseyeva, A.A.Kartamyshev, et al. ZhETF 82 (1982) 1007.

June 28, 1992, Tel Aviv University Preprint TAUP 1972/92

PION AND SIGMA POLARIZABILITIES AND RADIATIVE TRANSITIONS

Murray A. Moinester
Raymond and Beverly Sackler Faculty of Exact Sciences,
School of Physics and Astronomy
Tel Aviv University, 69978 Ramat Aviv, Israel
internet e-mail: MURRAY@TAUPHY.TAU.AC.IL

Workshop on Hadron Structure from Photo-Reactions at Intermediate Energies
Brookhaven National Laboratory, May 28-29, 1992, Eds. A. Nathan, A. Sandorfi

I. Introduction

Hadron electric (α) and magnetic (β) intrinsic polarizabilities[1-5] characterize the induced transient dipole moments of hadrons subjected to external oscillating electric $\vec{E}$ and magnetic $\vec{H}$ fields. The dipole moments are given by $\vec{d} = \alpha\vec{E}$ and by $\vec{\mu} = \beta\vec{H}$. The polarizabilities can be obtained from precise measurements of the gamma-hadron Compton scattering differential cross section. They probe the rigidity of the internal structure of baryons and mesons, since they are induced by the rearrangement of the hadron constituents via action of the photon electromagnetic fields during scattering. For the light charged pion, chiral symmetry leads to a precise prediction for the polarizabilities. For the heavier charged kaon, chiral perturbation theory may be applied to predict the polarizabilities. For these cases, the experimental polarizabilities subject the underlying chiral symmetry and chiral perturbation techniques of QCD to new and serious tests. The availability of high energy hyperon beams raises the possibility of investigating Compton scattering polarizabilities, radiative transitions, form factors and structure functions for Sigma hyperons. Such data are of particular interest because of problems arising in understanding the data on electromagnetic and weak properties of the ground state baryon octet. One such problem are the discrepancies in the naive quark model description of static magnetic moments. Pion and $\Sigma(1189)$ polarizabilities and associated $\Sigma(1385)$ radiative production (hereafter also designated Σ^*) will be measured in the Fermilab E781 SELEX experiment.[5,6] This experiment is primarily a study of the production and decay modes of charmed baryons. It includes searches[7] for HOP particles (Hexaquark H, Omegon O, Pentaquark P). It also includes a search for Primakoff production of hybrid ($q\bar{q}g$) mesons[8]; and Primakoff studies of pion and Σ polarizabilities and radiative transitions.

II. Sigma Polarizabilities and Radiative Transitions

Electromagnetic interactions of Σ's can be studied[5,6,9] in FNAL experiment E781 with high energy hyperon beams via the Primakoff interactions of incident Σ's with a virtual photon in the Coulomb field of a target nucleus of atomic number Z. The decay signature for $\Sigma^*(1385)$ $3/2^+$ production is clean as it decays to $\Lambda\pi$, and the Λ to π^-p. The process is shown in Fig. 1. Such radiative transition studies were first suggested by Lipkin[10] and considered in more detail afterwards.[5,11,12] The Σ Compton scattering and associated polarizabilities can be studied[5,9] following a Primakoff interaction by detecting the final state gamma ray and Σ in coincidence. The process is shown in Fig. 2 for a pion or Sigma beam. Sigma form factors and charge radii can be measured[5] by scattering 600 GeV Σ's from electrons in a liquid Hydrogen or a Carbon target. Such data test predictions of these quantities, such as the quenched lattice QCD calculations[13] that give a significantly larger radius (0.2 fm) for Σ^+ compared to Σ^-.

The Σ^+ (uus) and Σ^- (dds) baryons are of interest because electromagnetic observables are particularly sensitive to their underlying quark structure. The Σ^+ differs from the proton only by replacing the d quark by a strange quark which also has charge -1/3. Thus, any difference between the electromagnetic properties of the Σ^+ and proton can only arise from flavor SU(3) symmetry breaking. The two Σ states are isospin mirrors of one another, symmetrically placed in the same flavor SU(3) octet and have very similar strong interactions. However, their electromagnetic interactions are completely different because the Σ^+, like the nucleon and Ξ^o, have valence quarks of two flavors having the opposite sign of electric charge. External electromagnetic fields therefore exert forces in opposite directions on the two flavors and rotate spins in opposite directions, thereby producing internal excitation. The Σ^- on the other hand, and also the Ξ^-, have three valence quarks all with charge -1/3, and the principal effect of an external electromagnetic field is to exert forces in the same direction on all three valence quarks and rotate their spins in the same direction. This produces no internal excitation. We discuss below experimental implications of this effect, first noted[10] by a selection rule involving the U-spin SU(2) subgroup of SU(3). U-spin is conserved to all orders in any combination of electromagnetic interactions and strong interactions invariant under SU(3), and the resulting SU(3) prediction is that the Primakoff excitation $\Sigma^- \rightarrow \Sigma^{*-}$ is forbidden while excitation of $\Sigma^+ \rightarrow \Sigma^{*+}$ is allowed. The U-spin values of interest are U=1/2 for Σ^-, Σ^+, $\Sigma^+(1385)$ and U=3/2 for $\Sigma^-(1385)$.

The E1 and M1 Σ transitions are related to the intrinsic electric and magnetic Σ polarizabilities. We will elucidate below this connection, which can be tested experimentally. Hadron electric (α) and magnetic (β) intrinsic polarizabilities characterize the induced transient dipole moments. During γ-hadron Compton scattering, the lowest order scattering (Thomson) is determined by the charge and magnetic moment. The next order scattering (Rayleigh) is determined by the induced dipole moments. The Compton cross section data determine the Compton polarizabilities $\bar{\alpha}$ and $\bar{\beta}$ expressed here in Gaussian units of 10^{-43} cm^3. The angular distribution formulae for low γ-ray energies in terms of $\bar{\alpha}$ and $\bar{\beta}$ for γp scattering are given by Petrun'kin and L'vov,[1,2] and similar expressions apply for the Σ hyperons. Perturbation theory for the Σ^+, Σ^-, and proton polarizabilities

can be applied, leading to the expressions[1] of Petrun'kin:

$$\bar{\alpha} = 2\sum \frac{|\langle 0|\vec{d}_z|n\rangle|^2}{E_n - E_0} + \frac{1}{3}\frac{e^2}{M}\langle r^2\rangle = \alpha + \Delta\alpha, \qquad (1)$$

$$\bar{\beta} = 2\sum \frac{|\langle 0|\vec{\mu}_z|n\rangle|^2}{E_n - E_0} - k\frac{e^2}{M}\langle r^2\rangle = \beta + \Delta\beta. \qquad (2)$$

Here $\vec{d} = \sum e_k \vec{r}_k$ and $\vec{\mu}$ are the electric and magnetic dipole operator respectively, and the coefficient k will be discussed below. The first and second terms in these equations give the intrinsic and form factor (center of charge oscillation) contributions, respectively. The sums are over all E1 and M1 excitations. The intrinsic polarizabilities probe the internal structure of baryons and mesons.

Many theoretical and experimental polarizability studies have been made for the proton and neutron[14,15]; but none for the Σ. In the proton polarizability calculation of Weiner and Weise,[15] the intrinsic part is mainly due to the charged pion or kaon cloud surrounding the proton core. We consider here a much simpler non-relativistic quark bag calculation[1,5] with no pion cloud, for the analogous Σ^+ polarizabilities. We need to take into account the rms charge radii[13] of these hadrons ($R(\Sigma^+) \sim 0.96$ fm, $R(p) = 0.86$ fm, $R(\Sigma^-) \sim 0.76$ fm), the masses and rms radial positions[13] of the quarks ($m_s \approx 5/3\ m_{u,d}$; $r_{u,d} \sim 0.84$ fm, $r_s \sim 0.56$ fm for the Σ), and the intrinsic quark radius (taken to be to be $\rho_q = 0.41$ fm). The latter value is fixed here as previously[4] to achieve agreement with the dispersion sum rule for protons: $\bar{\alpha} + \bar{\beta} = 14.2$. We then obtain $k = 0.68, 0.60, 0.26$ for the proton, Σ^+, and Σ^- respectively.

The odd parity $\Sigma^*1/2^-$ and $\Sigma^*3/2^-$ states near 520 MeV excitation above the nucleon have the s orbit strange quark promoted to the p orbit. There are also excitations of the nonstrange quarks. The intrinsic contribution of eqn. 1 can be evaluated using closure by saturating the sum over these states, giving[1]:

$$\alpha_{\Sigma^+} \sim \frac{2}{\Delta E}\langle\Sigma^+|(\sum q_i z_i)^2|\Sigma^+\rangle^2 \sim \frac{2}{3}\frac{\langle r^2\rangle}{\Delta E}e^2\left(\frac{4}{9} + \frac{4}{9} + \frac{1}{9}\right) \approx 17.1. \qquad (3)$$

In principle, $< r^2 >= (m_q \Delta E)^{-1}$ for constituent quarks of mass $m_q \sim 0.34$ GeV bound in a harmonic oscillator well, so that $< r^2 >^{1/2} \sim 0.5$ fm is fixed by ΔE.[15] With a simplified calculation similar to eqn. 3, one can obtain reasonable agreement for proton polarizabilities[4] by taking $< r^2 >^{1/2}$ to be larger (equal to the experimental root mean square radius) and independent of ΔE. We follow this approach also for the Σ hyperon. The intrinsic magnetic polarizability can be evaluated by saturating the magnetic dipole excitations with the Σ^+ to Σ(1385) transition, giving[1,5]:

$$\beta_{\Sigma^+} \sim \frac{2}{M_{\Sigma^{*+}} - M_\Sigma}|\langle\Sigma^+|\vec{\mu}_z|\Sigma^*\rangle|^2 \sim \frac{2}{M_{\Sigma^{*+}} - M_\Sigma}\left(\frac{2\sqrt{2}}{3}\mu_{\Sigma^+}\right)^2 \sim 8.5, \qquad (4)$$

where μ_{Σ^+} is the Σ^+ magnetic moment. The Σ^+ to Σ^* magnetic dipole transition matrix element is written[1,5] in terms of the Σ^+ magnetic moment, following the nonrelativistic quark model. For β_{Σ^+}, the magnetic dipole transition to the Σ^* $3/2^+$ resonance saturates the magnetic dipole excitations, in analogy to the nucleon to Δ transition; the proton and Σ^+ have the same matrix element expression as members of the same U-spin doublet. For the proton intrinsic magnetic polarizability β_p, the analog of eqn. 4 gives[1] $\beta_p \approx 7.4$.

Consider matrix elements for magnetic moment operators $\vec{\mu}$ between states having the quark constituents of nucleons and Σ's. These are states (aab) for which the two quarks of flavor a are always nonstrange. In the SU(3) symmetry limit, the contributions to the magnetic moment of the odd d quark to μ_p and of the odd s quark to μ_Σ are equal. The fact that the magnetic moment of the Σ^+ is smaller than and that of the proton by 14% immediately shows that flavor SU(3) which predicts equal moments is broken. This breaking is much larger than expected and still lacks an adequate explanation. Consider experimental tests of SU(3) breaking mechanisms based on the assumptions that the u-flavor contributions to μ_p and μ_{Σ^+} are equal, that $SU(3)$ breaking only occurs in $\vec{\mu}_b$ where it is different for strange and nonstrange quarks, and that isospin symmetry is good. For magnetic moments, one can show[9] that the strange contribution to the magnetic moment is suppressed by an order of magnitude:

$$\frac{\mu_{\Sigma^+} + 2\mu_{\Sigma^-}}{\mu_p + 2\mu_n} \approx \frac{\langle\Sigma^+|\mu_s|\Sigma^+\rangle}{\langle p|\mu_d|p\rangle} \approx 0.11 \pm 0.04. \qquad (5)$$

The main physical difficulty is in the small value of the d quark contribution to the proton moment and the large contribution 2.45 n.m. of the u quarks. If the u quark contribution to μ_{Σ^+} is the same 2.45 n.m. as in the proton, then the experimental value $\mu_{\Sigma^+} = 2.42 \pm 0.02$ n.m. can be fit only by requiring a nearly vanishing s quark contribution.

That the strange quark contribution to μ_Σ is suppressed can also be seen from a different point of view. One can compare the the strange contributions to μ_Σ and μ_Λ, assuming only isospin symmetry and without using nucleon magnetic moments, thus minimizing effects of mass differences. One assumes that the spins of the nonstrange quarks in the Λ are coupled to zero, following conventional models. In this approximation[9]:

$$\frac{\mu_{\Sigma^+} + 2\mu_{\Sigma^-}}{3\mu_\Lambda} \approx \frac{\langle\Sigma^+|\mu_s|\Sigma^+\rangle}{\langle\Lambda|\mu_s|\Lambda\rangle} \approx 0.06 \pm 0.02 \qquad (6)$$

The strange quark contribution to μ_Σ is again seen to be anomalously low: only 6% of the strange contribution to μ_Λ and only 18% of the value -(1/3) obtained from the SU(6) wave function.

Experimental data on related processes may give additional insight. One such process involves octet-decuplet transitions for nucleons and Σ's. It will be interesting to measure these transitions and compare their systematics with those of the magnetic moments. In a description of SU(3) symmetry breaking in the Σ^- to Σ^{*-} transition, the ratio of M1 decay widths or of intrinsic magnetic polarizabilities for the Σ^- and proton can be estimated with the same assumptions described for eqn. 5. In that case[9,10]:

$$\frac{\Gamma(\Sigma \to \Sigma^{*-})}{\Gamma(p \to \Delta^+)} = \frac{(M_{\Sigma^{*-}} - M_{\Sigma^-})\beta_{\Sigma^-}}{(M_{\Delta^+} - M_p)\beta_p} \approx \frac{1}{9}\left(1 - \frac{\mu_s}{\mu_d}\right)^2 \approx 0.011. \qquad (7)$$

Here μ_s and μ_d are empirical magnetic moments of s and d quarks (estimated in a simple additive quark model[16] using proton, neutron, and Lambda magnetic moments, as $\mu_u = 1.852\mu_N$, $\mu_d = -0.972\mu_N$, $\mu_s = -0.613\mu_N$), the s and d values unequal due to SU(3) symmetry breaking. As shown in eqns. 5,6, μ_s may be significantly lower than the value fixed by the Lambda magnetic moment; which would significantly increase the predicted decay width of eqn. 7. Following the assumptions underlying eqns. 5-7, the Σ^- M1 transition width directly determines the relative magnitudes of the s and d-quark magnetic moments. Explicit quark model calculations[17] give a larger value of 0.034 for the ratio of eqn. 7, with $\Gamma(\Sigma^{*+}) = 104$ keV[17] and 117 keV[18]; and $\Gamma(\Sigma^{*-}) = 2.5$ keV.[17] Therefore these calculations correspond to $\Gamma(\Delta^+) = 74.3$ keV using eqn. 15 of Ref. 7. The Δ radiative width of the model is smaller than the experimental value, but this should not affect the reliability of the ratio calculation of eqn. 7. More recently, hyperon radiative transitions were calculated in a chiral bag model[19] and in an algebraic framework,[20,21] but these calculations are not yet available for the Σ transitions. One expects from eqns. (1-4,7) to observe very large and very small values of the intrinsic magnetic polarizability for the Σ^+ and Σ^-, respectively; and similarly for the Σ^* radiative decay width. With $\Delta E \sim 520$ MeV, we predict α_{Σ^+} =17.1, $\Delta\alpha_{\Sigma^+}$ =3.7, $\overline{\alpha_{\Sigma^+}}$ =20.8, β_{Σ^+} = 8.5, $\Delta\beta_{\Sigma^+}$ = -6.8, $\overline{\beta_{\Sigma^+}}$ = 1.7 . Similarly, α_{Σ^-} =3.4, $\Delta\alpha_{\Sigma^-}$ =2.3, $\overline{\alpha_{\Sigma^-}}$ =5.7, β_{Σ^-} = 0.12 from eqn. 7, $\Delta\beta_{\Sigma^-}$ = -1.8, and $\overline{\beta_{\Sigma^-}}$ = -1.7 .

The Σ beam at FNAL is polarized, so that asymmetry measurements are sensitive to the M1 or E2 nature of the exchanged photon, and therefore to the L=2 admixtures. The ratio E2/M1 of these amplitudes is a subject of considerable current interest[22,23] for the nucleon to Δ transition; so that measuring this ratio for the Σ^* (and Ξ^*) will be extremely valuable. The ratios may be different for Σ^*, Ξ^*, and Δ, given that the s-quark mass is significantly heavier than the d quark mass. The E2/M1 ratios for the Σ^{*-} and Σ^{*+}, would be similar if the SU(3) symmetry breaking in Σ^{*-} is comparable for both M1 and E2 transitions. However, the Σ^{*-} width estimate of Eqn. 7 is based on the form of the magnetic dipole operator, and is specific to a spin-flip M1 transition. The E2 transition width expected from SU(3) symmetry breaking depends on the form of the quadrupole operator; and on the extent to which the resulting Σ^{*-} state with L=2 has U=1/2 admixtures. One may expect therefore that the E2/M1 ratios are different for Σ^{*-} and Σ^{*+}.

III. Pion Polarizabilities

Recently, pion polarizabilty calculations were carried out by Bernard, Hiller, and Weise[24] emphasizing vector meson dominance diagrams, and by Bernard and Vautherin[25] within generalized SU(3) models. They find values for $\bar{\alpha}_\pi$ ranging from $\sim 7 - 14$. Holstein[26] shows that meson exchange via an axial meson pole diagram effectively provides the main contribution ($\bar{\alpha}_\pi = 2.6$) to the polarizability. For the $\gamma\pi$ interaction at low energy, chiral symmetry provides a rigorous way to make predictions. This approach[26-28] yields $\bar{\alpha}_\pi = -\bar{\beta}_\pi = 2.7 \pm 0.5$, where the uncertainty from Ref. 26 was set by the pion decay data used to fix the parameters of the Lagrangian. A recent quark confinement model calculation[29] gives $\bar{\alpha}_\pi \approx 3.63$ and $\bar{\beta}_\pi \approx -3.41$. Another theoretical approach based on dispersion sum rules[1,30] gives $\bar{\alpha}_\pi \approx 5.6$ and $\bar{\beta}_\pi \approx -5.2$, with very large (unstated) uncertainties.

For the pion polarizability, the $\gamma\pi$ scattering was measured[31,32] with 40 GeV pions at Serpukhov via radiative pion scattering in the nuclear Coulomb field ($\pi^- + Z \rightarrow \pi^- + Z +$ gamma) ; where the incident pion Compton scatters from a virtual photon in the Coulomb field of a nucleus of atomic number Z; and the final state gamma ray (typically 30 GeV) and pion (typically 10 GeV) were detected in coincidence. The process is shown in Fig. 2. This reaction is equivalent to $\gamma + \pi^- \rightarrow \gamma + \pi^-$ scattering for a laboratory gamma ray of several hundred MeV incident on a target π^- at rest. It is an example of the well tested Primakoff formalism[33,34] that relates processes involving real photon interactions to production cross sections involving the exchange of virtual photons. One test of the Primakoff formalism[34] is in fact a low-statistics radiative pion scattering experiment at 200 GeV, which determined $\gamma\pi$ Compton scattering cross sections that agreed with the Primakoff formalism to an accuracy of at least 8% at an 84% confidence level. Significant contributions of backgrounds would have spoiled the agreement. The statistics were too low to determine pion polarizabilities with reasonable uncertainties.

The pion electric polarizability $\bar{\alpha}_\pi$ was deduced[31,32] in a higher statistics experiment ($\sim$ 7000 events) to be:

$$\bar{\alpha}_\pi = -\bar{\beta}_\pi = 6.8 \pm 1.4_{stat} \pm 1.2_{syst}, \qquad (8)$$

where it was assumed in the analysis that $\bar{\alpha}_\pi + \bar{\beta}_\pi = 0$, as expected theoretically.[26] Charged pion polarizabilities were also deduced[35] from $\gamma\gamma \rightarrow \pi^+\pi^-$ data which is related to the Compton scattering by crossing symmetry; and from a Lebedev radiative pion photoproduction experiment,[36] $\gamma p \rightarrow \gamma\pi^+ n$, in which the incident γ-ray scatters from a virtual pion. The experimental values[35] for $\bar{\alpha}_\pi$ range from 2.2 to 26.3, and the large spread in values do not allow precision tests of any theory. The experimental situation points to the need for much higher quality data and more attention to the systematic uncertainties arising from different measurement and analysis techniques. A concerted experimental program on these questions is being developed at the LEGS,[37] DAΦNE,[38] and FNAL[5] facilities.

In the radiative pion scattering experiments, it was shown experimentally[31,32] and theoretically[39] that the Coulomb amplitude clearly dominates and yields sharp peaks in t-distributions at very small four momentum transfers to the target nucleus $t \leq 6\times10^{-4}(GeV/c)^2$. The gamma-pion Compton scattering for these experiments corresponds to gamma-ray energies in the range 60-600 MeV in the pion rest frame. The cross sections corresponding to the sharp peaks in the t-distributions for targets with different atomic number Z scaled as Z^2, further demonstrating the correspondence with the electromagnetic Compton effect. Background from other processes could easily be estimated and subtracted by extrapolating in t from events in the region of flat t-distribution of 3-8 $\times10^{-3}(GeV/c)^2$. The sources of these backgrounds are described below.

For gamma-pion Compton scattering, the Compton amplitude in principle may include contributions of pion or rho rescattering. The rescattering diagram (Fig. 3) includes two vertices, one for the pion strong interaction (with two real and two virtual pions), and one for the Compton effect with the virtual pions. Some of these contributions for the conditions of the 40 GeV pion experiment were evaluated theoretically[40] and were claimed to affect the determination of the pion polarizabilities at the level of 10%. Babusci et al.[35] give explicit and complete

formulae for one-loop rescatterings. Such effects were also discussed in connection with recent π^0 polarizability determinations.[35,41] Filkov[42] uses dispersion relationships to evaluate such rescatterings, implicitly taking into account loop corrections to all orders. In addition, the 200 GeV experiment[34] described above determined $\gamma\pi$ Compton scattering cross sections for E(V) = 240 - 1225 MeV, and the data agreed well with the Primakoff formalism. Significant contributions of rescattering diagrams would have spoiled the agreement.

Another background is the coherent strong process of pion elastic scattering accompanied by gamma emission. Such events when mediated by particle exchange will not have the sharp t-distribution peak of the Compton scattering. This process is described theoretically in terms of the exchange with the nucleus of a neutral meson such as a π^0, f_2, ρ, ω. Following this exchange, an intermediate state is formed which then decays to a gamma ray and a pion. In principle, diffractive production of a $\gamma\pi$ final state is also possible via elastic scattering mediated by Pomeron exchange, followed by bremsstrahlung. One may expect such a process to be very weak, but calculations are not available. The t-dependence would not be as steep, and the amplitude should be almost orthogonal to that from the Coulomb contribution. In the fit to the data, one could add a photon exchange and an incoherent part from pomeron exchange, and determine experimentally what is needed. However, it may not be easy to separate the contributions. One can expect also that the mass spectrum from the two sources may also be different. For an incident pion at 40 GeV and $\sqrt{s} \leq 3.2m_\pi$. Gal'perin *et al.*[39] estimated that particle exchange strong cross sections account for only 2.5% of the cross section below t= 2×10^{-4} $(GeV/c)^2$ for a carbon target, which is consistent with the data of Antipov *et al.*[31,32] This background is expected to decrease with increasing s, and this is consistent also with the t-distribution data for 200 GeV experiments.[33,34]

Other backgrounds come from the higher cross section inelastic channels $\gamma + \pi^- \rightarrow \rho^- \rightarrow \pi^- + \pi^0$; and $\gamma + \pi^- \rightarrow A_1(1260) \rightarrow 3\pi$. These were studied in their own right , the former[33] to measure the radiative decay of the ρ^-; and the latter[44] to study the radiative decay of the $A_1(1260)$. Background events result when only one of the gamma rays from a π^0 decay reaches the detector or exceeds the detector threshold, or when the detector angular resolution is inadequate to separate the two π^0 decay gamma rays.

One must also evaluate *electromagnetic* corrections to the process of radiative pion scattering of high energy pions in the Coulomb field of a nucleus, where the requirement is to measure only single photon bremsstrahlung emission. Here the detailed properties of the gamma detector are important, such as the photon detector threshold, t-resolution, and the two-photon angular resolution. For the setup of Antipov *et al.*[31,32] at 40 GeV with $t \leq 2 \times 10^{-4}$ $(GeV/c)^2$ for a carbon target, electromagnetic double bremsstrahlung and loop corrections (Fig. 4) were estimated[45] to affect polarizability determinations at the level of 30%. These corrections can be made smaller with improved detectors and lower detector thresholds. Such calculations need to be carried out for the conditions of the planned 600 GeV FNAL experiment. Here again, it is encouraging that the 200 GeV experiment was not significantly affected by such corrections.

To specifically illustrate some of the kinematics germane to a FNAL experiment, the reaction:

$$\pi + Z \rightarrow \pi' + Z' + \gamma' \tag{9}$$

is considered for a 600 GeV incident pion, where Z is the nuclear charge. The 4-momentum of each particle is P_π, P_Z, $P_{\pi'}$, $P_{Z'}$, k', respectively. In the one photon exchange domain, eqn. 9 is equivalent to:

$$\gamma + \pi \rightarrow \gamma' + \pi', \tag{10}$$

and the 4-momentum of the incident virtual photon is k = P_Z-$P_{Z'}$. The cross section for the reaction of eqn. 9 can be written as:

$$\frac{d\sigma}{dtdsd\Omega} = \frac{Z^2\alpha_f}{\pi} \frac{|F(t)|^2}{s - m_\pi^2} \frac{t - t_0}{t^2} \frac{d\sigma_{\gamma\pi}}{d\Omega}, \tag{11}$$

where $d\sigma_{\gamma\pi}/d\Omega$ is the unpolarized differential cross section for eqn. 10 (for real photons), t is the square of the four-momentum transfer to the nucleus, F(t) is the nuclear form factor (essentially unity at small t-values), $\sqrt{s}$ is the mass of the $\gamma\pi$ final state, and t_0 is the minimum value of t to produce a mass $\sqrt{s}$. The quantities s and t are Lorentz invariants. Eqn. 11 assumes that the atomic electrons do not screen the nuclear Coulomb field. This is valid as long as the incident energy is not too high, else t_0 will be so small so as to correspond to an impact parameter b large enough to be affected by the electron cloud of the atom ($t_0 \sim b^{-2}$). At 600 GeV, the impact parameter is $\sim$ 500 mfm, and the screening factor that may effectively reduce the Z value needs to be evaluated. No such factor was required to describe the 200 GeV radiative pion data,[34] where the impact parameter was $\sim$ 50 mfm. The analysis to determine polarizabilities by fitting the data use formula for $d\sigma_{\gamma\pi}/d\Omega$. This cross section depends on the polarizabilities and on s and on t_1, the square of the 4-momentum transfer between initial and final state γ's. We have:

$$t = k^2 \equiv -M(V)^2, \tag{12}$$

where k is the 4-momentum transferred to the nucleus, and M(V) is the virtual photon mass. Since $t = 2M_Z(E_{Z',lab} - M_Z) > 0$, the virtual photon mass is imaginary. To approximate real pion Compton scattering, the virtual photon must be almost real; and so M(V)<0.0167 GeV corresponding to $t < 2.8 \times 10^{-4} (GeV/c)^2$ can be required in the experiment. In addition,

$$-s = (P_{\pi'} + k')^2 \equiv -M(\gamma\pi)^2, \tag{13}$$

where $M(\gamma\pi)$ is the $\gamma\pi$ invariant mass. The minimum value for t[43] is given by:

$$t_0 \sim (s - m_\pi^2)^2/4|\vec{P}_\pi|^2, \tag{14}$$

corresponding to $t_0 \sim 5.4 \times 10^{-8} (GeV/c)^2$ for $\sqrt{s} = 1.75m_\pi$ at 600 GeV incident energy. If the gamma detector threshold is set very low, the minimum measurable transfer will approach t_0. With lead glass detectors,[31,32] a t-resolution of the order of $\sigma_t \sim 6.0 \times 10^{-4} (GeV/c)^2$ was achieved at 40 GeV, where the experimental γ-ray energy resolution was the main limiting factor. The t-distributions are plotted with a bin width that matches the t-resolution. This t-resolution therefore set the experimental maximum in t for accepted events, since the experimental Primakoff

cross section is taken from all the events in the first bin of the t-distribution. With an improved γ-ray detector, it should be possible to achieve somewhat better t-resolution, and to obtain a major fraction of the Compton cross section using an experimental maximum limit for accepted events of $t = 2.8 \times 10^{-4}$ (GeV/c)^2, or even lower. The maximum of the differential cross section for reaction (9) occurs at t=2t_0 and grows as $|t_0|^{-1} \sim (\vec{P}_\pi)^2$, where $\vec{P}_\pi$ is the laboratory incident pion 3-momentum. The integrated Compton cross section up to $t = 2.8 \times 10^{-4}$ (GeV/c)^2 grows less slowly, as $\ln(\vec{P}_\pi)$. Integrating the cross section expression eqn. 11 from t_0 to t=100t_0 gives essentially the entire Primakoff cross section one observes in the first t-bin. With this experimental limit and strong backgrounds that decrease with increasing incident energy, the percent strong background would decrease from the estimated[39] 2.5% at 40 GeV discussed previously to a yet smaller value at 600 GeV at FNAL. The strong backgrounds are associated with particle exchange, and such cross sections are known to fall rapidly with increasing energy. From this point of view, the t-resolution is not a critical parameter for 600 GeV experiments.

The energy of the incident photon in the pion rest frame is:

$$E(V) = (s - m_\pi{}^2 + t)/2m_\pi \sim (s - m_\pi{}^2)/2m_\pi \qquad (15)$$

at small t; so that the energy of the virtual photon is determined by s. The elemental cross section at low E(V) is a function of E(V), $cos(\theta)$, $\bar{\alpha}$, $\bar{\beta}$; where θ is the Compton scattering angle in the pion rest frame. In this frame, the nucleus Z represents a beam or cloud of virtual photons sweeping past the pion. One should require that E(V) be sufficiently low in energy, such that ρ meson production does not occur for an incident γ-ray on a target pion at rest. The γ-ray energy required to produce a ρ meson, not counting the ρ width, is given by:

$$\omega = E(V) = (M_\rho^2 - m_\pi^2)/(2m_\pi) = 2.0GeV. \qquad (16)$$

Considering the ρ width, one should limit the incident energy to be lower than 1 GeV, corresponding to $s < 15.3m_\pi^2$.

There is another condition that limits the s and t_1 range for the analysis. One fixes the polarizabilities by a maximum likelihood fit to the data, using eq. 11 with an appropriate formula for $d\sigma_{\gamma\pi}/d\Omega$. One can use for example the formulae from Filkov[42] based on a low energy expansion of the scattering amplitude or from Babusci et al.[35] based on chiral perturbation theory including all one-loop diagrams. The two formulae agree[35] only for $s=m_\pi^2$, where loop corrections are zero. Filkov claims that his formulae implicitly have all multi-loop diagrams included through the polarizabilities. Using the different formulae will lead to somewhat different results for the polarizabilities. The $\gamma\gamma \rightarrow \pi^+\pi^-$ reaction was analyzed[35] for pion polarizabilities with the condition that the invariant energy of the $\pi^+\pi^-$system be less than approximately 0.42 GeV. This requirement was set by the range of validity of the chiral perturbation formulae that were used in the fitting. By crossing symmetry, this limit for the Compton scattering translates to a maximum value of 0.42 GeV (or 3.m_π) for $\sqrt{-t_1}$. In the $\gamma\pi$ center of mass frame, the photon energy and momentum is given by :

$$\omega = K = (s - m_\pi{}^2)/2\sqrt{s} \qquad (17)$$

and

$$t_1 = -2K^2(1 - x) = -(1 - x)(s - m_\pi^2)^2/2s, \qquad (18)$$

where x = $\cos(\theta_{\gamma,\gamma'})$. For 180 degree scattering, x=-1, and the value of t_1 at x=-1 defines a curve in the s-t_1 plane, with:

$$t_1(-1) = -(s - m_\pi^2)^2/s. \qquad (19)$$

At s= 10.9m_π^2, t_1(-1) = -9.m_π^2. At lower values of s, the quantity -t_1 will be less than 9.m_π^2 for all angles up to 180 degrees. At higher values, it will satisfy this condition only for more forward angles. Thus, the conditions -t_1(max) < $9.m_\pi^2$ and $s < 15.3m_\pi^2$ together with eqn. 18 define a two-dimensional area in s-t_1 Compton scattering space, for which the one-loop chiral perturbation formulae may be used. Even in this space however, multi-loop diagrams can contribute. Filkov checked his Compton scattering formula by comparison with dispersion relationship calculations and claimed that the formula and dispersion relationships give comparable results to 10% for s up to 10.m_π^2 for all angles. In that case, it could also be used outside the restricted s-t_1 region just described for using the chiral perturbation theory formulae. The data analysis with both formulae could be done separately for different regions of s-t_1 space.

Consider the case of 600 GeV incident laboratory pions. Figures 5-6 show as a function of final photon laboratory angle for $M(\pi\gamma)/m_\pi$ = 1.75 and M(V) = 0.0167 GeV, the laboratory angles of the final state pion and γ-ray (Fig. 5); and the laboratory kinetic energy of the final pion and γ-ray (Fig. 6). The ranges in the figures are due to the azimuthal angle ranges ϕ of the recoiling nucleus. The figures show results in the laboratory frame for outgoing γ-rays emitted up to 5 mrad, and the corresponding outgoing pions emitted up to 0.3 mrad. The angular resolution for the pion is roughly 0.04 mrad due to multiple scattering in the Primakoff target and in the in-beam tracking detectors. Such resolution does not allow an adequate determination of the recoil azimuthal angle. The very small t associated with the pion polarizability data makes it difficult to define the normal to the production plane, and therefore the azimuthal angle. Otherwise, one could fix polarization direction of the virtual photon in Primakoff to be either helicity +1 or -1 along the exchange direction, and the angular distribution for decay into the final $\gamma\pi$ system would show a characteristic ϕ dependence with respect to this direction. The gamma ray energies considered then range from 0 - 400 GeV, and the corresponding outgoing pion energies range from 200 - 600 GeV. The corresponding Compton scattering angular range is 0 - 180 degrees in the π rest frame. In practice, the most forward Compton scattering angles are less accessible, as they correspond to the larger γ-ray angles in the laboratory frame which can miss the γ-ray detector, and where the γ-ray energies are also possibly below the detector threshold. But these forward angles are anyhow not sensitive to the polarizabilities, as discussed below. The corresponding γ-ray angles for the Sigma experiment extend to 14 mrad, exceeding the geometric acceptance of the detector.

The pion and gamma-ray angles in E781 are measured to high precision of $\pm$ 0.04 mrad; matching adequately the angular range shown in Figs. 5. The final state pion and Sigma will be measured[5,6] in the Fermi Lab E781 SELEX magnetic spectrometer while the final state γ-ray will be measured in a new segmented lead glass electromagnetic calorimeter. The laboratory decay length ($L = \gamma\beta c\tau$)

for pions and kaons and very high energy Σ's exceeds ten meters, so that easy magnetic detection is possible. Transition radiation detectors upstream of the target and ring Cerenkov detectors downstream will provide excellent particle identification. The data selection criteria requires one photon and one charged particle in the final state, their total energy consistent with the beam energy, small t, and other position, angle, and energy conditions. A suitable Primakoff trigger is being developed. At lower beam energies, the $\bar{p}$ and kaon fluxes are higher, and Primakoff studies become possible for these particles. As a check of systematic errors, one should study proton polarizabilities by the Primakoff effect, to compare to determinations with real γ-ray beams.

We consider briefly the uncertainties achievable for the polarizabilities in the FNAL E781 experiment, based on Monte Carlo simulations currently in progress. An important consideration is the information content of the data versus x and s, where x=cos(θ). In Fig. 7, we show the fraction of the $\gamma\pi$ Compton cross section arising from the $\bar{\alpha}$ terms in the $\gamma\pi$ center of mass cross section expression, for $\bar{\alpha}$=6.8, using the one-loop chiral Compton formulae. This figure shows that high s values and back angles (large t_1) have maximal information content for the polarizabilities. For example, the fraction of the cross section at back angles due to the polarizability term is only 5% at E(V) = 140 MeV, and roughly 30% at E(V) = 600 MeV. Starkov *et al.*[43] also give cross section predictions for pion Compton scattering. As discussed previously, the data analysis must be restricted in the s-t_1 space. The back angle region at high E(V) is not included in the analysis with the chiral formulae, but can be with the Filkov formula. The angular acceptance and detector threshold of the γ-ray calorimeter in E781 allows measuring more complete angular distributions than was achievable in the 40 GeV experiment.

We considered initially a beam energy of 600 GeV, a ^{12}C target, and an s-range of 2.2 - 4 m_π^2, corresponding to a Primakoff cross section of 2.6 μb, and E(V) $\sim$ 100-200 MeV. We take the π-Carbon total cross section at 600 GeV to be 192. mb, which is eight times the total inelastic π-nucleon cross section at 600 GeV. Considering shadowing for a light nucleus such as Carbon, approximately 8 nucleons are effective. We take the total inelastic cross section, since we require both a pion and gamma in the final state. We assume the use of a 5% interaction target which is required to achieve the rate needed for the charm trigger component of FNAL E781. The probability P per incident pion for a Primakoff interaction is then

$$P = 0.05 \times \frac{2.6 \times 10^{-6}}{192. \times 10^{-3}} = 6.8 \times 10^{-7}. \qquad (20)$$

The planned hyperon channel beam rate is 2 MHz, with roughly 60% Σ^- and 40% π^- beam composition. With an expected π^- rate of 0.8 MHz, one expects 0.5 Primakoff events per second. A Fermilab beam spill is 20 seconds, so that one expects 10 events per spill. There are 60 spills per hour, and therefore 600 events per hour. Since the experiment is approved to run in 1994/5 for 1600 beam hours, one expects roughly 1 million events in the E(V) energy region of 100 - 200 MeV. With such statistics, $\gamma\pi$ Compton scattering angular distributions can be determined separately for different ranges of s. We will analyze data in restricted s-t_1 regions for polarizability purposes, and at higher energies and angles for other physics involving multi-loop effects and the ρ meson properties. We cite here some initial Monte Carlo results for 40 and 600 GeV Primakoff experiments on Carbon, assuming the dispersion sum rule result $\bar{\alpha}+\bar{\beta}$ = 0.39 and also $\bar{\alpha}$=6.8. At 40 GeV, for 74,000 events in an s interval (2.2 - 4.)m_π^2, we find by fitting the simulated data that $\bar{\alpha} = 7.8 \pm 1.4$, roughly the uncertainty claimed by Antipov *et al.* for 10 times less events. This initial simulation includes only statistical errors, without the effects of experimental resolutions and acceptances. The reason we obtain a similar error to Antipov *et al.* is that they analyzed data at higher s (up to 10.m_π^2), and such data appear more sensitive to $\bar{\alpha}$. For E781 at 600 GeV, the Primakoff cross section is higher than at 40 GeV by a factor 1.7, and the statistics will be far superior than that of Antipov *et al.*. At 600 GeV, for 140,000 events in an s interval (2.2 - 4.)m_π^2, we find by fitting the simulated data that $\bar{\alpha}$ = 6.6 $\pm$ 0.9. For E781, with 10^6 events expected in this s interval, the statistical uncertainty will be reduced to 0.34 . A more correct analysis will restrict the angular range of such data, as described above. Data in different s-t_1 intervals will give independent values for the polarizability, which will help understand multi-loop effects, and thereby control the systematic uncertainties. Although the Monte Carlo simulations are not yet completed, the objective of obtaining pion polarizabilities with significantly smaller statistical and systematic uncertainties looks very promising.

IV. Conclusions

The beams at Fermilab invite hadron Compton scattering and radiative transition studies for different particle types, such as $\pi^{+,-}$, $K^{+,-}$, p, antiprotons, sigma and cascade and lambda hyperons, and others. Because these transitions involve the well understood electromagnetic process, they provide precision tests of the quark wave functions characterizing the configurations of the low lying excited states of hadrons. The 600 GeV beam energy at FNAL is important to get a good yield for low t events in the radiative scattering, and also to reduce backgrounds from the decay of unstable hadrons by significantly boosting their lifetime. We will measure the $\gamma\pi$ and $\gamma\vec{\Sigma}$ Compton scattering cross sections, thereby enabling precision determinations of the pion and Sigma polarizabilities. E781 will also measure the formation and decay of the Σ^-(1385) and Σ^+(1385) hyperon excited states. These various Σ and pion experiments, including studies of the sigma form factors described earlier, will allow serious tests of chiral symmetry and chiral perturbation theory; and of different available polarizability and radiative decay calculations in QCD. The Σ experiments will shed new light on puzzles associated with the size of the s-quark magnetic moment and the quark radial wave functions.

Acknowledgements

This work was supported by the U.S.-Israel Binational Science Foundation, Jerusalem, Israel. Thanks are due to S. Gerzon and G. Giordano for valuable collaborations on the Monte Carlo simulations; and to D. Babusci, S. Bellucci, M. Blecher, V. Chaloupka, P. Cooper, T. Ferbel, L. Filkov, L. Frankfort, J. Lach, H. J. Lipkin, A. L'vov, G. Matone, J. Russ, A. Sandorfi, and R. Woloshyn for valuable discussions.

Figure Captions

Fig. 1: Primakoff production of an excited $\Sigma^+(1385)$.

Fig. 2: Primakoff effect for Compton scattering of a pion or Sigma.

Fig. 3: Typical one-loop diagram for pion rescattering.

Fig. 4: Typical loop and double bremsstrahlung diagrams for electromagnetic corrections to the Compton effect.

Fig. 5: The laboratory angle of the final state pion as a function of the final state γ-ray angle for E(π)= 600 GeV incident energy, M(V)=0.0167 GeV, M($\pi\gamma$)/M(π)=1.75. The range of values is associated with the recoil polar angles of the nucleus.

Fig. 6: The laboratory energy of the final state pion and γ-ray as a function of the final state γ-ray angle for the conditions of Fig. 1.

Fig. 7: The fractional part of the two-body $\gamma\pi$ Compton scattering cross section due to polarizability, as a function of x=cos(θ) and s in the $\gamma\pi$ center of mass system.

Fig. 1:

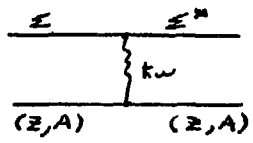

Fig. 2:

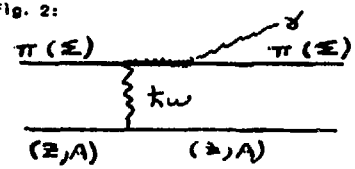

Fig. 3:

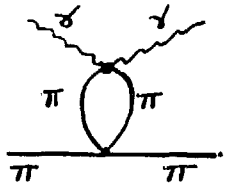

Fig. 4:

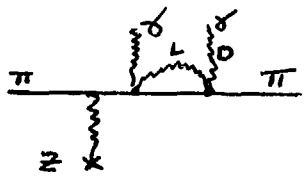

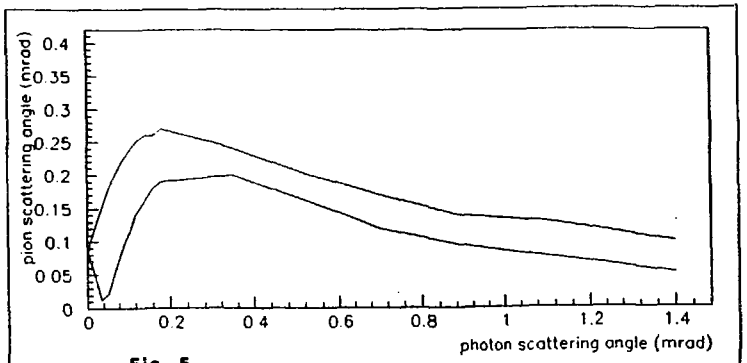

Fig. 5

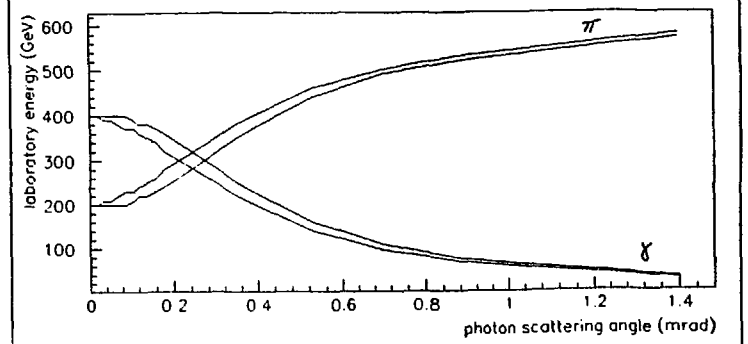

Fig. 6

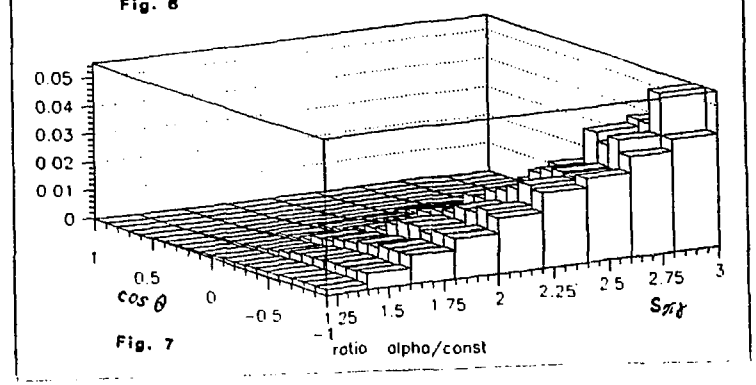

Fig. 7

REFERENCES

1. V. A. Petrun'kin, Sov. J. Part. Nucl. 12, 278 (1981).
2. A. I. L'vov, Sov. J. Nucl. Phys. 42, 583 (1985).
3. J. L. Friar, Workshop on Electron-Nucleus Scattering (1988, EIPC), Eds. A. Fabrocini *et al.*, World Scientific Publishing Co. (1989).
4. M. A. Moinester and M. Blecher, Proceedings of the Workshop on Science at the KAON Factory, July 1990, TRIUMF, Vancouver, B.C., Canada. TRIUMF preprint TRI-PP-90-60.
5. M. A. Moinester, Proceedings of the Conference on the Intersections Between Particle and Nuclear Physics, Tucson, Arizona, 1991, AIP Conference Proceedings 243, P. 553-558, 1992, Ed. W. Van Oers.
6. J. Russ, spokesman, FNAL E781, Institutions: Carnegie-Mellon, Fermilab, Beijing, SPNPI (St. Petersburg), ITEP (Moscow), U. Iowa, Sao Paulo, Rio de Janerio, U. Bristol, U. Washington, U. Rochester, and Tel Aviv U.
7. M. A. Moinester, C. B. Dover, H. J. Lipkin, BNL preprint BNL-47559, Phys. Rev. C., 1992, in press.
8. M. Zielinski *et al.*, Z. Phys. C - Particles and Fields 31, (1986) 545.
9. H. J. Lipkin and M. A. Moinester, Tel Aviv U. preprint TAUP 1968/92, Phys. Lett., 1992, in press.
10. H. J. Lipkin, Phys. Rev. D7, 846 (1973).
11. T. Goldman *et al.*, In Physics with LAMPF II, LA-9798-P, P. 319 (1984).
12. M. V. Hynes, In Physics with LAMPF II, LA-9798-P, P. 333 (1984).
13. D. B. Leinweber, R. M. Woloshyn, T. Draper, Phys. Rev. 43D, 1659 (1991).
14. J. Schmiedmayer *et al.*, Phys. Rev. Lett. 66, 1015 (1991).
15. R. Weiner and W. Weise, Phys. Lett. 159B, 85 (1985).
16. Particle Data Group, G.P.Yost et al., Phys. Lett. B204, 1 (1988).
17. J. W. Darewych *et al.*, Phys. Rev. 28D, 1125 (1983).
18. E. Kaxiras, E. J. Moniz, M. Soyeur, Phys. Rev. 32D, 695, (1985).
19. Y. Umino and F. Myhrer, Preprint SUNYSB-NTG-92-07, (Nucl. Phys. A).
20. F. Iachello and D. Kusnezov, Phys. Lett. 255B (1991) 493; Phys. Rev. D23 (1992), in press.
21. A. Leviatan, Abstract 35, International Conference on the Structure of Baryons and Related Mesons, June 1-4, 1992, Yale. U.
22. R. Davidson, N. Mukhopadhyay, R. Wittman, Phys. Rev. 43D, 71 (1991).
23. S. Nozawa, B. Blankleider, T.-S. H. Lee, Nucl. Phys. A513, 459 (1990).
24. V. Bernard, B. Hiller, W. Weise, Phys. Lett. B159, 85 (1988).
25. V. Bernard and D. Vautherin, Phys. Rev. D40, 1615 (1989).
26. B. R. Holstein, Comments Nucl. Part. Phys. 19, 239 (1990).
27. J. F. Donoghue and B. R. Holstein, Phys. Rev. 40D, 2378 (1989).
28. S. Bellucci, Proc. "Workshop on Physics and Detectors for DAFNE", Summary section, April 9-12, 1991 Frascati.
29. M. A. Ivanov and T. Mizutani, Phys. Rev. 45D, 1580 (1992).
30. L. V. Fil'kov, I. Guiasu, E. E. Radescu, Phys. Rev. 26D, 3146 (1982).
31. Yu. M. Antipov *et al.*, Phys. Lett. 121B, 445 (1983).
32. Yu. M. Antipov *et al.*, Z. Phys. C- Particles and Fields 26, 495 (1985).
33. T. Jensen *et al.*, Phys. Rev. 27D, 26 (1983).
34. M. Zielinski *et al.*, Phys. Rev. 29D, 2633 (1984).
35. D. Babusci, S. Bellucci, G. Giordano, G. Matone, A. M. Sandorfi, M. A. Moinester, Phys. Lett. B277, 158 (1992); and private communication.
36. T. A. Aibergenov et al., Czech. J. Phys. 36, 948 (1986).
37. A. M. Sandorfi *et al.*, IEEE NS30, 3083 (1983); C. E. Thorn et al., Nucl. Inst. Meth. A285, 447 (1989).
38. D. Babusci et al., "Workshop on Physics and Detectors for DAFNE" p. 383, April 9-12, 1991, Frascati.
39. A. S. Gal'perin *et al.*, Sov. J. Nucl. Phys. 32, 545 (1980).
40. G. V. Mitsel'makher and V. N. Pervushkin, Sov. J. Nucl. Phys. 37 (4), (1983).
41. A. E. Kaloshin and V. V. Serebryakov, Phys. Lett. 278B (1992) 198.
42. L. Filkov, Sov. J. Nucl. Phys. 41 (1985) 991; and private communication.
43. N. I. Starkov, L. V. Fil'kov, and V. A. Tsarev, Sov. J. Nucl. Phys. 36, 707 (1982).
44. M. Zielinski *et al.*, Phys. Rev. Lett. 52 (1984) 1195.
45. A. A. Akhundov, D. Yu Bardin, G. V. Mitsel'makher, Sov. J. Nucl. Phys. 37 (2), (1983).

The Quadrupole Amplitude in the $\gamma N \leftrightarrow \Delta$ Transition

A. M. Bernstein
Physics Department and Laboratory for Nuclear Science
Massachusetts Institute of Technology
Cambridge, MA 02139

S. Nozawa
Department of Physics
Queen's University, Kingston, Ontario, Canada K7L 3N6

M. A. Moinester
School of Physics and Astronomy
Raymond and Beverly Sackler Faculty of Exact Sciences
Tel Aviv University, 69978 Tel Aviv, Israel

Abstract

The presence of the tensor part of the color hyperfine interactions between quarks leads to a small electric quadrupole amplitude in the $\gamma N \leftrightarrow \Delta$ excitation. The difficulties in extracting this small amplitude with an appreciable background contribution from experiment is discussed. Furthermore, it is demonstrated that the available pion photoproduction data have a low sensitivity to the resonant (isospin $\frac{3}{2}$) electric quadrupole amplitude, $E_{1+}(\frac{3}{2})$. We show that $\gamma p \longrightarrow \pi^0 p$ cross sections near 0° and 180° and also those with polarized γ-rays near 90° will have the maximum sensitivity to the resonant $E_{1+}(\frac{3}{2})$ amplitude.

I Introduction

In analogy with the atomic hyperfine interaction, the interaction between quarks is believed to have a tensor component.[1,2] This gives the d-state admixture in the predominant s-state wave functions for the nucleon and Δ. This also leads to important predictions[2] about hadron structure including mass splitting, decay probabilities, nonzero quadrupole moments of the Δ and Ω^-, and a non-zero electric form factor for the neutron.[2,3] The tensor interaction between quarks also leads to a resonant ($I = \frac{3}{2}$) electric quadrupole amplitude $E_{1+}(\frac{3}{2})^*$ in the $\gamma N \leftrightarrow \Delta$ transition, which is primarily an $I = \frac{3}{2}$ magnetic dipole $M_{1+}(\frac{3}{2})$ transition. An accurate measurement of the $E_{1+}(\frac{3}{2})$ amplitude is therefore of great importance in testing nucleon models.

---

* The amplitudes are denoted by $E_{l+}(I)$ and $M_{l+}(I)$, where l is the orbital angular momentum of the photoproduced pion, the $\pm$ sign refers to the total pion- nucleon angular momentum $j = l \pm 1/2$, and I is the isospin of the πN system. Thus $E_{1+}(\frac{3}{2})$ is the resonant electric quadrupole amplitude (E2) and $M_{1+}(\frac{3}{2})$ is the resonant magnetic dipole amplitude (M1).

One would naturally turn to the multipole analyses[4] of the $N(\gamma,\pi)$ reaction in order to determine the resonant $E_{1+}(\frac{3}{2})$ amplitude or equivalently the ratio $R_{EM} = E_{1+}(\frac{3}{2})/M_{1+}(\frac{3}{2})$ (or E2/M1) for the resonant amplitudes. The determination of the resonant $E_{1+}(\frac{3}{2})$ amplitude is difficult for several reasons. First, it is small compared to the dominant $M_{1+}(\frac{3}{2})$ amplitude. Second the relative magnitude of the background is large. Therefore it is difficult to avoid a model dependence in separating the background contribution from the entire $E_{1+}(\frac{3}{2})$ amplitude to get the resonant part. Previous empirical attempts[5-10] obtained a range of values from 0 to -5% for R_{EM} using available data. Since these analyses were based on essentially the same data, the spread in the values reflects a systematic error in the analysis. In order to understand the reason for this systematic variation, we have made, for the first time, a quantitative estimate of the effect of the resonant $E_{1+}(\frac{3}{2})$ amplitude on the observables. This paper is primarily motivated by the fact that new experimental facilities and techniques have made a more sensitive and accurate measurement of the quantities which are sensitive to the quadrupole amplitude in the $\gamma N - \Delta$ transition feasible. However, as will be discussed below, before these measurements can be properly interpreted one must be able to distinguish between the signal and the background. One difficulty is that the quadrupole amplitude is typically calculated in the framework of a quark model in which the channel coupling to the continuum is neglected. In practice this means that a phenomenological hadronic model must be used to extract the quadrupole amplitude from experiment. The connection between the extracted amplitude and that of the quark model is not entirely clear. Ultimately one needs a quark model with realistic continuum coupling so that the experimental data can be directly predicted.

II General Constraints on Resonant Multipoles

Since the $E_{1+}(\frac{3}{2})$ amplitude is small and very likely to have a large background component in addition to the resonant part,[11,12,13] it is important to discuss the basic quantum mechanics of resonance amplitudes.[14] First consider resonances in πN scattering. These are most generally defined as poles in the S matrix. However for a strong resonance with a smooth background (eg the Δ) one can describe the phase shift δ (in the p_{33} channel) as:

$$\tan\delta(W) = \frac{\Gamma}{2}(W_r - W)^{-1} + A(W) \qquad (1)$$

where Γ is the full width at half maximum, W is the total CM energy, W_r is the resonance energy and A(W) is a slowly varying background term.[14] With Eq. (1) and $A = 0$, one obtains the usual Breit-Wigner resonance formula. At $W = W_r, \delta(W) = \frac{\pi}{2}$ so that the real part of the scattering amplitude goes to zero and the imaginary part goes through a maximum.

For the photoproduction amplitudes the main constraint comes from the Fermi-Watson theorem[15] which states that the multipoles M_α can be written in the form $M_\alpha(W) = |M_\alpha(W)| \exp i\delta_\alpha(W)$, where $\delta_\alpha(W)$ is the πN phase shift in the quantum state $\alpha = l, j, I$. For the 3,3 channel at resonance one notes that $\mathrm{Re}[M_\alpha(W_r)] = 0$. This is the only general constraint on the $M_{1+}(\frac{3}{2})$ and $E_{1+}(\frac{3}{2})$ multipoles.

The "electromagnetic ratio" R is defined as the E2/M1 ratio at resonance. At $W = W_r$ the real part of these amplitudes is zero so that R is the ratio of the imaginary parts of the amplitudes. For a strong resonance amplitude like the $M_{1+}(\frac{3}{2})$ the imaginary amplitude has a maximum at resonance. For the smaller $E_{1+}(\frac{3}{2})$ amplitude the imaginary part is close to zero. This is caused by a cancellation of the resonance and background amplitudes and will be discussed in detail in Section 3. One of the advantages of using a dynamical model is that we can separately demonstrate the effects of the dressed and bare $E_{1+}(\frac{3}{2})$ amplitude on the observables. We therefore define two electromagnetic ratios $R^R_{EM} = \frac{E^R_{1+}}{M^R_{1+}}$ = the "dressed"E2/M1 ratio and $R^\Delta_{EM} = \frac{E^\Delta_{1+}}{M^\Delta_{1+}}$ = the "bare"E2/M1 ratio.

We can now write the resonant multipole amplitudes (or equivalently the t matrix elements) in the form:[11,12,16]

$$M(W) = M_\Delta(W) + M_{VR}(W) + M_B(W) = M_R(W) + M_B(W) \tag{2}$$

where $M_\Delta(W)$ is the bare resonant amplitude, $M_{VR}(W)$ is the "vertex renormalization" (due to πN rescattering before Δ formation), $M_B(W)$ is the background amplitude, and $M_R(W) = M_\Delta(W) + M_{VR}(W)$ is the dressed resonant amplitude. These are discussed in more detail in Nozawa's talk.[16] The background term has final state interactions in non-resonant states and is unitary, i.e.

$$M_B(W) = |M_B(W)|e^{i\delta_B} \tag{3}$$

where $\delta_B(W)$ is the background phase shift in πN scattering. The dressed resonance is composed of the bare Δ plus the vertex renormalization; the bare Δ has the final state interaction in the resonant p_{33} channel and is unitary, i.e.

$$M_\Delta(W) = |M_\Delta(W)|e^{i\delta_{P33}} \tag{4}$$

The vertex renormalization term has the initial state interaction in the resonant p_{33} channel.

As has been discussed by many authors (see e.g. Ref. 13) the dressed Δ resonance is not unitary by itself although the entire amplitude M(W) is. One way to enforce unitarity by using the bare Δ amplitude is to write[13]

$$M_R(W) = M_\Delta(W)e^{i\phi} \tag{5}$$

where ϕ is an empirically determined amplitude which enforces unitarity; in this approach its dynamic origin is not clear. However by combining Eqs. 2 and 5 one can write:

$$M_R(W) = M_\Delta(W) + M_{VR}(W) = M_\Delta(W)e^{i\phi} \tag{6}$$

From Eq. 6 it is clear that the multiplicative phase factor ϕ is essentially represents the additive vertex renormalization.[16]

We conclude this section by noting that it is most appropriate to compare quark models without continuum coupling to the bare Δ amplitude and models which have pion clouds (eg the cloudy bag or chiral bag models) to the dressed Δ amplitude. We stress that this identification is intuitive and remains to be demonstrated by further calculations.

III The Resonant M1 and E2 Amplitudes and Their Effects on the Observables

We now present results for the $E_{1+}(\frac{3}{2})$ and $M_{1+}(\frac{3}{2})$ amplitudes calculated with the model of Nozawa, Blankleider and Lee (NBL),[11] which gives reasonable agreement with experimental data and has several attractive features. It is gauge invariant, preserves unitarity, and takes the off-shell final state πN interactions (FSI). The πN interaction used in the model reproduces the phase shift data. In this model the resonance $R^{\Delta}_{EM} \cong -3\%$ has been obtained from a fit to the data;[11] it can arbitrarily be set to zero to study the sensitivity of the observables to the $E_{1+}(\frac{3}{2})$ amplitude.

We stress that the primary use of this model is to determine the sensitivity of the observables to the quadrupole amplitude and to discuss the general question of how it can be obtained from experiment. The model employed here is sufficiently realistic to accomplish this goal since it is reasonable agreement with the data.

In Fig. 1 we show the calculated $M_{1+}(\frac{3}{2})$ and $E_{1+}(\frac{3}{2})$ amplitudes along with three empirical (energy dependent) values.[4,17] There is reasonable agreement for both $M_{1+}(\frac{3}{2})$ and $E_{1+}(\frac{3}{2})$ amplitudes. The $M_{1+}(\frac{3}{2})$ multipole has a typical Breit-Wigner resonance shape (Figs. 1a and 1b). As is required for a resonance, the real part of the $M_{1+}(\frac{3}{2})$ goes through zero at the resonance energy ($E\gamma = 340$ MeV, W = 1232 MeV). However, it can be seen that there is a significant background contribution in the real part of the $M_{1+}(\frac{3}{2})$ amplitude. The parameters of the NBL model were chosen to fit the Berends-Donnachie multipoles;[4] there are small differences between the Berends-Donnachie and Arndt *et al.*[17] $M_{1+}(\frac{3}{2})$ multipoles as can be seen in Figs. 1a and 1b.

Qualitatively the shape of $E_{1+}(\frac{3}{2})$ (Figs. 1c and 1d) indicates that it is not a simple resonance like $M_{1+}(\frac{3}{2})$. The fact that $|E_{1+}(\frac{3}{2})|$ amplitude goes through zero near the Δ resonance was first confirmed by Berends and Donnachie[4] and was subsequently demonstrated by Jurewiez[4] to be predicted by dispersion relations. It remained however for the recent theoretical models[9,11,12,13] to show physically that this unusual shape was due to a cancellation between the dressed resonant amplitude and the background. One obtains Re $E_{1+}(\frac{3}{2}) = 0$ at resonance Δ(W = 1235 MeV) as required by the Fermi-Watson theorem the unusual feature is that Im $E_{1+}(\frac{3}{2}) = 0$ slightly above resonance (in the NBL model this occurs at W = 1247 MeV). The fact that theses zero are so close to each other is a "dynamical accident." There are two important consequences of this background cancellation; 1) the observable effects of the E2 amplitude are reduced; and 2) it is important to separately determine the resonance and background contribution.

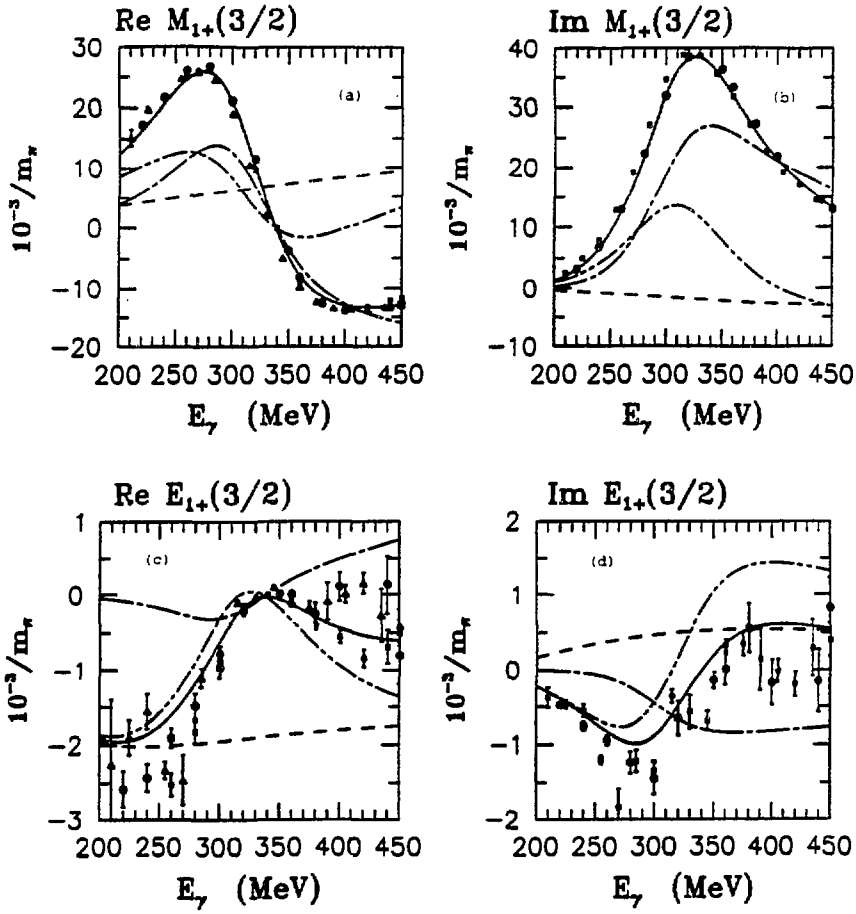

Figure 1. The $M_{1+}(\frac{3}{2})$ and $E_{1+}(\frac{3}{2})$ multipole amplitudes (in units of $10^{-3}/m_\pi$) as a function of the photon laboratory energy E_γ. The four sections of the figure are: 1a, Re $M_{1+}(\frac{3}{2})$; 1b, Im $M_{1+}(\frac{3}{2})$; 1c, Re $E_{1+}(\frac{3}{2})$; 1d, Im $E_{1+}(\frac{3}{2})$. The curves are: full calculation ————————; background - - - - - - - - - -; bare delta ——— - ———; and vertex renormalization plus background ——— - - ———. The points with the error bars are the empirical (energy dependent) multipole results of Pfeil and Schwela[4] ●, Berends and Donnachie [4] ▲, and Arndt *et. al.*[17] ■.

We now study the sensitivity of the cross sections for the $p(\gamma,\pi^0)$ reaction to the resonant $E_{1+}(\frac{3}{2})$ amplitude with both polarized and unpolarized photons. Calculations have been performed for the cross sections for unpolarized photons ($\sigma_{\rm unpol}$), photons polarized parallel to the production plane ($\sigma_\parallel$), and photons polarized perpendicular to the production plane ($\sigma_\perp$). They are related to each other by

$$\frac{d\sigma_{\rm unpol}(\theta)}{d\Omega} = \frac{1}{2}\left(\frac{d\sigma_\perp(\theta)}{d\Omega} + \frac{d\sigma_\parallel(\theta)}{d\Omega}\right) \tag{7}$$

where θ is the pion production angle. It should be pointed out that cross sections $\sigma_{\rm unpol}$, $\sigma_\parallel$ and $\sigma_\perp$ become identical at $\theta = 0$ and π where they are equally sensitive to the $E_{1+}(\frac{3}{2})$ amplitude.

We now present numerical results obtained by the NBL model.[11] First we define the ratio of the cross sections with and without the *resonant* E2 amplitude as follows.

$$R_\alpha = \frac{d\sigma_\alpha(\text{with E2})}{\mathrm{d}\Omega} \Big/ \frac{d\sigma_\alpha(\text{zero resonant E2})}{\mathrm{d}\Omega}, \tag{8}$$

where $\alpha \equiv$ unpol, $\|$ and $\perp$. We show the calculated results for R_α for the bare Δ in Fig. 2a, for the dressed Δ in Fig. 2b and for the entire $E_{1+}(\frac{3}{2})$ amplitude in Fig. 2c. Note how different these three sensitivity curves are. For the bare Δ the curves are symmetric about 90°, for the dressed Δ they are not, and for the entire $E_{1+}(\frac{3}{2})$ amplitude the effect is smallest. This indicates the large effect that the background has in canceling the resonant signal. In all cases there is the greatest sensitivity for parallel polarized photons. For E2/M1 = −3% there is a 15% increase in $R_\|$ for the bare Δ near $\theta = 90°$. We conclude that the measurement of the cross section for parallel polarized photons is the most sensitive measurement of the E2 amplitude. Such data is presently being taken at the LEGS facility in Brookhaven.[23]

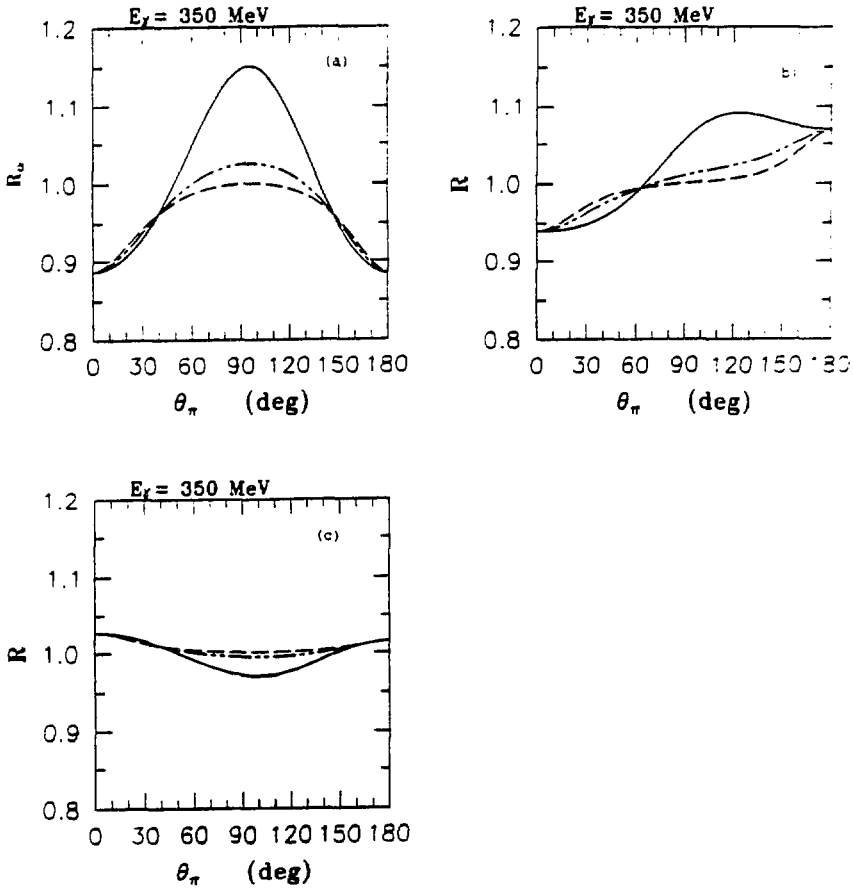

Figure 2. The calculated ratios R_α for the $p(\gamma, \pi^0)$ reaction are shown for: a) the bare Δ; b) the dressed Δ; and c) the full $E_{1+}(\frac{3}{2})$ amplitude. The curves correspond to R_{unpol} (—— - - ——), $R_\|$ (——————) and $R_\perp$ (- - - - - - - - - -).

Note that for the unpolarized cross section there is the maximum sensitivity to the E2 component for $\theta \sim 0°$ and 180°. At present there is only unpolarized data at medium angles[18] where there is little sensitivity to the E2 amplitude. It is therefore surprising that multipole analyses have been able to obtain any accurate determinations of the $E_{1+}(\frac{3}{2})$ amplitude based on the existing data base. We note that a new set of $p(\gamma,\pi^0)$ data in the Δ region has just been obtained at Mainz[19] with convergence near 0° and 180° which should give valuable information on the subject.

We show in Fig. 3a the predicted unpolarized cross section. In order to demonstrate the importance of the background E2 amplitude, we have added two curves: the cross sections without the bare $E_{1+}(\frac{3}{2})$ amplitude and without the dressed $E_{1+}(\frac{3}{2})$ amplitude. In Fig. 3b we show the calculated polarized cross sections. It can be seen that the parallel cross section is smaller and not as angular dependent as the perpendicular cross section.

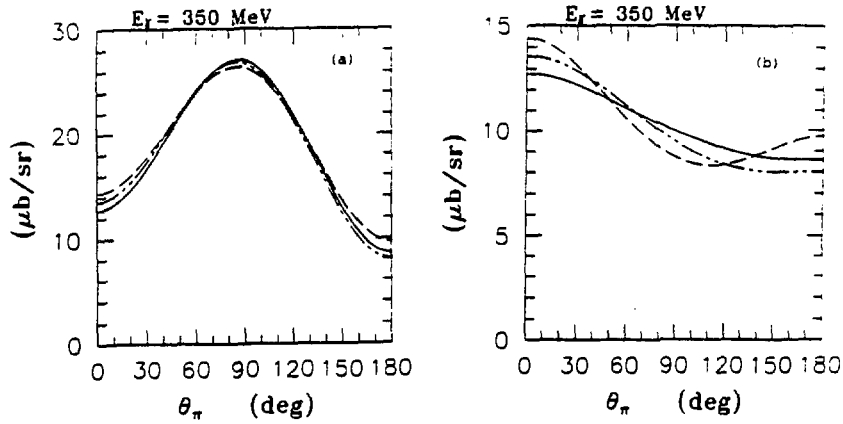

Figure 3. Cross sections for the $p(\gamma,\pi^0)$ reaction at E_γ=350 MeV. Fig. 3a are the unpolarized cross sections. The curves are: ——————— full $E_{1+}(\frac{3}{2})$ amplitude; - - - - - - - - - - no bare Δ $E_{1+}(\frac{3}{2})$ amplitude; and ——— - - ——— no dressed $E_{1+}(\frac{3}{2})\Delta$ amplitude. Curves in 3b present the polarized cross section $\sigma_{\|}$ for E_γ=350 MeV.

We have also examined the sensitivity of the conventional polarization observables in the (γ,π) reaction.[10,20] These are the polarized target asymmetry and the polarized recoil nucleon asymmetry. We have found that they have similar sensitivities (up to 15% for E2/M1=−3%) as we have presented for the polarized photon cross sections. Since the measurements involving target or(low energy) recoil polarization are more difficult than the proposed measurement here, we do not show these results.

IV Previous Determinations of the E2/M1 Ratio

Having presented the results of the E2/M1 sensitivity on the observables, we are now in a position to discuss the E2/M1 ratio obtained in the literature. The most recent version

of the Review of Particle Properties[21] lists four values of the E2/M1 ratio; $-1.1 \pm 0.4\%$ and $-1.5 \pm 0.2\%$ from the two papers of Davidson *et al.*,[7] $+3.7 \pm 0.4\%$ from Tanabe and Ohta,[12] and $-1.3 \pm 0.5\%$ from the last analysis performed by the particle data group.[6] These values, although not all that are found in the literature, have been obtained with quite differing assumptions and actually represent different quantities.

The analysis of the particle data group is based on the two helicity amplitudes $A_{1/2}$ and $A_{3/2}$. The E2/M1 ratio of $-1.3 \pm 0.5\%$ is then obtained from the measured helicity amplitudes.[6] This means that no background contribution has been subtracted. The quoted error is based on the measured uncertainties in the helicity amplitudes and does not reflect any systematic errors in the extraction of the E2/M1 ratio. We note that this value is for the dressed Δ coupling.

The most ambitious effort to determine the E2/M1 ratio from the multipoles is due to Davidson and Mukhopadhyay.[7] They assumed K matrix forms for the photo-pion production pion-nucleon scattering ($K_{\gamma\pi}$ and $K_{\pi\pi}$ respectively);

$$K_{\gamma\pi} = A/(W_R - W) + B$$

$$K_{\pi\pi} = C/(W_R - W) + D \tag{9}$$

where A, B, C, and D are smoothly varying functions of W (in practice they were assumed to be constant near resonance). From this the t matrix elements (multipoles) are calculated. At $W = W_R$, the resonance energy, one obtains[7] Re $t_{\gamma\pi} = 0$, in agreement with the Fermi-Watson theorem, and Im $t_{\gamma\pi} = A/C$, the ratio of the K matrix residues for the photo-production and pion scattering. Note that the K matrix background term B does not contribute at resonance. This assumption therefore represents the strong model dependent choice for the t matrix (multipoles), that there is no background contribution. As we have shown in Section 3, and also others[12] including Davidson *et al.*,[13] using an effective Lagrangian, there is a large background term which is comparable to the resonant amplitude for the $E_{1+}(\frac{3}{2})$ multipole. We therefore conclude that the "model independent..."[7] method of Davidson and Mukhopadhyay is in effect a highly restrictive (no background) determination of the E2/M1 ratio. Once that is understood the results are interesting. A number of multipole solutions to the data were analyzed with a uniform procedure and the E2/M1 ratios were obtained; the results varied from $-0.6 \pm 1.0\%$ to $-2.3 \pm 1.0\%$. Since the multipole analyses were based on essentially the same data base this spread in the values represents a systematic uncertainty in the E2/M1 ratio. The values should not be combined statistically as if they were independent measurements of the same quantity. In fact it is a triumph of the multipole analyses that given the lack of sensitivity of the data to the E2 amplitude (as shown in Section 3) that the results of the different multipole analyses are so consistent. Finally we note that the E2/M1 ratios obtained by Davidson *et al.*,[7] could be for the bare coupling.[16] The reason is that the use of the unitarization procedure used in Ref. 7 is effectively equivalent to the vertex renormalization discussed in Section 2.

There have been several empirical attempts to subtract a background contribution in the $E_{1+}(\frac{3}{2})$ amplitude.[8,10] The results are -0.6% and -1.9% respectively for the dressed amplitude. A third approach[9,11,18–21] uses a model to calculate the background amplitude,

then determines the resonance contribution by fitting the empirical $E_{1+}(\frac{3}{2})$ amplitude. The results for the bare Δ amplitude are $-(3.1 \pm 1.3)\%$ for the model presented here,[11] $-(1.5 \pm 0.72)\%$,[13] -4%,[22] 0%[9] and $+4\%$.[12] It is clear that there is a significant model dependence for the extracted E2/M1 ratio; much of this is probably due to the different off shell treatment of the πN scattering in the final state.

V Conclusions

We have shown that the $\gamma p \rightarrow \pi^0 p$ reaction is most sensitive to the resonant E2 amplitude for photons polarized in the reaction plane or for unpolarized photons producing pions near 0° and 180°. We have also shown that the resonant E2 multipole has a large background contribution which almost cancels out the resonant contribution. We have not addressed the question of whether dedicated data taken to determine R_{EM} will enable one to make an accurate background subtraction for the $E_{1+}(\frac{3}{2})$ amplitude. We believe that it may be possible after one obtains data that have different sensitivities to the background amplitude. It may also help to determine the quadrupole amplitude by different techniques such as Compton scattering[23] and also by the $p(\vec{e}, e'\pi^0)p$ reaction.[22] Each of these reactions will have differing sensitivities to the background and resonant amplitudes and may enable one to make a model independent background subtraction or at least to test different background models. In particular the fifth structure function in the pion electroproduction experiments are particularly sensitive to the background amplitudes.

In summary, we have also demonstrated that the spread in the values for E2/M1 obtained in previous analyses is probably due to the fact that they are based on data which do not have the angular coverage or polarization data that is sufficiently sensitive to the resonant E2 amplitude. In addition there is a sizable background contribution to the $E_{1+}(\frac{3}{2})$ amplitude which has been neglected in several analysis.[6,7] We have also shown that more accurate determination of the E2/M1 ratio requires new data from dedicated experiments; the required experimental accuracy will be 1% (or better) since the predicted effects are 10 to 20%. Cross section measurements using polarized photon beams are very sensitive to the E2/M1 ratio; such data is presently being taken at LEGS.[23] Measurements of the unpolarized cross sections near 0° and 180° will help untangle the background and resonant amplitudes; such data has been recently taken at Mainz.[19] Although we have focused out attention on the $p(\gamma, \pi^0)$ reaction we note that measurements of charged pions are also important to perform the isospin decomposition.

Acknowledgments

We would like to thank T. S. H. Lee, N. C. Mukhopadhyay, O. V. Sorokin, and R. S. Wittman for stimulating discussions and T. P. Welch for suggestions on the manuscript. This work was supported by the Department of Energy under contract no. DE-AC02-76ERO3069, National Sciences and Engineering Research Council of Canada (NSERC), and the U.S.-Israel Binational Science Foundation (BSF), Jerusalem, Israel.

References

1. S.L. Glashow, Physica **A96**, 27 (1979). For recent reviews of this subject see the articles by F. E. Close, S. Capstick, R. H. Dalitz and N. Isgur in Excited Baryons 1988, G. Adams, N. C. Mukhopadhyay, and P. Stoler editors, World Scientific.
2. For a review of the color magnetism model see N. Isgur, G. Karl, and R. Koniuk, Phys. Rev. **D25**, 239 (1982).
3. R. Carlitz, S. D. Ellis, and R. Savit, Phys. Lett. **64B**, 85 (1976); N. Isgur, G. Karl, and D. W. L. Sprung, Phys. Rev. **D23**, 163 (1981).
4. W. Pfeil and S. Schwela, Nucl. Phys. **B45**, 379 (1972); F. A. Berends and A. Donnachie, Nucl. Phys. **B84**, 342 (1975); and A. Jurewicz, J. Phys. G, 5 (1979).
5. For a review of the determination of the E2/M1 ratio see the articles by N. C. Mukhopadhyay, C. N. Papanicolas, and O. A. Rondon-Aramayo in the Topical Workshop on Excited Baryons 1988, G.Adams, N. C. Mukhopadhyay, and P. Stoler editors, World Scientific.
6. Particle Data Group, M. Aguilar-Benitez *et al.*, Phys. Lett. **170B**, 1 (1986).
7. *R. M. Davidson and N. C. Mukhopadhyay, Phys. Rev* **D42**, *20 (1990). R. Davidson,* N. C. Mukhopadhyay, and R. Wittman, Phys. Rev. Lett. **56**, 804 (1986).
8. A. S. Omelaenko and O. V. Sorokin, Sov. J. Nucl. Phys. **38**, 398 (1983).
9. R. Cenni, G. Dillon, and P. Christillin, Nuovo Cimento **97A**, 1 (1987).
10. See the articles by V. F. Grushin and A. I. Lebedev and B. V. Mangazeyev in Photoproduction of Pions and on Nucleons and Nuclei, Nova Science Publishers, N.Y., translation of the Proceedings of the Lebedev Physics Institute, Academy of Sciences of the USSR, Vol. 186 (1988); V. F. Grushin *et al*, JETP Lett. **39**, 491 (1984); I. I. Miroshnichenko *et al.*, Yad Fiz. **32**, 659 (1980).
11. S. Nozawa, B. Blankleider, and T.-S. H. Lee, Nucl. Phys. **A513**, 459 (1990).
12. H. Tanabe and K. Ohta, Phys. Rev. **C31**, 1876 (1986), and S. N. Yang, J. Phys. **G11**, L205 (1985).
13. R. M. Davidson, N. C. Mukhopadhyay, and R. S. Wittman, Phys. Rev. **D43**, 71 (1991).
14. See eg, B. H. Bransden and R. G. Moorhouse, The Pion-Nucleon System, Princeton University Press (1973).
15. See B. T. Feld, Models of Elementary Particles and references therein.
16. See the talk of S. Nozawa, in these proceedings.
17. R. A. Arndt, R. L. Workman, Z. Li, and L. D. Roper, Phys. Rev **C42**, 1853 (1990).
18. D. Menze, W. Pfeil, and R. Wilcke, ZAED Compilation of Pion Photoproduction Data, University of Bonn, 1977.
19. Mainz experiment A2 (7-90), H. Ströker spokesman.
20. F. A. Berends and A. Donnachie, Nucl. Phys **B4**,1 (1967), A. A. Belyaev *et al*, Nucl. Phys. **B213**, 201 (1983).
21. Review of Particle Properties, K. Hisasa *et al.*, Phys. Rev. **D45**, No. 11, 1 June 1992.
22. J. M. Laget, Nucl. Phys. **A481**, 765 (1988).
23. A. M. Sandorfi *et al.*, experiment in progress at LEGS, and Proceedings of the Sixth Course of the International School of Intermediate Energy Nuclear Physics, Venice, Italy, July (1988), C. Schaerf, Ed.; A. M. Sandorfi *et al.*, IEEE **NS30**, 3083 (1983); and C. E. Thorn *et al.*, Nucl. Inst. Meth. **A285**, 447 (1989).

Pion photoproduction and $\gamma N \leftrightarrow \Delta$ amplitudes

S. Nozawa and B. Castel
Department of Physics, Queen's University, Kingston, Ontario, Canada K7L 3N6

Abstract

We review a dynamical model for the pion photoproduction on the nucleon. With the model, we explore sensitivities of observables to the E2 (or E_{1+}) multipole amplitude in the $\gamma N \leftrightarrow \Delta$ transition. It will be demonstrated that the cross section with polarized photons has a significant sensitivity to the E2 amplitude. The model prediction will be compared with the most recent LEGS data.

1. Introduction

Study of the M1 (or M_{1+}) and E2 (or E_{1+}) amplitudes of the $\gamma N \leftrightarrow \Delta$ transition has been done by many authors both experimentally and theoretically. It has been known that the tensor interaction between quarks gives the D-state admixture in the predominant S-state wave functions of the nucleon and the Δ. Non-vanishing E2 amplitude is one of the signals of the D-state admixture. Therefore it is extremely important to determine the E2 amplitude in order to test various quark model predictions. However, it is extremely difficult to determine the E2 amplitude accurately. The main reason is that the E2 amplitude is very small compared with the predominant M1 amplitude. Second, a model dependence is unavoidable in separating the background amplitude to extract the resonance amplitude. In this paper, we would like to address two questions. (i) What is model dependent and what is model independent? (ii) What is the most sensitive observable to the E2 amplitude? In section 2, we derive the Watson theorem. A dynamical model will be introduced in section 3. Numerical results for the M1 and E2 amplitudes will be presented in section 4. In section 5, the E2/M1 sensitivity will be explored using the polarized photon cross sections. Finally, the model prediction will be compared with the most recent LEGS data.

2. The Watson theorem

Let us first derive the Watson theorem[1]. It requires (i) the unitarity of the S-matrix and (ii) the time-reversal invariance of the T-matrix. The unitarity condition for each partial wave implies

$$S^\ell S^{\ell\dagger} = I, \tag{1}$$

where $\ell \equiv L_{2T2J}$ denotes the partial wave (P_{33}, etc.) and I is the unit matrix. The T-matrix is defined by

$$S^\ell = I - 2\pi i \rho T^\ell, \tag{2}$$

where ρ is the phase space factor, and S^ℓ and T^ℓ are

$$S^\ell = \begin{pmatrix} s^\ell_{\pi\pi} & s^\ell_{\pi\gamma} \\ s^\ell_{\gamma\pi} & s^\ell_{\gamma\gamma} \end{pmatrix}, \quad T^\ell = \begin{pmatrix} t^\ell_{\pi\pi} & t^\ell_{\pi\gamma} \\ t^\ell_{\gamma\pi} & t^\ell_{\gamma\gamma} \end{pmatrix}. \tag{3}$$

Here $\pi\pi$, $\pi\gamma$, $\gamma\pi$ and $\gamma\gamma$ denote $\pi N \to \pi N$, $\pi N \to \gamma N$, $\gamma N \to \pi N$ and $\gamma N \to \gamma N$, respectively. Inserting eqs. (2) and (3) into eq. (1), one obtains four coupled equations. The relevant piece for the photoproduction is

$$t^{\ell}_{\gamma\pi} - t^{\ell *}_{\pi\gamma} = -2\pi i\rho\,(t^{\ell}_{\pi\pi}t^{\ell *}_{\gamma\pi} + t^{\ell}_{\pi\gamma}t^{\ell *}_{\gamma\gamma}). \tag{4}$$

Assuming time-reversal invariance of the T-matrix, i.e. $t^{\ell}_{\pi\gamma} = t^{\ell}_{\gamma\pi}$ and dropping the second term of the RHS which is suppressed by a factor α ($=\frac{1}{137}$), eq. (4) is simplified.

$$t^{\ell}_{\gamma\pi} \simeq (1 - 2\pi i\rho\, t^{\ell}_{\pi\pi})\, t^{\ell *}_{\gamma\pi} = e^{2i\delta^{\ell}_{\pi\pi}}\, t^{\ell *}_{\gamma\pi}. \tag{5}$$

Multiplying $t^{\ell}_{\gamma\pi}$ to eq. (5), one finally obtains the Watson theorem's prediction.

$$t^{\ell}_{\gamma\pi} = \mid t^{\ell}_{\gamma\pi} \mid e^{i\delta^{\ell}_{\pi\pi}}. \tag{6}$$

Namely, the pion photoproduction amplitude has the same phase $e^{i\delta^{\ell}_{\pi\pi}}$ as the πN scattering. It is important to note that the Watson theorem is model independent.

Let us now consider a case that the amplitude contains resonance (R) and background (B) components, for example, P_{33}. The T-matrices are decomposed into

$$t_{\pi\pi} = t^{R}_{\pi\pi} + t^{B}_{\pi\pi} \tag{7.a}$$

$$t_{\gamma\pi} = t^{R}_{\gamma\pi} + t^{B}_{\gamma\pi}. \tag{7.b}$$

Note that the superscript ℓ has been dropped in eq. (7). Inserting eq. (7) into eq. (4), one finds that the background amplitude is unitary, whereas the resonance amplitude is not. The background amplitude is expressed by

$$t^{B}_{\gamma\pi} = \mid t^{B}_{\gamma\pi} \mid e^{i\delta_B}, \tag{8}$$

where δ_B is the background πN phase shift. Now, the question is how to unitarize the RHS of eq. (7.b). In fact, the unitarization method is not unique. For example, Olsson[2] introduced the following method. (i) First assume that the resonance amplitude is modified by a multiplicative phase factor $e^{i\phi}$, i.e.

$$t^{R}_{\gamma\pi} \to \mid t^{\Delta}_{\gamma\pi} \mid e^{i(\delta_{P33}+\phi)}, \tag{9}$$

where $t^{\Delta}_{\gamma\pi}$ is the unitary Δ-resonance amplitude. (ii) Then impose the Watson theorem to determine ϕ. This implies the following condition.

$$\mid t_{\gamma\pi} \mid e^{i\delta_{P33}} = \mid t^{\Delta}_{\gamma\pi} \mid e^{i(\delta_{P33}+\phi)} + \mid t^{B}_{\gamma\pi} \mid e^{i\delta_B}, \tag{10}$$

where δ_{P33} is the P_{33} πN phase shift. The parameter ϕ is determined as follows.

$$\sin\phi = \frac{\mid t^{B}_{\gamma\pi} \mid}{\mid t^{\Delta}_{\gamma\pi} \mid} \sin(\delta_{P33} - \delta_B) \tag{11.a}$$

$$\mid t_{\gamma\pi} \mid = \mid t^{\Delta}_{\gamma\pi} \mid \frac{\sin(\delta_{P33} + \phi - \delta_B)}{\sin(\delta_{P33} - \delta_B)}. \tag{11.b}$$

Note that $|\ t^{\Delta}_{\gamma\pi}\ |$ in eq. (11) is in general $|\ t^{R}_{\gamma\pi}\ |$ as shown in Refs. 3 and 4. It is important to note that eq. (11) has been derived with the assumption of eq. (9). We will compare this unitarization method with the coupled channel approach in section 3. Furthermore, the determination of ϕ is model dependent for the following reasons. (i) The determination of $t^{B}_{\pi\pi}$ (and therefore $t^{B}_{\gamma\pi}$) is model dependent. For example, there are zero background ($t^{B}_{\pi\pi}$=0), on-shell $t^{B}_{\pi\pi}$ and off-shell $t^{B}_{\pi\pi}$ models. (ii) The determination of $t^{R}_{\gamma\pi}$ is also model dependent. We will discuss this issue in section 3.

To leave this section, the following point should be emphasized. One may want to ask a question. What is the physical origin of the parameter ϕ in eq. (10)? The Watson theorem will not be able to explain the dynamical origin of ϕ. Only dynamical models can answer this question. We will discuss this issue in section 3.

3. Coupled channel method and a dynamical model

We will briefly describe a dynamical model of Nozawa, Blankleider and Lee (NBL)[5]. There exists other dynamical models by Tanabe and Ohta[4] and by Yang[6] which were constructed in the same spirit. The model starts with the coupled channel Lippmann-Schwinger equation.

$$T = V + T G_0 V, \tag{12}$$

where G_0 is a free πN propagator. The potential V is given by

$$V = \begin{pmatrix} v_{\pi\pi} & v_{\pi\gamma} \\ v_{\gamma\pi} & v_{\gamma\gamma} \end{pmatrix}. \tag{13}$$

Inserting eqs. (3) and (13) into eq. (12), one obtains the following equations.

$$t_{\pi\pi} = v_{\pi\pi} + t_{\pi\pi} G_0 v_{\pi\pi}. \tag{14.a}$$

$$t_{\gamma\pi} = v_{\gamma\pi} + t_{\pi\pi} G_0 v_{\gamma\pi}. \tag{14.b}$$

$$t_{\gamma\gamma} = v_{\gamma\gamma} + t_{\gamma\pi} G_0 v_{\gamma\pi}. \tag{14.c}$$

In deriving eq. (14), we have dropped terms suppressed by a factor α. Solving the integral equation of eq. (14.a) for a given $v_{\pi\pi}$, one obtains $t_{\pi\pi}$. Inserting this into eq. (14.b) and integrating over intermediate πN states, the pion photoproduction $t_{\gamma\pi}$ matrix is obtained. Similarly, the Compton scattering T-matrix is derived by eq. (14.c).

Let us now consider the P_{33} partial wave. The amplitude is decomposed into resonance and background components as shown in eq. (7). We have shown the graphical representation in Fig. 1.

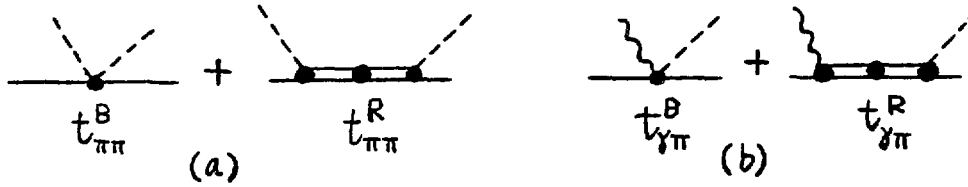

Fig. 1 Graphical representation of the T-matrices. (a) $t_{\pi\pi}$ and (b) $t_{\gamma\pi}$.

The background $t^B_{\gamma\pi}$ matrix satisfies

$$t^B_{\gamma\pi} = v^B_{\gamma\pi} + t^B_{\pi\pi} G_0 v^B_{\gamma\pi}. \tag{15}$$

It is therefore separately unitary (see eq. (8)). Furthermore the resonance amplitude $t^R_{\gamma\pi}$ has two components.

$$t^R_{\gamma\pi} = t^\Delta_{\gamma\pi} + t^{VR}_{\gamma\pi}. \tag{16}$$

These amplitudes are graphically presented in Fig. 2.

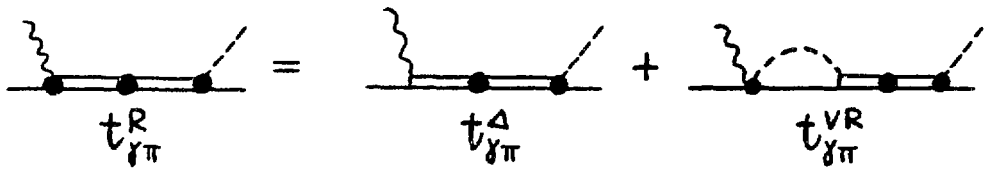

Fig. 2 Graphical representation of the resonance $t^R_{\gamma\pi}$ matrix.

The first term $t^\Delta_{\gamma N}$ is the unitary Δ-amplitude, i.e.

$$t^\Delta_{\gamma\pi} = | t^\Delta_{\gamma\pi} | e^{i\delta_{P33}}. \tag{17}$$

It should be emphasized that the $\gamma N\Delta$-vertex has bare coupling constants G_M and G_E, whereas the $\pi N\Delta$-vertex and the Δ-propagator are all dressed. The second term $t^{VR}_{\gamma\pi}$ is the rescattering amplitude which leads to dressing of the $\gamma N\Delta$-vertex. We call it the vertex renormalization (VR) amplitude. Equation (7.b) now becomes

$$t_{\gamma\pi} = t^\Delta_{\gamma\pi} + t^{VR}_{\gamma\pi} + t^B_{\gamma\pi}. \tag{18}$$

It is important to note that eq. (18) is a general consequence of the present approach based on the coupled channel Lippmann-Schwinger equation. Comparing eq. (18) with the RHS of eq. (10), it is clear that $t^{VR}_{\gamma\pi}$ is the dynamical origin of the parameter ϕ introduced in Olsson's unitarization method. It should be noted that the additive $t^{VR}_{\gamma\pi}$ amplitude modifies the Δ-amplitude, whereas the multiplicative phase $e^{i\phi}$ does in eq. (10). In the coupled channel approach, unitarity is guaranteed by the $t^{VR}_{\gamma\pi}$ term. The parameter ϕ is no longer necessary. However, this approach requires knowledge of the half-off-shell $t_{\pi\pi}$ matrix, where the model dependence does come in.

The construction of the NBL model is as follows. (i) First, the model assumes separable forms for the πN potential $v_{\pi\pi}$. This has the advantage that the integral equation (14.a) can be solved analytically and therefore the πN T-matrix $t_{\pi\pi}$ has an analytic form. For P_{11} and P_{33} partial waves, the potential consists of resonance and background terms, whereas other partial waves are parameterized in terms of 2-term separable potentials. All parameters in the potential are fixed by fitting πN phase shift data up to the pion kinetic energy E_{lab}=500 MeV. (ii) The pion photoproduction potential $v_{\gamma\pi}$ is the Born amplitude with the standard pseudovector πN Lagrangian

plus ρ- and ω-exchange diagrams. They are graphically shown in Fig. 3a~f. The Δ-resonance diagram is shown in Fig. 3g. It should be noted that the model satisfies gauge invariance even after the integration of the half-off-shell πN T-matrix.

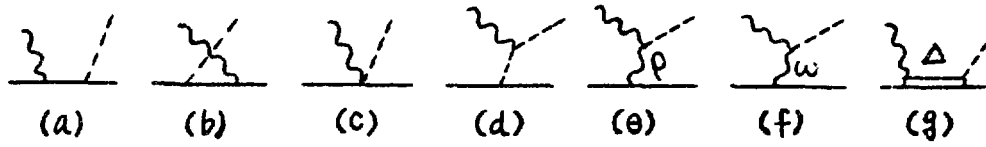

Fig. 3 Diagrams for the pion photoproduction.

The $\gamma N\Delta$-vertex has two coupling constants for the real photon case, i.e. G_M and G_E. They are called the magnetic dipole (M1) and the electric quadrupole (E2) coupling constants, respectively. In the NBL model, they are treated as free parameters. The model has a third parameter Λ by introducing a cut-off form factor

$$F_{\rm cut}(k) = \frac{k^2}{k^2 + \Lambda^2} \tag{19}$$

in eq. (14.b) in order to make the integral over the momentum k converge.

4. M1 and E2 amplitudes of the model

The three parameters G_M, G_E and Λ are determined in the following manner. For a given Λ, we determine G_M and G_E to give a best fit to the M1 and E2 amplitudes. We obtained the following results. (i) For Λ=350 MeV/c, G_M=2.80 and G_E=0.05. (ii) For Λ=650 MeV/c, G_M=2.28 and G_E=0.07. (iii) For Λ=900 MeV/c, G_M=2.30 and G_E=0.08. The ratios of the E2 and M1 amplitudes correspond to (i) E2/M1=−1.8%, (ii) E2/M1=−3.1% and (iii) E2/M1=−3.5%, respectively. These three cases give equally good fit to the M1 and E2 amplitudes. However, case (ii) was found to give an over-all best agreement for differential cross section data. In Figs. 4 and 5, we display the result of the M1 and E2 multipoles for case (ii) E2/M1=−3.1%.

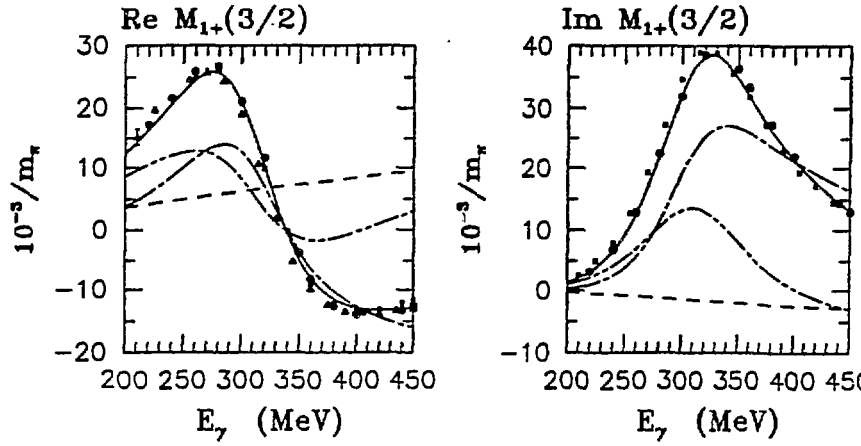

Fig. 4 M1 multipole amplitude.

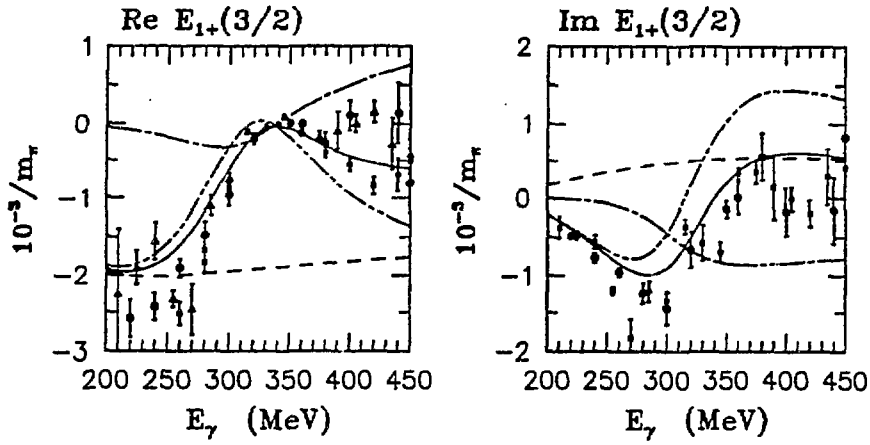

Fig. 5 E2 multipole amplitude.

The solid curve is the full amplitude $t_{\gamma\pi}$. The dashed curve, dot-dashed curve and dot-dot-dashed curve are extractions of the $t^B_{\gamma\pi}$, $t^\Delta_{\gamma\pi}$ and $t^B_{\gamma\pi} + t^{VR}_{\gamma\pi}$ amplitudes, respectively. The circle, triangle and square correspond to the result of the multipole analyses by Refs. 7, 8 and 9, respectively. The background amplitude $t^B_{\gamma\pi}$ has a smooth energy dependence as expected. The values of $t^B_{\gamma\pi}$ agree with the result of Figs. 12 and 13 in Ref. 10. The background amplitude is significantly large for the E2 amplitude. The resonance-like energy dependence of the dot-dot-dashed curve is due to the vertex renormalization amplitude $t^{VR}_{\gamma\pi}$.

Let us now compare the obtained result E2/M1=−3.1%[5] with the literature. The values are E2/M1=−(0.59 ± 1.01)% to −(2.25 ± 1.02)%[11], −(1.5 ± 0.72)%[10], −4%[6], 0%[12] and +4%.[4]. The following comment should be noted. The K-matrix formalism was used in Ref. 11. Although the K-matrix $K_{\pi\pi}$ contains a background contribution, the resulting T-matrix $t_{\pi\pi}$ contains no background $t^B_{\pi\pi}$. According to these E2/M1 values, it is clear that there is a significant model dependence in the extraction. This might be due to the following reasons. (i) Different unitarization methods used. As mentioned earlier, Refs. 5 and 10 gave a similar background $t^B_{\gamma\pi}$ contribution. Therefore the difference must come from $t^R_{\gamma\pi}$, namely due to different unitarization methods. Olsson's method and its variations were used in Refs. 3 and 10-12, whereas the coupled channel method with dynamical models was used in Refs. 4-6. It is also evident that there is a significant model dependence among the dynamical models[4−6]. (ii) This will be probably due to different half-off-shell πN T-matrices. As far as the present situation is concerned, all we can say about the E2/M1 ratio is that it is small, a few percent with probably a negative sign.

In this circumstance, it is extremely important to study the $\gamma N \leftrightarrow \Delta$ amplitude more extensively. In particular, it will be essential to use direct information such as cross sections and asymmetries without relying on the multipole analyses. We will study the sensitivity of polarized cross sections to the E2 amplitude in the next section.

5. Sensitivity of cross sections to the E2 amplitude

Various predictions of the NBL model for differential cross sections and asymmetries have been given in Ref. 5. In this paper, special attention will be payed to the differential cross sections for unpolarized photons ($\sigma_{\rm unpol}$), for photons polarized parallel to the production plane ($\sigma_{||}$) and for photons polarized perpendicular to the production plane ($\sigma_{\perp}$). Details will be presented elsewhere[13]. Here $\sigma_{\rm unpol}$ is the average of $\sigma_{||}$ and $\sigma_{\perp}$. Note that the cross sections $\sigma_{\rm unpol}$, $\sigma_{||}$ and $\sigma_{\perp}$ become identical at $\theta = 0$ and π, where they are equally sensitive to the E2 amplitude. However, it is difficult to detect pions at the forward and backward angles and no data are presently available there. We therefore study the cross sections near $\theta = \frac{\pi}{2}$, which is preferred experimentally.

Keeping S, P and D-wave multipoles, one can write the cross sections at $\theta = \frac{\pi}{2}$ as

$$\frac{d\sigma_{\perp}(\frac{\pi}{2})}{d\Omega} = \frac{k}{\omega_q}\left\{ \mid E_{0+} - D_{\perp} \mid^2 + \mid P_{\perp} \mid^2 \right\} \qquad (20.a)$$

$$\frac{d\sigma_{||}(\frac{\pi}{2})}{d\Omega} = \frac{k}{\omega_q}\left\{ \mid E_{0+} - D_{||} \mid^2 + \mid P_{||} \mid^2 \right\}, \qquad (20.b)$$

where k and ω_q are the pion momentum and the photon energy in the CM system. In eq. (20), E_{0+} is the S-wave amplitude, and $P_{\perp}$ and $P_{||}$ are P-wave amplitudes given by $P_{\perp} = 2M_{1+} + M_{1-}$ and $P_{||} = 3E_{1+} - M_{1+} + M_{1-}$. Similarly, $D_{\perp}$ and $D_{||}$ are D-wave amplitudes. It is evident that at $\theta = \frac{\pi}{2}$, $\sigma_{||}$ has a maximum sensitivity to E2, whereas $\sigma_{\perp}$ has no sensitivity. We define R_{α} by the ratio of the cross sections with and without the resonance E2 amplitude. Here α denotes unpol, $||$ and $\perp$. The numerical results for R_{α} are shown in Fig. 6. For E2/M1=−3.1%, $R_{||}$ is increased by 15% at $\theta = \frac{\pi}{2}$, whereas $R_{\rm unpol}$ and $R_{\perp}$ have much smaller effects. The measurement of $\sigma_{||}$ will be therefore a sensitive observable of the resonance E2 amplitude.

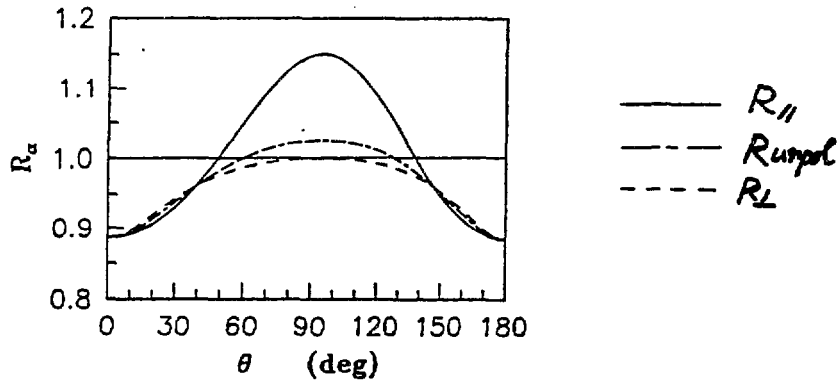

Fig. 6 Calculated ratios $R_{||}$, $R_{\perp}$ and $R_{\rm unpol}$ at E_{γ}=350 MeV.

Recently, polarized cross sections have been measured at the LEGS facility[14,15]. We have compared the NBL model prediction with the data[15]. In Fig. 7, we show (a) the energy dependence of $\sigma_{||}/\sigma_{\perp}$, and (b) the unpolarized cross section. The solid and dashed curves correspond to the full calculations with E2/M1=−3.1% and E2/M1=0%,

respectively. At E_γ=314 MeV, agreement between the NBL model and the data is reasonable. However, the discrepancy increases for lower energies.

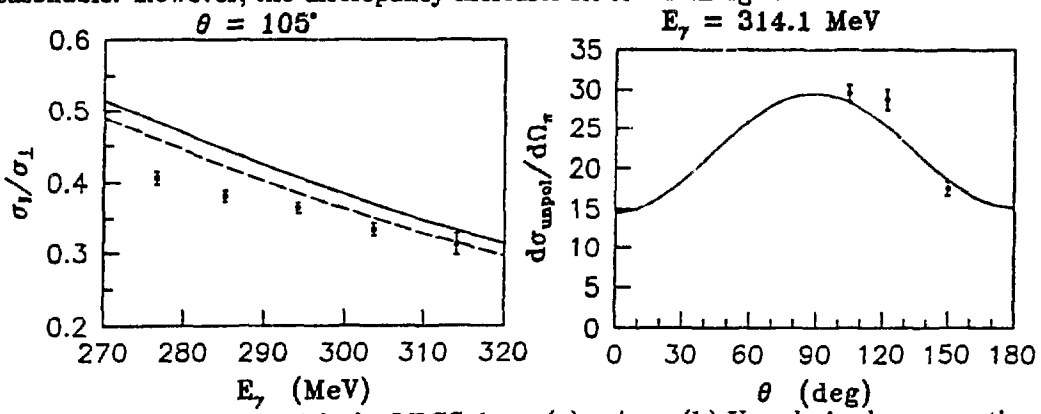

Fig. 7 Comparison with the LEGS data. (a) $\sigma_\parallel/\sigma_\perp$. (b) Unpolarized cross section.

In summary, we have reviewed the coupled channel method with a dynamical model of the pion photoproduction. A detailed comparison has been made between the coupled channel approach and Olsson's unitarization method. A sensitivity study has been also made for the E2 amplitude using cross sections with polarized photons. Finally, the NBL model prediction has been compared with the most recent LEGS data.

The authors would like to thank Dr. Andrew Sandorfi for providing the recent LEGS data before its publication. This work was supported in part by the National Sciences and Engineering Research Council of Canada (NSERC). One of us (SN) is grateful to the Queen's University Advisory Research Committee for additional support.

References

1. K. M. Watson, Phys. Rev. **95**, 228 (1954).
2. M. G. Olsson, Nucl. Phys. **B78**, 55 (1974).
3. R. S. Wittman, R. M. Davidson and N. C. Mukhopadhyay, Phys. Lett. **B142**, 336 (1984).
4. H. Tanabe and K. Ohta, Phys. Rev. **C31**, 1876 (1986).
5. S. Nozawa, B. Blankleider, and T. S. H. Lee, Nucl. Phys. **A513**, 459 (1990).
6. S. N. Yang, J. Phys. **G11**, L205 (1985).
7. W. Pfeil and S. Schwela, Nucl. Phys. **B45**, 379 (1972).
8. F. A. Berends and A. Donnachie, Nucl. Phys. **B84**, 342 (1975).
9. R. A. Arndt, R. L. Workman, Z. Li, and L. D. Roper, Phys. Rev **C42**, 1853 (1990).
10. R. M. Davidson, N. C. Mukhopadhyay, and R. S. Wittman, Phys. Rev. **D43**, 71 (1991).
11. R. M. Davidson and N. C. Mukhopadhyay, Phys. Rev **D42**, 20 (1990).
12. R. Cenni, G. Dillon, and P. Christillin, Nuovo Cimento **97A**, 1 (1987).
13. A. M. Bernstein, S. Nozawa and M. A. Moinester, in preparation.
14. A. M. Sandorfi *et al.*, IEEE **NS30**, 3083 (1983); C. E. Thorn *et al.*, Nucl. Inst. Meth. **A285**, 447 (1989).
15. A. M. Sandorfi, LEGS Data Release #L2-5.1 (April, 1992) and #L2-5.2 (May, 1992).

Effective Lagrangians, Watson's theorem and the E2/M1 mixing ratio in the excitation of the Delta resonance

R.M. Davidson *Inst. für Kernphysik, Johannes Gutenberg Univ., 6500 Mainz, W. Germany*

Abstract

We investigate theoretical uncertainties and model dependence in the extraction of the nucleon-delta(1232) electromagnetic transition amplitudes from the multipole data base. Our starting point is an effective Lagrangian incorporating chiral symmetry, which includes at the tree level the pseudovector Born terms, leading t-channel vector meson exchanges, and s and u channel delta exchanges. The nucleon-delta magnetic dipole (M1) and electric quadrupole (E2) transition amplitudes are expressed in terms of two independent gauge couplings at the $\gamma N\Delta$ vertex. After unitarizing the tree level amplitude, the gauge couplings are fitted to various multipole data sets, thus determining E2 and M1. Although there is much sensitivity to the method used to unitarize the amplitude, we extract the E2/M1 ratio to be negative, with a magnitude around 1.5%.

1 Introduction

Although quantum chromodynamics (QCD) has been around for 20 years, it still has not been solved in the non-perturbative domain, and several "QCD-inspired" models [1] have been developed to help shed light on the quark-gluon structure of the hadrons. Partial wave analyses of elastic pion-nucleon (πN) scattering reveal numerous baryon resonances (N^*), the masses of which the baryon models can, for the most part, reproduce. More powerful tests of these models are provided by the electroweak transitions between an N^* and N. Aided by a new generation of accelerators and detectors, new experimental efforts aimed at studying the γNN^* vertices are under way at places such as Bates, Brookhaven, Mainz, and in the future, CEBAF.

In this contribution, we will examine some of the model dependence involved in extracting the nucleon-delta(1232) magnetic dipole (M1) and electric quadrupole (E2) transition amplitudes from the extant multipole data base. The E2 amplitude is of special importance in the testing of baryon models. Its value is predicted to be zero in the simplest quark models, and a non-zero value is a signal for the existence of a tensor force between the quarks, arising for example from one-gluon exchange.

In the next section, we will review Watson's theorem [2] and its relevance to pion photoproduction (γ, π) in the delta resonance region. There is also a brief discussion of the general problem of separating a multipole into its background and resonant parts. In section 3, we discuss how this problem is "solved" in the effective Lagrangian approach, and how Watson's theorem is implemented. In section 4, we present our results for E2 and M1, as well as a comparison with the data. The last section contains a summary and conclusions.

2 Watson's theorem

Let us first recall what Watson's theorem [2] is, and then discuss the assumptions needed to derive the theorem. First, define $\phi_{J,P,T}$ to be the phase of a (γ, π) multipole with total spin J, parity P, and leading to a final πN state with isospin T. Watson's theorem states that $\phi_{J,P,T} = \delta_{J,P,T}$, where $\delta_{J,P,T}$ is the elastic πN phase shift with quantum numbers J,P,T. In particular, for the resonant multipoles $E_{1+}^{3/2}$ (due to an E2 photon) and $M_{1+}^{3/2}$ (due to an M1 photon),

$$E_{1+}^{3/2}, M_{1+}^{3/2} = C_{E,M} e^{i\delta_{33}}, \tag{1}$$

where C_E and C_M are real quantities and δ_{33} is the πN phase shift in the $J^P = 3/2^+$, T=3/2 channel.

Watson's theorem follows directly from unitarity and the assumption of one dominate channel (in our case the πN channel), which is equivalent to assuming that the πN phase shift is real for the partial wave in question. Therefore, above the two pion threshold Watson's theorem is no longer strictly valid. However, it generally remains a good approximation throughout the delta region because the inelasticities are small, with the possible exception of the P11 channel (corresponding to the $M_{1-}^{1/2}$ multipole). Even below the two pion threshold there are corrections to Watson's theorem. One correction is due to the Compton phase shift, i.e. a term of order e^2 (e the charge of the proton) compared to the strong interaction. The second correction is due to isospin breaking, for example the differences in the pion masses. This second correction is obviously important in the very near threshold region, but as pointed out by Berends and Donnachie [3], care must also be taken near the peak of the delta because different charge states of the delta (with different masses) may be excited in photoproduction than in πN scattering.

Apart from being a constraint that (γ, π) models should satisfy, Watson's theorem is also useful for multipole analyses in the delta region. Denoting some observable by $\mathcal{O}_i$(W,x), with W the total cm energy and x the cm scattering angle, we recall that the observables are bi-linears in the multipoles,

$$\mathcal{O}_i(W,x) \sim \left[\sum_{l=0}^{\infty} a_l^i(x)\mathcal{M}_l(W)\right]^2, \tag{2}$$

where $\mathcal{M}_l$'s are the multipoles, l is the πN angular momentum, and a_l^i are known functions. In most cases, only the l = 0,1 multipoles are fitted to the data with the higher l multipoles taken either from dispersion relations or from the nucleon Born terms. As the multipoles are complex quantitites, we see that Watson's theorem reduces in half the number of parameters that need to be fitted to the data.

In figure 1 we show the real parts of $M_{1+}^{3/2}$ and $E_{1+}^{3/2}$ obtained from three different multipole analyses (BD, GET, MIR; see ref. [3]). Below we discuss the curves in this figure. The $M_{1+}^{3/2}$ (fig. 1b) clearly shows a resonant structure, but it is not clear if the $E_{1+}^{3/2}$ (fig. 1a) has a resonant contribution. Regarding the consistency of the different multipole sets, we are not surprised that there is disagreement for the $E_{1+}^{3/2}$, since it is a relatively small multipole, but the discrepancies appearing in the $M_{1+}^{3/2}$ are surprising. It is even more alarming when one considers that the errors given for the $M_{1+}^{3/2}$ are 1% or less. It is hoped that the new experiments will help resolve these discrepancies.

Now that we have the multipoles, we still must seperate them into their background and resonant parts in order to get E2 and M1 which we want to compare with the baryon models. In general, we expect a resonant multipole $\mathcal{A}$ to be of the form

$$\mathcal{A} = B + \frac{M_\Delta \sqrt{\Gamma_\gamma(W)\Gamma_\pi(W)}}{W^2 - M_\Delta^2 + iM_\Delta\Gamma_\pi(W)}, \tag{3}$$

where M_Δ is the mass of the delta, Γ_γ the photon decay width, Γ_π the pion decay width, and B is the background contribution which varies smoothly with energy. The first problem is that we must make sure the above amplitude satisfies Watson's theorem. The second problem is what to take for the energy dependence of the widths and how to check if they have a reasonable energy dependence. The third problem is what to take for B and if there is any way to check B; this is of particular importance when analyzing the $E_{1+}^{3/2}$. These problems will be addressed in the next section.

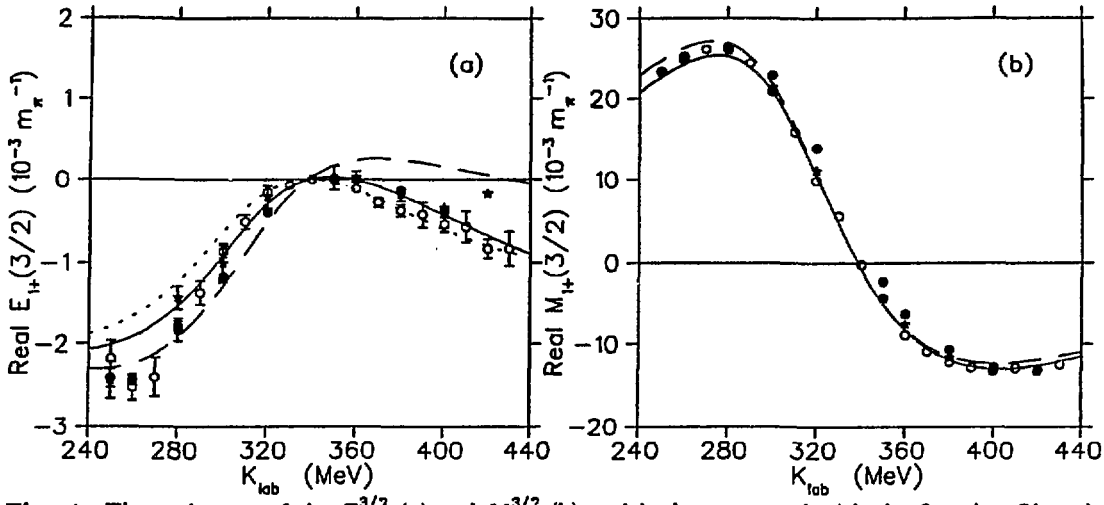

Fig. 1. The real parts of the $E_{1+}^{3/2}$ (a) and $M_{1+}^{3/2}$ (b) multipoles compared with the fit using Olsson's method (solid line) and Noelle's method (dashed line). The dotted line in fig. 1a is obtained from Olsson's method by turning off the resonant contribution. The data are from BD (open circles), MIR (solid circles), and GET (stars). See ref. 3 for abbreviations.

3 The effective Lagrangian approach

The effective Lagrangian approach has long been used to study low energy πN scattering and pion photoproduction [4]. We follow and extend these previous works. The main advantage of this approach is the simplicity in which important symmetries can be incorporated: chiral symmetry, gauge invariance, Lorentz invariance, etc. The main disadvantage is that it is not clear how to implement unitarity. Here, we consider three methods to unitarize the amplitude, Olsson's method [5], Noelle's method [6], and the K-matrix method [7].

We start a comparison of these unitarization methods by looking at πN scattering in the resonant P33 channel. Starting from the effective Lagrangian for the $\pi N\Delta$ vertex [7], we obtain a contribution to the partial wave $f_{1+}^{3/2}$

$$qf_{1+}^{\Delta} = \frac{M_\Delta \Gamma_\pi(W)}{M_\Delta^2 - W^2} \equiv \frac{1}{\epsilon} \equiv tan\delta_R, \tag{4}$$

$$\Gamma_\pi(W) = \frac{g_{\pi N\Delta}^2 (E+M) q^3 (W+M_\Delta)}{24\pi\mu^2 W M_\Delta}, \tag{5}$$

where $g_{\pi N\Delta}$ is the pion-nucleon-delta coupling constant, E is the final nucleon energy, q is the pion three momentum, M is the nucleon mass, and μ is the pion mass. We see that the effective Lagrangian gives a prediction for the energy dependence of the pion width. Taking into account a background contribution at the tree level of the form $qf_{1+}^{B} \equiv tan\delta_B$, the three different unitarization methods give for δ_{33}

$$tan\delta_{33} = \frac{1 + \epsilon tan\delta_B}{\epsilon + \eta tan\delta_B}, \tag{6}$$

where η =+1, -1, 0 for the Olsson, Noelle, and K-matrix methods respectively. An interesting feature is that value(s) of $tan\delta_{33}$ can be found in all three methods at which $g_{\pi N\Delta}$ and M_Δ can be found independently of $tan\delta_B$. Thus, $tan\delta_R$ is known and δ_B can be determined from eqn. 6 using the experimental δ_{33}. This method however does not tell us how reasonable the energy dependence of the width is, and therefore it is useful to assume some form for $tan\delta_B$ and fit the

parameters to δ_{33}. Taking $tan\delta_B = a(q/\mu)^3 + b(q/\mu)^5$, we find $(g_{\pi N\Delta}, M_\Delta) = (1.94, 1217)$, (2.46, 1250), and (2.16, 1232) for the Olsson, Noelle and K-matrix methods respectively (M_Δ in MeV). These values agree within a few percent with those obtained from the special values of $tan\delta_{33}$. In each case, assumming an error of 1 degree for δ_{33} at every energy, the χ^2_{DF} is 0.45 and $a \approx 0.1$, $b \approx$ -0.01. Note the model dependence of $g_{\pi N\Delta}$ and M_Δ, which will carry over into our determination of E2 and M1.

Having determined $\Gamma_\pi(W)$, which gives a good description of δ_{33}, we now proceed to the (γ, π) channel. For the background contribution, we take the pseudovector Born terms, which are known to dominate at threshold [7], and provide a smooth extrapolation to higher energies. This part of the amplitude has no free parameters and contributes to all the multipoles including the $M_{1+}^{3/2}$ and the $E_{1+}^{3/2}$. We have also included t-channel ω and ρ exchanges. The couplings here are not well known, and will lead to some additional uncertainty in our determination of E2 and M1. The last part of the amplitude comes from s- and u-channel delta exchange. The s-channel delta exchange produces resonant contributions in the $E_{1+}^{3/2}$ and $M_{1+}^{3/2}$ multipoles, and the u-channel delta contributes to all the isovector multipoles. *Therefore, all the isovector multipoles must be fitted when determining E2 and M1, not just the $E_{1+}^{3/2}$ and $M_{1+}^{3/2}$.*

The last step is to unitarize the multipoles. For a non-resonant multipole A_B, this is achieved by $A_B \rightarrow A_B cos\delta e^{i\delta}$, where δ is the appropriate πN phase shift. For the resonant multipoles, the different methods give

$$A_{Ol} = e^{i\delta_{33}}\left[A_B cos(\delta_{33} - \delta_B) + \sqrt{1 - \frac{A_B^2}{N^2}} N sin(\delta_{33} - \delta_B)\right], \tag{7}$$

$$A_N = e^{i\delta_{33}}\left[A_B cos\delta_{33} + N sin(\delta_{33} - \delta_B)\right], \tag{8}$$

$$A_K = e^{i\delta_{33}}\left[A_B cos\delta_{33} + \frac{N}{\epsilon} cos\delta_{33}\right], \tag{9}$$

where A refers to either the $E_{1+}^{3/2}$ or the $M_{1+}^{3/2}$ multipole, and the subscript denotes the unitarization method (Ol=Olsson, N=Noelle, K=K-matrix). Note that Watson's theorem is manifestly satisfied. A_B is the projection of the background (all terms excluding the s channel delta) into the resonant multipole. Also,

$$N_M = C\left[g_{1\Delta}(3W + M) - g_{2\Delta}\frac{W(W - M)}{2M}\right], \tag{10}$$

$$N_E = -C(W - M)\left[g_{1\Delta} - g_{2\Delta}\frac{W}{2M}\right]; C = \frac{e\sqrt{E_i + M}k\mu}{4g_{\pi N\Delta}\sqrt{E + M}q^2 M(W + M)}, \tag{11}$$

where E_i is the intial nucleon energy and k is the photon three momentum. In these equations, $g_{1\Delta}$ and $g_{2\Delta}$ are the gauge couplings that are fitted to the data and determine E2 and M1. Specifically,

$$M1 = \frac{e}{12M}\sqrt{\frac{k_\Delta}{M_\Delta M}}\left[g_{1\Delta}(3M_\Delta + M) - g_{2\Delta}\frac{M_\Delta(M_\Delta - M)}{2M}\right] \tag{12}$$

$$E2 = \frac{-e}{6M}\frac{k_\Delta}{(M_\Delta + M)}\sqrt{\frac{k_\Delta M_\Delta}{M}}\left[g_{1\Delta} - g_{2\Delta}\frac{M_\Delta}{2M}\right], \tag{13}$$

where k_Δ is the photon energy evaluated at W = M_Δ.

Another nice feature of this approach is that the parameters that determine the background contribution in the resonant multipoles also determine the nonresonant multipoles, therefore *the accuracy of the background contribution to the resonant multipoles can be tested by how well the model reproduces the nonresonant multipoles.*

An alternate approach to (γ,π) is the "dynamical" model [8]. Many of the input ingredients are the same as presented here; the PV Born terms, an s channel delta, and sometimes ω exchange. These are used as driving terms in either the Lippmann-Schwinger equation or a reduced Bethe-Salpeter equation, and the problem of how to unitarize the amplitude is avoided since these equations satisfy unitarity. The price one pays for this is the introduction of additional parameters coming from the form factors which are needed to make the integrals convergent. The Born terms are multiplied by the same common form factor which is not expected on physical grounds, but it simplifies the gauge invariance constraint. Finally, it is not clear if some double counting is going on, in the sense that part of the dispersive integral is already contained in the couplings and masses. The K-matrix method considered here has been shown [8, 7] to result when only the absorptive part of the rescattering integral is kept, i.e. this method assumes that the dispersive part of the integral only renormalizes the couplings and masses to their physical values and that the energy dependence away from their points of definition are unimportant.

4 Results

Having now obtained a unitarized amplitude, the gauge couplings are fitted to various extant multipole sets [3] using the three different unitarization methods. We find that the extracted E2 and M1 are quite sensitive to the method of unitarization, which is not surprising considering that the different methods give quite different values for $g_{\pi N\Delta}$, and $N_{E,M} \propto 1/g_{\pi N\Delta}$ (see eqns. 10-11). Considering all data sets, we find: M1 = 250±16, E2=-4.05±0.91, and E2/M1=-1.63±0.37% for Olsson's method; M1=333±16, E2= -8.34±3.45, and E2/M1=-2.50±0.98% for Noelle's method; M1=283±10, E2=-4.72±0.96, and E2/M1=-1.68±0.32% for the K-matrix method, where E2 and M1 are in units of $10^{-3}GeV^{-1/2}$. The errors here reflect the spread of values obtained from fitting the different data sets. Considering all the fits, including those with different ω couplings, our final results are M1=285±37, E2=-4.60±2.58, and E2/M1=-1.57±0.72%.

In figure 1 we show the fits to the resonant multipoles using Olsson's method (solid line) and Noelle's method (dashed line) compared to the data of BD (open circles), MIR (solid circles), and GET (stars) (see ref. [3] for the meaning of the abbreviations). Visually the fits look quite good, but due to the extremely small error bars the χ^2_{DF}'s can be quite large (see ref. [7] for more details). For the $E^{3/2}_{1+}$ we also show what happens if the resonant delta contribution is turned off in this multipole (dotted line). We see that it gives a very good fit to the data, but the χ^2 for this multipole is about 40% larger than that obtained using Olsson's method with the resonant contribution.

In figure 2 we show two of the background multipoles, namely the $E^{3/2}_{0+}$ and $M^{1/2}_{1-}$ compared with the data of BD (open circles) and PS (solid circles). The $M^{1/2}_{1-}$ has a large contribution from the u-channel delta exchange, indicated by the difference between the solid line and the dashed line. Again we see discrepancies between the data sets.

The observables for (γ,π) are well reproduced for all charge channels for energies (photon lab energy) $\lesssim$ 450 MeV and cm angles $\lesssim 120°$ for $p\pi^0$ production and $\lesssim 150°$ for charged pion production. In figure 3 we show some results for $\gamma p \to p\pi^0$ using Olsson's method (solid line) and Noelle's method (dashed line). Although Noelle's method does a better job in fitting the cross sections at these angles than Olsson's method does (figs. 3a,b) it totally fails for the observables related to the photon asymmetry (figs. 3c,d). While Olsson's method gives excellent agreement with the older data [9, 10] for the photon asymmetry (Σ), it is in disagreement with the new Brookhaven data [11] for $\sigma_\parallel/\sigma_\perp = (1-\Sigma)/(1+\Sigma)$. We also notice in fig. 3b a discrepancy between the new Brookhaven data and the older Bonn data [9]. As the Bonn data weighed in heavily in the multipole analyses, it will be interesting to see what the new Brookhaven data imply for the multipoles, particularly the $E^{3/2}_{1+}$ and $M^{3/2}_{1+}$.

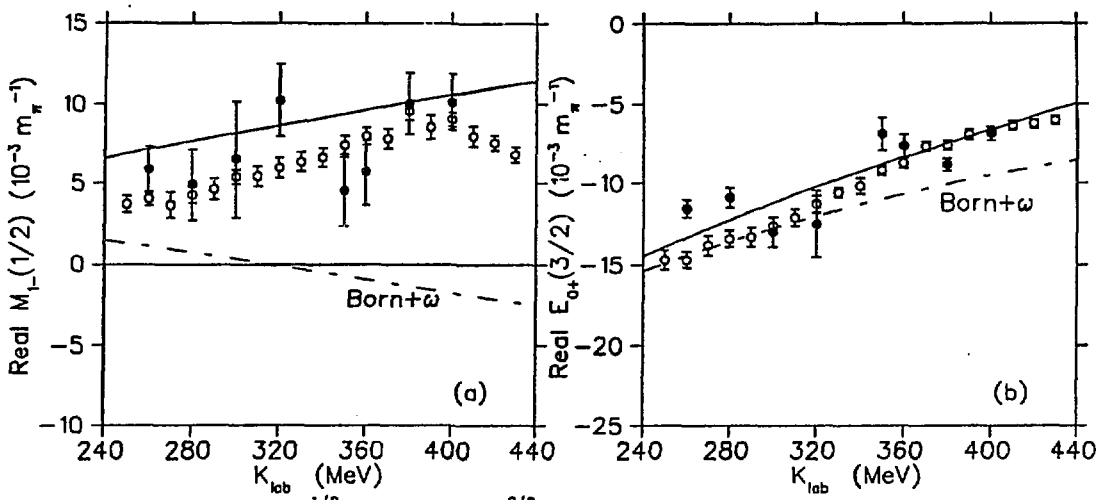

Fig. 2. The real parts of $M_{1-}^{1/2}$ (fig. 2a) and $E_{0+}^{3/2}$ (fig. 2b). The dashed curve is the contribution from the Born and ω exchanges, while the solid curve is the full calculation. The data are from BD (open circles) and PS (solid circles) [3].

5 Summary and conclusions

We have considered an effective Lagrangian model for (γ, π) production in the delta resonance region in an effort to extract the E2 and M1 nucleon-delta transition amplitudes from the extant multipole data sets. The amplitude is evaluated in the tree approxiamtion, and subsequently unitarized according to three different methods. The parameters determining the E2 and M1 are then fitted to different multipole sets, and the accuracy of the background contribution in the resonant multipoles is gauged by how well the nonresonant multipoles are reproduced. Although different multipole data sets imply different values for the E2 and M1, we find that the largest uncertainty in these extracted amplitudes arises from the ambiguity (in this approach) of how to unitarize the amplitude. Despite the large sensitivity to the unitarization method, we find E2/M1 = -1.57±0.72%.

In the near future we can look forward to higher quality data for (γ, π) production in the delta resonance region and beyond, and hopefully a better determination of the multipoles. The theoretical challenges will be many. The new data will push the current (γ, π) models to the limit, eventually resulting in a better understanding of pion photoproduction. Second, given the multipoles, we must decide on a suitable defintion of E2 and M1, as many definitions now exist in the literature. As an illustration of this point, one only need to consider the different values of $g_{\pi N\Delta}$ obtained from the different unitarization methods considered here. Third, the quantitative comparison of E2 and M1 with predictions from essentially static baryon models can be pushed only so far. The real test of these models will be in direct comparison with the scattering data.

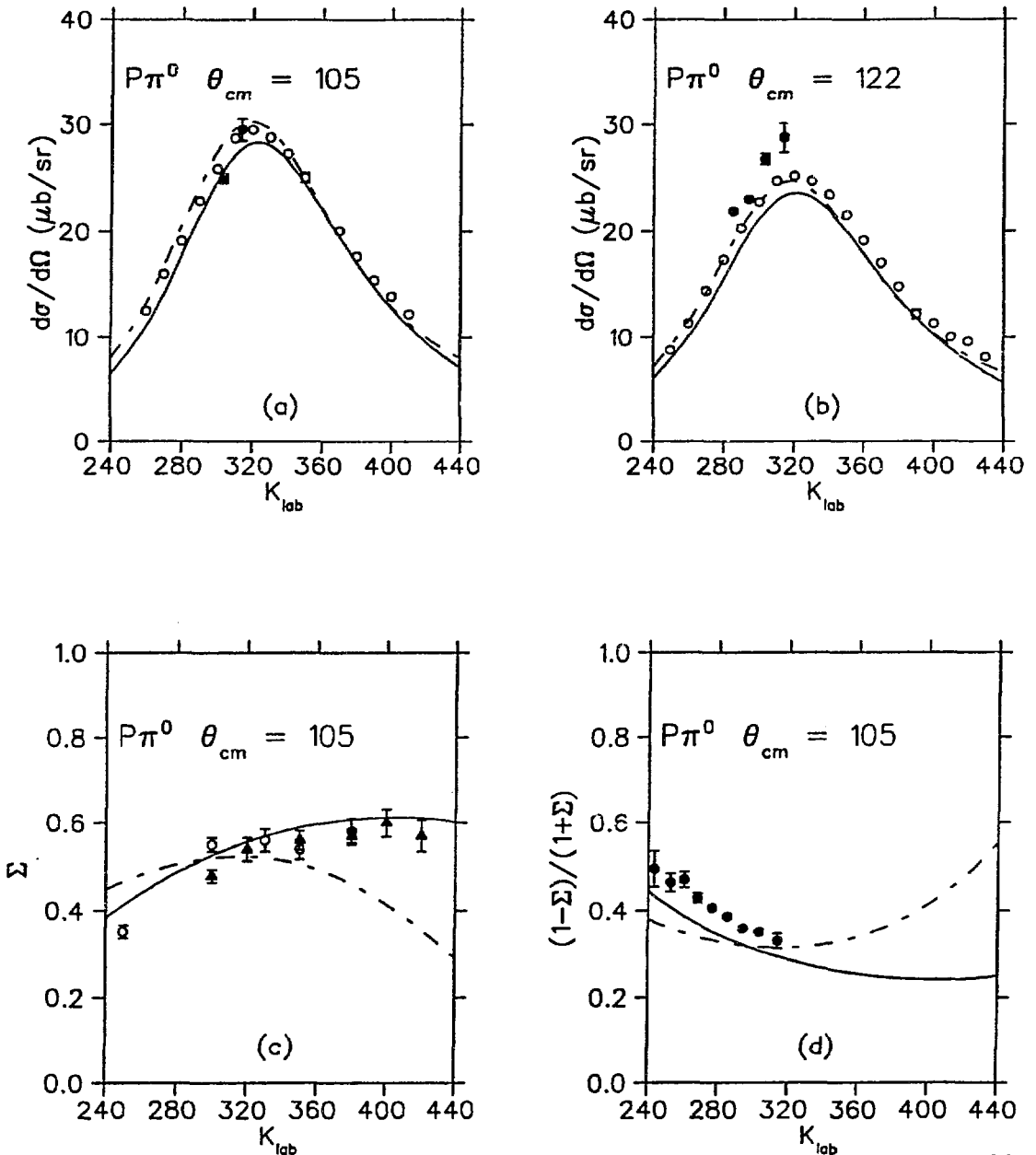

Fig. 3. *Differential cross sections for $\gamma p \rightarrow p\pi^0$ at 105° (fig. 3a) and 122° (fig. 3b). Data are from [9] (open circles) and [11] (solid circles). Fig. 3c shows $\Sigma(105°)$ while fig. 3d is $\sigma_{\parallel}/\sigma_{\perp}$ also at 105°. The open circles are from ref. [9], the triangles from ref. [10], and the solid circles from ref. [11]. The solid curve is obtained using Olsson's method, while the dashed curve is obtained from Noelle's method.*

References

[1] S.L. Glashow, Physica **A96** 27 (1979). N. Isgur, G. Karl, and R. Koniuk, Phys. Rev. **D25**, 2394 (1982). M. Bourdeau and N.C. Mukhopadhyay, Phys. Rev. Lett. **58**, 976 (1987) and **63**, 335 (1989). G. Kälbermann and J.M. Eisenberg, Phys. Rev. **D34**, 3472 (1983). G.S. Adkins, C.R. Nappi, and E. Witten, Nucl. Phys. **B228**, 552 (1983). T.D. Cohen and W. Broniowski, Phys. Rev. **D34**, 3472 (1986).

[2] K.M. Watson, Phys. Rev. **95**, 228 (1954). E. Fermi, Supp. Nuovo Cimento **10**, 17 (1955).

[3] F. Berends and A. Donnachie, Nucl. Phys. **B84**, 342 (1975) (BD). W. Pfeil and D. Schwela, Nucl Phys. **B45**, 379 (1972) (PS). V.A. Get'man, V.M. Sanin, Yu Telegin, and S.V. Shalaskil, Sov. J. Nucl. Phys. **38**, 230 (1983) (GET). V.F. Grushin A.A. Shikanyan, E.M. Leikin, and A. Ya Rotvain, Sov. J. Nucl. Phys. **38**, 881 (1983) (GRU). I.I. Miroshnichenko, V.I. Nikiforov, V.M. Samin, P.V. Sorokin, and S.V. Shalatskil, Sov. J. Nucl. Phys. **32**, 339 (1980) (MIR). The initials at the end are used in the text to refer to specific data sets.

[4] R.D. Pecci, Phys. Rev. **181**, 1902 (1969). M.G. Olsson and E.T. Osypowski, Nucl. Phys. **B87**, 399 (1975) and Phys. Rev. **D17**, 174 (1978).

[5] M.G. Olsson, Nucl. Phys. **B78**, 55 (1974).

[6] P. Noelle, Prog. Theor. Phys. **60**, 778 (1978).

[7] R.M. Davidson, N.C. Mukhopadhyay and R.S. Wittman, Phys. Rev. **D43**, 71 (1991). M. Benmerrouche, R.M. Davidson, and N.C. Mukhopadhyay, Phys. Rev. **C39**, 2339 (1989).

[8] S. Nozawa, B. Blankleider, and T.-S. Lee, Nucl. Phys. **A513**, 459 (1990). H. Tanabe and K. Ohta, Phys. Rev. **C31**, 1876 (1985). S.N. Yang, J. Phys. **G11**, L205 (1985). See also Nozawa's contribution to this workshop.

[9] D. Menze, W. Pfeil, and R. Wilcke, Bonn compilation of pion photoproduction data.

[10] A.A. Belyaev et al., Sov. J. Nucl. Physics **35**, 401 (1982).

[11] LEGS data releases nos. L2-5.1 and L2-5.2 (1992).

New Measurements of the $p(\vec{\gamma},\pi^\circ)$ Reaction at LEGS

M. A. Khandaker[6], G. S. Blanpied[4], M. Blecher[6],
A. Caracappa[1], C. Djalali[4] , M-A. Duval[4], G. Giordano[2],
S. Hoblit[5], O. C. Kistner[1], G. Matone[2], L. Miceli[1],
W.K. Mize[4], B.M. Preedom[4], A.M. Sandorfi[1], C. Schaerf[3],
R. M. Sealock[5], C. E. Thorn[1], S. T. Thornton[5], K. Vaziri[7],
C. S. Whisnant[1,4], X. Zhao[6], and M. A. Moinester[8]

(The LEGS collaboration)

[1]*Physics Department, Brookhaven National Laboratory, Upton, NY, 11973*
[2]*INFN-Laboratori Nazionali di Frascati, Frascati, Italy*
[3]*Universita di Roma and INFN-Sezione di Roma, Rome, Italy*
[4]*Department of Physics, University of South Carolina, Columbia, SC, 29208*
[5]*Department of Physics, University of Virginia, Charlottesville, VA, 22903*
[6]*Physics Dept., Virginia Polytechnic Institute & State University, Blacksburg, VA, 24061*
[7]*Rensselaer Polytechnic Institute, Troy, NY, 12180-3590*
[8]*School of Physics and Astronomy, Tel Aviv University, 69978 Tel Aviv, Israel*

Results from three independent measurements of the $p(\vec{\gamma},\pi^\circ)$ reaction are presented for incident photon energies between 243 and 314 MeV. The ratio of cross sections measured with orthogonal states of linear polarization is sensitive to the $E2$ excitation of the Δ resonance. Comparisons are made to the predictions of various models, all of which fail to reproduce these data.

I. INTRODUCTION

Essentially all constituent quark models invoke a tensor interaction between the quarks in a proton which comes about through one-gluon exchange. This tensor force between quarks mixes a D state into what would otherwise be a purely S wave proton. The D wave component breaks spherical symmetry, resulting in a non-vanishing $< r^2 Y_2 >$ matrix element for the nucleon and a static quadrupole moment and deformation for its first excited state, the delta (Δ) resonance, at about 320 MeV. The magnitude and sign of this D state component are quite sensitive to the internal structure of the proton and have been of great interest in recent years [1].

The experimental signature of such a D wave component lies in the excitation of the nucleon to the Δ. The Δ is excited mainly by $M1$ photons which induce quark-

spin-flip transitions. If there is a D wave component in the Δ then this transition can also be excited by $E2$ photons. The challenge is to evaluate the relative magnitude of this $E2$ excitation in the presence of the dominant $M1$ transition. A variety of models predict this mixing ratio to be quite small, anywhere from -0.9% to -6% [2], so that a high degree of precision is demanded of experiment.

The isospin (I) 3/2 Δ decays with a 99.4% branch to a pion-nucleon (πN) final state. An $E2$ photon will produce a P-wave pion so that, in the Chew-Goldberger-Low-Nambu notation [3], the mixing ratio of interest is written in terms of photo-pion multipoles as E_{1+}/M_{1+}. There have been many determinations of the I=3/2 parts of these multipoles from existing pion photo-production data. For the most part, these agree on the dominant M_{1+} amplitude but differ on smaller components such as E_{1+}. The photo-pion multipoles are usually constrained to satisfy Watson's theorem [4], a particular form of Unitarity which fixes their phases in terms of the πN phase shifts. Although this is strictly valid only below 2π threshold (309 MeV), it is usually imposed at higher energies. To extract the part of the I=3/2 E_{1+} multipole associated with the Δ requires a further decomposition of this amplitude into resonant and background components. This decomposition is not unique, and in recent years many models have been reported, quoting values ranging from +4% to -8% for the ratio of the resonant parts of the I=3/2 E_{1+} and M_{1+} amplitudes [5].

II. POLARIZATION OBSERVABLES IN PION PRODUCTION

In charged-pion production, Δ excitation interferes with a large non-resonant E_{0+} background which obscures the presence of E_{1+} components. However, the situation is much more favorable in π° production, where backgrounds are greatly reduced. The sensitivities in reactions not involving a polarization observable are extremely small. Effects in recoil polarization measurements, $p(\gamma,\vec{p})\pi^\circ$, are also expected to be quite small. The polarized target asymmetry from $\vec{p}(\gamma,\pi^\circ)$ should exhibit some sensitivity to an E_{1+} component, but only at extreme forward and backward angles where measurements are difficult. The pion photo-production observable that is most sensitive to the E_{1+} multipole is associated with the $p(\vec{\gamma},\pi^\circ)$ reaction. Calculated cross sections for different orientations of linear polarization are shown in fig. 1. The thick-solid and thick-dashed lines assume that the incoming photon's electric field vector is parallel and perpendicular to the reaction plane, respectively. The thin lines give the corresponding predictions for the case when the resonant part of the E_{1+} is set to zero. (These are from the model of ref. [6]. Other models predict the same qualitative behavior.)

For all but extreme forward and backward angles, reactions with the perpendicular orientation of the beam polarization vector are completely insensitive to the $E2$ mixing in the Δ. Essentially all the sensitivity comes from reactions with the parallel polarization geometry. (The perpendicular cross section is much bigger than the parallel and dominates unpolarized measurements, thus rendering the unpolarized cross section insensitive.) This is actually a rather convenient situation, since the ratio of

parallel/perpendicular cross sections ($d\sigma_{\parallel}/d\sigma_{\perp}$) can now be formed. All of the sensitivity to the E_{1+} multipole will be preserved through the numerator of this ratio, and at the same time most of the systematic experimental uncertainties will cancel out.

The cross section for $\gamma p \rightarrow \pi^{\circ} p$ can be measured by detecting either the recoil proton or the two photons from the decay of the π°. The efficiency of the latter changes with both angle and incident γ energy, which is not desirable when studying small effects. Detecting the recoil protons avoids this problem, although at forward angles the proton energy becomes quite low.

III. MEASUREMENTS AT LEGS

New measurements of the $p(\vec{\gamma},p)\pi^{\circ}$ reaction have been made at the Laser Electron Gamma Source (LEGS) located at the National Synchrotron Light Source of Brookhaven National Laboratory [7]. Linearly polarized γ rays up to 319 MeV were produced by backscattering polarized ultra-violet laser light from 2.5 GeV electrons. The γ-ray energy was determined, to typically 5 MeV, by detecting the scattered electrons in a tagging spectrometer [8]. Many of the details of these measurements are similar to those described in ref. [9].

To test the sensitivity to systematic uncertainties that may survive the $d\sigma_{\parallel}/d\sigma_{\perp}$ cross section ratio, three independent experiments have been conducted with different detectors, different methods of defining the γ-ray energy and monitoring the γ-flux, different polarizations, and using two targets of liquid hydrogen having different cell configurations. All of the data in various energy intervals from 243 MeV to 314 MeV were collected simultaneously. The main characteristics of these experiments are summarized in Table I.

The μ-Strip detector of Exp. L2s consisted of four planes of silicon microstrips, providing track reconstruction for each proton, followed by a 1-cm-thick plastic scintillator and backed by a 25-cm-deep NaI(Tl) crystal. The array of Phoswich detectors in Exp. L2p were composites of 1-2 mm of CaF_2 followed by 30-50 cm of plastic scintillator. During the latter experiment, data were also collected simultaneously at 122° and 150° CM. The operation of the μ-Strip and Phoswich detectors are described in greater detail in ref. [9]. The detector of Exp. L5 was a 1-cm-thick plastic scintillator followed by a 25-cm-deep NaI(Tl) crystal. In each detector system, protons were selected by imposing cuts in energy-loss and total energy deposition. During analysis of data from the μ-Strip array, the photon tag was ignored and the γ-ray energy was reconstructed from the measured proton energy and momentum vector. Only tagged-photon data were collected during Exps. L2p and L5. For Exp. L2s, the γ-ray flux in each energy interval was calculated in a Monte Carlo simulation of the laser-backscattering process, normalized to the total tagged flux. For Exps. L2p and L5, the tagged flux as a function of energy was monitored by counting the Compton-scattered electrons in coincidence with e^+e^- pairs produced in thin, high-Z converters that remained in the γ-beam throughout the experiments. During all of

the experiments, the polarization was randomly flipped between directions parallel and perpendicular to the reaction plane at a frequency averaging once every 180 sec. The contribution from unpolarized bremsstrahlung in the residual gas of the electron-beam vacuum chamber (< 1%) was also monitored every 180 sec. During Exp. L2, the laser light was partially depolarized, while for Exp. L5 its polarization was nearly 100%. The resulting polarizations of the high energy γ-rays are given in Table I. The targets were liquid-hydrogen-filled cylinders, 3.8 cm in diameter transverse to the γ-ray beam during Exp. L2 and 10.0 cm along the beam during Exp. L5. Background contributions from reactions within the walls of the target chambers and of the vacuum chamber windows were subtracted in measurements with the targets filled with ^{4}He gas, normalized to the same integrated γ-flux.

IV. NEW RESULTS

The $d\sigma_{||}/d\sigma_{\perp}$ cross section ratios measured at 105° in the three experiments are plotted in fig. 2. The error bars reflect the combined statistical and polarization-dependent systematic uncertainty. In each of the three experiments, the recoil-proton spectrum was integrated over $p(\vec{\gamma},p)\gamma$ events as well as those from π°-production. In $(\vec{\gamma},p)\pi^\circ$, the parallel cross section is much smaller than the perpendicular, while the reverse is true in Compton scattering, and the $d\sigma_{||}/d\sigma_{\perp}$ ratio amplifies this difference over what would otherwise be a negligble effect. The $p(\vec{\gamma},p)\gamma$ contribution was calculated using the Compton-partial-wave amplitudes of ref. [10]. The Compton-corrected weighted-mean of these results is plotted as the solid circles in the bottom panel of fig. 3. The reduced χ^2 of the measurements from the three experiments relative to this weighted-mean is 1.8 over the overlapping energy range of these data sets. Data at 122° and 150° CM, taken during Exp. L2p, are also shown. Previously published data, open symbols, are generally consistent with these results, albeit with larger errors [11, 12].

V. COMPARISON OF DATA WITH MODEL CALCULATIONS

Plotted with the data of fig. 3 are the results of two recent model calculations. The curves lying generally above the data (labeled as NBL) are the work of Nozawa, Blankleider and Lee [6], and result from evaluation of the various diagrams for photo-pion production. Final state interactions (FSI) between the outgoing π and N are explicitly taken into account, and the imaginary parts of the amplitudes are determined by πN scattering phase shifts in such a way that Watson's theorem is automatically satisfied. The constants of the model are determined in a fit of the full (Δ + calculated-non-resonant background) $M_{1+}(I = 3/2)$ and $E_{1+}(I = 3/2)$ amplitudes to published multipoles. Fitting the constants of their model to the Berends and Donnachie (BD) photo-pion multipoles [13], Nozawa *et al.* deduced a mixing ratio of -3.1%. The predictions for the $d\sigma_{||}/d\sigma_{\perp}$ ratio are shown as the long-dashed-short-dashed curves in the figures. The dashed-dotted curves are obtained by setting the

$E_{1+}(I = 3/2)$ resonant term to zero.

The curves lying generally below the data (labeled as DMW) are the work of Davidson, Mukhopadhyay and Wittman [14]. In their approach, photo-production is described in terms of effective Lagrangians with five free parameters. FSI are not explicitly treated and the resulting amplitudes are real, which would violate Watson's theorem. These amplitudes are then multiplied by an exponential containing the πN phase shifts. This recovers Unitarity and effectively includes some FSI implicitly. The methods of decomposing the resulting multipoles into background and resonant components is not unique, and several are discussed in ref. [14]. In fig. 3 we show calculations in which the background and resonant parts have been made separately Unitary (refered to as the "Olsson method" in ref. [14]), since these results are closest to the data. Using the same set of BD multipoles [13], Davidson *et al.* deduce a resonant E_{1+}/M_{1+} mixing ratio of -1.4%. The DMW predictions for the $d\sigma_{\parallel}/d\sigma_{\perp}$ ratio are shown as the solid curves in fig. 3. The dashed curves are obtained by setting the resonant part of the $E_{1+}(I = 3/2)$ amplitude to zero. Although the DMW value of -1.4% for the mixing ratio is about half of that deduced by NBL (-3.1%), it must be remembered that the latter reflects the "bare" $\gamma N\Delta$ coupling, without any dressing from FSI, while that of the DMW calculation implicitly includes the effects of FSI at some level.

At 105°, where the sensitivity to a resonant $E2$ component is nearly maximal, both full calculations approach the data near the peak of the Δ (about 320 MeV). However, the energy dependence of $d\sigma_{\parallel}/d\sigma_{\perp}$ ratio provides the crucial test of the resonance-background decomposition, and here both models fail rather badly. At larger angles the comparison with Nozawa *et al.* becomes dramatically worse, while those of Davidson *et al.* become much more reasonable.

It is interesting to compare the NBL and DMW curves with direct predictions of the BD multipoles. The latter are published as fixed-energy solutions. Since energy-dependent fluctuations in these are averaged out in the process of fitting the model parameters, the appropriate comparison should be to predictions made with a smoothed-energy-dependent form of these multipoles. These are shown as the dashed curves, labeled (BDLE) in fig. 3 [15]. The full calculations of both the NBL and the DMW models should reproduce the BDLE curves which were used to fix their model parameters. Neither do, and there are two possible reasons for the large discrepancies evident here: (1) the description of the physical processes in both of the models is incomplete; or (2) although one of the models may provide a sufficiently complete description of the $p(\vec{\gamma}, \pi^{\circ})$ reaction, the multipole set used to fix model parameters is flawed. In fact, the data of fig. 3 question the validity of existing multipole decompositions, at least for small amplitudes. Although the predictions of the BDLE solution are in fairly good agreement with the 105° results, this appears fortuitous since the agreement at the larger angles is quite poor.

A number of π-production experiments have been completed since the BD analysis, most noteably the measurements of spin observables made at Khar'kov [11, 12]

However, the inclusion of these data into a multipole analysis does not lead to a superior representation of the E_{1+} sensitive $d\sigma_{\parallel}/d\sigma_{\perp}$ ratio [16]. This is at least partly due to the larger errors on previously published polarization data, and partly to ambiguities in the analysis resulting from the systematic uncertainties associated with the various unpolarized measurements.

The accuracy of the present data set would be sufficient to distinguish differences equivalent to $\sim 1/3$ of the separation between the full and 0%–$E2$ calculations of fig. 3. However, the large discrepancies between the measured $d\sigma_{\parallel}/d\sigma_{\perp}$ ratios and the various calculations described above must be resolved before attempting to confront QCD-Hadron models with a resonant $E2$ component of Δ excitation. Although new experiments are needed, particularly large sets of simultaneously measured observables with few systematic uncertainties, it is doubtful that this could bring both the NBL and DMW model predictions into agreement.

The LEGS collaboration is supported by the U.S. Department of Energy under Contracts No. DE-AC02-76-CH00016 and No. DE-FG05-89ER40501, and in part by the Istituto Nazionale di Fisica Nucleare (Italy) and the U.S. National Science Foundation. One of us (A.M.S.) would like to thank Drs. R. Arndt, R. Davidson, H. Lee, S. Nozawa and R. Workman for many stimulating discussions, and for providing the various calculations that are included here.

TABLES

TABLE I. Different characteristics of the $p(\vec{\gamma},p)\pi^{\circ}$ experiments at 105° CM.

Expt.#	Detector	E_{γ}–definition	γ–Flux	γ–Polarization	Target
L2s	μ-Strip	Kin-reconstruction	Monte Carlo	83.0±1.5 %	3.8 cm
L2p	Phoswich	E_e Tagging	Tagged e^+e^-	83.0±1.5 %	3.8 cm
L5	NaI(Tl)	E_e Tagging	Tagged e^+e^-	95.0±1.0 %	10.0 cm

REFERENCES

[1] S.L. Glashow, Physica **A96**, 27 (1979). M. Giannini, Rep. Prog. Phys. **54**, 453 (1991) and ref. contained therein.

[2] N.C. Mukhopadhyay, Topical Workshop on Excited Baryons-1988, Eds. G. Adams, N. Mukhopadhyay, P. Stoler, World Sci. 205, 1989.

[3] G. F. Chew, M. Goldberger, F. Low, Y. Nambu, Phys. Rev. **106**, 1345 (1957).

[4] K. M. Watson, Phys. Rev. **95**, 228 (1954).

[5] See, for example, H. Tanabe and K. Ohta, Phys. Rev. **C31**, 1876 (1985); S. N. Yang, J. Phys. bf G11,L205 (1985); and refs. [6] and [14] below.

[6] S. Nozawa, B. Blankleider and T.-S.H. Lee, Nucl. Phys. **A513**, 459 (1990), and priv. comm.

[7] A. M. Sandorfi *et al.*, IEEE **NS-30**, 3083 (1983).

[8] C. E. Thorn *et al.*, Nucl. Inst. Meth. **A285**, 447 (1989).

[9] The LEGS Collaboration, G.S. Blanpied *et al.*, Phys. Rev. Lett. **67**, 1206 (1991).

[10] A.M. Sandorfi *et al.*, Topical Workshop on Excited Baryons-1988, Eds. G. Adams, N. Mukhopadhyay, P. Stoler, World Sci. 256, 1989; W. Pfeil *et al.*, Nucl. Phys. **B73**, 166 (1974).

[11] V. B. Ganenko *et al.*, Sov. J. Nucl. Phys., **23**, 162 (1976).

[12] A. A. Belyaev *et al.*, Sov. J. Nucl. Phys., **35**, 401 (1982).

[13] F.A. Berends and A. Donnachie, Nucl. Phys. **B84**, 342 (1975).

[14] R.M. Davidson, N.C. Mukhopadhyay and R.S. Whittman, Phys. Rev. **D43**, 71 (1991), and priv. comm.

[15] R. A. Arndt *et al.*, Phys. Rev. **D42**, 1853 (1990); BDLE solution calculated with the VPI-code SAID.

[16] For example, solutions SP89 or SP92 from SAID [15]

FIGURES

FIG. 1. Cross sections for different orientations of linear polarization, either parallel (Par) or perpendicular (Perp) to the $(\vec{\gamma}, \pi^\circ)$ reaction plane, and either with or without a resonant $E_{1+}(I = 3/2)$ component [6].

FIG. 2. Data from the three new experiments at 105° CM (Table I). Errors reflect the combined statistical and polarization-dependent systematic uncertainties.

FIG. 3. Shown as the solid circles are $p(\vec{\gamma}, \pi^\circ)p$ data for 150° CM (top) and 122° CM (middle), together with the weighted-mean of the data from fig. 2 at 105° CM (Bottom). Previous results are from ref. [11] (open squares) and from ref. [12] (open diamonds). The NBL calculations are from ref. [6], BDLE are from ref. [15], and the DMW are from ref. [14].

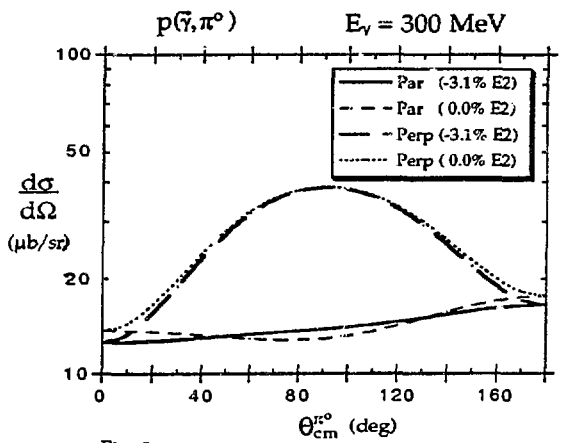

Fig. 1

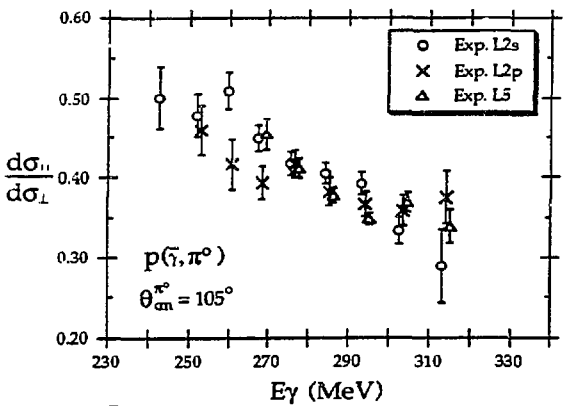

Fig. 2

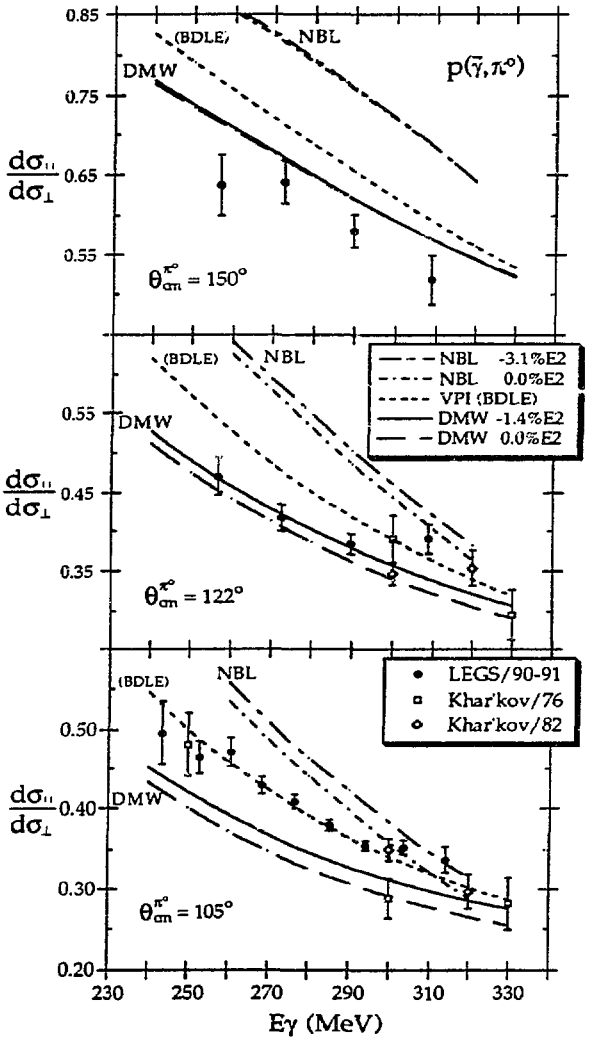

Fig. 3

Multipole Analyses and Photo-decay Couplings at Intermediate Energies

Ron L. Workman, Richard A. Arndt, and Zhu-jun Li

Department of Physics
Virginia Polytechnic Institute and State University, Blacksburg, VA 24061

Abstract

We describe the results of several multipole analyses of pion-photoproduction data to 2 GeV in the lab photon energy. Comparisons are made with previous analyses. The photo-decay couplings for the delta are examined in detail. Problems in the representation of photoproduction data are discussed, with an emphasis on the recent LEGS data.

We have recently completed a number of studies of the pion-photoproduction reaction to 2 GeV in the lab photon energy. Underlying these studies is a multipole analysis[1,2] of the existing data base. Both energy-dependent (EDS) and single-energy solutions (SES) have been obtained in an attempt to reduce the model-dependence of our results. We have extracted resonance photo-decay couplings and have compared these results with results from previous analyses and quark model predictions. A preliminary version of these results was given at Hadron 91[1].

The present results are based on the same coupled-channel K-matrix approach discussed previously[1,2]. Our final result (dubbed SM92 and accessible through the interactive SAID program[3]) gives an improved fit to the highest energy data contained in our data base. The underlying πN scattering input comes from our most recent πN analysis, which is constrained to satisfy fixed-t dispersion relations[4].

In a comparison with two other recent analyses[5,6] of this reaction, we favor the results of Crawford and Morton[6]. A brief comparison is given in Table I.

Table I. Comparison of other recent analyses.

Analysis	Energy Range	No. of Data	χ^2/datum
Arai/Fujii[5]	1.8 GeV	7768	13.2
Crawford/Morton[6]	2.9 GeV	8839	2.4

The differences in χ^2 are probably not very meaningful, as they are dependent upon the choice of data and the method used to determine the relative normalizations of different measurements. We do, however, find rather large deviations from the results of Arai and Fujii[5]. Our data base is also considerably larger than the data sets used in Refs.[5,6]. In general, the pion photoproduction data base is 'noisier' than the πN or NN sets. The $\chi^2/datum$ is given in Table II for several recent VPI analyses.

Table II. Comparison of $\chi^2/datum$ for various reactions.

Reaction	Energy Range	χ^2/datum
$\gamma N \to N\pi$	1.8 GeV	42761/11921 = 3.6
πN	2.1 GeV	60577/22072 = 2.7
pp	1.6 GeV	24862/12156 = 2.0
np	1.1 GeV	14874/ 7772 = 1.9

In addition to our analysis to 1.8 GeV, we have generated several low-energy solutions to 500 MeV. Comparisons with our 1.8 GeV solution show that the extension to higher energies has not degraded the fit to low-energy data.

From these solutions we have extracted the E2/M1 ratio, using a ratio of $\mathrm{Im}(E_{1+}^{3/2})$ to $\mathrm{Im}(M_{1+}^{3/2})$ at the resonance position. Prior to the inclusion of the recent Σ measurements from LEGS, we found values consistently between -1% and -2% in agreement with the results of Mukhopadhyay and co-workers[7]. Three solution are compared in Table III.

Table III. Comparison of VPI solution (pre-LEGS data).

Solution	E2/M1	χ^2/data(LEGS)
V400 (400 MeV)	-1.5%	168/20
SP89 (1 GeV)	-1.4%	412/20
SP92 (1.8 GeV)	-1.3%	405/20

However, if the background-resonance separation proposed by Lee[8] was used, very different values resulted for both the E2/M1 ratio and the $\Delta(1232)$ photo-decay amplitudes. Christillin and Dillon[9] have explored this difference in terms of 'bare' and 'dressed' couplings. This decomposition also seems to result in an improved agreement with the NRQM predictions.

An unusual feature of the E2 multipole, which existed in the SES of Refs. 2 and 10, is now less evident. Recall that these analyses suggested that the E2 multipole had a second zero near 450 MeV. This behavior was in marked disagreement with that displayed by EDS[1,2]. [Anyone who has worried about this feature may find Fig. 2 of Ref. 11 interesting.] In our most recent EDS (SM92), the SES and EDS show much better agreement near 450 MeV - with little evidence for a second zero.

While the above comments might imply that we have converged on correct values for the E2 and M1 amplitudes, one significant problem remains. The very recent LEGS beam-asymmetry (Σ) data[12] is not well represented by the solutions in Table III. The measurements at 150^o and 122^o are reasonably well predicted. At 105^o we seem to miss the measured data by an overall normalization. The LEGS data was subsequently

added to our data base and revised fits were obtained. The resulting χ^2 for the LEGS data was reduced but remained large.

At this point we began to play 'games' with our fits and LEGS data in order to find the source of this conflict. As a first test, we gave the LEGS data microscopic errors in order to force a fit. The results were interesting. The forced fit (F500) gave a reasonable representation of the existing P, Σ and T data (over the energy range of the LEGS experiment). The cross section data, unfortunately, suffered a large increase in χ^2.

Table IV. Comparison of fits including the LEGS data.

Solution	E2/M1	$\chi^2/data$ (LEGS)
SM92 (1.8 GeV)	−1.5%	124/20
B500 (500 MeV)	−1.5%	132/20
F500 (500 MeV)	−2.9%	29/20

The forced fit (F500) is compared to un-forced fits in Table IV. Given that F500 does poorly in fitting cross sections, the rather large shift in E2/M1 should be taken with caution. A general trend, however, is that a good fit to the LEGS Σ data tends to produce an E2/M1 ratio which is larger in magnitude. We can also say that it is 'not easy' to find a good fit to both this Σ data and differential cross section data - implying a data conflict. The situation is not likely to improve without a significant improvement in the quality of the photoproduction data base.

While this Workshop is not specifically directed toward the photoproduction of pions at high and low energies, we will make a few comments (as this will more fully describe our multipole solution). The low-energy behavior of our solution is primarily constrained by recent measurements of $\pi^- p \to n\gamma$ and $\gamma p \to p\pi^0$ near threshold. Our solutions give a reasonable account of both the recent Saclay and Mainz data.

The high-energy behavior of our EDS was studied via the isospin-decomposed Gerasimov-Drell-Hearn sum rules[13,14]. The vector-vector and vector-scalar sum rules displayed pleasing convergence properties at the high energy end of our solution. The scalar-scalar sum rule [which measures a very small component of the photoproduction reaction] was less well behaved. While the vector-scalar sum rule appeared to converge below 2 GeV, the resulting value [from the integral over photo-absorption cross sections] had a sign opposite to that predicted. We may now be able to explain this descrepancy in terms of an extended current algebra.

A connection between the GDH sum rule and current commutation relations was demonstrated by Kawarabayashi and Suzuki[15]. In particular, it was shown that an additional contribution to the isovector-isoscalar sum rule would result from certain current algebras containing Schwinger terms. Such an extended current algebra has

recently been proposed by Chang and Liang[16]. If we assume the above algebra, the following sum rule results

$$\frac{2\pi^2\alpha}{M^2}[(\kappa_p)^2-(\kappa_n)^2]+S=\int_{\omega_0}^{\infty}\frac{[\sigma_{3/2}(\omega)-\sigma_{1/2}(\omega)]_p-[\sigma_{3/2}(\omega)-\sigma_{1/2}(\omega)]_n}{\omega}d\omega. \quad (1)$$

The contribution S, due to the extension term, has the value

$$S=\frac{\alpha G_A}{3F_\pi^2}. \quad (2)$$

The left-hand-side of Eq.(2) gives a prediction of $109\mu b$. The right-hand-side is equal to twice the isovector-isoscalar integral. This has been estimated in Refs.13 and 14. A value near $70\mu b$ was estimated in Ref.14. This quantity has a rather large uncertainty. No error has been assigned to contributions coming from the $\gamma p \to \pi\pi N$ process. The integral has also been cut off at 2 GeV in the laboratory photon energy. It is remarkable that this additional contribution to the sum rule has even the correct magnitude to explain the current discrepancy.

While our solution is consistent with a previous analysis of Crawford and Morton, and has a reasonable low- and high-energy behavior, precise determinations of the photo-decay amplitudes are hindered by the existance of conflicting measurement in our data base. The apparent conflicts between recent sets of LEGS data and previous measurements suggest that more experimental work will be required before we may achieve a consensus on the E2/M1 ratio.

This work was supported in part by the U.S. Department of Energy Grant DE-AS05-76ER04928.

REFERENCES

[1]Z. Li, R.A. Arndt, L.D. Roper and R.L. Workman, contrib. to Hadron 91, Baryon 92, and submitted for publication.

[2]R.A. Arndt, R.L. Workman, Z. Li and L.D. Roper, Phys. Rev. **C 42**, 1853 (1990); 1864 (1990).

[3]Access SAID via a TELNET call to VTINTE.PHYS.VT.EDU or 128.173.7.3. The logon/password is: PHYSICS/QUANTUM.

[4]R.A. Arndt, unpublished.

[5]I. Arai and H. Fujii, Nucl. Phys. **B194**, 251 (1982).

[6]R.L. Crawford and W.T. Morton, Nucl. Phys. **B211**, 1 (1983); Particle Data Group, Phys. Lett. **B239**, 1 (1990).

[7]R.M. Davidson, N.C. Mukhopadhyay and R.S. Wittman, Phys. Rev. **D 43**, 71 (1991), and references therein.

[8]T.S.H. Lee, private communications and contribution to Baryons 92.

[9]P.Christillin and Dillon, J. Phys. **G15**, 967 (1989).

[10]F.A. Berends and A. Donnachie, Nucl. Phys. **B84**, 342 (1975).

[11]A. Jurewicz, Phys. Rev. **D 28**, 1604 (1983).

[12]A. Sandorfi, private communications.

[13]I. Karliner, Phys. Rev. **D 7**, 2717 (1973).

[14]R.L. Workman and R.A. Arndt, Phys Rev. **D 45**, 1789 (1992).

[15]K. Kawarabayashi and M. Suzuki, Phys. Rev. **152**, 1383 (1966).

[16]L.N. Chang and Y. Liang, Phys. Lett. **B 268**, 64 (1991); Phys. Rev. **D 45**, 2121 (1992); L.N. Chang, Y. Liang and R.L. Workman, contrib. to Baryons 92, and submitted to Phys. Rev. Lett.

Compton scattering off the proton at SAL

University of Saskatchewan,
Saskatchewan Accelerator Laboratory:

E.L. Hallin, D. Amendt, J.C. Bergstrom,
H.S. Caplan, R.Igarashi, D.M.Skopik

Boston University:

E.C.Booth, D. Delli Carpini, J.P. Miller

University of Illinois:

A.M.Nathan, B.E. MacGibbon, F.J. Federspiel

Abstract

The proton Compton effect has been studied in the region between the threshold for pion photoproduction and the $\Delta(1232)$. The measurements were performed using a bremsstrahlung endpoint technique and the high duty factor electron beam available at the Saskatchewan Accelerator Laboratory (SAL)[1]. The elastically scattered photons were detected with approximately 1.5% energy resolution using the Boston University NaI total absorption scintillation detector[2]. Angular distributions have been determined for $136\text{MeV} \leq E_\gamma \leq 288\text{MeV}$ and for angles in the range $50° < \theta_{cm} < 150°$. These angular distributions and the excitation functions derived from them are in excellent agreement with recent theoretical analyses [3,4].

Introduction

Elastic photon scattering from the proton has been investigated by a number of groups in the region near the $\Delta(1232)$ resonance [5,6,7,8,9]. In this energy regime, Compton scattering experiments are difficult due to the combination of the low cross sections for this process and the high cross section for the dominant background process (the decay of photo-produced neutral pions). Unfortunately, poor energy resolution and difficulties in absolute flux normalization in some of these earlier experiments have made the understanding of these data difficult. The current experiment addresses this situation by providing the first high resolution, systematic study of the proton Compton effect in the energy regime between 136MeV and 288MeV.

Experimental Method

A diagram of experimental area two (EA2) at SAL is shown in Figure 1. An approximately 50% duty factor electron beam was used to produce a bremsstrahlung photon beam by passing it through an aluminum radiator whose thickness was 0.01 radiation lengths. The bremsstrahlung endpoint energies were 298 MeV, 244 MeV, 200 MeV and 170 MeV. The primary beam current was monitored by dumping it into a water cooled copper beam stop. A 1 cm diameter by 30 cm long lead collimator together with 1m of dense concrete shielding and a sweep magnet were used to produce a relatively clean 2.5cm diameter photon beam on the liquid hydrogen target, which was 10.2 cm in diameter and 12.7 cm long. The detector was the high resolution total absorption NaI(Tl) scintillation counter designed at Boston University [2]. It consists of a cylindrical core of NaI surrounded by four annular NaI segments. This core is encased in a plastic scintillator annulus which, together with plastic veto counters in front of and behind the detector, was used to efficiently reject the cosmic ray background. Neutron backgrounds were reduced to acceptable levels through careful geometrical shielding of the detector. A 12.5 cm tungsten collimator was used to define the detector aperture. The photon flux was monitored continuously by measuring the energy deposited in a quantameter which was well shielded from room backgrounds.

At each beam energy, the response of the detector was measured by rotating it to zero degrees and allowing a greatly reduced photon flux to directly enter the crystal. This served to establish a reference point for the gain determination. This reference point was determined by fitting an EGS4 [10] simulated detector response function to the measured zero degree spectrum. This response function was calculated by using an incident bremsstrahlung spectrum of the appropriate endpoint energy. [11] A range of angles were measured for each energy; during the detector move (which usually took about half an hour) a thorium source was placed in the aperture of the detector to allow the gains of the quadrants to be monitored.

For each angle, a series of target empty and full runs would be accumulated. A typical full/empty cycle would require about 6-8 hours and, depending on the energy and angle, each point would require of order 1 day to acquire acceptable statistics in the photon yield region of interest. A yield spectrum for endpoint energy 200 MeV and lab angle 135 degrees is shown in Figure 2. The vertical lines indicate the approximate boundary of the region of interest. The region of interest is that region which should contain only elastically scattered photons and is defined by the interval between the most energetic photon possible from the decay of photo-produced neutral pions and the kinematic endpoint. The large π° background is clearly visible.

Data reduction

Figure 3 shows the same yield spectrum once the target empty background has been subtracted. Backgrounds were subtracted normalized to the quantameter counts with a correction for the fact that about 2% of the hydrogen remained in the target for the so-called target empty runs. The solid line in this figure was produced by simulating the detector response to π° decay photons and to a Compton scattered incident bremsstrahlung spectrum. These incident spectra had an arbitrary normalization and were used only to determine the appropriate shapes of the detector response. The incident spectra were determined using a technique first reported by Cocconi and Silverman [12] together with the photoproduction cross section compilation of Genzel, Joos and Pfeil [13]. Cocconi and Silverman parametrize the π° photoproduction cross section and then develop an analytic expression for the energy and angle distribution of the decay photons in terms of this parametrization. A Monte Carlo code was written to fold this distribution together with an incident bremsstrahlung spectrum. The success of this method is evident from the excellent agreement between the normalized calculated detector response curve and the background subtracted data. The sharp edge of the π° decay spectrum served as an excellent check on the energy calibration of the detector. This procedure was applied to each energy and angle combination to determine accurate regions of interest in the detected spectra. Especially for the lower energies, this region of interest was often large enough to allow several sub-bins with reasonable statistics in each bin. At the lowest energies, this allowed a consistency check since the same energy and angle combination was often measured with two different machine energies.

Once the bins have been determined, the remaining steps in the extraction of the differential cross sections are straightforward. Since the detector response function for monochromatic photons is not flat, it is necessary to determine the efficiency with which a given bin integrates the photon flux. The EGS4 simulation of the detector was written so that this efficiency could be easily determined. An energy spectrum is accumulated leaving the target and compared with the energy spectrum of the detected photons. The ratio of counts in equivalent bins in these two spectra then gives the efficiency. This also includes the effect of absorption as the scattered photon travels from the target to the detector. A simple Monte Carlo code was written to determine the detector solid angle, allowing for the effects of the extended target. Finally, an EGS4 simulation of the quantameter was carried out to verify that the photon flux monitoring with this device was in fact energy independent and that the calibration constant for it was reasonable.

One all the appropriate factors were determined, the differential cross sections were

$$\frac{d\sigma}{d\Omega}(\theta, \bar{E}) = \varepsilon(\mathrm{E1,E2}) \times \frac{C}{N_\gamma \Omega N_t}$$

calculated according to the above formula, where the quantities are defined as

C = detected photon flux in the region of interest
N_t = number of scattering centers in the target
Ω = detector solid angle
N_γ = incident photon flux corresponding to the region of interest

E1 and E2 are the energy endpoints of the region of interest, and ε is the efficiency (including absorption) for this region. The number density of protons in the target cell was calculated as $(5.37\pm0.11)\times10^{23}\,cm^{-2}$. The error in the flux normalization due to photon absorption in the target was estimated to be less than 0.5%.

Figure 4 shows the four most complete angular distributions together with the theoretical angular distributions as calculated from a theoretical dispersion relation analysis due to L'vov [3]. The agreement with his analysis is excellent.

Figure 5 shows an excitation curve near the threshold region at 45 degrees. This curve demonstrates the consistency with which cross sections were determined over the entire range of machine energies. The solid curve is from a multipole analysis by one of the authors (J.C. Bergstrom) based in part on the multipoles of Pfeil et al. [14]. It is of interest to note the behavior in the region of the pion photo-production threshold. The influence of the cusp is clearly evident; when the cusp amplitude is used with a multiplication factor of 1, the agreement between theory and experiment is excellent. Reducing or increasing the influence of the cusp worsens this agreement dramatically as indicated.

Conclusions

The excellent agreement between measured and calculated angular distributions in the energy regime investigated lends support to the dispersion relation calculations of L'vov [3]. We see definite evidence for the unitary cusp in the near threshold compton scattering from the proton.

Figure Captions

Figure 1: A scale diagram of experimental area 2 (EA2) at SAL, showing the detector and it shielding as it would be located for a forward angle measurement.

Figure 2: A summed yield spectrum for incident electron energy of 200.2 MeV and lab angle of 134.8 degrees. The region of interest is indicated by vertical lines. The left most is one detector resolution above the π° decay endpoint and the right most is the kinematic endpoint. The influence of the π° decay background is evident.

Figure 3: A comparison between the EGS4 simulation of the detector response and the target empty background subtracted yield spectrum. The calculated spectrum is only normalized, not fit.

Figure 4: Angular distributions for 150 MeV, 185 MeV, 232 MeV and 288 MeV average incident photon energies. The solid curves are calculated from the dispersion theory of L'vov [3].

Figure 5: An excitation function at 45 degrees. Data points are interpolated as required from the measured angular distributions. The solid curve is derived from the multipole analysis of Pfeil and Schwela [15].

References

[1] L.O. Dallin, High Duty Factor Monochromatic Extraction From Eros Ph.D. Thesis, Univ.of Sask.(1990), **SAL Report No. 38.**

[2] J. P. Miller et al., *Nucl. Instrum. Methods Phys. Res.* **A270** (1988) 431.

[3] A. L'vov, *private communication*, and V.A. Petrun'kin, *Sov. J. Nucl. Phys.*, **12**(3), May - June (1981), 278

[4] M. Benmerrouche and N.C. Mukopadhyay, *Rensselaer Physics Preprint* No. **RPI-N76-92** (1992).

5] Bernardini et al., *Nuovo Cim.* **18** (1960) 1203.

6] J.W. DeWire et al., *Phys. Rev.* **124** (1961) 909-912

[7] P.S. Baranov et al.,*Sov. J. Nucl. Phys.*, **3**(6), December (1966) 791 - 797

[8] E.R. Gray and A.O. Hanson, *Phys. Rev.*, **160** (1967) 160

[9] H. Genzel et al., *Z. Physik* **279** (1976) 399 - 406

[10] W.R. Nelson, H. Hirayama and D.W.O. Rogers, *EGS4 Code System*, **SLAC-265**, 1985.

[11] J. L. Matthews and R. O. Owens, *Nucl. Instrum. Methods*, **111** (1973) 157.

[12] G. Cocconi and A. Silverman, *Phys. Rev.* **88** (1952) 1230-1233.

[13] H. Genzel, P. Joos, and W. Pfeil, *Photoproduction of Elementary Particles*, ed. H. Schopper, Springer-Verlag, New York 1973.

[14] W. Pfeil et al., *Nucl. Phys.* **B73** (1974) 166-188.

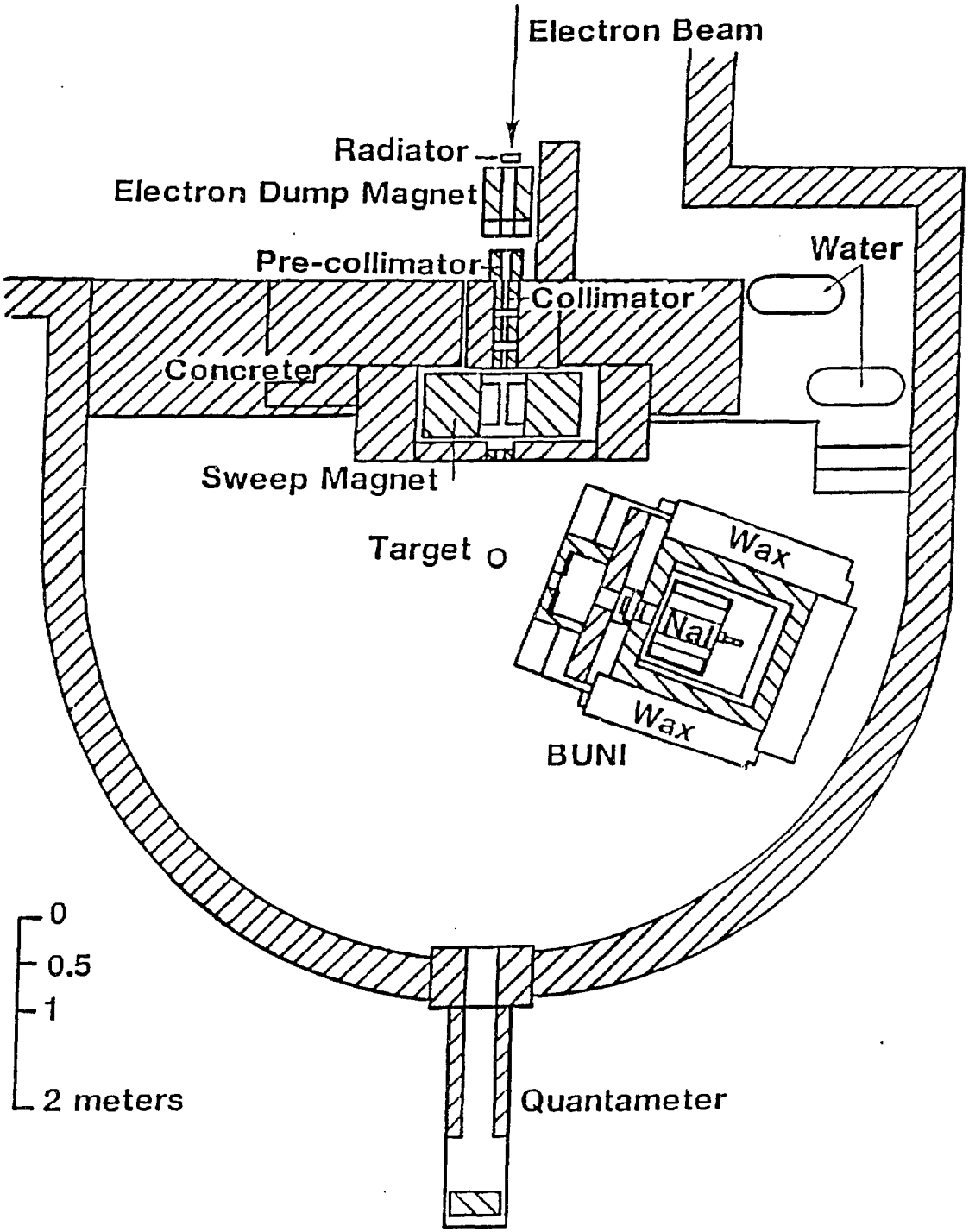
Electron Beam
Radiator
Electron Dump Magnet
Pre-collimator
Collimator
Water
Concreter
Sweep Magnet
Target
Wax
NaI
Wax
BUNI
0
0.5
1
2 meters
Quantameter

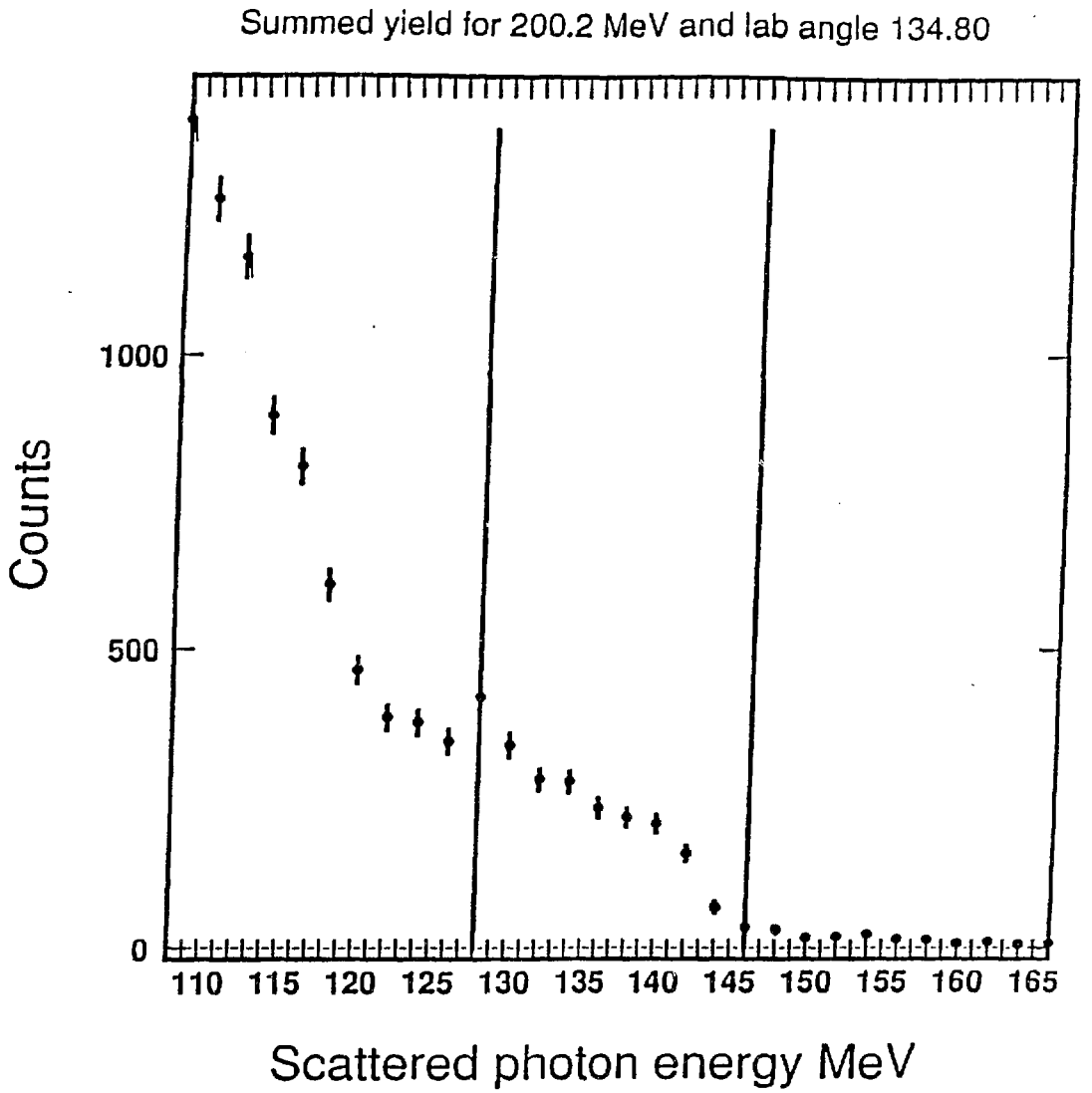
Summed yield for 200.2 MeV and lab angle 134.80
Counts
1000
500
0
110 115 120 125 130 135 140 145 150 155 160 165
Scattered photon energy MeV

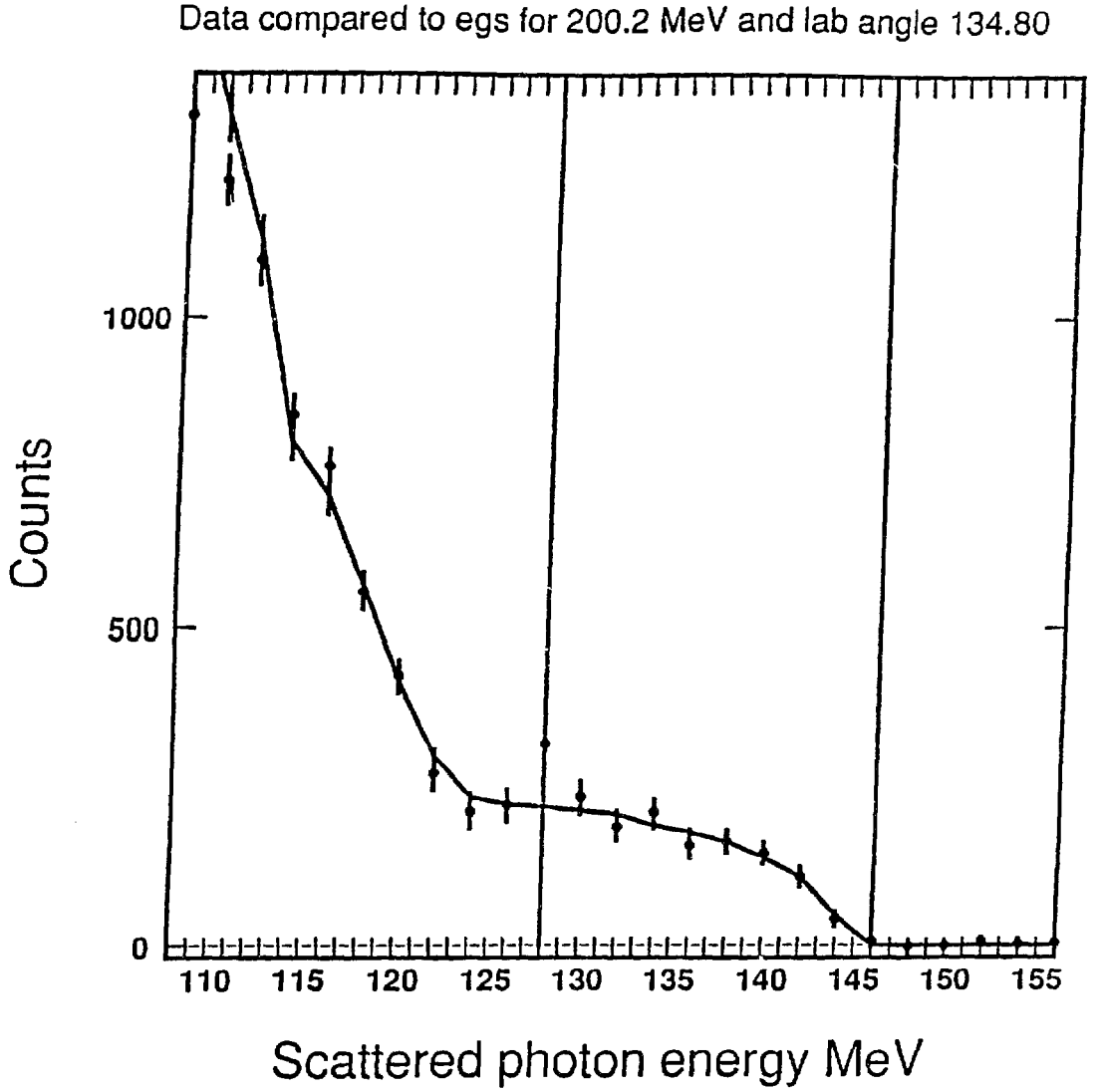
Data compared to egs for 200.2 MeV and lab angle 134.80
Counts
1000
500
0
110
115
120
125
130
135
140
145
150
155
Scattered photon energy MeV

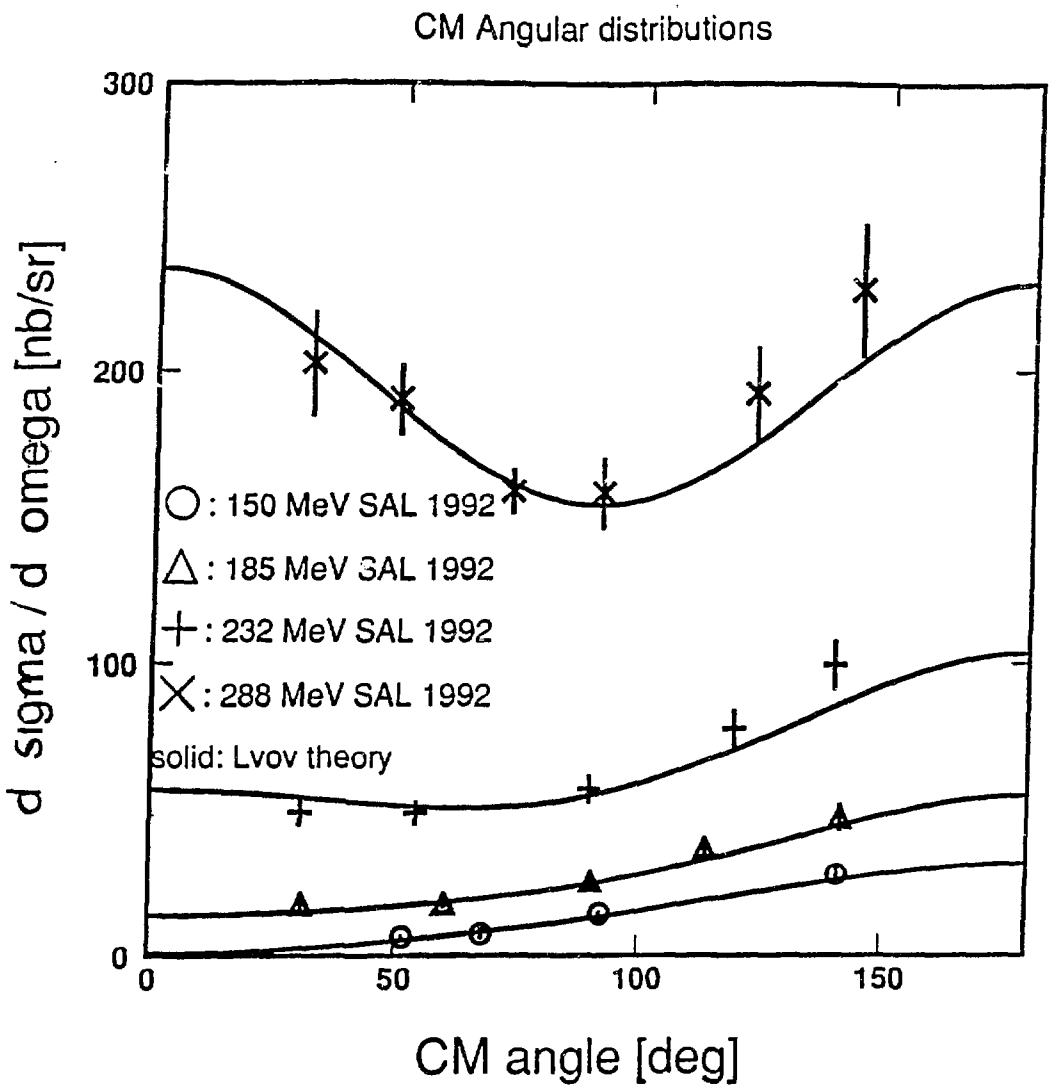
CM Angular distributions
d sigma / d omega [nb/sr]
300
200
100
0
0
50
100
150
CM angle [deg]
○ : 150 MeV SAL 1992
△ : 185 MeV SAL 1992
+ : 232 MeV SAL 1992
× : 288 MeV SAL 1992
solid: Lvov theory

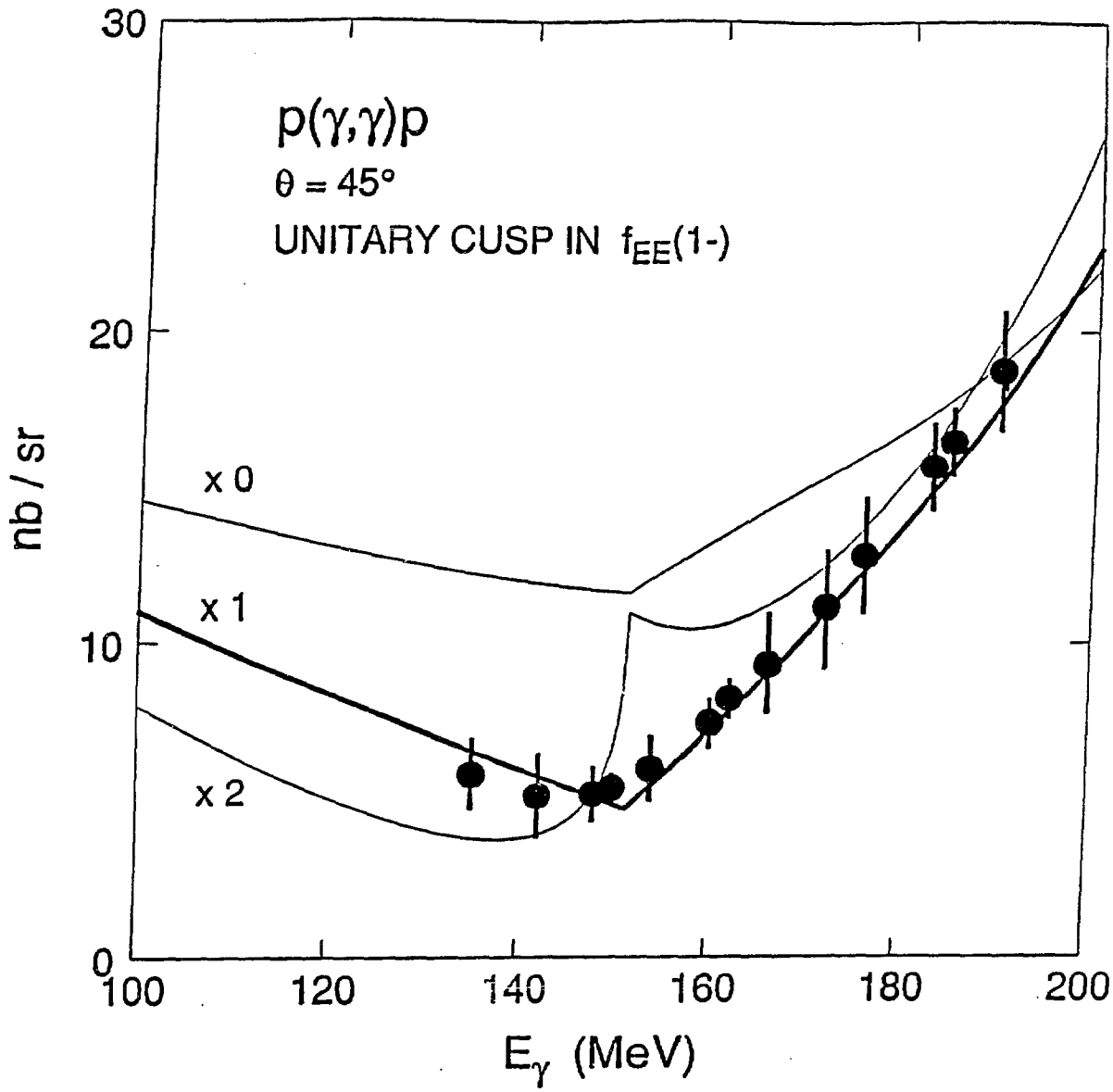
p(γ,γ)p
θ = 45°
UNITARY CUSP IN $f_{EE}(1-)$
x 0
x 1
x 2
nb / sr
E_γ (MeV)
0
10
20
30
100
120
140
160
180
200

CONNECTIONS BETWEEN COMPTON SCATTERING AND PION PHOTOPRODUCTION IN THE DELTA REGION*

NIMAI C. MUKHOPADHYAY and M. BENMERROUCHE
Physics Department, Rensselaer Polytechnic Institute
Troy, New York 12180–3590, USA

ABSTRACT

Using textbook tools like analyticity, unitarity and optical theorem, we discuss the relationship between pion–nucleon scattering, pion photoproduction and Compton scattering in the $\Delta(1232)$ resonance region. We review the relevant data and draw conclusions pertinent to the QCD–inspired models.

1. Introduction

Feynman[1], in his seminal text on photon–hadron interaction, has stressed the advantage of probing hadrons with a particle of known structure and interaction, and has considered photons the best in this regard, since no other particles, with the possible exceptions of leptons, are known as well. Compton Scattering (CS) is thus a classic way of probing hadrons: photon comes in and goes out, leaving the target hadron in its ground state, and thus neatly hiding all the hadronic violence in the intermediate state. In the Thomson limit, the CS cross–section is given by the only operative scale in the problem, viz., the charge e and the Compton wavelength of the hadron, $r_0 \sim \frac{1}{m}$, m being the mass of the hadron. In the photon energy region corresponding to the $\Delta(1232)$ excitation, however, the magnetic dipole and even the electric quadrupole excitation of the $\Delta(1232)$ becomes important. In this paper, we shall be concerned about these basic amplitudes, which are of great interest to the topical investigations[2] of hadron structure.[3] The reader is invited to consult our more elaborate discussion[4] elsewhere on the CS, for numerical and physics details that will be omitted in this paper.

The rest of the paper will be divided as follows: Section 2, a discussion of the Fermi–Watson theorem and a precise determination of the imaginary part of the magnetic Compton amplitude; Section 3, the use of the optical theorem to determine the forward Compton amplitude; Section 4, resolution of an apparent unitarity crisis; Section 5, possible determination of the E2/M1 amplitude ratio in the $N \leftrightarrow \Delta$ transition via the CS; Section 6, a summary of our conclusions.

*Invited Paper, Workshop on Hadron Structure from Photo–reactions at Intermediate Energies, Brookhaven National Laboratory, May 28–29, 1992. Presented by N.C. Mukhopadhyay.

2. A Precise Extraction of the Magnetic Compton Amplitude from the Pion–Nucleon Scattering and Pion Photoproduction

Let us consider the π N elastic scattering and pion photoproduction in the spin–isospin 3/2 channel relevant to the $\Delta(1232)$ excitation. For the latter, let us restrict ourselves to the dominant magnetic dipole amplitude. The 2x2 S–matrix is

$$S=\begin{bmatrix} \eta\, e^{2i\delta_1} & i\sqrt{1-\eta^2}\; e^{i(\delta_1+\delta_2)} \\ i\sqrt{1-\eta^2}\; e^{i(\delta_1+\delta_2)} & \eta\, e^{2i\delta_2} \end{bmatrix}, \qquad (1)$$

where η is the elasticity parameter, δ_1 and δ_2 are the strong and Compton phase shifts in the I = J = 3/2 channel. The off–diagonal matrix elements are equal due to time–reversal invariance, and they display the famous Fermi–Watson[5] phase, $\delta_1+\delta_2$, often approximated[6] in the literature by δ_1. Since we are interested in the CS, we shall not do that approximation, and use the recent analysis of pion photoproduction by Grushin et al.[7], which determines real and imaginary parts of the photopion production T–matrix element separately. Using the definition

$$T = i(1-S)/2, \qquad (2)$$

we have

$$\begin{aligned} \text{Re } T_{22} &= \tfrac{1}{2}\,\eta \sin 2\delta_2, \qquad (3) \\ \text{Im } T_{22} &= \tfrac{1}{2}\,(1-\eta\cos 2\delta_2). \end{aligned}$$

We know δ_1 from the pion–nucleon phase shift analyses[8], and we can determine $\psi = \delta_1+\delta_2$, from Grushin et al.'s analysis:

$$\tan\psi = \text{Im } T_{12}/\text{Re } T_{12}. \qquad (4)$$

Likewise, we set

$$\eta = \sqrt{1 - 4|T_{12}|^2}\,. \qquad (5)$$

We can thus determine the magnetic Compton amplitudes for proton, using the relations

$$f_{MM}^{1+(3)} \simeq \frac{T_{22}}{2k}\,, \qquad f_{MM}^{1+} \approx \frac{2}{3}\, f_{MM}^{1+(3)}\,, \qquad (6)$$

whereby small isospin – 1/2 contribution for the proton target is neglected, k is the photon cm momentum.

This method allows us to determine the Compton amplitude Im f_{MM}^{1+} most accurately at a certain energy close to the Δ–pole. Thus, the combination of the VPI phase shifts[8] and the Grushin et al. analyses[7] yield

$$\text{Im } f_{MM}^{1+} = 15.4 \pm 0.2, \tag{7}$$

in unity of $10^{-4}/m_{\pi^+}$, at $E_\gamma = 348$ MeV, the photon lab energy, corresponding to the cm energy W = 1239 MeV. Using instead the Karlsruhe[8] phase shifts, we get

$$\text{Im } f_{MM}^{1+} = 15.7 \pm 0.2, \tag{7'}$$

in the same units, for $E_\gamma = 343$ MeV or W = 1235 MeV. These can be measured in direct CS experiments to check consistency of the above analytical inputs. This would be of direct interest to the on–going Compton scattering experiments planned at the Brookhaven LEGS facility.[20] Also, the LEGS experiments reported at this conference[23] on the (γ,π°) reaction may be able to improve on the results (7), (7') reported above.

While this particular extraction is quite precise, it suffers from some limitations: (1) it is not helpful to determine Re f_{MM}^{1+}; (2) it *depends* on the various phase shift analyses; (3) away from the above "magic" energy determined by the phase shifts, the method loses accuracy[4]; (4) we have ignored the resonant E2 and the I = 1/2 contributions; these are small, but for better accuracy, they should be included. Thus, it is no replacement for a direct experimental determination, if we wish to know T_{22} as a function of E_γ.

3. Forward Compton Amplitude via the Optical Theorem from the Photohadron Experiments

One interesting independent check on the consistency and accuracy of the multipole data base of pion photoproduction can be provided by the application of optical theorem[9] for the total photohadron cross–section, on which some older data exist[10]. The optical theorem relates the total photohadron cross–section σ_T to the forward Compton amplitude f_1.

$$\sigma_T = \frac{4\pi}{E_\gamma} \text{Im } f_1, \tag{8}$$

where the expression for f_1 is given in terms of the various Compton multipoles by the classic work of Gell–Mann, Goldberger and Thirring[11]:

$$f_1 = \frac{E_\gamma}{k}(2 f_{MM}^{1+} + \dots), \tag{9}$$

where (...) represents other s– and p–wave contributions not shown (the d–wave contributions are small). From the multipole data base of Grushin et al.[7], we extract at $E_\gamma = 320$ MeV,

$$\text{Im } f_1 \approx 13.3 \pm 0.6\ \mu b\ \text{GeV}, \tag{10}$$

ignoring the d–wave terms. From the total photohadron cross–section measurements of Armstrong et al., we get

$$\text{Im } f_1 = 13.2 \pm 0.2,\ 13.0 \pm 0.2, \tag{11}$$

in the same units, at $E_\gamma = 315$ and 340 MeV respectively. The nice agreement of (10) and (11) checks the consistency of the multipole data base of Grushin et al., and adds confidence to the extraction (7), (7′) of the Im f^{1+}_{MM}, in a manner that is independent of a direct CS experiment, another text–book illustration of the Compton physics.

4. Unitarity Crisis in Compton Scattering?

Since the appearance of the Bonn studies[12] on CS in the delta region, there has existed a problem that has not been properly explained: the apparent violation of the unitary lower bound[13] on the CS cross–section at $E_\gamma = 320$ MeV, $\theta = 90°$ (the CS angle in the cm frame). The bounds are obtained as follows: Let us write the differential cross–section for the CS in terms of the relevant amplitudes $\phi_i (i = 1, ..6)$,

$$\frac{d\sigma}{d\Omega} = \frac{1}{2} \sum_{i=1}^{6} \eta_i \, |\phi_i|^2, \tag{12}$$

where η_i's are positive integers. Thus, the lower bound on the cross–section is obtained by setting the real parts of the ϕ_i to be zero:

$$\frac{d\sigma}{d\Omega} \geq \frac{d\sigma}{d\Omega}\Big|_{\text{Re}\phi_i = 0}. \tag{13}$$

The imaginary parts of the amplitudes ϕ_i can be obtained by using the unitarity equation for the T–matrix:

$$\text{Im} T_{ij} = \sum_k T_{ik} \, T^*_{ji}. \tag{14}$$

Thus, for the magnetic Compton amplitude

$$\text{Im } f^{1+}_{MM} = q \sum_c |M^c_{1+}|^2 + \ldots, \tag{15}$$

where q is the pion cm momentum, c are the physical channels ($\pi^+ n$, $\pi^0 p$ for the $\gamma p \to \gamma p$ process), (...) represents small corrections, and

$$T^c_{12} = \sqrt{2qk}\, M^c_{1+}, \tag{16}$$

Our test of the bound (13), using the pion photoproduction multipoles of Grushin et al.[7], shows no problem[4] with the Bonn data[12]. This is comforting: possibly the unitarity problem of the Pfeil et al.[13] has an origin in the underestimation of the errors of their multipole data base. This may also be due to the fact that Pfeil et al. have ignored the Compton phase δ_2 in extracting their photoproduction multipoles, thereby introducing "minor" errors for pion photoproduction, which are substantial for the CS. The unitarity tests bear a reexamination at a better precision than what we can provide from the Grushin et al. multipole data base. *So far we detect no unitarity crisis.* Finally, the new data taken at Mainz on the Compton scattering, now being

analyzed,firmly indicate that the new experiments show a nice consistency with the unitary lower band at $E_\gamma = 320$ MeV. We are grateful to M. Sanzone[24] for sharing this good news at this meeting.

5. Precise Measurements of Nucleon to Delta Resonant Electromagnetic Amplitudes: Future Prospects

We finally come to the subject matter with direct bearing on hadron structure[3,14-19]: determination of resonant helicity (or equivalently, multipole) amplitudes in the nucleon to delta electromagnetic transition, which we can probe sensitively via the CS. At the outset, we should stress to the reader the results that we have obtained[2] through our many years of research at RPI : the dominant magnetic dipole amplitude, extracted from the pion photoproduction data, is considerably larger than the predictions[14] of the Isgur–Karl quark shell model, while the electric quadrupole amplitude, so extracted, agrees in sign with the prediction of this model, though the magnitude seems to be bigger. The predictions of the Maryland school, for example, in which a combination of quark and meson effects in the structure of the hadrons is explored, are given by Cohen and Broniowski[3], in the long–wave length approximation,

$$M1 \simeq 204,\ E2 \simeq -11,\ A\ 1/2 \simeq -86,\ A\ 3/2 \simeq -186, \tag{17}$$

while the best determination from our photoproduction analysis is[2]:

$$M1 = 285\pm37,\ E2 = -4.6\pm2.6,\ A1/2 = -135\pm16,\ A3/2 = -251\pm33, \tag{18}$$

all in units of 10^{-3} $GeV^{-1/2}$. The important point to note is that the Maryland theoretical E2 amplitude in (17) is considerably *larger* than the empirical RPI value, while the former M1 amplitude is considerably *smaller*, even after factoring in the approximation in (17). Latest quark model calculations by Simon Capstick[25] do not improve the discrepancy between quark model[14] and our results, although the "bare" delta properties extracted by Nozawa, Lee and Blankleider[26] are much closer to the quark model. Finally, Robson[27] finds evidence for new corrections to quark model results.

The Compton scattering provides us with a new opportunity[4] to probe these amplitudes with considerable sensitivity. The dominant magnetic dipole Compton amplitude f^{1+}_{MM}, imaginary part of which is related to the M1 nucleon to delta amplitude by Eq. (15), sets the scale of the Compton observables in the delta region. Thus, we have,

$$\frac{d\sigma}{d\Omega} \simeq \frac{(3x^2+7)}{2}\,|f^{1+}_{MM}|^2,\ S \simeq 3(1-x^2)\,|f^{1+}_{MM}|^2,$$
$$\frac{d\sigma_{\|}}{d\sigma_{\perp}} \simeq \frac{5}{3x^2+2}, \tag{19}$$

where $x = \cos\theta$, all quantities are in the γ–N cm frame, $S = d\sigma_{\|}/d\Omega - d\sigma_{\perp}/d\Omega$, with $\|$ and $\perp$ representing the photon polarization parallel and perpendicular to the scattering plane, θ is the scattering angle. *In the limit of vanishing of real parts of all CS amplitude, the recoil nucleon polarization vanishes.* These are powerful results that

can be tested in future precise CS experiments, such as those that are currently underway at Mainz or the Brookhaven light source (LEGS).

A bonus of these experimental possibilities is to have a handle on the E2 amplitude, which is very tiny and yet theoretically very interesting. We recall that this amplitude would be zero in the naive SU(6) or $SU(6)_W$ limit[15]; it is sensitive to the color hyperfine interaction[16] due to one–gluon exchange between quarks. In the bag model[17], it is directly sensitive to the deformation of the hadron bag. In the Skyrme model[18], it is large and non–zero, but is difficult to estimate, as it is in the sub–leading order of the effective N_c expansion (N_c, the number of colors), and is sensitive[19] to the issue of current conservation in such models, and to the problem of keeping track of retardation effects (early estimates take long–wave length limits of this observable, thereby yielding a result that is not immediately comparable[19] to experiments). These problems should be also relevant to the work of the Maryland school[3], and hence the theoretical uncertainties of the estimates (17) need to be explored.

Happily, our investigations[4] indicate that the Compton observables S and $\frac{d\sigma_{\parallel}}{d\sigma_{\perp}}$ are quite sensitive to the variation of the E2 to M1 amplitude ratio at $\theta = 90°$, while $\frac{d\sigma}{d\Omega}$ is not as much sensitive at this angle. Thus, simultaneous measurements of these observables would be a step in the right direction – a step that is being currently explored at Brookhaven[20]. We must pay tribute here to Andy Sandorfi and his able collaborators at Brookhaven for their pioneering efforts at LEGS to make this possible at BNL.

An extrapolation[21] of the extracted resonant M1 amplitude from the delta peak to much lower energies indicates that it is consistent with recent measurments[22] of the magnetic polarizability of the proton at low energies. This is another check on the accuracy of the nucleon to delta amplitudes.

6. Conclusions

We summarize our conclusions on the Compton scattering in the delta (1232) region off nucleons:

(a) Unitarity[4,5] and information on pion–nucleon phase shifts[8], along with multipoles from the photoproduction of pions[7], allow us a precise determination of the amplitude Im f^{1+}_{MM} at a particular energy close to the delta pole. This is of crucial interest to hadron models.

(b) Optical theorem[9,11] and photohadron experiments[10] yield an independent consistency check on the magnetic Compton amplitude in (a).

(c) The Bonn data[12] on the Compton scattering of photons at $E_\gamma = 320$ MeV are consistent with the unitary lower bound extracted from the photopion multipole data base of Grushin et al.[7] Thus, the apparent unitarity crisis, reported by the Bonn group, is now resolved. There is, however, a lot of room for improvement on the experimental precision of this data base.

(d) There is an experimental opportunity[20] to explore the nucleon to delta electromagnetic resonant amplitudes via the Compton scattering at a precision so far unavailable. This prospect is enhanced by the availability of the polarized photons at

laser–driven light sources.[20]

7. Acknowledgement

We are grateful to Alan Nathan and Andy Sandorfi for their invitation. We thank A. Bernstein, R. Davidson, A. Nathan, S. Nozawa, A. Sandorfi, R. Wittman, R. Workman, and L. Zhang for discussions. This research has been supported by the U.S. Department of Energy, under grant #DE–FG02–88ER40448.A004. Part of this work has also been reported in an invited paper at the Conf. on Medium and High Energy Nuclear Physics, Calcutta, India (Dec. 1991).

8. References

1. R.P. Feynman, *Photon–Hadron Interactions* (Benjamin, Reading, Mass., 1972) p. 3.

2. N.C. Mukhopadhyay, in *Excited Baryons 1988*, eds. G. Adams, N.C. Mukhopadhyay and P. Stoler (World Scientific, Singapore, 1989), p. 205. R.M. Davidson and N.C. Mukhopadhyay, Phys. Rev. D42 (1990) 20. R.M. Davidson, N.C. Mukhopadhyay and R.S. Wittman, Phys. Rev. D43 (1991) 71.

3. M.C. Birse and M.K. Banerjee, Phys. Rev. D31 (1985) 118. T.D. Cohen and W. Broniowski, Phys. Rev. D34 (1986) 3472, and priv. com. (1991). W. Broniowski, this conf.

4. M. Benmerrouche and N.C. Mukhopadhyay, RPI preprint No. RPI–N76–92 (1992), Phys. Rev. D (in press).

5. K.M. Watson, Phys. Rev. 95 (1954) 228. E. Fermi, Supp. Nuovo Cim. 10 (1955) 17.

6. W. Pfeil and D. Schwela, Nucl. Phys. B45 (1972) 379. F.A. Berends and A. Donnachie, Nucl. Phys. B58 (1973) 378.

7. V.F. Grushin et al., Sov. J. Nucl. Phys. 38 (1983) 881.

8. R. Koch and E. Pietarinen, Nucl. Phys. A336 (1980) 331. R.A. Arndt et al., Phys. Rev. D32 (1985) 1085.

9. See, for example, L.I. Schiff, *Quantum Mechanics* (McGraw Hill, New York, 1968) p. 137.

10. T.A. Armstrong et al., Phys. Rev. D5 (1972) 1640.

11. M. Gell–Mann, M.L. Goldberger and W. Thirring, Phys. Rev. 95 (1954) 1612.

12. H. Genzel et al., Z. Physik A279 (1976) 399.

13. W. Pfeil, H. Rollnik and S. Stankowski, Nucl. Phys. B73 (1974) 166.

14. N. Isgur, G. Karl and R. Koniuk, Phys. Rev. D25 (1982) 2394. See also, S.S. Gershtein, and G.V. Dzhikiya, Sov. J. Nucl. Phys. 34 (1981) 870; M. Bourdeau and N.C. Mukhopadhyay, Phys. Rev. Lett. 58 (1987) 976 and 63 (1989) 335; S. Capstick and G. Karl, Phys. Rev. D41 (1990) 2767.

15. G. Becchi and G. Morpurgo, Phys. Lett. 17 (1965) 352; H. Harari and H.J. Lipkin, Phys. Rev. B140 (1965) 1617.

16. A. DeRújula, H. Georgi and S.L. Glashow, Phys. Rev. D12 (1975) 147.

17. G. Kälbermann and J.M. Eisenberg, Phys. Rev. D28 (1983) 71; A. Araki and A.N. Kamal, Phys. Rev. D29 (1984) 1345. See also G.E. Brown, Nucl. Phys. A358 (1981) 51c, and in *Excited Baryons 1988* (Ref. 2).

18. G.S. Adkins, C.R. Nappi and E. Witten, Nucl. Phys. B228 (1983) 552; G.S. Adkins and C.R. Nappi, Nucl. Phys. B249 (1985) 507; A. Wirzba and W. Weise, Phys. Lett. B188 (1987) 6.

19. L. Zhang and N.C. Mukhopadhyay, to be published.

20. A. Sandorfi et al., in *Excited Baryons 1988* (Ref. 2), and priv. comm. (1992). A. Sandorfi, invited talk at the Baryons–92 Conf. (Yale University, June 1992), to be published.

21. N.C. Mukhopadhyay, A. Nathan and L. Zhang, in preparation.

22. F.J. Federspiel et al., Phys. Rev. Lett. 67 (1991) 1511. A. Zieger et al., Phys. Lett. B278, 34 (1992). See U. Meissner, this conf., for a review of the latest results in the Chiral Perturbation Theory (χPT). For magnetic polarizability, the treatment of the $\Delta(1232)$ is still a problem in the χPT.

23. M. Khandeker, this conf.

24. M. Sanzone, this conf. and priv. comm. (June 1992).

25. S. Capstick, CEBAF preprint # CEBAF–TH–92–09, 1992, to be published.

26. S. Nozawa, this conf.; T.–S.H. Lee, Invited Talk at the Baryons–92 Conf. (Yale University, June, 1992), to be published, and references herein.

27. D. Robson, to be published, and the Report at the CEBAF Workshop (June 1992).

Single-Pion Electroproduction and the $\Delta^+ \to P + \gamma$ Transverse One-Half and Scalar Helicity Transition Form Factors--An Algebraic Approach.

ABSTRACT

Milton D. Slaughter[*]
Department of Physics
University of New Orleans
New Orleans, Louisiana

and

S. Oneda
Center for Theoretical Physics, University of Maryland
College Park, Maryland

Single-pion electroproduction $(\gamma + p \to \Delta^+ \to \pi^0 + p)$ and the $\Delta^+ \to p + \gamma$ transverse one-half helicity transition form factor $h_3(q^2) \propto (G_M^*(q^2) - 3G_E^*(q^2)) \propto (M_{1^+}^{(3/2)}(q^2) + 3E_{1^+}^{(3/2)}(q^2))$ and the scalar transition form factor $h_1(q^2) \propto G_C^*(q^2) \propto S_{1^+}^{(3/2)}(q^2)$ are examined using equal-time commutation relations (ETCRs) and the dynamical concept of asymptotic $SU_F(2)$ symmetry and realization. Utilizing as input only $g_A^{np}(q^2)$, the well-known isovector part of the proton magnetic moment $G_M^V(q^2)$, and the isovector part of the proton electric form factor $G_E^V(q^2)$, a direct calculation of $h_1(q^2)$ and $h_3(q^2)$ is made. The scalar quadrupole amplitude $S_{1^+}^{(3/2)}(q^2)$ is calculated with results in good agreement with experiment. The ratio of the electric quadrupole moment to the magnetic dipole moment $(E_{1^+}/M_{1^+})_{q^2=0} \equiv$ electromagnetic ratio (EMR) is also calculated as a function of $G_M^*(0)$ and is shown to be a very sensitive function of the Δ mass. Our treatment is *completely relativistic*. Current conservation is guaranteed.

[*] Supported in part by NSF Grant No. PHY-9012374

Relativistic effects, QCD mixing angles and $N\to N\gamma$ and $\Delta\to N\gamma$ transition form factors

I. G. Aznauryan

Yerevan Physics Institute, Alikhanian Brothers St. 2

375036, Yerevan, Armenia, CIS

Abstract

It is shown that relativistic effects, considered in the framework of a relativistic quark model constructed in infinite momentum frame, improve the agreement between theory and experiment for $\Delta\to N\gamma$ transition. They enlarge the magnitudes of the amplitudes $A^p_{1/2}$ and $A^p_{3/2}$ and suppress with increasing Q^2 the magnetic form factor of $\Delta\to N\gamma$ transition in comparison with proton magnetic form factor. The additional inclusion of not large QCD-inspired mixings of multiplet $[56',0^+]$ into the N and the Δ improves further the agreement with experiment for this form factor and permits to describe its Q^2-dependence at $Q^2< 3$ GeV^2. Predominantly due to the relativistic effects non-zero values for electric and Coulombic form factors of $\Delta\to N\gamma$ transition are obtained. It is predicted that the electric form factor is positive at $Q^2< 0.2$ GeV^2 and changes its sign with increasing Q^2, so the magnitude of helicity asymmetry should be lower than 0.5 at $Q^2> 0.2$ GeV^2.

ELECTROPRODUCTION STUDIES OF THE N→Δ TRANSITION AT BATES AND AT CEBAF

C. N. Papanicolas
University of Illinois at Urbana-Champaign
Department of Physics and Nuclear Physics Laboratory
1110 W. Green Street
Urbana, IL 61801 USA

ABSTRACT

The nucleon resonance programs pursued at Bates and at CEBAF place particular emphasis on the study of $\Delta^+(1232)$ resonance. A number of experiments have been approved that seek to precisely determine the resonant quadrupole amplitude in the N→Δ transition. The experimental evidence available from earlier electroproduction experiments and recent theoretical predictions are reviewed in order to provide a perspective on the planed measurements. The goals and the scope of the approved experiments at Bates and at CEBAF, are then presented.

INTRODUCTION

Among the few crucial observables needed to guide the QCD inspired phenomenology, the strength of the quadrupole excitation of the $\Delta^+(1232)$ has emerged as a particularly sensitive one. At the two US electron scattering facilities which can address this question through electroproduction, Bates and CEBAF, extensive efforts are underway preparing for an experimental program which ought to provide the necessary and much desired experimental information.

The nucleon resonance program at the Bates Linear Accelerator Facility, a facility capable of providing intense high quality electron beams with a maximum energy of 1 GeV, is limited to the study of only the $\Delta^+(1232)$ resonance at low momentum transfers. At CEBAF, where beams of superb quality of energies exceeding 4 GeV are anticipated, resonances of masses up to 2.5 GeV can comfortably be studied through electroproduction. The kinematic restrictions for an H(e,e'p) experiment at these two facilities are best understood with the help of Figure 1. The electron spectrometer angle (dashed curve), and the proton emission angles (shaded band) are shown as a function of momentum transfer (Q^2). Momentum transfers exceeding 0.6 GeV^2 become impractical at Bates; at CEBAF one can reach momentum transfers of 5 (GeV/c)^2. The solid line in the middle of the shaded band gives the direction of the momentum transfer. The width of the band, typically of the order 40° for Bates and 10° for CEBAF, gives the opening angle of the cone within which all of the decay protons (from the Δ) may be detected. It is worth pointing out that at Bates the momentum transfer vector typically lies only 30° from the beam direction and the reaction cone always straddles the beam. Clearly these are not the ideal conditions to study nucleon resonances. At CEBAF where the higher incident beam allows expanded kinematic flexibility, the narrow reaction cone, within which the angular distribution needs to be mapped, puts much tougher restriction on the instrumental accuracy that needs to be achieved.

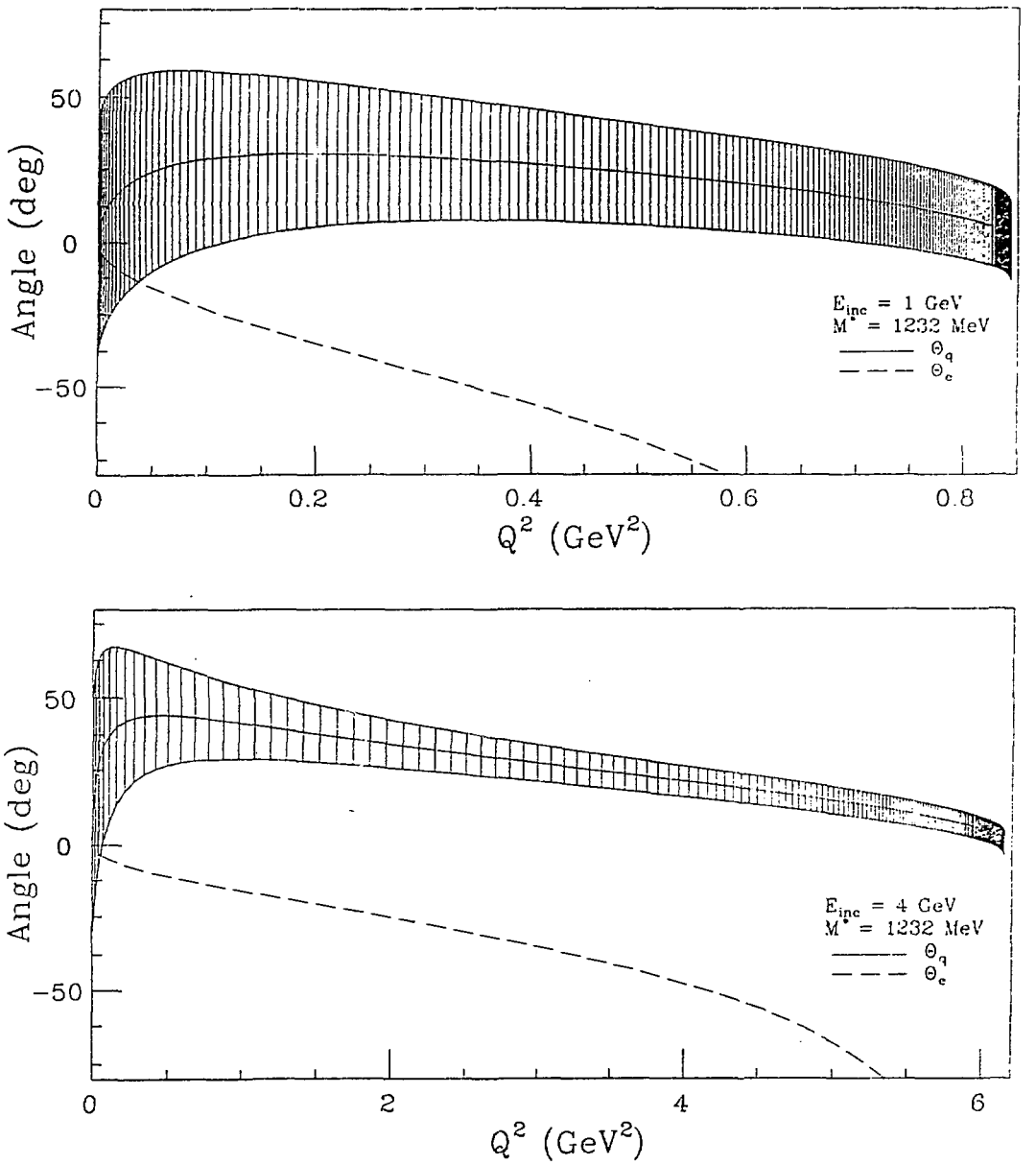

Figure 1: The electron angle, Θ_e, (dashed) and proton lab decay cone, (shaded band) for kinematics appropriate to Bates (top figure) and for CEBAF (bottom) for the study of the N→Δ transition in H(e, e'p) experiments. as a function of Q^2.

THEORETICAL MOTIVATION

S. Glashow in 1979 suggested [10] that most of the shortcomings of the MIT bag model [7] could be overcome if spherical symmetry was not imposed as a prerequisite. In microscopic terms the abandonment of the spherical shape can be understood in analogy to the case of the deuteron. As in the case of the N-N interaction the interaction between quarks is believed to have a tensor component [13]. In the case of nuclei this leads to the famous d-state admixture and to the deformation of the deuteron. At the quark level, this leads to d-state admixtures in the N(939) and the $\Delta^+(1232)$ and the "deformation" of the nucleon. As it is to be expected, such an important effect leads to many other consequences about hadron structure: a non-zero electric form factor for the neutron, mass splittings and modified decay probabilities.

The intrinsic deformation of the spin-$\frac{1}{2}$ object cannot be measured directly; it has to be inferred from transition amplitudes, as in the case of spin-0 or spin-$\frac{1}{2}$ nuclei. The transition amplitudes for the N$\rightarrow\Delta$ excitation are the most obvious candidates. The $\Delta^+(1232)$ in spherical models can be excited only through a pure spin-flip transition, which can proceed only through an M1 (magnetic dipole) excitation. Deformation introduces d-state admixtures in the ground state of the nucleon and/or in the Δ which allow quadrupole transitions in addition to the spin flip M1. Departure from spherical symmetry implies a new observable – the Electric quadrupole to Magnetic dipole amplitude Ratio (EMR). If virtual photons are used then in addition to E2 (Electric Quadrupole) a C2 excitation (Quadrupole Coulombic) is allowed and by analogy to the EMR the CMR (C2 to M1 Ratio) can be defined. These, well understood observables, are therefore of great importance in testing our understanding of the nucleon.

Following Glashow's suggestion, an intense theoretical activity emerged, which continues to date unabated, exploring the values that the EMR ratio can assume in different models of the nucleon. In Table 1 we present a collection of results representative of the various models. The most remarkable feature of this table is the rather narrow range of values

Theory	EMR (×100)	Reference
SU(6)	0.00	[2, 12]
MIT Bag	0.00	[7]
Chiral Bag	−0.92	[6]
Chiral Bag	−1.8	[23]
Constituent	−0.32 to +0.5	[9]
Quark	+0.7	[13]
Models	−0.69, −0.23	[24]
	−0.6, −0.3	[4]
	−0.65	[11]
Skyrme	−5.0	[1]
Model	−2.6 to −4.9	[25]

Table 1: Theoretical Predictions for EMR

predicted by the various models. The predicted values of the EMR are typically small, negative, and with the exception of certain Skyrme predictions, always below 0.02 in absolute value.

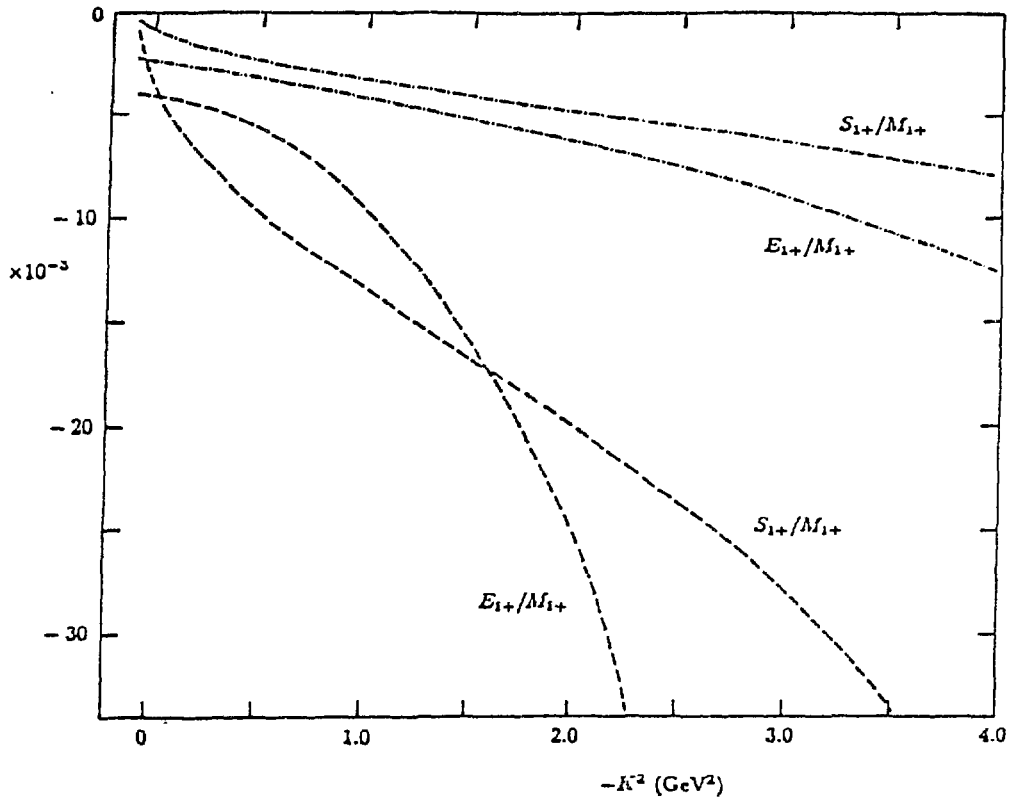

Figure 2: Representative multipole ratios, E_{1+}/M_{1+} and S_{1+}/M_{1+}, from the work of Capstick and Karl [5] for the Isgur, Karl, and Koniuk [13] model (dashed curves) and with relativized wavefunctions (dot-dashed curves).

The momentum transfer behavior of EMR and CMR is potentially a very sensitive observable that has remained, until recently, unexplored. S. A. Gogilidze *et al.* [11], Nozawa *et al.* [19], and Capstick and Karl [5] have studied the Q^2 behavior of the S_{1+}, M_{1+}, and E_{1+} multipoles within their respective models. Typical and illustrative of the expected magnitude and Q^2 behavior are the results of Capstick and Karl. The EMR and CMR values resulting from their calculation are shown in Figure 2 as functions of Q^2.

The situation in the case of the N→Δ transition is rather unique, because the two limits of Q^2 ($Q^2 \rightarrow 0$) and ($Q^2 \rightarrow \infty$) are well understood. We have seen that at the photon point ($Q^2 = 0$) the EMR should be very small and in the SU(6) limit it should be zero. Work by Carlson [10] based on the sound assumption that helicity is conserved and that photons couple to quarks directly (no resonant behavior) lead to the conclusion that the asymptotic value of EMR must be 1.0. It is then obvious why one needs to establish the validity of these two limits and then proceed to examine the Q^2 evolution of EMR and CMR.

AVAILABLE EXPERIMENTAL EVIDENCE

Although the region of the first nucleon resonance has been extensively studied at many laboratories with a wide variety of experimental techniques, no clear evidence has emerged for the existence of the quadrupole excitation of the Δ. The majority of these investigations are more than twenty years old. They were carried out at high energy facilities such as DESY, BONN, Daresbury (NINA) and Tokyo as part of broad investigations on nucleon resonances with the main emphasis placed on understanding the $\gamma_v NN^*$ vertex. They predate Glashow's suggestion so no particular care was taken in addressing the question of "nucleon deformation". The discovery of J/ψ in 1974 radically changed the perspective of the high energy physics community; the nucleon resonance programs were terminated and the experimental facilities were shut down. When the renewed theoretical interest emerged in the eighties, it was no longer possible to pursue such measurements.

The experimental evidence has been recently reviewed [18] and there is no need to repeat it here. However it is worth restating the most significant conclusions:

a. The region of low Q^2 has been probed repeatedly with photoproduction and with inclusive and coincidence electron scattering. None of the measurements were originally intended to obtain precise information on the quadrupole excitation of the Δ.
b. Repeated attempts to analyze the available photoproduction data yield small ($\leq$4%) negative values for the EMR. This due to the various model assumptions introduced in the analysis of the data which are not reach enough to both check the various model assumptions and produce the obviously very small value of the EMR. Evidently richer data involving either the use of polarized tagged photons and/or the use of virtual photos are needed.
c. All of the available electroproduction measurements are limited to an accuracy of about 5%. New measurements must find ways to limit systematic error to well below this level if they are to contribute to the determination of the amplitude of the resonant quadrupole excitation of the Δ.
d. Given the present status of theory the low momentum transfer region is most important. In this region the present data are quite old and most suspect. The Q^2 evolution of CMR and EMR will be particularly valuable.

ELECTROPRODUCTION AT BATES AND AT CEBAF

The anticipated availability of high quality cw beams at Bates and at CEBAF and the superb instrumentation build to exploit them offers the possibility to address the question of "nucleon deformation" with an improvement in accuracy of about an order of magnitude over the existing measurements. Two experiments have been approved for Bates which will attempt to measure this effect at low values of Q^2 and three at CEBAF which will extend these measurements to intermediate values of momentum transfer. It is hoped that the Bates measurements will establish the magnitude of the effect while the CEBAF measurements will determine its evolution as a function of Q^2. All approved experiments and their extensions rely on the accurate detection of interference response functions either through out-of-plane detection or through focal plane polarimetry. Each response function exhibits different sensitivities, and by measuring simultaneously a number of

them it is hoped to gain enough information so as to both determine the background amplitudes and to isolate the resonant piece of the quadrupole amplitude.

BATES EXPERIMENTS

a. Experiment #87-09

This experiment will study the N→Δ transition in the $(\vec{e}, e'\gamma)$ and $(\vec{e}, e'\pi^\circ)$ channels: It is possible to access these two electrocoincidence channels simultaneously through a kinematically complete $H(\vec{e}, e'p)$ experiment. The background contributions are of different nature than the resonant E2/C2 contributions in the two channels, and therefore an important cross check on the model dependence is offered through the comparison of results obtained from these two channels. In coincident electron scattering with polarized electrons (no polarized targets or detection of recoil polarization) three interference functions are accessible: W_{TL} the transverse-longitudinal interference, W_{TT} the transverse-transverse interference, and $\tilde{W}_{TL}$ the imaginary part of the transverse longitudinal interference (commonly referred to as the fifth structure function). Theoretical studies suggest that W_{TT} is insensitive to the presence of resonant quadrupole excitation, W_{TL} is highly sensitive to it, and $\tilde{W}_{TL}$ is highly sensitive to the interference of Born terms with the resonant Δ excitation. If only resonant amplitudes were present, then $\tilde{W}_{TL}$ would vanish identically, thus providing an observable particularly sensitive to the background term. Detection of this observable requires both a polarized beam and out-of-plane detection; both will be available for #87-09. This valuable new observable was detected for the first time only last year at Bates [17].

These dependences are illustrated in Figure 3 where the sensitivity of each response, accessible in coincident electron scattering, to the resonant quadrupole excitation is shown. The two curves for each response correspond to two versions of the unitarized Blomqvist-Laget (B-L) model. The standard B-L model in addition to the Born terms includes a phenomenological M1 excitation of the Δ, but it does not allow for resonant quadrupole excitation. Its prediction for the kinematics discussed here are represented by the dashed curves. The B-L model has been extended [15] so a resonant quadrupole excitation of the Δ is also allowed. The magnitude of the resonant quadrupole excitation has been adjusted to yield a value for $\mathrm{Re}(S_{1+}M_{1-})/(M_{1+})^2 = -0.04$, which reproduces reasonably well the experimental data. The predictions of this model are depicted as solid curves in Figure 3. Experimentally the obvious task is to map these responses as a function of θ_p (equivalent to θ_π^*)and try to distinguish between the two predictions. This is the goal of the Bates #87-09 experiment, where these functions will be studied at $Q^2 = -0.07$ GeV^2 and -0.12 GeV^2 and for energy loss varying between the pion emission threshold and the Ropper resonance.

It is obvious that measurements seeking to isolate small amplitudes in a given process run the risk of being masked by systematic error. The proposed technique in experiment #87-09 addresses this problem by the use of four simultaneous measurements of the outgoing proton. The required four magnetic spectrometers of DQ design are currently under construction [8]. This method, which is described in detail in ref. [22], allows the isolation of the interference structure functions with greatly reduced error. Actually the tolerances of the OOPS (Out Of Plane Spectrometer) system of Bates were driven by the requirements imposed by experiment #87-09. The simultaneous measurement of four

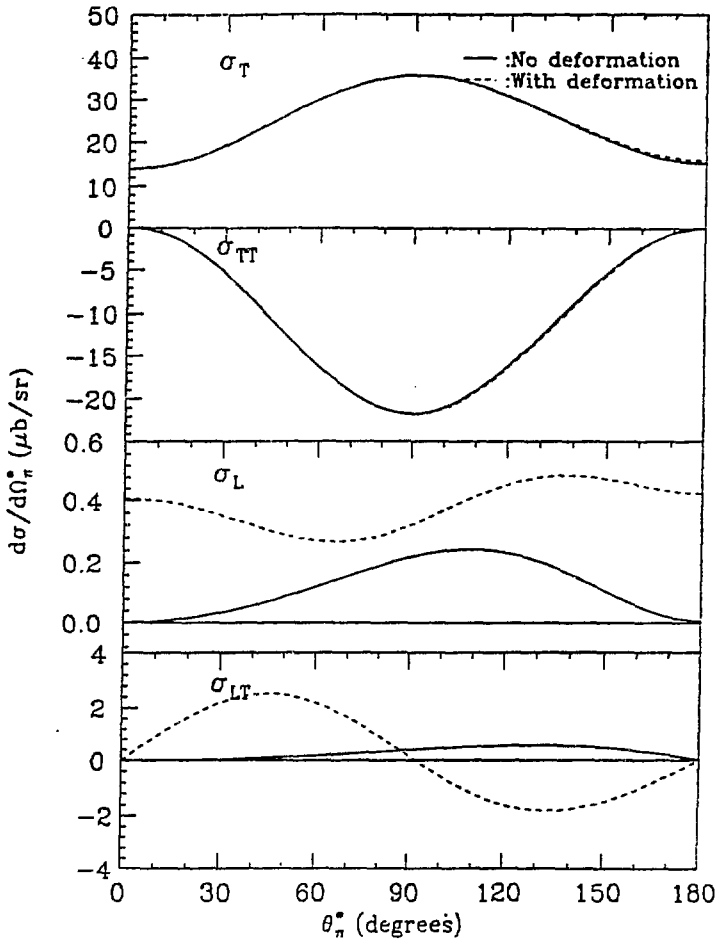

Figure 3: Response functions calculated by Laget [3, 15] for the kinematics of Bates Exp. #87-09. The solid curves indicate results expected if the resonant quadrupole is identically zero, while the dashed curves include a resonant quadrupole excitation compatible with EMR= -0.04.

coincident cross sections significantly reduces the systematic error. This is achieved by reducing the task of isolating structure functions to that of making a set of asymmetry measurements. In Figure 4 the asymmetry which corresponds to the W_{TL} responce in the Laget model is shown. In the same figure the expected errors in the measurement (which include both systematic and statisitcal contributions) are shown - the result of an extensive Monte Carlo study of the experiment. The OOPS system is in its final year of construction. Measurements on the N$\rightarrow\Delta$ are expected to commence in late 1993.

b. Experiment #89-03 A complementary approach to the measurement of the interference structure functions involves the use of focal plane polarimetry. In this approach, the goal of the experiment is to make a precise measurement of the $H(\vec{e},e'\vec{p})\pi^\circ$ reaction at the maximum of the Δ resonance. Six individual response functions, $R^l_{LT'}$, $R^t_{LT'}$, R^n_{LT},

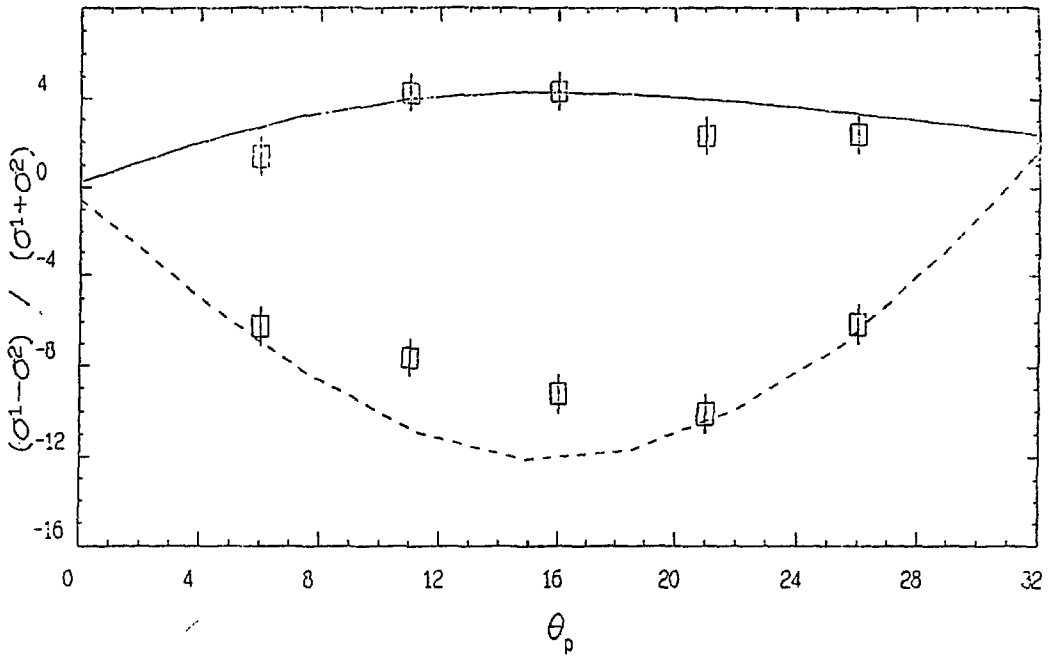

Figure 4: Experimentally accessible asymmetry corresponding to the W_{TL} response [20] evaluated using the results of Laget[3, 15]. The solid curve indicates the result expected if the resonant quadrupole is identically zero, while the dashed curves include a resonant quadrupole excitation compatible with EMR= -0.04.

R_{LT}, $R^l_{TT'}$, and $R^t_{TT'}$, can be separated. The superscripts indicate the additional decomposition that can be achieved through the detection of the direction of polarization of the outgoing proton [16]. In addition, the experiment can determine the combinations $2\epsilon R^n_L + R^n_T + \epsilon R^n_{TT}$ and $2\epsilon R^n_L + R^n_T - \epsilon R^n_{TT}$. Three of the LT-type response functions are highly sensitive to the presence of a resonant quadrupole (S_{1+}) amplitude. The inherent redundancy in these observables will allow the S_{1+} contribution to be isolated from the several other amplitudes present in each response function. The other LT-type response, R^n_{LT}, will characterize the influence of other (resonant and non-resonant) amplitudes since it, like the "fifth" response function $\tilde{W}_{TL}$, identically vanishes for an isolated resonance. Figure 5 illustrates the expected precision of the experiment in a measurement of the R^n_{LT} structure function. Finally knowledge of the two TT'-type response functions will allow the dominant $|M_{1+}|$ term to be accurately determined and, by isolating it, one can deduce the remaining transverse strength, most of which is expected to come from the resonant E_{1+} multipole. Experiment #89-03 will be performed at $Q^2 = -0.07$ GeV^2 so as to sample these additional structure functions at the same momentum transfer value as experiment #87-09.

The construction of the Bates Focal Plane Polarimeter is nearing completion; it is expected that it will be calibrated during the next year at IUCF and be installed at the focal plane of the OHIPS spectrometer. #89-03 is expected to run after a deuteron recoil polarization measurement at Bates but well in advance of the CEBAF experiments.

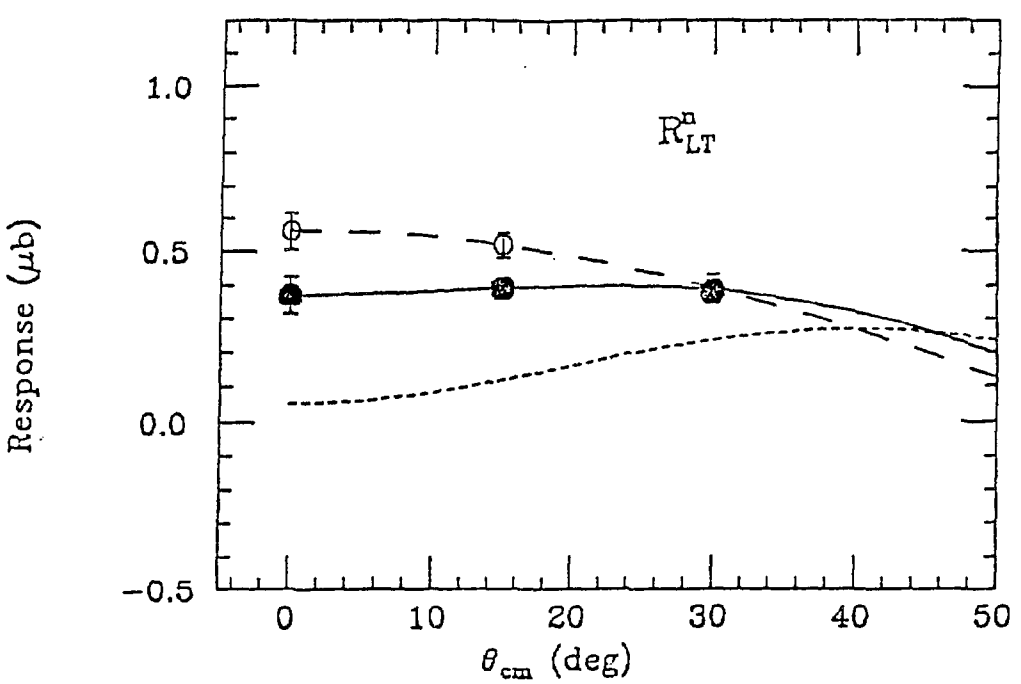

Figure 5: Bates Exp. # 89-03: the R^n_{LT} response function. Error bars illustrate the projected experimental precision. Curves represent a full calculation according to the Devenish-Lyth parametrization (solid), a calculation with S_{1+} and E_{1+} multipoles set to zero (long dashed), and a calculation with Born terms set to zero (short dashed).

CEBAF EXPERIMENTS

A very extensive research program on nucleon resonances with particular emphasis on the N→Δ transition is planned at CEBAF. At this time two experiments have been approved for Hall B which plan to use the CLAS (The CEBAF Large Acceptance Spectrometer) and one is approved to run in Hall-A. They are the following:

a. 89-037 Electroproduction of the $P_{33}(1232)$ Resonance, V. Burkert, spokesman.
b. 89-042 A measurement of the Electron Asymmetry in $p(\vec{e}, e'\pi^0)$and $p(\vec{e}, e'\pi^+)$in the Mass Region of the $P_{33}(1232)$ for $Q^2 \leq 2(GeV/c)^2$, V. Burkert, spokesman.
c. 91-011 High Precision Separation of Polarized Structure Functions In Electroproduction and Roper Resonances, S. Frulani and R. W. Lourie Co-spokesmen.

The CLAS experiments take advantage of the large solid angle of the device (3.2π) and the large momentum bite of about 0.1 - 4.0 GeV/c for a standard field setting, to access a very wide angular range for all momentum transfers in this kinematic window. The wide angular coverage includes out-of-plane detection and the advantages it brings. In exp 89-037 the channels $H(e, e'\pi^+)n$ and $H(e, e'p)\pi^0$ will be studied simultaneously in the Q^2 range from 0.2 to 4.0 $(GeV/c)^2$. The expected statistical accuracy compared to a number of recent theoretical results for the Q^2 dependence of the EMR are shown in Figure 6.

The availability of polarized beams at CEBAF and the inherent out-of-plane detection of CLAS allows the measurement of the fifth structure function at much higher momentum

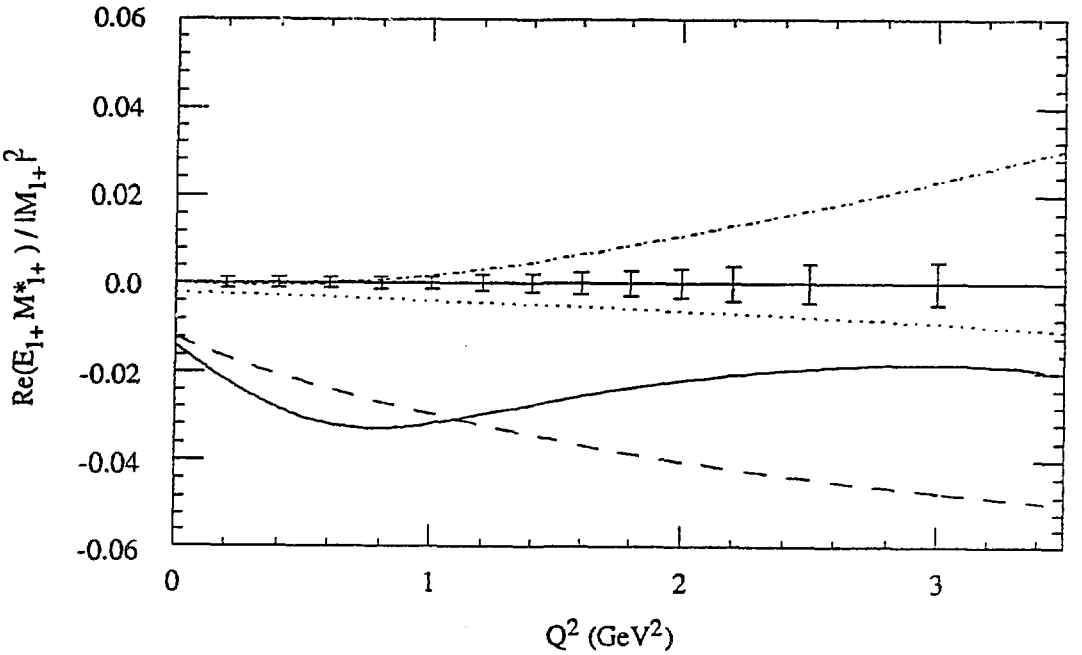

Figure 6: Monte Carlo estimation of the statistical accuracy with which the EMR will be obtained in CEBAF experiment 89-037. Theoretical calculations are from Warns *et al.*[26] (solid: relativized, dashed: nonrelativistic), Capstick and Karl [5] (dotted), and Koerner [14] (dot-dash)

transfers than OOPS. The goal of experiment 89-042 is to measure the $Im(S_0 M^*_{1+})$ and $Im(S_{1+} M^*_{1+})$ in the region of the $P_{33}(1232)$ Resonance for Q^2 below 3 $(GeV/c)^2$.

CEBAF experiment 91-011 is an extension of the recoil polarization of Bates to the CEBAF kinematic regime. The Hall-A focal polarimeter measurements will complement the more extensive investigations of the $P_{33}(1232)$ Resonance with CLAS. In Figure 7. two of the response functions expected to be measured in this experiment are shown with the estimated statisitical uncertainty and some representative theoretical results.

SUMMARY AND CONCLUSIONS

The resonant quadrupole excitation amplitude of the $\Delta^+(1232)$ provides a particularly valuable observable for understanding the structure of the nucleon. It can provide unambiguous information on the question of nucleon deformation and on the nature and magnitude of the inter quark tensor interaction. The Bates program which is anticipates to commence in the fall of 1993 is hoped that it will provide new precise data at low momentum transfers. It will be followed by an extensive program at CEBAF which will provide us with the evolution of this amplitude in momentum space.

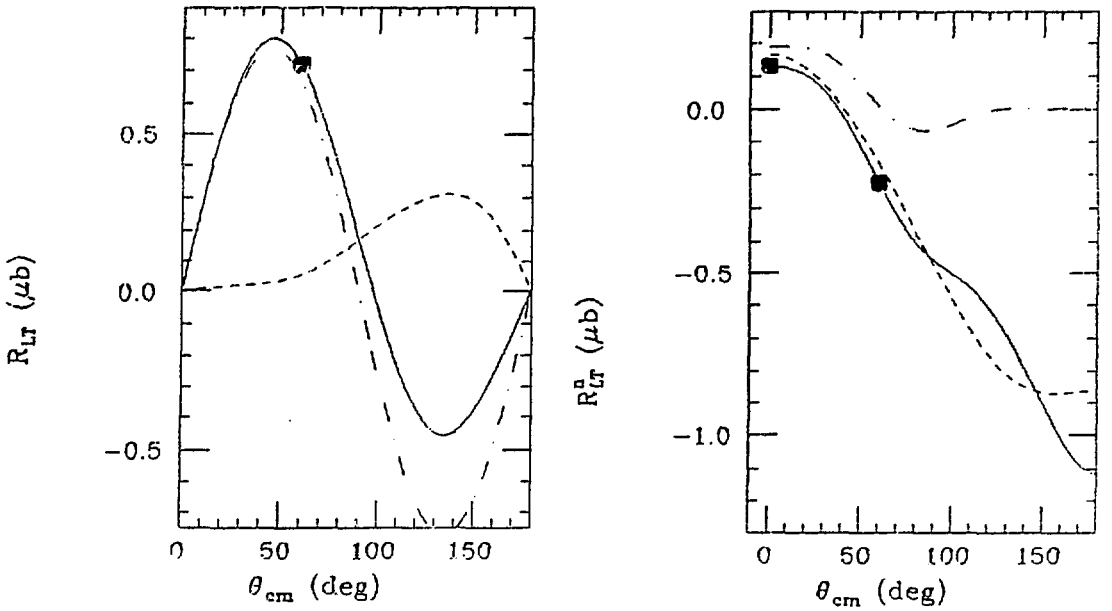

Figure 7: Two of the Response functions that will be measured in CEBAF Exp 91-011. The error bars arepresentative of the projected accuracy. Curves represent a full calculation according to the Devenish-Lyth parametrization (solid), a calculation with S_{1+} and E_{1+} multipoles set to zero (long dashed), and a calculation with Born terms set to zero (short dashed).

ACKNOWLEDGMENTS

I am indebted to Dr. V. Burkert for providing me with information concerning the CEBAF program, and my colleagues at UIUC Dr. S.E. Williamson, S. Dolfini and J. Mandeville for help in the preparation of this talk. The work reported here is supported in part by the National Science Foundation under grant NSF PHY 89-21146.

REFERENCES

[1] Adkins, G. S. and C. R. Nappi, Nucl. Phys. **B249**, 507 (1985).
[2] Becchi, C. and G. Morpurgo, Phys. Rev. **140**, B687 (1965).
[3] Blomquist, I. and J. M. Laget, Nucl. Phys. **A280**, 405 (1977).
[4] Bourdeau, M. and N. Mukhopadhyay, Phys. Rev. Lett. **58**, 976 (1987).
[5] Capstick, S. and G. Karl, Phys. Rev. **D41**, 2767 (1990).
[6] Carlson, C. E., Phys. Rev. **D34**, 2704 (1986).
[7] Chodos, A. *et al.*, Phys. Rev. **D9**, 3471 (1974); Chodos, A. *et al.*, Phys. Rev. **D10**, 2599 (1974); Chodos, A. and C. B. Thorn, Phys. Rev. **D12**, 2733 (1975).
[8] Dolfini, S. *et al.*, "Out-of-Plane Spectrometer Design Report Update," presented to Bates PAC, July 1988; S. Dolfini, *et al.*, Bull. Amer. Phys. Soc. **33**, 1578 (1988).
[9] Gershtein, S. S. and G. V. Dzhikiya, Sov. J. Nucl. Phys. **34**, 870 (1981).
[10] Glashow, S. L., Physica **96A**, 27 (1979).

[11] Gogilidze, S. A., Yu. S. Surovtsev, and F. G. Tkebuchava, Yad. Fiz. **45**, 1085 (1987).
[12] Harari, H. and H. Lipkin, Phys. Rev. **140**, B1617 (1965).
[13] Isgur, N. and G. Karl, Phys. Rev. **D18**, 4187 (1978); **D12**, 147 (1979); Isgur, N., G. Karl, and R. Koniuk, Phys. Rev. **D25**, 2394 (1986).
[14] Koerner J.G., Z. Phys. **C33**, 529 (1987)
[15] Laget, J. M., Nucl. Phys. **A481**, 765 (1988); private communication.
[16] Lourie, R. W., Nucl. Phys. **A509**, 653 (1990).
[17] Mandeville J. *et al.*To be published.
[18] Mukhopadhyay, N. C., in the proceedings of *Excited Baryons 1988* (Troy, New York, August 1988), World Scientific, Ed. G. Adams, N. C. Mukhopadhyay, P. Stoler, pp. 205; C. N. Papanicolas, *ibid.*, pp 235.
[19] Nozawa S., Blankleider B., and Lee H. T. S., Nucl. Phys. **A513**, 459 (1990).
[20] Papanicolas, C. N. (spokesman), Bates Proposal #87-09 (1987)
[21] R. W. Lourie and V. Burkert (co-spokesmen), Bates Proposal #89-03 (1989).
[22] Papanicolas, C. N. *et al.*, Nucl. Phys. **A497**, 509c (1989).
[23] Pfeil, W. and D. Schwela, Nucl. Phys. **B45**, 379 (1972).
[24] Weyrauch, M. and H. J. Weber, Phys. Lett., **B171**, 13 (1986).
[25] Wirzba, A. and W. Weise, Phys. Lett. **B188**, 6 (1987).
[26] Warns M., Schroder H., Pfeil W. and Rollnick H., Z. Phys. **C45**, 613 and 627 (1990).

Description of a Nucleon in Nuclear Matter

G. G. Bunatian
Joint Institute for Nuclear Research , Dubna , Russia

The nonlinear cloudy bag model,CBM /1/,is generalized to describe a nucleon in a nuclear matter at various density ρ and temperature T /2/.The influence of the nuclear medium on the bag-nucleon in the framework of CBM is due to the modification of the equation describing the CBM pion field π. These changes are accounted for in the CBM by including in the CBM lagrangian the pion polarization operator $\Pi(\rho,T)$.The free pion propagator D is replaced in a nuclear medium by $D(\rho,T)$.The changing of the pion field π and propagator D leads via the CBM equations to the modification of the bag size R and quark momentum p, determined simultaneously from these equations,and then to modifications of other bag-nucleon characteristics:the total energy E, r.m.s. radii $\langle r^2\rangle^{1/2}$, magnetic moment μ ,polarizability α and so on,which all are expressed as the expectation values $\langle\hat{A}\rangle$ of the corresponding operators $\hat{A}$ in the bag-nucleon state The quantity $\Pi(\rho,T)$was studied in the works /3/ whose results are used in our investigations.As we have obtained,the nucleon size R in the nuclear matter at normal density ρ_0 and zero temperature T=0 decreases by $\sim$ 5% and the quarks momentum p also decreases,however, insignificantly,by $\sim$ 1-2%.On the other hand,the values of the r.m.s.radii $\langle r^2\rangle^{1/2}$ increases by $\sim$ 15% for a proton and by $\sim$ 100% for neutron.We have found also that polarizability of a nucleon in nuclear matter is roughly two times as much than one of the free nucleon.

Our calculations are selfconsistant.If at the given T and ρ the CBM equations have the simultaneous solution for the pion field,bag size R_e and quarks momentum p_e,the total energy E(R) as the function on R will have absolute minimum just at this solution $R=R_e$ .But,if it turns out that at high enough density $\rho>\rho_c$ or temperature $T>T_c$ the CBM equations have no simultaneous solution and respectively energy E(R) has no minimum,it manifests that the nuclear matter does not consist then of the common three-quark bags only,the other,non-nucleon phase appearance has to be expected.The increase of the ρ and T values leads to the pion mode softening and then to strengthening of the CBM pion field,to the enhancement of the virtual "pion cloud" of the bag which causes eventually the nucleon-bag nonstability in a nuclear matter at $T>T_c$ and $\rho>\rho_c$ .Our estimations give for the quantities ρ_c and T_c values $\rho_c=(1.5\text{-}2)\rho_0$,$T=(1\text{-}1.5)(m_\pi c^2)=(140\text{-}210)$MeV.

References

1.A.W.Thomas,Adv.Nucl.Phys.13 (1984) 1
2.G.G.Bunatian,Sov.J.Nucl.Phys.49 (1989) 664;49 (1989) 847;43 (1986) 188;51 (1990) 790.Nucl. Phys.A509 (1990) 736.
3.G.G.Bunatian,Sov.J.Nucl.Phys.30 (1979) 131;31 (1980) 613;41 (1985) 33;41 (1985) 560;36 (1982) 656.Nucl.Phys.A404 (1983) 525

n,e-Amplitude Estimate Independent of Nuclear Scattering Model

V.G.Nikolenko, A.B.Popov
Joint Institute for Nuclear Research, 141980 Dubna, SU

The physical importance of the n,e-amplitude b_{ne} consists in the fact that it allows determination of the neutron mean square charge radius that is proportional to $(b_{ne} - a_F)$, where the Foldy term $a_F = -1.468$ mfm.

It is important to note that, in spite of the many year investigation, the problem of b_{ne} estimation has not been solved. All known precise results fall into two groups: one near $-1.55(5)$ mfm [1-3] and the other near $-1.32(4)$ mfm in the range critical for sign assignment to the neutron mean square charge radius .

So, the obtained in [2] value of b_{ne} differs from the estimates of refs [4,5] by nearly 10 errors and, as we have shown [6], this is connected with different mathematical descriptions of the measured effects. But the difference between the values $-1.49(5)$ [1], $-1.55(2)$ [3] and $-1.31(4)$ [4,5] has not found any explanation up to now. And so, estimates of b_{ne} from [5] depend on the reliability and precision of the rich set of coherent amplitude b_{coh} values (for Bi) obtained in different years on the gravitational spectrometer and (in the last time) on the interferometer and lie essentially beyond error limits. These b_{coh} lead to the values of b_{ne} from -1.32(3) to -1.43(3). Such uncertainty evokes the necessity of analysis of the measurement and data processing methods. Here one more approach to n,e-amplitude estimation is proposed. The nuclear scattering cross section $\sigma_s(0) \quad 4\pi R'^2(0)$ is calculated by extrapolation of known scattering cross sections from the energy region of tens or hundreds eV to $E \Rightarrow 0$. The values of b_{ne} are obtained from a comparison of $\sigma_s(0)$ and $4\pi b_{coh}$ with $b_{coh} = R'(0) + b_{ne}Z$. The authors discuss also the discrepancy between the existing b_{ne} estimates and conclude that it is yet impossible to reliably determine the neutron mean square charge radius. The obtained "nonmodel" estimates of b_{ne} agree nicely with the results [5].

Method	Bi	Pb
$R'_0 = const$ [5]	-1.30 ± 0.06	-1.32 ± 0.04
$R'_0 = const$ [6]	-1.30 ± 0.04	-1.32 ± 0.03
Extrapolation $\sigma_s \Rightarrow 0$	-1.33 ± 0.03	-1.32 ± 0.03

References

1. Melkonian, E., et.al.: Phys. Rev. 1959, **114**, p.1471.
2. Alexandrov, Y., et.al.: Sov. J. Nucl. Phys., 1986,**44**, p.900.
3. Alexandrov, Yu., et.al.: Yadernaya Fisika, 1974,**20**, p.1190.
4. Krohn, V., Ringo, G.:Phys.Rev., 1973,**D8**, p.1305.
5. Koester, L., et.al.: Z. Phys. A , 1988, **329**, p.229.
6. Nikolenko, V., Popov, A.: Z. Phys. A - Hadrons and Nuclei, 1992, **341**, p. 365.

Δ-RESONANCE EFFECTS IN POLARIZATION OBSERVABLES OF ^{3}He$(\gamma,\pi^+)^3$H

S.S. Kamalov[1], L. Tiator[1], and C. Bennhold[2]

[1] Institut für Kernphysik, Universität Mainz, D6500 Mainz, Germany
[2]TRIUMF, 4004 Wesbrook Mall, Vancouver, B.C., V6T 2A3, Canada

In recent publications[1,2] we have reported on new investigations of pion scattering and pion photoproduction on the trinucleon ^{3}He and ^{3}H. In a model using realistic three-body wave function and realistic pion-nuclear interaction with spin and isospin degrees of freedom we have obtained a good agreement with all available data for the cross section in pion photoproduction and both for the target asymmetry and cross section in pion scattering.

In the present work the polarization observables Σ (photon asymmetry), T and P (target and recoil asymmetries) for ^{3}He$(\gamma,\pi^+)^3$H at various kinematics are presented. The process is described in a recently developed *nonlocal* coupled-channel framework[1)] that employs three-body Faddeev wave functions and incorporates two-step processes such as ^{3}He$(\gamma,\pi^o)^3$He$(\pi^o,\pi^+)^3$H. Enhancement effects of the contributions from small components of the ^{3}He wave function as well as from the E^{Δ}_{1+} multipole in production operator to the polarization observables have been investigated. The results are presented in Fig.1 where the solid (dashed) curves are calculations with (without) D-state components of the three-body wave function and with the full production operator. The dash-dotted (dotted) curves are calculations without E^{Δ}_{1+} (only with Born terms) and with the full wave function. Experimental data are from Ref.[3)].

We found that the energy dependence for T, P and especially Σ observables at $\theta_\pi = 90^0$ are sensitive to the D-state components of the ^{3}He three-body wave function. Around E_γ = 350–400 MeV a small D-state component with only 1% probability reduces Σ by up to 30%, leaving a clear signal that should be detectable experimentally. At this region the photon asymmetry Σ is also very sensitive to the presence of the $E2$ transition in the $\gamma N\Delta$ vertex which defines the E^{Δ}_{1+} multipole. Above E_γ=350 MeV large differences appear between our computations without and with the $E2$. The presence of an $E2$ which is in our calculations about -5% of the dominant $M1$ transition[4)] enhances Σ at E_γ=400 MeV by almost a factor of two. We found that such effects arise entirely due to an interference between S- and D-state components of the ^{3}He wave function. The corresponding contribution is enhanced by the large Kroll-Ruderman E_{0+} multipole which is absent in Σ for a pure S-shell wave function, as well as for the photon asymmetry of the elementary process. The observables T and P are insensitive to the $E2$ transition up to E_γ=500 MeV. So we find the photon asymmetry Σ to be useful to study details in the trinucleon wave function, such as D-state components, as well as the $E2/M1$ ratio.

In Fig.1c,d we show our predictions for the T and P observables at $\Theta_{c.m.} = 30^0$ as a function of the photon energy. In this angular region these observables are basically insensitive to pion rescattering. Using simple harmonic oscillator S-shell wave functions leads to almost identical results as calculations with the full Faddeev amplitudes. The same conclusion holds for the photon asymmetry Σ. Thus PWIA with simple S-shell wave functions is a good approximation for polarization observables in pion photoproduction at small angles. Here the simple relations

$$\Sigma(^3\mathrm{He}) = \Sigma(p)\,,\quad T(^3\mathrm{He}) = -P(p)\,,\quad P(^3\mathrm{He}) = -T(p) \qquad (1)$$

between the polarization observables on ^{3}He and on the proton are fulfilled. Furthermore, in this region the contribution from the Δ-isobar is very important (compare dotted and solid curves). Therefore, we believe that this is a good kinematical region to study the dominant Δ-isobar properties inside the nuclear medium. Should an experiment find deviations from the simple relations (1) at forward direction, this would indicate medium modifications of the delta propagator in the ^{3}He nucleus.

1) S.S. Kamalov, L. Tiator, C. Bennhold, Few Body Systems 10 (1991) 143
2) C. Bennhold, B.K. Jennings, L. Tiator, and S.S. Kamalov, Nucl. Phys A (1992) (in press)
3) B. Bellinghausen et al., Nucl. Phys. A470 (1987) 429
4) J.M. Laget, Nucl. Phys. A481 (1988) 765

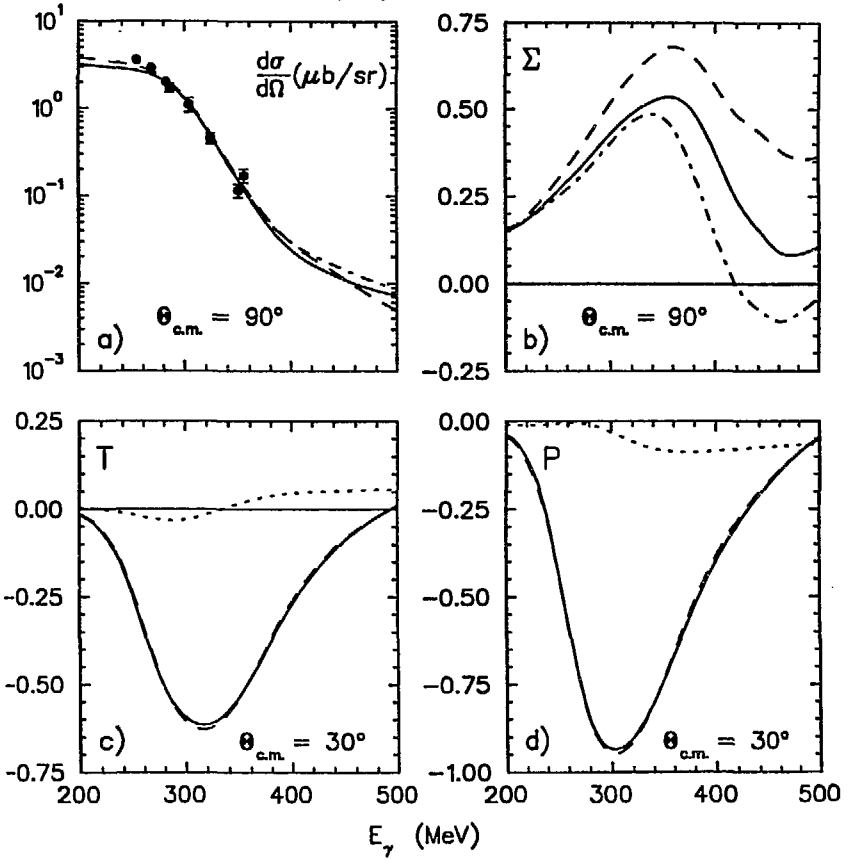

PARTICIPANTS LIST

NAME	INSTITUTE and E-MAIL ADDRESS
Arndt, Richard	Virginia Polytechnic Inst. & State University PHYS0@VTVM1
Aybergenov, Token	Lebedev Physical Institut H01TOK@DHHDESY3
Aznauryan, Ina	Yerevan Physics Institute EGIYAN@CEBAF
Benmerrouche, Mohamed	Rensselaer Polytechnic Institute BENMER@NIMAI.PHYS.RPI.EDU
Bergstrom, Jack	University of Saskatchewan BERGSTROM@SKATTER.USASK.CA
Bernstein, Aron	Massachusetts Institute of Technology BERNSTEIN@MITLNS
Blecher, Marvin	Virginia Polytechnic Inst. & State University BLECHER@VTINTE
Booth, Edward	Boston University BOOTH@BUPHYC
Broniowski, Wojciech	University of Maryland WOJTEK@QUARK.UMD.EDU
Bunatian, George	Joint Institute for Nuclear Research, Dubna LNFNP@LNP.JINR.DUBNA.SU
Davidson, Richard	University of Mainz DAVIDSON@VKPMZA.KPH.Uni-Mainz.de
Federspiel, Fred	Los Alamos National Laboratory, LAMPF FEDERSPIEL@LAMPF.BITNET
Feldman, Jerry	University of Saskatchewan FELDMAN@SKATTER.USASK.CA
Fil'kov, Lev	Lebedev Physical Institut H01BPS@DHHDESY3
Fiolhais, Manuel	University of Coimbra TMANUEL@FTEOR1.CFTUC.PT
Garino, Gerard	University of Illinois GARINO@UIUCNPL
Giordano, Giofranco	Frascati National Laboratory GIORDANO@IRMLNF
Hallin, Emil	University of Saskatchewan EMIL@SKATTER.USASK.CA
Hayward, Evans	Duke University EHAY@NISTCS2
Hoblit, Sam	LEGS/University of Virginia HOBLIT@BNLCL1

Ivanov, Mikhail	Joint Institute for Nuclear Research, Dubna MIZUTANI@VTVM1
Kettler, Thomas	Massachusetts Institute of Technology KETTLER@PIERRE.MIT.EDU
Khandaker, Mahbub	LEGS/Virginia Polytechnic Inst. & State University KHANDAKER@BNLCL1
Kistner, Ottmar	LEGS, Brookhaven National Laboratory KISTNER@BNLCL1
Kobayashi, T.	Rensselaer Polytechnic Institute KOBAT@RPIMEP.PHYS.RPI.EDU
Kopecky, Stefan	Inst. Kernphysik KOPECKY@EATI.UNA.AC.AT
Krusche, B.	University of Giessen BERND@DGIPIG5
Leeb, Helmut	University of Vienna LEEB@EKPISL.TUWIEN.AC.AT
Li, Zhujun	Virginia Polytechnic Inst. & State University LIZ@VTCC1
Lipkin, Harry	Weizmann Institute of Science FTLIPKIN@WEIZMANN
L'vov, Anatoli	Lebedev Physical Institut LVOV@SCI.FIAN.MSK.SU
MacGibbon, Bruce	University of Illinois MACGIBBON@UINPLA.NPL.UIUC.EDU
Matinian, Sergei	Yerevan Physics Inst. EGIYAN@CEBAF
Matone, Gianni	Frascati National Laboratory MATONE@IRMLNF
Maximon, Leonard	George Washington University MAX@GWUVM
Meissner, Ulf-G.	University of Bern MEISSNER@ITP.UNIBE.CH
Menze, Dietmar	University of Bonn MENZE@PIB1.PHYSIK.UNI-BONN.DE
Miceli, Lino	LEGS, Brookhaven National Laboratory MICELI@BNLCL1
Miller, James	Boston University MILLER@BUPHYC
Moinester, Murray	Tel Aviv University MURRAY@TAUPHY.TAU.AC.IL
Mukhopadhyay, Nimai	Rensselaer Polytechnic Institute USEREBC2@RPITSMTS
Nathan, Alan	University of Illinois NATHAN@UIUCNPL
Nozawa, Satoshi	Queen's University NOZAWA@QUCDNAST

Papanicolas, Costas	University of Illinois COSTAS@UIUCNPL
Preedom, Barry	University of South Carolina N530005@UNIVSCVM
Rebreyend, Dominique	LEGS/University of South Carolina Rebreyend@BNLCL1
Sandorfi, Andrew	LEGS, Brookhaven National Laboratory SANDORFI@BNLCL1
Sanzone, Marcella	Universita Genova SANZONE@GENOVA.INFN.IT
Scadron, Mike	University of Arizona SCADRON@ARIZVMS
Schaerf, Carlo	University of Rome 39992::SCHAERF
Schmiedmayer, Jorg	Massachusetts Institute of Technology SCH@AMO.MIT.EDU
Schoch, Bertholα	University of Bonn SCHOCH@PIB1.PHYSIK.UNI-BONN.DE
Sealock, Richard	University of Virginia SEALOCK@VIRGINIA
Slaughter, Milton	University of New Orleans MDSPH@UNO
Surya, Yohanes	College of William & Mary SURYA@CEBAF
Tam, April	LEGS/University of South Carolina TAM@BNLCL1
Teichmeister, Claudia	University of Vienna TEICHTM@EKPI51.TUWIEN.AC.AT
Thorn, Craig	LEGS, Brookhaven National Laboratory THORN@BNLCL1
Thornton, Stephen	University of Virginia STT@VIRGINIA.EDU
Welch, Pat	Massachusetts Institute of Technology PWELCH@MITLNS.MIT.EDU
Wells, Doug	University of Washington WELLS@NPL.NPL.WASHINGTON.EDU
Whisnant, Steve	LEGS/University of South Carolina WHISNANT@NUC003.PSC.SCAROLINA.EDU
Workman, Ron	Virginia Polytechnic Inst. & State University WORKMANRL@VTVM1
Zhao, Mike	LEGS/Virginia Polytechnic Inst. & State University MZHAO@BNLCL1